

Research into Resistojet Rockets for Small Satellite Applications

by
Captain Timothy J. Lawrence

October 1998

**A thesis submitted for the degree of Doctor of Philosophy at the Department of
Electronic and Electrical Engineering, University of Surrey, Guildford, Surrey, UK.**

DTIC QUALITY INSPECTED 2

ABSTRACT

This effort investigated the use of resistojets for small satellite stationkeeping missions. Small satellites create unique system constraints, compared to larger spacecraft, that have not been investigated thoroughly for stationkeeping missions. These constraints are: cost, power, volume, mass, safety, and thrust. Whilst all these constraints have been considered in off-the shelf-systems used through out the aerospace community, current systems may not be appropriate or affordable for cost-effective small satellite applications. Cold gas systems have low performance, hydrazine and ammonia systems use toxic propellants, and arcjets, electrostatic and electromagnetic electric propulsion systems have low thrust to input power ratios. Thus, electric propulsion using resistojets operating at low power, ~100W, and using liquid propellants, water and nitrous oxide, have re-emerged as attractive propulsion options for small satellites.

The research objective was to investigate a resistojet thruster that could satisfy the six constraints mentioned above and provide the design tools for future applications. To obtain this goal, three phases of research were conceptually required. Two resistojet thrusters have been developed which utilise a packed bed of silicon carbide particles with a cartridge heater for the heat exchanger. A thermodynamic model has been developed to study and optimise the thruster design and a series of practical performance tests with both nitrous oxide and water have been completed at the USAF Research Laboratory using the NASA Jet Propulsion Laboratory inverted pendulum thrust stand. Endurance tests, ~300 hours in duration, were conducted to determine lifetime limitations and failure modes. Friction losses were characterised in small nozzles, 0.12 mm diameter. The first ever self-sustaining, 0 power, but not at full decomposition temperature, nitrous oxide reaction for resistojet application was observed. The results were very encouraging and resistojet thrusters are now proposed for future USAF - 120 kg MightySATII.1, and SSTL - 300 kg UoSAT-12 small satellite missions.

The results presented in this dissertation show for the first time that water and nitrous oxide resistojets are advantageous for small satellite missions. The results has increased the state of the art in resistojet and small satellite propulsion. This is evident in the total development cost of the nitrous oxide system is the same price (£93,000) compared to the industry standard hydrazine thruster. This impact on the industry state of the art is evident in the outside funding received for the programme and eventual flight on two spacecraft in 1999 and 2000.

Table of Contents

| | |
|---|------------|
| ABSTRACT | ii |
| LIST OF FIGURES | vi |
| LIST OF TABLES | x |
| ACKNOWLEDGEMENTS | xii |
| 1. INTRODUCTION | |
| 1.1. BACKGROUND | 1-2 |
| 1.1.1. Small Satellites | 1-2 |
| 1.1.2. Propulsion Systems | 1-5 |
| 1.1.3. Small Satellite Constraints | 1-8 |
| 1.2. RESEARCH PLAN..... | 1-11 |
| 1.2.1. Hypothesis | 1-12 |
| 1.2.2. Research Goals and Tasks | 1-13 |
| 1.3. PUBLICATIONS / OUTSIDE FUNDING..... | 1-14 |
| 1.4. REFERENCES | 1-16 |
| 2. RESISTOJET TECHNOLOGY OPTIONS | |
| 2.1. STATIONKEEPING PROPULSION OVERVIEW | 2-2 |
| 2.1.1. Fundamentals | 2-2 |
| 2.1.2. Electric Propulsion Systems | 2-10 |
| 2.1.3. Cold Gas Propulsion Systems | 2-17 |
| 2.1.4. Chemical Propulsion Systems | 2-18 |
| 2.1.5. Analysis | 2-20 |
| 2.2. RESISTOJET HISTORY..... | 2-24 |
| 2.2.1. Past Flight Systems | 2-24 |
| 2.2.2. Water Resistojet Systems | 2-27 |
| 2.2.3. Existing Flight Qualified Resistojet Systems | 2-32 |
| 2.3. RESISTOJET DESIGN APPROACH | 2-35 |
| 2.4. BOILING / HEAT TRANSFER | 2-42 |
| 2.5. NEW DESIGN APPROACH..... | 2-47 |
| 2.6. CONCLUSIONS | 2-61 |
| 2.7. REFERENCES | 2-62 |
| 3. PROOF OF CONCEPT RESEARCH PHASE | |

Table of Contents

| | |
|---|-------------|
| 3.1. GOALS AND OBJECTIVES..... | 3-2 |
| 3.2. THRUSTER DESIGN AND EXPERIMENTAL APPARATUS..... | 3-2 |
| 3.2.1. <i>Thruster and Water Experimental Apparatus</i> | 3-2 |
| 3.2.2. <i>Nitrous Oxide Experimental Apparatus</i> | 3-8 |
| 3.3. EXPERIMENTAL RESULTS | 3-10 |
| 3.3.1. <i>Water Experimental Test Observations</i> | 3-10 |
| 3.3.2. <i>Water Experimental Results</i> | 3-17 |
| 3.3.3. <i>Nitrous Oxide Experimental Test Observations</i> | 3-21 |
| 3.3.4. <i>Nitrous Oxide Experimental Results</i> | 3-21 |
| 3.4. MODELLING RESULTS | 3-23 |
| 3.5. CONCLUSIONS | 3-32 |
| 3.6. REFERENCES | 3-33 |
| 4. PROTOTYPE RESEARCH PHASE | |
| 4.1. GOALS AND OBJECTIVES..... | 4-2 |
| 4.2. THRUSTER DESIGN AND EXPERIMENTAL APPARATUS..... | 4-2 |
| 4.3. EXPERIMENTAL RESULTS | 4-6 |
| 4.4. MODELLING RESULTS | 4-13 |
| 4.5. CONCLUSIONS | 4-20 |
| 4.6. REFERENCES | 4-21 |
| 5. PROTOFLIGHT RESEARCH PHASE | |
| 5.1. GOALS AND OBJECTIVES..... | 5-2 |
| 5.2. THRUSTER DESIGN AND EXPERIMENTAL APPARATUS..... | 5-2 |
| 5.3. EXPERIMENTAL RESULTS | 5-19 |
| 5.4. MODELLING RESULTS | 5-28 |
| 5.5. CONCLUSIONS | 5-38 |
| 5.6. REFERENCES | 5-39 |
| 6. FLIGHT SYSTEMS | |
| 6.1. FLIGHT DESIGN..... | 6-2 |
| 6.1.1. <i>Design Approach</i> | 6-2 |
| 6.1.2. <i>Other Approaches</i> | 6-5 |
| 6.2. UOSAT-12 | 6-7 |
| 6.2.1. <i>Spacecraft & Mission</i> | 6-7 |
| 6.2.2. <i>Resistojet Application</i> | 6-11 |
| 6.3. MIGHTYSATII.1 | 6-17 |
| 6.3.1. <i>Mission and Spacecraft</i> | 6-17 |
| 6.4. REFERENCES | 6-24 |

Table of Contents

7. CONCLUSIONS

| | |
|---|------------|
| 7.1. RESULTS | 7-2 |
| 7.2. CONCLUSIONS | 7-2 |
| 7.2.1. <i>Small Satellite Constraints</i> | 7-3 |
| 7.2.2. <i>Engineering Accomplishments</i> | 7-3 |
| 7.2.3. <i>Scientific</i> | 7-4 |
| 7.2.4. <i>Performance</i> | 7-5 |
| 7.3. ACCOMPLISHMENTS | 7-5 |

| | |
|---|------------|
| APPENDIX A THERMAL MODEL SOURCE CODE | A-1 |
|---|------------|

| | |
|--|------------|
| APPENDIX B ENGINEERING DRAWINGS | B-1 |
|--|------------|

| | |
|--|------------|
| APPENDIX C ATTITUDE CONTROL SIMULATIONS | C-1 |
|--|------------|

| | |
|------------------------------------|------------|
| APPENDIX D MIGHTYSATIL1 SOW | D-1 |
|------------------------------------|------------|

**ATTACHED CD-ROM CONTAINS ALL OF THE EXPERIMENT DATA AND
SUPPORTING ANALYSIS
POCKET**

List of Figures

| | |
|--|--------|
| Figure 1-1 Diagram of University of Surrey Minisatellite | p.1-3 |
| Figure 1-2 MightySAT11.1 Spacecraft Bus | p.1-4 |
| Figure 1-3 MightySAT11.1 Payloads..... | p.1-4 |
| Figure 1-4 Plot of Table 1-3 Showing Trends of the Various Stationkeeping Propulsion Systems | p.1-9 |
| Figure 1-5 Hypothesis Diagram..... | p.1-12 |
| Figure 1-6 Research Approach | p.1-13 |
| Figure 2-1 Resistojet..... | p.2-11 |
| Figure 2-2 100 kW Arcjet | p.2-11 |
| Figure 2-3 Ion Thruster..... | p.2-13 |
| Figure 2-4 FEEP System | p.2-14 |
| Figure 2-5 MPD Thruster | p.2-15 |
| Figure 2-6 Hall Thruster | p.2-15 |
| Figure 2-7 PPT | p.2-16 |
| Figure 2-8 Prototypic Nitrogen Cold Gas System for Small Satellite Application..... | p.2-18 |
| Figure 2-9 Cut Away View of a Hydrazine Mono-Propellant Thruster..... | p.2-20 |
| Figure 2-10 Picture of Vela Spacecraft | p.2-25 |
| Figure 2-11 Pictures of 50 W Pulsed Resistojet | p.2-26 |
| Figure 2-12 Primex Resistojet | p.2-33 |
| Figure 2-13 EHT-15 Ammonia Thruster..... | p.2-34 |
| Figure 2-14 Isp and Density Isp for a Resistojet with a Chamber Temperature of 1000K | p.2-36 |
| Figure 2-15 Frozen Flow Efficiency Versus Isp for Various Working Fluids | p.2-38 |
| Figure 2-16 Energy Break Down for Previous Water Resistojet Systems | p.2-43 |
| Figure 2-17 Typical Heat Transfer Regimes for Boiling in Flow Channel..... | p.2-44 |
| Figure 2-18 Typical Boiling Heat Transfer Performance..... | p.2-45 |
| Figure 2-19 Typical Two Phase Flow Patterns | p.2-46 |
| Figure 2-20 First Order Resistojet Mass Flow Requirements as a Function of Power | p.2-49 |
| Figure 2-21 Isp vs. Area Ratio for a Water Resistojet Operating @ 1 bar and a Chamber Temperature of 900 K | p.2-51 |
| Figure 2-22 Design Approach Flow Chart | p.2-56 |
| Figure 2-23 Predicted Performance for a Water Resistojet with Various Bed Materials..... | p.2-60 |
| Figure 2-24 Packed Bed vs. Heated Tube Resistojet Thruster. Dimensions 60 mm x 180 mm @ 400 W and 10 Bar Pressure | p.2-60 |

List of Figures

| | |
|--|--------|
| Figure 3-1 Hedin 560 W @ 28 V Cartridge Heater | p.3-3 |
| Figure 3-2 Cut-away diagram of proof of concept thruster..... | p.3-4 |
| Figure 3-3 Schematic of Experimental Apparatus | p.3-5 |
| Figure 3-4 Picture of the Experimental Apparatus..... | p.3-6 |
| Figure 3-5 Flowmeter Regression for Calibration..... | p.3-7 |
| Figure 3-6 Nitrous Oxide Test Apparatus for Proof of Concept Thruster | p.3-9 |
| Figure 3-7 Picture of Leak Areas on Resistojet | p.3-11 |
| Figure 3-8 Drawing of Copper/Sand System..... | p.3-14 |
| Figure 3-9 Pictures During Testing | p.3-16 |
| Figure 3-10 Bed Testing with No Flow..... | p.3-17 |
| Figure 3-11 Comparison of Various Bed Materials | p.3-17 |
| Figure 3-12 Massflow vs. Time for SiC Water Proof of Concept Test..... | p.3-18 |
| Figure 3-13 Chamber Pressure versus Time for SiC Water Proof of Concept Test | p.3-18 |
| Figure 3-14 Chamber Temperatures versus Time for SiC Water Proof of Concept Test..... | p.3-19 |
| Figure 3-15 Power/mass flow rate for SiC Water Test..... | p.3-19 |
| Figure 3-16 Mass flow rate vs. Time for Proof of Concept Nitrous Oxide Resistojet..... | p.3-21 |
| Figure 3-17 Chamber Pressure vs. Time for Proof of Concept Nitrous Oxide Resistojet | p.3-21 |
| Figure 3-18 Chamber Temperature vs. Time for Proof of Concept Nitrous Oxide Resistojet. | p.3-21 |
| Figure 3-19 Efficiency versus Time for Proof of Concept Nitrous Oxide Resistojet @ 200 W | p.3-22 |
| Figure 3-20 Heat Transfer Efficiency Based Upon Kinetic Energy for Proof of Concept Thruster | p.3-23 |
| Figure 3-21 Heat Transfer Efficiency Based Kinetic Energy for Proof of Concept Thruster | p.3-23 |
| Figure 3-22 Heat Transfer Efficiency Using New Thermocouple Location for Nitrous Oxide Experiment | p.3-24 |
| Figure 3-23 Comparison of C* Efficiencies for the Various Heat Transfer Material. The Test Parameters (Power, Flow, Pressure) Were Very Similar for These Experiments | p.3-26 |
| Figure 3-24 Convective Heat Transfer Efficiency Results Assuming a Cp of 4187 J/kgK and 2060 J/kgK | p.3-27 |
| Figure 3-25 Comparison of Thermodynamic Efficiencies for the Heat Transfer Methods for One Stainless Steel Test | p.3-28 |

List of Figures

| | |
|---|--------|
| Figure 3-26 Comparison of Thermal Model to Measured Chamber Temperature for the Proof of Concept Thruster Experiment | p.3-31 |
| Figure 4-1 Heater Comparison Sea Level Test @ 225 W Power..... | p.4-3 |
| Figure 4-2 Prototype Thruster | p.4-4 |
| Figure 4-3 Prototype Chamber Temperature Prediction using the Thermal Model versus Proof of Concept Test Results | p.4-5 |
| Figure 4-4 Change of performance with addition of IPA (0- 90% mixtures by mass) | p.4-6 |
| Figure 4-5 Pictures of Prototype Resistojet..... | p.4-7 |
| Figure 4-6 Comparison of Proof of Concept and Prototype Resistojets @ sea level..... | p.4-8 |
| Figure 4-7 Comparison of Thruster Performance with Respect to Gravity in Vacuum using Water as the working fluid @ 200 W | p.4-9 |
| Figure 4-8 Thrust versus time for one of the Prototype trials | p.4-10 |
| Figure 4-9 Thrust versus for two of the Resistojets used in the Prototype programme | p4-11 |
| Figure 4-10 Oxidation Rates of Ordinary Steel as a Function of Temperature | p.4-11 |
| Figure 4-11 Scanning Electron Microscope view of the Nozzle Exit Area | p.4-12 |
| Figure 4-12 SiC and MgO Catalyst | p.4-13 |
| Figure 4-13 Chamber Temperature vs. Time for Prototype Water Resistojet | p.4-14 |
| Figure 4-14 Chamber Pressure vs. Time for Prototype Water Resistojet | p.4-14 |
| Figure 4-15 Mass flow rate vs. Time for Prototype Water Resistojet..... | p.4-14 |
| Figure 4-16 Chamber efficiency vs. time for Water Prototype Experiment | p.4-15 |
| Figure 4-17 Mass flow vs. time for 100 W Prototype Resistojet Test | p.4-15 |
| Figure 4-18 Chamber Pressure vs. Time for Nitrous Experiment..... | p.4-16 |
| Figure 4-19 Chamber Temperature vs. Time for the Same Experiment, power shut off with mass flow continuous at 110 minutes | p.4-16 |
| Figure 4-20 Chamber efficiency for 100 W Nitrous Oxide Experiment..... | p.4-17 |
| Figure 4-21 Comparison of heat transfer efficiency for prototype nitrogen experiment .. | p.4-18 |
| Figure 4-22 Comparison of Heat Transfer Efficiency for Prototype Water Experiment ... | p4-18 |
| Figure 4-23 Comparison of Heat Transfer Efficiency for Prototype Nitrous Oxide Experiment | p.4-19 |
| Figure 4-24 Comparison of Thermal Model to Measured Temperature for Prototype Thruster | p.4-20 |
| Figure 5-1 Expansion Ratio vs. Isp for Ideal Water and Nitrous Oxide Prototype Test Conditions | p.5-5 |
| Figure 5-2 Reynolds Number versus Area Ratio for Water Prototype Test..... | p5-6 |
| Figure 5-3 Area Ratio vs. Knudsen Number for Water Prototype Thruster | p.5-7 |

List of Figures

| | |
|---|--------|
| Figure 5-4 Prototype Simulations versus Prototype Test Data for Nitrous Oxide | p.5-8 |
| Figure 5-5 Reynolds Number versus Area Ratio for 0.19 mm throat diameter Protoflight Nozzle Simulation | p.5-9 |
| Figure 5-6 Reynolds Number versus Area Ratio for 0.69 mm Protoflight Nozzle | p.5-9 |
| Figure 5-7 Comparison of Knudsen Numbers for Prototype and Protoflight Thrusters ... | p.5-10 |
| Figure 5-8 Drawing and picture of Protoflight thruster | p.5-11 |
| Figure 5-9 NASA JPL Inverted Thrust Stand and Drawing of core elements of the Thrust Stand..... | p.5-13 |
| Figure 5-10 Picture of test facility and procedure | p.5-14 |
| Figure 5-11 Thermal Drift in Prototype Thrust Measurement | p.5-18 |
| Figure 5-12 Catch and Weigh for Prototype Flow meter | p.5-19 |
| Figure 5-13 Thrust versus time for Protoflight#2 thruster | p.5-20 |
| Figure 5-14 Isp versus Time for Long Endurance Test Using Protoflight Thruster#2 | p.5-21 |
| Figure 5-15 Temperature versus Time for Protoflight#4 Thruster..... | p.5-21 |
| Figure 5-16 Protoflight#4 thruster glowing and picture of Thruster after Test | p.5-22 |
| Figure 5-17 Validation for Using Micropore Insulation | p.5-22 |
| Figure 5-18 Prototype Comparison Test- Catalyst not much impact on performance..... | p.5-24 |
| Figure 5-19 Before and after pictures of the SiC bed material | p.5-24 |
| Figure 5-20 Silicon Oxide deposits in nozzle throat - amorphous deposition | p.5-25 |
| Figure 5-21 Dengritic crystal growth | p.5-25 |
| Figure 5-22 Silicon Oxide deposits on inner wall of screen mesh | p.5-26 |
| Figure 5-23 Amount of Silicon and Oxygen in the bed Material before and after a firingp.5-23 | |
| Figure 5-24 ICP Analysis of water..... | p.5-27 |
| Figure 5-25 Treated and Green Silicon carbide SEM oxygen content..... | p.5-27 |
| Figure 5-26 Chamber pressure versus time for Protoflight Thruster | p.5-28 |
| Figure 5-27 Massflow rate vs. time for Protoflight Thruster | p.5-29 |
| Figure 5-28 Chamber Temperature vs. Time for Protoflight#4 | p.5-29 |
| Figure 5-29 Thrust versus Time for Protoflight#4 | p.5-29 |
| Figure 5-30Efficiency vs. Time for Protoflight#4..... | p.5-30 |
| Figure 5-31 Isp versus Time for Protoflight#4..... | p.5-30 |
| Figure 5-32 Heat transfer efficiency versus time for the Protoflight#4 | p.5-31 |
| Figure 5-33 Massflow vs. Time for Protoflight#4 Water Test..... | p.5-31 |
| Figure 5-34 Pressure vs. Time for the same water experiment | p.5-32 |
| Figure5-35 Chamber Temperature vs. Time for same water experiment..... | p.5-32 |
| Figure 5-36 Heat Transfer Efficiency vs. Time for Protoflight#4 600 W Test..... | p.5-32 |

List of Figures

| | |
|---|--------|
| Figure 5-37 Isp versus Time for 600 W Protoflight Thruster | p.5-33 |
| Figure 5-38 Efficiency vs. Time for Protoflight Water Test | p.5-33 |
| Figure 5-39 Comparison of thermal model simulations to test data | p.5-38 |
| Figure 6-1 100 W Thermal Simulation for Both Working Fluids | p.6-3 |
| Figure 6-2 Knudsen Numbers for Protoflight#4 and 0.3mm Flight Nozzle..... | p.6-4 |
| Figure 6-3 Reynolds Number for 0.3mm throat diameter | p.6-4 |
| Figure 6-4 SINDA-3D Simulation of the Flight Resistojet..... | p.6-5 |
| Figure 6-5 UoSAT-12 Propulsion System Architecture..... | p.6-8 |
| Figure 6-6 UoSAT-12 Propulsion System Pictures..... | p.6-9 |
| Figure 6-7 Top Down View of UoSAT-12 showing the resistojet thruster location | p.6-13 |
| Figure 6-8 Picture of UoSAT-12 Engineering Model and Flight Resistojet..... | p.6-14 |
| Figure 6-9 Flight Thruster Subassemblies..... | p.6-14 |
| Figure 6-10 Polyflex Expulsion system..... | p.6-17 |
| Figure 6-11 MightySATII.1 Spacecraft bus | p.6-17 |
| Figure 6-12 MightySATII.1 Payloads | p.6-18 |
| Figure 6-13 Mission tradeoffs for high drag orbit..... | p.6-18 |
| Figure 6-14 MightySATII.1 Flight Design integrated to the expulsion system..... | p.6-19 |
| Figure 6-15 Pressurised Feed System Schematic | p.6-20 |
| Figure 6-16 Installation Envelope | p.6-21 |

List of Tables

| | |
|--|--------|
| Table 1-1 Spacecraft Specifications for UoSAT-12 and MightySATII.1 | p.1-5 |
| Table 1-2 Various Low Thrust Propulsion Options | p.1-7 |
| Table 1-3 Comparison Of Specific Thrust and Density Specific Impulse for Various Stationkeeping Systems..... | p.1-9 |
| Table 1-4 Comparison of 2 Possible Small Satellite Propulsion Systems | p.1-11 |
| Table 1-5 Summary of Research Goals, Tasks, and the Chapter of the Thesis Where They are Addressed | p.1-14 |
| Table 2-1 Attitude Control Actuators | p.2-8 |
| Table 2-2 Pro's and Con's of In-House Versus Off-the Shelf Systems | p.2-9 |
| Table 2-3 Specific Impulse Performance for Various Gases | p.2-17 |
| Table 2-4 Performance Parameters for Nitrogen versus Helium Cold Gas Thruster Options | p.2-18 |
| Table 2-5 MR-106E Hydrazine Mono-propellant Thruster Performance Data | p.2-19 |
| Table 2-6 Comparison of Various Systems for a 3 Year Small Satellite Stationkeeping Mission..... | p.2-21 |
| Table 2-7 Comparison of Various Systems for a High Drag (Space Shuttle) Experimental Volume Constrained Mission..... | p.2-24 |
| Table 2-8 Specifications of 1st Resistojet-90 W TRW Resistojet for Vela Spacecraft. ... | p.2-24 |
| Table 2-9 Flight Qualified Resistojet Systems | p.2-25 |
| Table 2-10 History of Water Resistojet Systems | p.2-28 |
| Table 2-11 Unresolved Theoretical and Practical Problems in Past Programmes | p.2-32 |
| Table 2-12 Primex MR-502 Hydrazine Resistojet Specifications | p.2-33 |
| Table 2-13 EHT-15 Specifications..... | p.2-34 |
| Table 2-14 Comparison of Various Working Fluids @ 100 W Input Power (100 % Power Conversion Efficiency) and 1000 K..... | p.2-36 |
| Table 2-15 Performance Prediction for HiPEHT Resistojet Based Upon Empirical Results | p.2-39 |
| Table 2-16 Comparison of Aston's Model Versus Engineering Model Thruster | p.2-41 |
| Table 2-17 Initial Performance Calculations..... | p.2-48 |
| Table 2-18 Initial Design Trades | p.2-52 |
| Table 2-19 Comparison of Various Resistojet Designs | p.2-58 |
| Table2-20 Bed Materials Investigated..... | p.2-60 |
| Table 3-1 Summary of Test Observations..... | p.3-15 |

List of Tables

| | |
|--|--------|
| Table 3-2 Summary of Performance for Proof of Concept Thruster..... | p.3-30 |
| Table 4-1 Prototype Thruster Specifications | p.4-5 |
| Table 4-2 Test Parameters for Prototype Thruster Tests..... | p.4-7 |
| Table 4-3 Comparison of Prototype Experiment Propellant Performance..... | p.4-19 |
| Table 5-1 Nozzle Performance of Prototype Thruster | p.5-4 |
| Table 5-2 Specifications for Simulation and Test Data | p.5-8 |
| Table 5-3 Protoflight Specifications..... | p.5-11 |
| Table 5-4 Comparison of Performance for Prototype and Protoflight Thruster for Water Experiments | p.5-23 |
| Table 5-5 Comparison of Performance for Prototype and Protoflight thrusters for Nitrous Oxide Experiments | p.5-23 |
| Table 5-6 Summary of Prototype and Protoflight Test Results | p.5-37 |
| Table 6-1 Flow Conditions for Thermal Simulations | p.6-3 |
| Table 6-2 Use of empirical data to generate performance data for the design of nitrous oxide resistojets..... | p.6-6 |
| Table 6-3 Mass break down for UoSAT-12 cold gas system..... | p.6-10 |
| Table 6-4 Cold Gas System Performance..... | p.6-10 |
| Table 6-5 System mass and specification..... | p.6-15 |
| Table 6-6 System Specifications | p.6-19 |
| Table 6-7 Expulsion System Components..... | p.6-20 |
| Table 7-1 Summary of research goals, their specific corresponding tasks, and the results obtained in the research programme | p.7-2 |
| Table 7-2 Resistojet Programme Cost Break Down..... | p.7-6 |

ACKNOWLEDGEMENTS

During the course of my research, I have been supported financially by the United States Air Force, United States Air Force Academy, University of Surrey Department of Electrical Engineering, and by Surrey Satellite Technology Limited.

Royal Ordnance, Rocket Motors Division, Wescott, have provided test facilities and support that were important in the resistojet testing process.

Dr Ron Spores, Dr Greg Spanjers, Mr Jamie Malak, Lt Jason Leduc, Mr Daron Bromaghin, and the other Edwards AFB AFRL Electric Propulsion Laboratory staff donated their test facilities and technical support that were vital in characterizing the performance of the resistojet. It also has been a pleasure working with them further on the MightySATII.1 programme.

Professor Martin Sweeting had the confidence and vision to start this resistojet research effort. He also created a challenging academic atmosphere that is world class and I will never forget. I am deeply grateful to him.

Mr Malcolm Paul was the technical foundation of this research effort. With his practical knowledge of rocketry, he made the impossible happen. I will always cherish having the opportunity to work with him.

Major Jerry Sellers was an excellent mentor from my first day in the UK. His support and guidance were crucial in getting me to where I am today.

EVERYONE at SSTL/CSER! I enjoyed all of our technical and social activities over the past 3 years. Words can not express all my appreciation to my new international mix of friends. Thank you for putting up with a loud American for the last 3 years. At least productivity should increase when I leave ☺

My Channel Swimming Coaches, Freda and Alison Streeter, are the best Channel Swimming people involved in the sport and serve as excellent role models in long distance swimming and

for coming up with the motivation and energy to work through a Ph.D. They also gave me something to do on the weekend whilst in England 😊.

A special thanks to my friends in the UK and back in the US. Thank you for your support and being there when I needed you.

Last, but not least, a special thank you to my family for all of their love and support through the years. Yes mom, it is turned in. 😊

Chapter 1

Introduction

1. INTRODUCTION

1.1. BACKGROUND

1.2. RESEARCH PLAN

1.3. PUBLICATIONS / OUTSIDE FUNDING

1.4. REFERENCES

This chapter serves as an introduction to the thesis and provides an overview of research into resistojet rockets for small satellite applications. The chapter begins with a brief background section describing small satellites and future mission requirements. From these requirements and using two upcoming missions under investigation by the University of Surrey and the United States Air Force, propulsion systems are needed for these missions with unique constraints that only pertain to small satellites. This serves as the motivation for an investigation into resistojets for small satellite applications and narrows the scope of research. From this, a detailed experimental research road map is developed that shows the three conceptual phases, subject to the constraints, which were needed to produce the resistojet thruster and thermodynamic model. Each of these phases are presented which shows how several tasks were developed to accomplish the research objectives and also serves as an outline for the remaining chapters of the thesis. The chapter ends with a list of publications written during this research and a brief description of outside funding that was received.

1. Introduction

1.1. Background

This section presents a brief introduction to small satellites and serves to motivate the research. The small satellite research going on at the University of Surrey and in the United States Air Force is introduced. A brief discussion of the various types of propulsion systems that could be used for these upcoming missions is then presented. The unique constraints of using propulsion systems for low cost small satellite stationkeeping missions are defined. The section concludes by showing that the research represents a new approach to solve these unique small satellite constraints.

1.1.1. Small Satellites

1.1.1.1. UoSAT Micro and Minisatellites

Surrey Satellite Technology Limited (SSTL) at the University of Surrey has been designing small, inexpensive, and sophisticated microsatellites for 18 years. Traditionally, each microsatellite has had a mass of approximately 50 kg. Since 1981, University of Surrey satellites (UoSATs) have shown that small, reliable satellites can be built and operated at costs far less than one would find in the mainstream aerospace industry. The typical bus consists of a series (10-12) of modular trays (module boxes - approximately 350 mm x 350 mm x 100 mm) that are divided into power, ADCS, OBC, transputers, GPS, telemetry, and payload individual module boxes. The module boxes are stacked, bolted together, and surrounded by 4 solar arrays to form the complete satellite which measures approximately 800 mm in height. The existing microsatellites have used a 6 m gravity gradient boom and magnet-torquers for attitude control.

The SSTL/UoSAT team have logged over 50 orbit years of operational experience with 11 spacecraft in space. All of these spacecraft have operated in the relatively benign environment of LEO (low earth orbit). As secondary payloads, they have had to make do with whatever orbit the launcher provided. Natural orbit perturbations (drag, J2, etc.) were acceptable. Over the years, these pioneering small satellite missions have proven that effective communication, remote sensing and space science can be done from a low-cost platform. As these missions have evolved, various technical challenges in on-board data handling, low-power communication, autonomous operations and low-cost engineering have been met and solved. All of these successful missions have led the SSTL engineers to consider enhancing the current microsatellite mission capability. These enhanced missions include: GEO communications, lunar exploration, LEO constellations, and SAR missions. However, a new type of bus was needed to support some of these future small satellite missions.

In 1995, SSTL engineers started developing a flexible, multi-mission minisatellite. With an approximate mass of 300 kg, the minisatellite structural design builds on the modular approach used

in the UoSAT microsattellites in a way that allows maximum re-use of subsystems between the two platforms. A diagram of the minisatellite is shown in Figure 1-1. As this is written, the first flight of this new satellite bus, dubbed UoSAT-12, is in critical design for a launch in April 1999.

The technical objectives for the minisatellite mission strike a compromise between all the features a flexible minisatellite bus would have and what can be achieved within the available budget and time scale. The following technical objectives have been defined for the UoSAT-12 mission:

- Demonstrate a commercially viable minisatellite bus with industry-standard support systems
 - 28 VDC power bus
 - 1 MBPS S-band down-link
- Demonstrate that enhanced core microsatellite technologies can be used in a minisatellite:
 - Intel 386-based on board computers (OBC)
 - Low-rate VHF/UHF data links
 - Distributed TT&C via control area network (CAN)
- Demonstrate major new subsystems:
 - Enhanced attitude determination and control capability
 - Propulsion system capability with orbit maintenance and attitude control
- Enhance existing UoSAT payloads using resources of the minisatellite to provide operational demonstration of:
 - High-resolution (<30 m) multi-spectral visible imaging and 10 m monochromatic imaging
 - Store-and-forward communications to small terminals

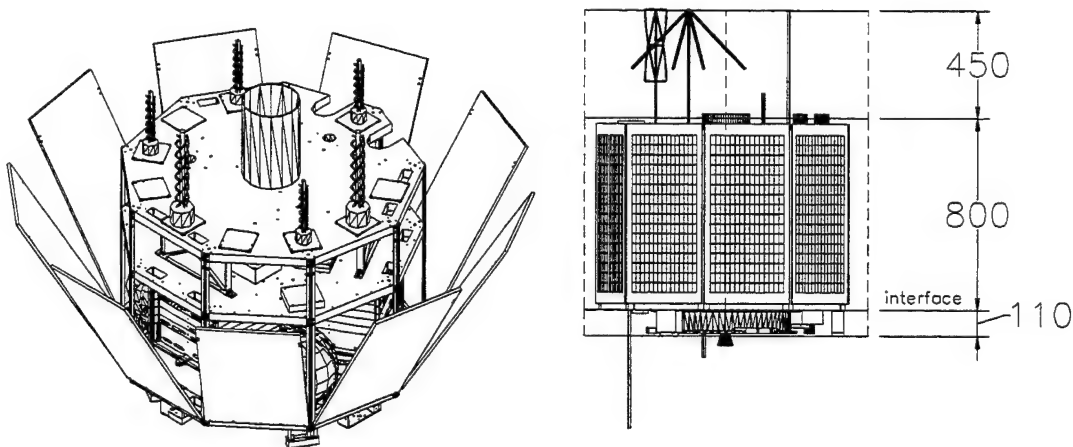


Figure 1-1: Diagram of University of Surrey Minisatellite (dimensions in mm)

1.1.1.2. USAF MightySatII.1 Mission

The MightySatII.1 is a flagship mission of the USAF AFRL (United States Air Force Research Laboratory). Using the theme, “faster, cheaper, better”, the USAF has decided that low cost small satellite platforms are useful for launching its own Department of Defence (DOD) payloads from the

research laboratories in a quick and cheap manner. The MightySat series is a test bed to demonstrate this concept. It is developed with SSTL in mind with a target total cost budget of £6.25 million. The programme is managed from the Space Vehicles Directorate of AFRL at Kirtland Air Force Base (AFB), NM. Spectrum Astro, of Gilbert, AZ, successfully completed a Detailed Design Review in February 1998 and is currently building the first in a series of MightySat II spacecraft. MightySat II.1, known as Sindri, is scheduled for launch in January, 2000. Figure 1-2 shows the spacecraft and the bus components. Figure 1-3 shows the various payloads.

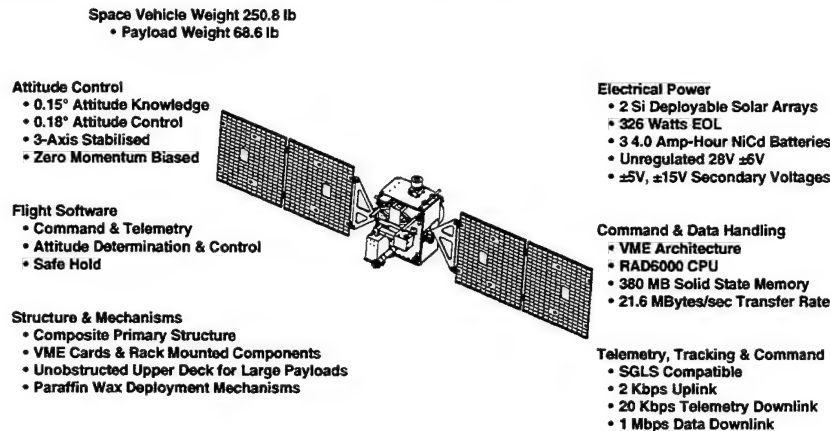


Figure 1-2: MightySATII.1 Spacecraft bus from [Spectrum, 98]

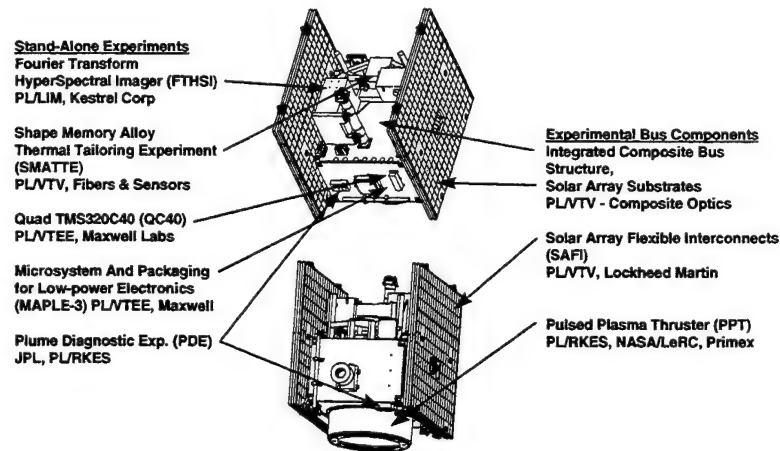


Figure 1-3: MightySATII.1 Payloads from [Spectrum, 98]

UoSAT-12 and MightySatII.1 need propulsion systems to fully exploit their mission capability. UoSAT-12 will require orbit maintenance for remote sensing application and MightySatII.1 will need orbit maintenance to increase the spacecraft lifetime. Propulsion systems are a common feature on virtually all larger satellites. However, UoSAT-12 and MightySatII.1 pose new requirements uncommon to these types of propulsion systems. These requirements are shown in Table 1-1.

| Description | UoSAT-12 | MightySatII.1 |
|---|---------------------|------------------|
| Mission | Experimental | Experimental |
| On orbit average power (W) | 140 | 326 |
| Volume (mm) | 700 (o.d.) x 800 | 685 x 990 x 1300 |
| Available propulsion system volume - tanks (mm) | 300 x 300 x 100 | 300 x 300 x 100 |
| Mass (kg) | 300 | 114 |
| Attitude Control - both 3 axis control, Pointing accuracy (deg) | 0.1 - 0.5 | 0.18 |
| Initial Orbit (km) | 650 sun synchronous | 200 |
| Launch Vehicle | Dnepr | Space Shuttle |

Table 1-1: Spacecraft Specifications for UoSAT-12 and MightySATII.1

The objective of the propulsion system for these missions is to maximise the ΔV capability to the spacecraft subject to the constraints. Since the missions are experimental, the volume allowed in Table 1-1 for the propulsion systems will most likely grow on future missions to take over more of the available volume. These missions provided the motivation for starting research in resistojet technology. The study can begin by surveying propulsion options available for such missions.

1.1.2. Propulsion Systems

Propulsion systems are divided into three classes:

- *Orbit Manoeuvring*-- the ability to move from an initial parking orbit to an escape trajectory or insert into a final mission orbit, e.g. changing from geosynchronous transfer orbit to geosynchronous orbit.
- *Orbit Maintenance (stationkeeping)* -- the ability to maintain a specific orbit against drag and other perturbations, or to phase the orbit to maintain proper angular separation within a constellation.
- *Attitude Control* -- the ability to rotate the spacecraft to reorient sensors or dump momentum, especially beyond LEO where magnet torquers and gravity gradient stabilisation are not viable options.

Propulsion systems are an integral part of most commercial and military spacecraft. However, because of their prohibitive cost and complexity (at least £100,000), their use on larger minisatellites consumes a disproportional share of the mission budget (~25%- 50%) [Sellers,96A]. Thus, a low-cost propulsion option is needed for small spacecraft to evolve economically beyond the niche of LEO (low Earth orbit) and exploit emerging new opportunities.

The first opportunities to demonstrate a low cost propulsion system are to provide stationkeeping propulsion for the UoSAT-12 and MightySATII.1 missions discussed in the last section. Table 1-2 describes several different propulsion system options surveyed to meet the stationkeeping mission requirements. These systems are discussed in greater detail in Chapter 2.

From Table 1-2, a satellite designer may be tempted to rush out and buy an Ion, MPD, or PPT thruster since they offer the highest performance. For example, an Ion system would only require a couple of kilograms out of 300 kg to provide the mission ΔV ! Thus, the satellite designer could have more mass for payload. Unfortunately, I_{sp} alone is not the only factor in determining the best propulsion system. From the advantages and disadvantages shown in Table 1-2, a satellite designer discovers that there may be more to the equation than just performance.

| System | Operating Principle | Isp (sec) | Power (kW) | "Off the Shelf System" Exists | Adv / Disadv |
|----------------------------|--|--------------|---------------|----------------------------------|--|
| Water resistojet | inputs electric energy into a heat exchanger to thermally expand a working fluid | 150-220 | 0.1-0.6 | N | ADV: safety, simple, thrust, power (100 W) DISADV: poor performance |
| Xenon ion thruster | applies an electrostatic force to ionised atoms | 2585 | 0.4 - 2 | Y | ADV: high Isp DISADV: power, \$\$\$, thrust |
| Hydrazine arcjet | discharges an arc into propellant to heat a working fluid | 500 | 0.5 - 1.8 | Y | ADV: high Isp DISADV: high power requirement (> 500 W), \$\$\$ |
| MPD Magneto-plasdynamic | sends electric current through a plasma which interacts with magnetic fields to generate thrust | 2000 | 0.43 - 1000 | N | ADV: high Isp DISADV: power requirement |
| FEEP | electrostatic force to ionised atoms | 6000 | 0.06 | N | ADV: high ISP DISADV: thrust |
| Ammonia microwave | uses photons to form a plasma for the Lorentz force to generate acceleration in the working fluid | 550 | 0.1- 0.6 | N | ADV: low power requirement (100 W) DISADV: still in fundamental research phase |
| Nitrogen cold gas | uses stored energy of a compressed gas to develop thrust | 65 | 0 | Y | ADV: inexpensive DISADV: low Isp |
| Hydrazine resistojet | resistojet except that hydrazine decomposition products (hydrazine exposed to a catalyst) are the working fluid | 300 | 0.35 - 0.51 | Y | ADV: high Isp DISADV: high power requirement (>300 W for hydrazine), \$\$\$, safety |
| Nitrous Oxide Resistojet | resistojet with additional energy input from nitrous decomposition | 135- 150 | 0-0.3 | N | ADV: safety, power, thrust DISADV: low Isp |
| Hydrazine | hydrazine decomposition products (hydrazine exposed to a catalyst) produce thermal energy | 220 | 0 | Y | ADV: power, thrust, performance DISADV: safety, \$\$\$ |
| Ammonia Resistojet | resistojet with ammonia working fluid | 296 | 0.1-0.45 | Y | ADV: low power, high Isp DISADV: safety, thrust |
| Pulsed Plasma thruster | uses a Lorentz force generated by the interaction of an arc passing from anode to cathode with self-induced magnetic fields to accelerate a small quantity of vaporised Teflon | 1500 | 0.01 | Y | ADV: low power requirement (>10 W), Isp DISADV: integration issues, \$\$\$, thrust |

Table 1-2: Various Low-thrust Propulsion Options [Humble, 1996], [Meyers, 1996]

1.1.3. Small Satellite Constraints

Previous work by Sellers [Sellers,96B] developed a methodology for studying the cost of propulsion systems for various missions. Sellers set out to define all the dimensions that encompass total propulsion system cost. He developed a nine dimensional cost paradigm that weighs:

- Propellant Mass
- Propellant Volume
- Total Elapsed Thrust time (to complete all ΔV)
- Power Required
- System Price
- Technical Risk (to the program)
- Safety (to deal with inherent personal risk)
- Integration
- Logistics

These metrics were analysed for the UoSAT-12 and MightySat missions. From this analysis, 6 metrics emerged that are important to small satellite stationkeeping missions. These are:

- Cost – the total price of these spacecraft is in the £4,000,000 - £6,000,000 range. Propulsion costs can not absorb much of that budget.
- Power – with an on - orbit average power level ranging from 140 - 326 W, many of the systems in Table 1-2 will require too much power, especially since electric propulsion thermal devices require 10's of minutes to reach steady state.
- Volume – 100 mm x 100 mm x 300 mm for tank storage is a tight constraint. The storage density of the propellant becomes an important consideration
- Mass – the system must have enough performance for the needed ΔV and stay within the small mass constraints
- Integration – since these spacecraft are being launched at either a remote Russian site with little infrastructure or out of the Space Shuttle Payload Bay, safety and ease of integration to the spacecraft is important
- Thrust – for high drag orbits, thrust will be an important factor in moving the spacecraft in a reasonable amount of time for the required manoeuvre. Depending on the orbit, some systems may not be able to move the spacecraft at all due to drag losses for the given thrust.

Table 1-3 and Figure 1-4 show how the systems presented in Table 1-2 can be compared using these metrics. The first column in Table 1-3 lists the *specific thrust* for each system. The specific thrust is the input power the propulsion system requires in the chamber divided by the thrust produced from the system. The lower the value the better, since the thruster is producing the thrust with little input required from the spacecraft power system. The second column in Table 1-3 shows the *density specific impulse*. *Density specific impulse* is defined as the product of the propellant average specific gravity and the specific impulse of the thruster. It is an important parameter for small satellites since it takes into account the performance of the thruster (propellant mass) **and** the volume of propellant needed, rather than just the mass. The higher the value the better, since less propellant mass and storage volume are needed to accomplish the mission.

| System | Input Power / Thrust (W/mN) | Density Isp (sec) |
|--------------------------|-----------------------------|-------------------|
| Nitrogen cold gas | 0 | 7 |
| Hydrazine | 0 | 222 |
| Nitrous Oxide Resistojet | 0.6 | 105 |
| Hydrazine Resistojet | 1.9 | 304 |
| Water Resistojet | 2.7 | 182 |
| Ammonia Arcjet | 6.5 | 372 |
| Hydrazine Arcjet | 9 | 507 |
| Ammonia Resistojet | 15 | 228 |
| Hall Thruster | 16 | 695 |
| Xe Ion | 26 | 982 |
| PPT | 27 | 2000 |
| FEPP | 60 | 11000 |

Table 1-3: Comparison of Specific Thrust and Density Specific Impulse for Various Stationkeeping Systems

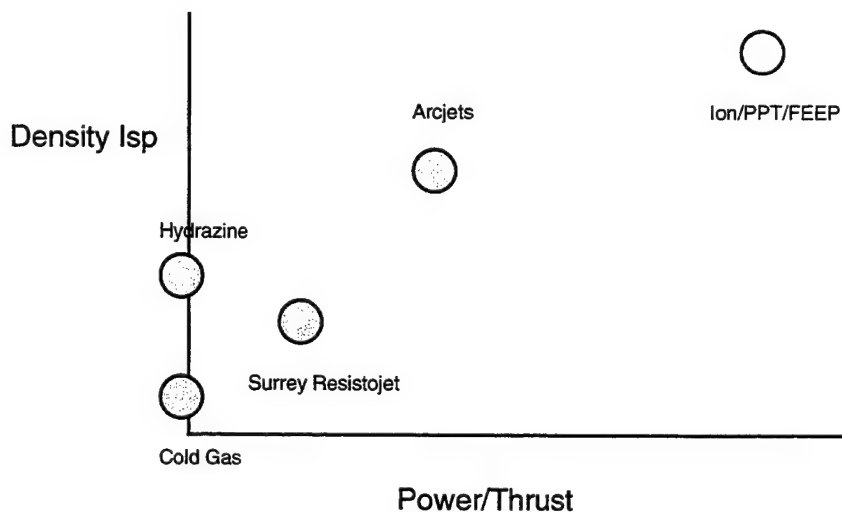


Figure 1-4: Plot of Table 1-3 Showing Trends of the Various Stationkeeping Propulsion Systems

Figure 1-4 presents 4 out of the 6 metrics for evaluating small satellite propulsion systems. The remaining two, cost and integration, are more esoteric. ROM costs were received for some of the systems (thrusters only):

- Ion: £1,000,000 [Clauss, 95]
- Cold Gas: £3,500 [Fleming, 95]
- Hydrazine Resistojet: £100,000 [Primex, 95]

However, as Sellers discovered in his research programme, there are additional costs then just the price of the thruster. For example, hydrazine due to its toxicity, has additional handling charges compared to other non-toxic propellants such as water, nitrous oxide, and nitrogen. These charges are (from [Sellers, 96A] and [Paul, 98]):

- SCAPE Suits and other handling equipment: £15,000
- 200 litres of hydrazine: £17,500
- Storage and facility: £5,000
- Shipping (in UK): £500
- Shipping to remote Russian launch sites : £50,000

Integration issues can also increase the TOTAL propulsion system price. The systems that use toxic propellants will require extra safety costs in handling during spacecraft assembly, same prices as above, especially at remote Russian launch sites where equipment will have to be brought to the site. Integration costs for toxic propellants also include training of personnel, and extra GSE equipment needed at the launch site compared to non-toxic systems.

Safety issues are also important in the research and development phase and integration of the propulsion system. A water resistojet or nitrogen cold gas system will allow testing to occur in University laboratories instead of remote concrete blockhouses.

Now that the metrics for small satellite stationkeeping missions have been outlined, the best system needs to be determined. A good example is to compare a PPT system with a nitrous oxide resistojet. Table 1-4 shows an analysis conducted on these two systems. Applying the results in Table 1-4, to the metrics:

- Engine Price: N/A, both systems under development
- Power: both are at 100 W, but due to the low *specific thrust* of the PPT system, it will have to be operated longer to accomplish the same ΔV . This will be important for power constrained spacecraft like UoSAT-12, 144 W on orbit average power, where firing time will be limited.
- Volume: PPT is better due to the low amount of Teflon propellant needed. Capacitor and power conditioning system add to the volume though.
- Mass: equal. Capacitor and other PPT support structure are additional weight even though it is an order of magnitude higher *Isp*.
- Integration: both propellants are easy to handle. EMI with other electronic components is an issue for the PPT.
- Thrust: The resistojet almost achieves a two orders of magnitude increase in thrust for the same input power. This is evident in the trip time required, which will be even worse in high drag orbits, like the 200 km MightySatII.1 orbit.

| System | Pulsed Plasma Thruster | Nitrous Oxide Resistojet |
|--|------------------------|--------------------------|
| Power | 100 W | 100 W |
| Isp | 1500 sec | 150 sec |
| Density Isp | 3465 sec | 107 sec |
| Thrust | 1 mN | 50 mN |
| ΔV (UoSAT-12 - 300 kg experimental mission) | 5.4 | 5.4 |
| Mass of propellant | 0.1 kg | 1.1 kg |
| System mass | 6 kg | 8kg |
| Firing time for ΔV | 19 days | 6 hours |
| Change in semi-major axis (assuming initial orbit is 720 km) | 7 km | 7km |

Table 1-4 Comparison of 2 possible small satellite propulsion systems

After analysing the remaining systems presented in Table 1-3 and Figure 1-4, an interesting result occurs. The electrostatic propulsion systems are not suitable for stationkeeping due to their high *specific thrust* values. Arcjets can also be classified into this category. Cold gas systems have small power requirements, but low efficiency. The remaining systems are off-the-shelf toxic resistojets and mono-propellant thrusters, or a new non toxic resistojet. If a non-toxic resistojet system can be produced with a high *density specific impulse*, it could be very attractive for small satellite stationkeeping missions. This led to the choice of water and nitrous oxide as propellants for a resistojet system. Since there were no **off-the-shelf** resistojet systems, a research plan was formulated to start investigating this technology option.

1.2. Research Plan

This section shows how a resistojet technology research programme was developed to solve the small satellite constraints mentioned in the last section. It presents a hypothesis that a resistojet is the best option for small satellite stationkeeping missions. The issues and problems associated with resistojet design and modelling are described, which led to the plan of attack for breaking down these problems into three conceptual phases. Each phase presents experimental and modelling results with synergistic goals for the next research phase. The section concludes with an introduction to the remaining chapters of the thesis.

1.2.1. Hypothesis

Figure 1-5 shows the hypothesis and work plan for the resistojet research programme.

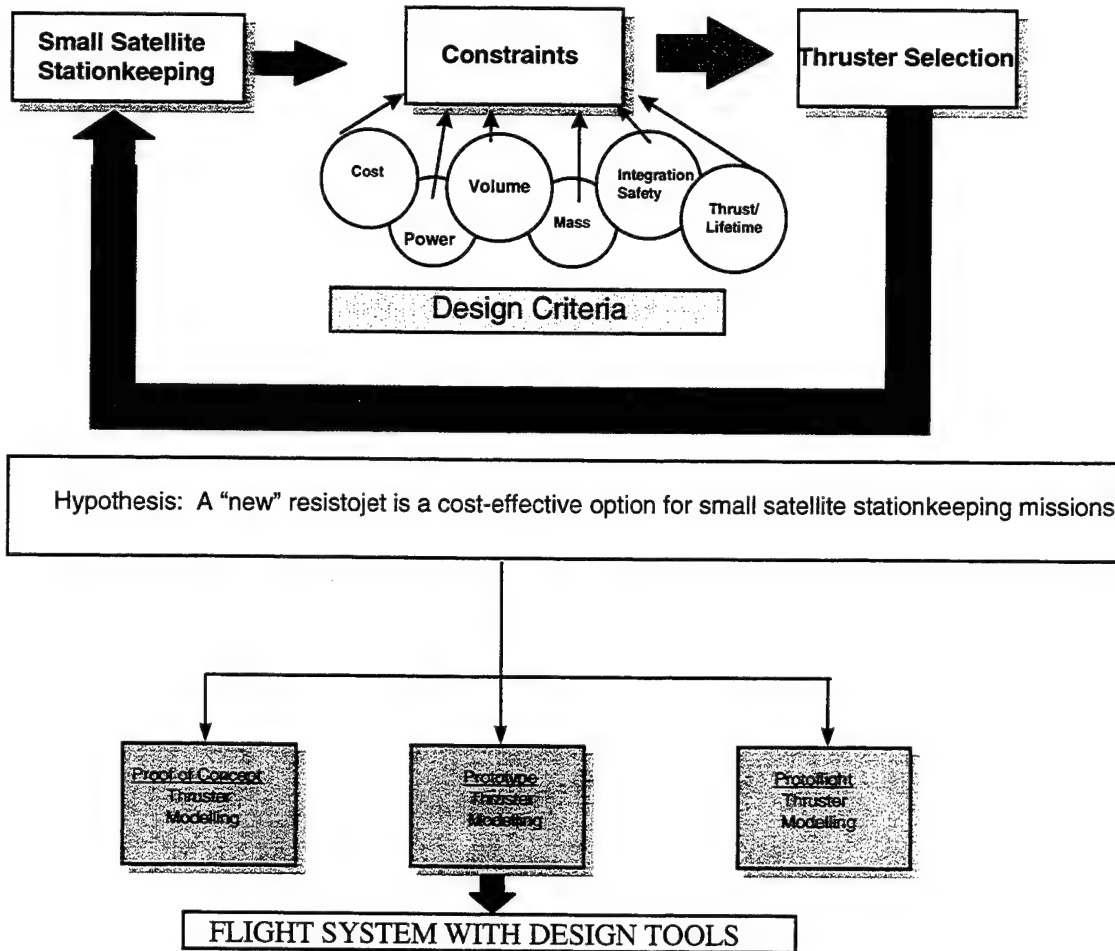


Figure 1-5: Hypothesis Diagram

The hypothesis is that a resistojet, subject to the constraints mentioned in the previous section, is the cost effective solution to solving the stationkeeping problem for small satellites. From this, a research approach was developed to break the research down into specific phases.

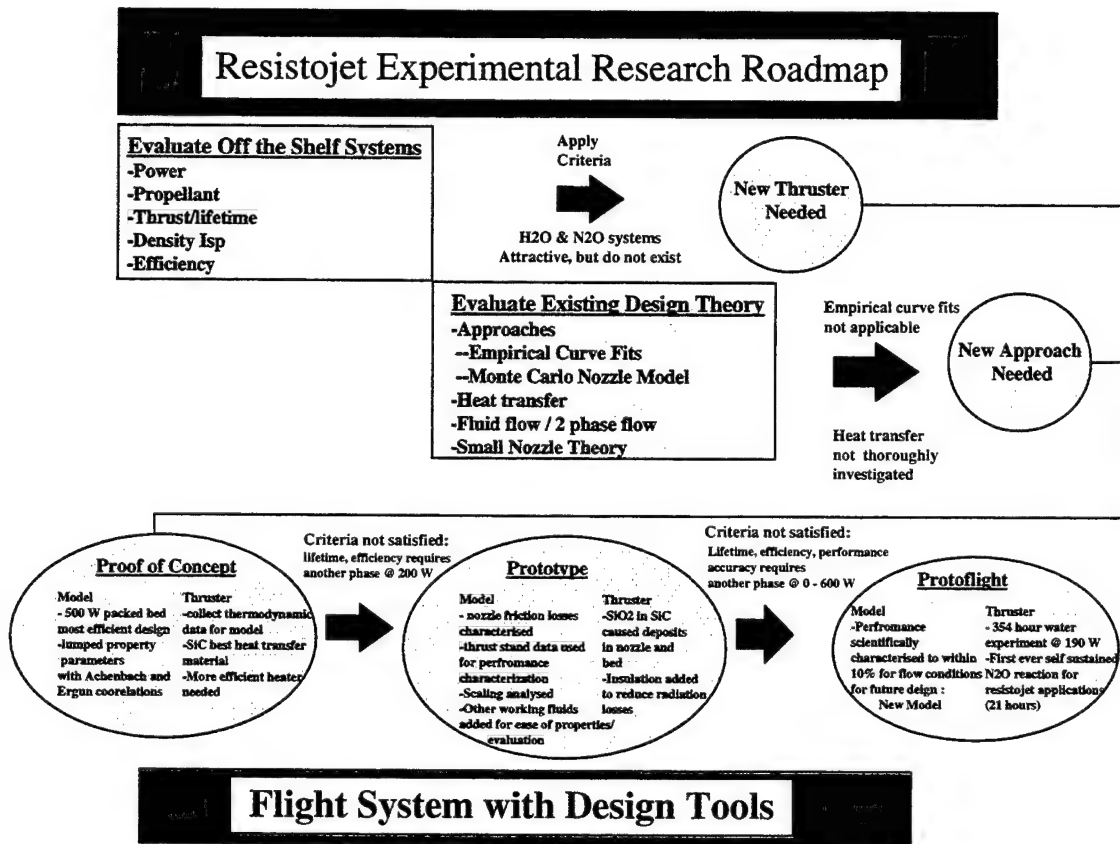


Figure 1-6: Research Approach

The research approach shows that the two objectives of the research programme are to produce a flight resistojet system, and associated design tools, subject to the constraints. There were three phases in the programme: proof-of-concept, prototype, and protoflight. Under each phase, the research can be further broken down into two problem areas where research was needed to solve specific problems in experimental testing and modelling. Once these problems were addressed in each phase, they also served to set goals for the next phase of research. The next section will address these specific problems in greater detail.

1.2.2. Research Goals and Tasks

Table 1-5 shows the research goals and tasks for each phase of the research programme. The associated task to solve these goals for each phase and the chapter in the thesis where they are discussed is also presented.

| Research Phase | Goals | Tasks | Chapter |
|-----------------------------|---|--|---------|
| Proof of Concept | <ul style="list-style-type: none"> Design packed bed system @500 W using water as the working fluid - collect data to verify thermal analyses Collect data / observe fluid flow for thermal model | <ul style="list-style-type: none"> Built thruster that fired for 27 hours using 6 different bed materials. Identified engineering issues for next phase - efficiency, lifetime | 2, 3 |
| Prototype | <ul style="list-style-type: none"> Design 200 W thruster with new heater and SiC bed material for better efficiency Improve thermal model - use gases with easier properties for benchmark Calculate heat transfer efficiency, thrust, Isp | <ul style="list-style-type: none"> Two thrusters fired for 150 hours Friction losses in nozzle reduced performance up to 90 % Oxidation of bed material reduced lifetime - discovered by using Electron Microscope Issues for next phase : efficiency and lifetime | 4 |
| Protoflight | <ul style="list-style-type: none"> Improve Design Calculate heat transfer efficiency, thrust, Isp Improve thermal model Obtain endurance data obtainable for a flight system | <ul style="list-style-type: none"> Tested for a total of 450 hours in vacuum with He, N₂, H₂O, H₂O/Methanol, N₂O, and N₂O with MgO catalyst @powers from 0 - 600 W, pressures from 3 - 100 bar using a thrust stand Observed first self-sustaining N₂O reaction for resistojets . Density Isp of 182 sec for water and 105 sec for nitrous oxide with 0 power applications makes flight systems attractive modelling within 10 % of experimental results | 5 |
| UoSAT-12 Flight System | <ul style="list-style-type: none"> Design flight system | <ul style="list-style-type: none"> Use ALL results to design 100 W N₂O system | 6 |
| MightySATII.1 Flight System | <ul style="list-style-type: none"> Design flight system | <ul style="list-style-type: none"> Use ALL results to design 100 W H₂O system | 6 |

Table 1-5: Summary of research goals, tasks and the chapter of the thesis where they are addressed.

1.3. Publications / Outside Funding

Below is a list of publications during the first two and one half years of the research. Additional publications are envisioned after completion of this thesis:

- Co-authored with Dr Jerry Sellers and Mr. Malcolm Paul, "Results of Low Cost Propulsion System Research for Small Satellite Application" for the 3rd Annual Small Satellite Symposium, Annecy, France, 24 - 28 June 1996.
- Authored, "Results of Low-Cost Propulsion System Research for Small Satellite Application", 5th Annual Advanced Technology Workshop, INSAT, Toulouse, France 8 - 10 Jul 96
- Co-authored with Dr. Jerry Sellers and Mr. Malcolm Paul, "Results from Small Satellite System Research" for AIAA Joint Propulsion Conference, 1 - 3 July 1996, Orlando, Florida.

Chapter 1: Introduction

- Authored, “UoSAT Minisat Resistojet Thruster” for AMSAT-UK 96, University of Surrey, 25-27 July 1996.
- Authored, “Performance Testing of a Resistojet Thruster For Small Satellite Applications” for AMSAT-UK 98, University of Surrey, 31 July 1998.
- Authored with Dr Jerry Sellers, Dr Jeff Ward, and Mr Malcolm Paul, “Results of Low-Cost Electric Propulsion System Research for Small Satellite Application” for 10th AIAA/USU Small Satellite Conference, 16 - 19 September 1996, Logan, Utah.
- Authored with Professor Martin Sweeting, Mr Malcolm Paul, Dr Jerry Sellers, Dr Ron Humble, and Cadet Jenn Drum, “Results of Cold Gas and Resistojet Research for Small Satellite Application”, 11th AIAA/USU Small Satellite Conference, 15 - 18 September 1997, Logan Utah.
- Authored with Professor Martin Sweeting, Mr Malcolm Paul, Mr Lee Cowie, and Dr Jerry Sellers. “Results of Low-Cost Propulsion Activities at the University of Surrey”, 2nd ESA Space Propulsion Conference, ESTEC, Netherlands, 27-29 May 1997.
- Authored with Professor Martin Sweeting, Mr. Malcolm Paul, Dr Jerry Sellers, Dr Ronald Spores, Dr Greg Spanjers, Lt Jason Leduc, and Mr Jamie Malak “Performance Testing of a Resistojet Thruster For Small Satellite Applications” for AIAA Joint Propulsion Conference, 6-9 July, Cleveland, Ohio.
- Authored with Professor Martin Sweeting, Dr Jerry Sellers, and Lt Jason Leduc, “Low-Cost Orbit Manoeuvres for Minisatellites Using Novel Water Resistojet Thrusters” for 49th IAF Conference, Melbourne, Australia, 28 Sep - 2 Oct 1998. Named top paper for session and will appear in IAF *Ad Astra*.
- Submitted abstract for AIAA Journal of Propulsion and Power, requested to present paper for special edition on microsatellite propulsion, 25 Sep 98.

This research was also sponsored by two outside contracts. The first one was from USAFA/EOARD to investigate the feasibility of using the resistojet as a starting mechanism for a nitrous oxide hybrid motor. The second effort was from the USAF AFRL/ Electric Propulsion Laboratory and EOARD to investigate flying a 100 W water resistojet on the MightySAT II.1 mission. These two efforts totaled ~ £45,000.

1.4. References

- [Cassidy, 95] Personal phone conversation with Mr Joe Cassidy, Primex, December, 1995.
- [Clauss, 95] Personal phone conversation with Mr Craig Clauss, Atlantic Research Company, December, 1995.
- [Fleming, 95] Personal phone conversation with Mr Alan Fleming, Arde, December, 1995.
- [Humble, 95] Henry, Gary, N., and Larson, Wiley J., *Space Propulsion Analysis and Design*, New York: McGraw-Hill, Inc., 1995.
- [Larson, 92] Wertz, J.R. (ed.), *Space Mission Analysis and Design*, 2 ed., Microcosm, Inc. Torrance, California and Kluwer Academic Publishers, Dordrecht, The Netherlands, 1992.
- [Meyers, 94] Oleson, S.R., "Small Satellite Propulsion Options," AIAA 94-2997, 30th Joint Propulsion Conference, Indianapolis, Indiana, June 27-29, 1994.
- [Sellers, 96A] "Investigation into Low-Cost Propulsion Systems for Small Satellite Missions", Ph.D. Thesis, Department of Electrical Engineering, CSER, University of Surrey, Guildford, UK June, 1996.
- [Sellers, 96B] Lawrence, T.J., Paul, M., "Results of Low-Cost Propulsion System Research for Small Satellite Application," Presented at the 3rd International Symposium on Small Satellite Systems and Services, Annecy, France, June 24-28, 1996.

Chapter 2

Resistojet Technology Options

2. RESISTOJET TECHNOLOGY OPTIONS

2.1. STATIONKEEPING PROPULSION OVERVIEW

2.2. RESISTOJET HISTORY

2.3. RESISTOJET DESIGN APPROACH

2.4. BOILING / HEAT TRANSFER

2.5. NEW DESIGN APPROACH

2.6. CONCLUSIONS

2.7. REFERENCES

This chapter presents the results of a background survey on resistojets and design techniques. The chapter begins by presenting a brief overview of electric propulsion systems. Resistojets that have flown in space are next discussed. Past water resistojets and the problems associated with the designs are then presented. A brief discussion of existing flight qualified resistojets and their limitations for small satellite applications is shown. The current state of the art approach to resistojets with design models is described. The specific heat transfer issues related to resistojets and the special considerations needed for water heat transfer and boiling are highlighted. The chapter concludes with a presentation of a new resistojets design approach. This design approach shows that a packed bed is the best system for the start of the experimentation phase of resistojets research.

2. Resistojet Technology Options

2.1. Stationkeeping Propulsion Overview

A brief discussion on stationkeeping propulsion systems is presented in this section. More detailed system trades are presented which shows the motivation for starting a resistojet research programme.

2.1.1. Fundamentals

As mentioned in Chapter 1, there are 6 important parameters for evaluating low-cost options stationkeeping propulsion. These are:

- mass
- volume
- power
- thrust
- integration
- cost

There are equations that can serve as useful tools in evaluating these metrics for various small satellite stationkeeping propulsion systems. This section introduces these equations.

The equation that is useful in determining how much **mass** a propulsion system will use in its mission is *specific impulse*. *Specific impulse* is defined as:

$$Isp = \frac{F}{\dot{m}g_o} \quad (2-1)$$

where:

Isp = specific impulse (s)

F = thrust magnitude (N)

\dot{m} = massflowrate (kg / s)

g_o = gravitational acceleration @ sea level (9.81 m/s²)

Specific impulse describes the thrust derived from a system as a function of the propellant weight flow rate. It is a measure of rocket efficiency. Higher values of *specific impulse* are desirable because the rocket produces more total impulse for a given mass of propellant. For propulsion systems that produce thrust by converting thermal energy into kinetic energy, *specific impulse* can be expressed as:

$$Isp = \frac{c}{g_o} \quad (2-2)$$

where:

c = effective exhaust velocity (m/s)

$$c = V_{exit} + A_{exit} (P_e - P_a) / \dot{m} \quad (2-3)$$

where:

$$V_{exit} = \sqrt{\frac{2 \cdot \gamma \cdot R_u \cdot T_0}{(\gamma - 1) \cdot M} \cdot \left[1 - \left(\frac{P_e}{P_0}\right)^{\gamma-1/\gamma}\right]} \quad (2-4)$$

V_{exit} = nozzle exit velocity (m/s)

R_u = universal gas constant (8314.41 J/kmol*K)

T_0 = chamber temperature (K)

P_e = exit pressure (Pa)

P_0 = chamber pressure (Pa)

M = molecular mass of gas (kg/kmol)

γ = ratio of specific heats (no dimensions)

A_{exit} = nozzle exit area (m²)

\dot{m} = mass flow rate (kg/s)

The full derivation of Equations 2-3 and 2-4 are in [Humble, 95]. Equation 2-4 expresses the nozzle exit velocity and is valid according to the following assumptions for describing the propellant flow from the rocket chamber through the nozzle exit:

- steady, one-dimensional, isentropic (adiabatic and reversible) flow
- no significant changes in potential energy
- no shaft work or shear work done
- a calorically perfect gas
- constant heat capacity over the temperature range
- rocket chamber represents stagnation conditions - velocity much less than exit velocity

The variables in Equation 2-4 show that the *specific impulse* is a function of the chamber temperature, pressure, and choice of propellant (s) - molecular mass and ratio of specific heats.

Density specific impulse is used to determine the propellant **volume** requirements. Density specific impulse is defined as the product of the propellant average specific gravity and the specific impulse:

$$DensityIsp = \delta_{av} * Isp \quad (2-5)$$

where:

δ_{av} = average specific gravity (no dimensions)

Isp = specific impulse (s)

Density Isp = density specific impulse (s)

The density specific impulse is an important parameter for small satellites since it takes into account the volume of propellant needed, rather than the mass. In satellites like UoSAT-12 and MightySatII.1, volume is a tighter commodity than mass.

Power is another important parameter in small satellite systems. Since most small spacecraft have very low power output (e.g. UoSAT-12 has a total of 144 W continuous power in sunlight for a 720 km orbit), it is important to determine how much power various electric propulsion systems use and the resultant thrust they produce. The power consumed for cold gas and chemical propulsion is negligible compared to electric propulsion systems. A good first order approximation for determining this in electric systems is :

$$F = \frac{2P}{C} \quad (2-6)$$

where:

F = thrust (N)

P = Input Power (W)

C = effective exhaust velocity (m/s)

Thus, the thrust produced from the electric system directly scales with the input power.

The **thrust** the propulsion system produces is important for several reasons:

- Power required - for electric systems
- Trip time to do the manoeuvre
- Ability to move the spacecraft in high drag orbits
- Attitude control issues

The thrust related to power relation is shown in Equation 2-6. The trip time can be approximated as:

$$TGO = \frac{\Delta V}{accel \left(1 + 3Vratio + 3Vratio^2 \right)} \quad (2-7)$$

$$Vratio = \frac{\Delta V}{6I_{sp}g_o}$$

where:

ΔV = velocity needed for spacecraft to do orbital manoeuvre (m/s)

I_{sp} = specific impulse (sec)

g_o = gravitational constant @ sea level (m/s²)

$accel$ = thrust/mass of spacecraft (m/s²)

TGO = time to do manoeuvre (seconds) from [Sellers, 96]

The ΔV from equation 2-7 can be expressed with two approaches. There are many ways to express this equation, this application applies to stationkeeping missions. The first expression is defined as the rocket equation :

$$\Delta V = Isp g_o \ln \frac{M_i}{M_f} \quad (2-8)$$

where:

ΔV = velocity needed for spacecraft to do orbital manoeuvre (m/s)

Isp = specific impulse (sec)

g_o = gravitational constant @ sea level (9.81 m/s²)

M_i = mass of spacecraft before firing (kg)

M_f = mass of spacecraft after firing (kg)

This equation predicts the velocity needed for the spacecraft to do the orbital manoeuvre based upon the performance of the propulsion system and the amount of propellant on board. This equation would be useful in volume limited cases (e.g. 1 module box on a microsatellite - 300 mm x 300 mm x 100 mm) to calculate how much ΔV the propulsion system could produce for the limited volume. The other expression (Equation 2-9) is determined from an analysis of the spacecraft stationkeeping requirements.

$$\Delta V_{Stationkeeping} = \Delta V_{Drag} + \Delta V_{momentumwheeldumping} + \Delta V_{phasin g} + \Delta V_{planechange} + \Delta V_{deorbit} \quad (2-9)$$

where:

$$\Delta V_{drag} = \rho a V \pi (C_D A / m) \quad (2-10)$$

per circular orbit

ρ =atmospheric density (1.24 x 10⁻¹⁴ kg/m³ for 750 km circular orbit)

a = semi-major axis (km)

V = space craft velocity (m/s)

C_D = Drag coefficient = 2.2

A = spacecraft cross sectional area (m²)

m = spacecraft mass

$$M_p = \frac{I}{Isp g_o}$$

$$I = npulse * nwheels * 365daysperyear * nyears * firingdurationperpulse * F \quad (2-11)$$

$$F = \frac{H}{Lt}$$

where:

H = stored momentum in wheel (Nms)

L = moment arm (m)

t = burn time (sec)

$$\Delta V_{\text{momentumwheeldumping}} = Isp g_o \ln \frac{M_i}{M_f} \quad (2-12)$$

where:

M_i = Initial spacecraft mass (kg)

M_f = final spacecraft mass (kg) = $M_i - M_p$

M_p = propellant mass (kg)

Isp = rocket efficiency (s)

$$\Delta V_{\text{phasin g}} = \text{driftrate} \times (V / 1080) \text{ m / s per deg / orbit} \quad (2-13)$$

where:

V = spacecraft velocity (m/s)

$$\Delta V_{\text{planechange}} = 2V \sin\left(\frac{\phi}{2}\right) \quad (2-14)$$

where:

V = spacecraft velocity (m/s)

ϕ = inclination change (deg)

$$\Delta V_{\text{deorbit}} = V \left(1 - \sqrt{\frac{2R_E}{R_E + r}}\right) \quad (2-15)$$

where:

V = spacecraft velocity (m/s)

R_E = radius of the earth (m)

r = radius of the orbit (m)

All of the terms in Equation 2-9 depend on the orbit. The drag term predicts how much velocity will be needed to keep the spacecraft in the same circular orbit to counter the force of drag. The higher the orbit, the less atmosphere, hence the less velocity required. Equations 2- 11 and 2-12 show the velocity needed to dump momentum from the wheels on the spacecraft. This velocity is related to the rotation rate of the wheels and the propulsion system on board. If the spacecraft is in a constellation, it will need to be re-phased relative to the other spacecraft. Equation 2-13 shows the velocity required

relative to the spacecraft's drift rate and orbit velocity. Equation 2- 14 expresses the velocity required to change the inclination of the spacecraft's orbit. This is sometimes required for stationkeeping, due to perturbations in the spacecraft's orbit from the oblateness of the earth. The last equation shows the velocity required to de-orbit the spacecraft. This may be a requirement in the future, even for LEO satellites due to the growing number of spacecraft in orbit. [Larson, 1992]

There are other analytical means of evaluating the **thrust** the spacecraft produces relative to the spacecraft. The first one applies in high drag orbits. The acceleration the spacecraft produces can be expressed as:

$$a(t) = \frac{F}{m(t)} - \frac{D}{m(t)} \quad (2-16)$$

where:

F = thrust of propulsion system (N)

D = drag = $1/2\rho AC_D V^2$

m = spacecraft mass (kg)

t = time (s)

If a very low thrust system is placed on too big of a platform, even for small satellites, in a high drag orbit (high atmospheric density), the platform will not be able to overcome the drag. This could become a factor in the highly efficient, but low thrust electric propulsion systems.

The last impact of **thrust** on small satellites is attitude control. The propulsion system must be able to move the spacecraft, but not cause severe attitude control concerns while it is firing. The easiest way to rectify this, is to place the thrust vector along the spacecraft centre of gravity. However, some margin does need to be considered for thrust misalignment, uncertainties in the location of the centre of gravity, and change in the centre of gravity over time due to propellant being expelled from the spacecraft. A conservative equation that can express the disturbance torque generated due to these effects (derived from [Larson, 92]) is:

$$T_{thrustdisturbancetorque} = F * 0.07 \quad (2-17)$$

where:

F = thrust of system (N)

T = thrust disturbance torque (Nm)

The spacecraft must have actuators that can counter this disturbance torque. Table 2-1 shows the actuators and the torque they can produce.

| Actuator | Typical Performance Range | Weight (kg) | Power (W) |
|------------------------------|--|---|-----------|
| Thrusters | | | |
| Hot gas | 0.5 to 9,000 N | Thruster: 1 kg, tanks and propellant depend on smallsat mass and volume | 0 |
| Cold gas | < 5N To get torque, multiply by thruster location to cg - moment arm (.1 - 1.5 m) = $T = F * \text{moment arm}$ | Thruster: 0.5 kg, tanks and propellant depend on smallsat mass and volume | 0 |
| Reaction and momentum wheels | 0.4 to 400 Nms for momentum wheels at 1200 to 5000 rpm: max torques from 0.01 to 1 Nm | 2 to 20 | 5 to 110 |
| Control moment gyros (CMG) | 25 to 500 Nm of torque | >40 | 90 to 150 |
| Magnetic torquers | 1 to 4000 $\text{Am}^2 = 4.7 \times 10^{-4}$ Nm to 0.18Nm for 800km orbit and max Earth field of 0.4 gauss | 0.4 to 50 | 0.6 to 16 |

Table 2-1: Attitude Control Actuators from [Larson, 92]

Integration and safety parameters are difficult to quantify in straightforward equations like the previous four parameters. From data already introduced in Chapter 1, toxic systems will require more infrastructure for applications ranging from research and development, qualification testing, to launch integration. The use of toxic propellants can add up to £90,000 to the propulsion system budget. [Paul, 1998] Most of this is a one-off infrastructure cost, but in the initial propulsion system analysis for small satellites, it needs to be considered. The other **integration** issue to consider is the decision to buy the propulsion system off-the-shelf versus building it in house. Analysis of the first 4 parameters may make this a moot point since there are no off the shelf systems that can meet the user requirements. However, constraints may be relaxed to meet an off-the-shelf system if the user feels it is more advantageous. Sellers presents pro and con arguments for both options in Table 2-2. The user can weigh these arguments and then include it in the overall analysis with the other parameters.

| Option | Advantages | Disadvantages |
|-----------------------------------|---|---|
| <i>Building Hardware In-House</i> | <p>YOU...</p> <ul style="list-style-type: none"> • Control the specifications and performance • Control the design and interfaces • Control the schedule • Control the cost • Can introduce new or untried technology • Spend over-head costs within your organisation • Gain expertise that should make it even cheaper next time | <p>YOU...</p> <ul style="list-style-type: none"> • Carry all the risk • Need the in-house expertise to design the entire component and manufacture it • Need to space qualify it • Need to acceptance test it |
| <i>Buying Hardware</i> | <p>YOU...</p> <ul style="list-style-type: none"> • Share risk with supplier • Use tried and tested hardware • May reduce or avoid development costs • Learn from subcontractors | <p>YOU...</p> <ul style="list-style-type: none"> • Have less control over specifications • Have less control over schedule and cost • Spend overhead outside your organisation • Do not learn how to do it yourself next time |

Table 2-2: Pro's and Con's of In-house versus Off-the-Shelf Systems from [Sellers, 96]

The last parameter is **cost**. This is another parameter that is difficult to quantify. There have been various cost models applied to spacecraft, and spacecraft components such as propulsion, but there are no tools that could be directly used for evaluating various propulsion systems, without using an "engineering judgement" type of decision making. Sellers developed a total cost figure of merit methodology using his 9 parameters discussed in Chapter 1 [Sellers, 96]. The methodology produces total cost figure of merits for each system considered based upon assigning weights to the 9 different parameters in the paradigm. The method allows the user to input varying mission requirements, and decide the propulsion system that best meets the mission. Unfortunately, it does rely on "engineering judgement" in assigning the importance of the parameters for the various propulsion systems.

Since many of the stationkeeping systems discovered in the literature survey phase of the research are still under research and development, cost modelling is very difficult. Many of systems can not present a projected engine price [ESTEC, 97]. However, the best proposed solution is to take the industry standard system for stationkeeping, a hydrazine resistojet, and use that as the cost benchmark. Primex quotes a ROM cost for the MR-502 engine as £100,000 [Cassidy, 95]. If a new system represents a low-cost option for small satellites, it should be under this price.

Now that the six parameters have been introduced, it is time to decide which systems best meet these requirements for small satellite stationkeeping. However, it is better to introduce the various propulsion systems first to provide relevant background information before the parametric analysis is conducted. Electric propulsion, chemical, and cold gas systems will be discussed.

2.1.2. Electric Propulsion Systems

Electric propulsion systems can be categorised into three main areas:

1. *Electrothermal*-- electrical energy is used to directly heat a working fluid. The resulting hot gas is then expanded through a converging-diverging nozzle to achieve high exhaust velocities. These systems convert thermal energy to kinetic energy.
2. *Electrostatic*-- electrical energy is directly converted into kinetic energy. Electrostatic forces are applied to charged particles to accelerate the propellant.
3. *Electromagnetic*-- electromagnetic forces directly accelerate the reaction mass. This is done by the interaction of electric and magnetic fields on a highly ionised propellant plasma.

This section introduces these various electric propulsion systems and provides relevant background information to the parameters introduced in the past section.

2.1.2.1. Electrothermal

Resistojets, arcjets, and microwave are the three types of electrothermal thrusters. A resistojet functions by passing the propellant flow over an electrically heated solid surface. An arcjet passes the flow through an arc discharge. Finally, a microwave thruster works by high-frequency excitation. In each case, the maximum temperature the chamber and nozzle surfaces can tolerate, and the gas-kinetic and thermodynamic properties of the propellant primarily determine the attainable exhaust velocity.

Many potential resistojet configurations have been investigated. They have been operated at input power levels from 1 W to over 60 kW. Typical thrusts lie between several mN to a few N, with Isp's from 100 - 1000 seconds. Many different propellants such as hydrogen, carbon dioxide, methane, nitrogen, hydrazine, ammonia, helium, argon, air, and water have been investigated for space application. The advantages of resistojets are:

- simplicity
- high thrust density
- high heat transfer efficiency with given input power
- wide spectrum of propellants

The major disadvantage of resistojets, as compared to other forms of electrical propulsion, are the low specific impulse. However, as far as the metrics for stationkeeping, they represent a good balance of power, density Isp, and thrust. [Stuttgart, 98]

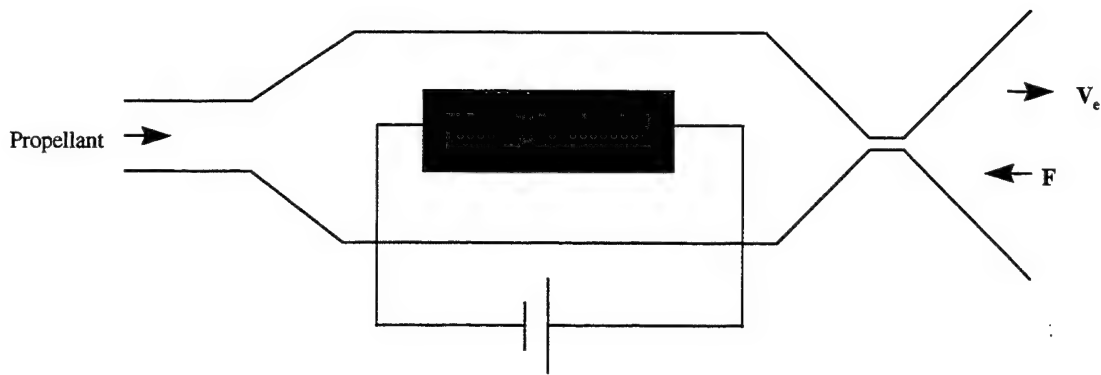


Figure 2-1: Resistojet

Arcjets have been developed using a wide variety of propellants, notably hydrogen, ammonia, and hydrazine. The arcjet systems have three basic elements:

1. the engine
2. the power source and conditioner
3. propellant subsystem

The engine is the smallest component in size and mass of the entire system. Added mass is needed for the power conditioning system to convert spacecraft voltages from $\sim 28\text{V}$ to $100 - 1000\text{ V}$. This power conditioning is required for arc operation. Arcjets are configured to confine the extremely hot plasma column to the centre and keep a relatively cooler flow at the outer wall. This arrangement allows average chamber stagnation temperatures to reach $4000 - 5000\text{ K}$, and measured specific impulse values of $1000 - 2000$ seconds using hydrogen. Engines have been operated for periods of days at power levels of $2 - 3\text{ kW}$, and for shorter periods at 200 kW .

Currently, arcjets are used on Lockheed Martin Aerospace series 7000 spacecraft that include Telstar 4 and Intelsat 7 spacecraft. These arcjets use hydrazine, operate at 1.5 kW and are qualified for 1500 hours of operation. Several low power arcjets are in development at NASA Lewis and the University of Stuttgart for operation in the $400 - 800\text{ W}$ range with *specific impulses* in the range of $300 - 560$ sec. The University of Illinois is also investigating a pulsed 50 W helium arcjet. [Stuttgart, 98] [NASA Lewis, 98].



Figure 2-2: 100 kW Arcjet from [Stuttgart , 98]

Even though arcjets have high performance and thrust, their power requirement is high for small satellite application. The lowest power flight qualified system is a 750 W continuous ammonia system developed by the University of Stuttgart for the AMSAT Phase 3D spacecraft. Arc spiralling and frozen flow issues have impeded development at the lower power levels. There is no data currently published on the performance of the University of Illinois pulsed system.

Microwave thrusters have been under development at Penn State University for the last 15 years. Conceptual designs have been presented in papers [Micci, 96]. The USAF has started to develop a 100 W ammonia and water system due to be funded in the next three years [Micci, 98]. Microwave thrusters are attractive due to their power, performance and thrust. The small satellite industry will be interested in their operation, if a system can be developed and integrated into a spacecraft.

2.1.2.2. Electrostatic

Ion and FEEP (Field Emission Electric Propulsion) are the two major types of electrostatic propulsion systems. In ion propulsion, the propellant atoms are ionised by electron bombardment at the ion source. Then the positive ions are accelerated to very high velocities by an electric field established between the ion source and the accelerating electrode. After acceleration, the ion beam may be partially decelerated by a decelerating electrode, and it is then electrically neutralised by a stream of electrons, which are injected into the exhaust beam. FEEP thrusters, unlike ion engines, directly extract the ions from the liquid phase. Thrust is obtained by exhausting a beam, mainly composed of singly ionised atoms, produced by field emission [CPIA, 98] [NASA Lewis, 98].

Ion propulsion is under extensive development, particularly for North-South stationkeeping of large GEO communications spacecraft. The first commercial use of ion propulsion was recently begun aboard the Hughes Galaxy III-R communications satellite, which uses four 0.424 kW Hughes XIPS-13 thrusters. The first European Retrievable Carrier mission (EURECA-1) used a German Daimler-Benz 0.44kW Radiofrequency Ionisation Thruster (RIT-10). Two improved RIT-10 thrusters will be used along with two British Matra Marconi Space UK-10 Xe ion thrusters on ESA's ARTEMIS satellite. NASA is also investigating the use of their 30-cm xenon ion engine system for interplanetary exploration as part of the Millennium Programme. NASA JPL plans to fly this thruster on Deep Space 1 (DS-1) in the fall of 1998. DS-1 will be launched into Earth orbit by a Delta II rocket, and the its ion propulsion system will drive it to distant encounters with a comet and one or two asteroids [Beattie, 98].

The thruster requires a power-processing unit that electrically transforms the spacecraft voltages into those required by the various subsystems of the thruster. Current designs use xenon, argon, or krypton for the propellant while earlier designs employed mercury and cesium. To achieve high

performance, the feed system must provide both high pressure (most likely supercritical) storage and low flow rate distribution to the thruster [CPIA, 98] [NASA Lewis, 98].

Typical input power ranges from 424 - 2.5kW. Total system mass is on the order of 12 - 18 kg. The power-processing unit usually drives this and the systems required in ionising the gas. Isp's range from 2550-3200 sec. The rated life is 8,000 hr @ 2.5 kW. The main drawbacks of ion systems are their thrust / power ratio. They are also very expensive ~£1 million per system [Claus, 95].

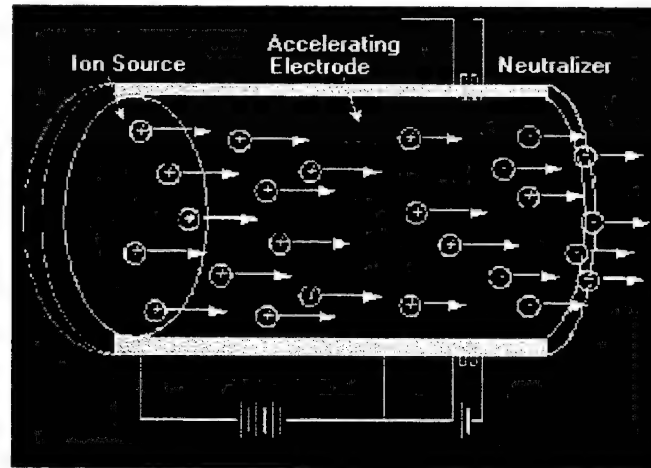


Figure 2-3: Ion Thruster from [Stuttgart, 98]

FEEP delivers very low thrust with very high accuracy and controllability. The application range of FEEP covers the $1\mu\text{N}$ - 2mN thrust range. The thruster can accelerate a large number of different liquid metals or alloys; cesium proved to be the best choice due to its molecular weight and its low ionisation potential. The thruster's main features are:

- very high specific impulse (~6000 sec)
- low system mass and size
- no moving parts
- self-contained propellant reservoir.

The FEEP technology is developed at Centrospazio under ESA/ESTEC and ASI funding. FEEP is baselined for the ESA Horizon 2000 Plus LISA and the JPL OMEGA missions, both multi-spacecraft gravitational wave detectors, and for the Italian proposed test of the Equivalence Principle on the Galileo Galilei - GG satellite. The disadvantage of FEEP for stationkeeping of small satellites is the same as ion propulsion, a low thrust to power ratio (60 W/mN). There are no system costs as of yet since it is still under development [Centrospazio, 98].

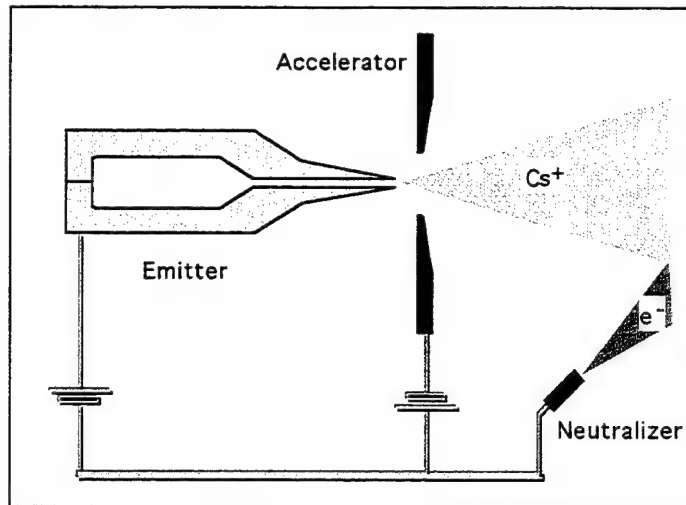


Figure 2-4: FEEP System from [Centrosazio, 98]

2.1.2.3. Electromagnetic

Magnetoplasmadynamic (MPD), HALL or Stationary Plasma Thrusters (SPT), and Pulsed Plasma Thrusters (PPT) are electromagnetic systems. MPD thrusters use an electrical arc discharge, like an arcjet. The propellant plasma is accelerated by the interaction of the arc and the self-induced and applied magnetic fields. SPT thrusters use the Hall effect to set up an electrostatic field, which accelerates the propellant ions. PPTs accelerate the propellant plasma by interaction of an electric arc current with a self-induced magnetic field.

An experimental 0.43kW, repetitively pulsed, hydrazine MPD arcjet thruster was recently launched on the Japanese Space Flyer Unit Mission One by and H-II rocket. MPD thrusters have demonstrated high performance and high power handling capabilities that make them attractive for primary propulsion applications, if their low efficiencies and limited lifetimes can be overcome. These factors have kept most MPD thrusters at the development level. Research is underway by ESA to understand the basic physical processes taking place in purely electromagnetic devices. Experimental activities underway include electrical characterisation, performance measurements and plume diagnostics as a function of the thruster geometry and scale, operating under a broad range of conditions [CPIA, 98] [Stuttgart, 98] [NASA Lewis, 98].

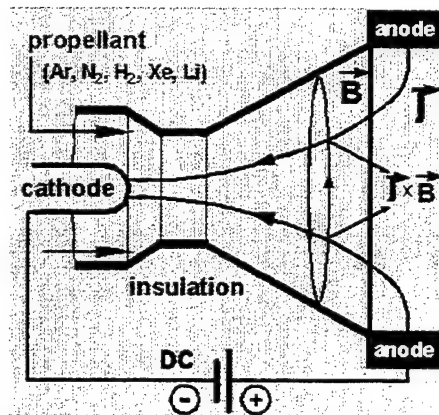


Figure 2-5: MPD Thruster from [Stuttgart, 98]

Several Hall thrusters have been developed and flown on spacecraft built in the former Soviet Union. The thruster works by developing an axial electric field between discharge electrodes. The field interacts with a radial magnetic field that generates a “Hall” current in an azimuthal direction. This current, in turn, reacts against a magnetic field to generate a force on the propellant in the downstream axial direction. The unique feature of this device is that the major current flow is the Hall current perpendicular to the electric field, hence the name Hall thruster. The device operates in a steady state mode and achieves I_{sp} 's from 1000 - 2000 sec. Input power levels range from 0.5- 2.5 kW. The 2.5 kW thruster has a rated lifetime of 1,000 hours. International Space Technology, inc. (ISTI) is the joint venture formed by Space Systems/Loral, Fakel Enterprises (Russia), the Research Institute of Applied Mechanics and Electrodynamics of the Moscow Aviation Institute (MAI/Russia), and its other international partners to commercialise SPT's for use on Western spacecraft. The AFRL Electric Propulsion Laboratory has also funded industry and academia to build their own Hall systems. The disadvantage for small satellite application of the Hall system is its high input power requirement [CPIA,98] [Spores, 98] [NASA Lewis, 98].

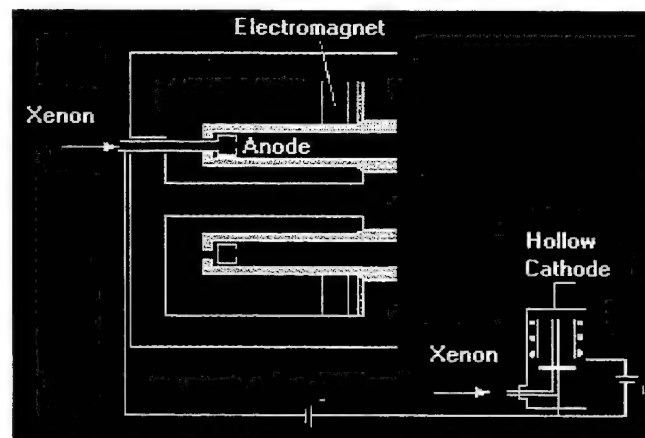


Figure 2-6: Hall Thruster from [Stuttgart, 98]

A PPT thruster consists of two parallel flat-plate electrodes separated by a Teflon propellant bar at the upstream end of the discharge volume. The electrodes are connected to a capacitor that provides a high current, high power pulse to the electrodes once the inter-electrode gap is made conducting by

the discharge of a small ignitor plug mounted in the cathode electrode. Once triggered, the main discharge current flows along the surface of the Teflon propellant bar in a thin sheet and ablates a portion that is subsequently electromagnetically accelerated downstream. The actual acceleration force arises from the vector cross product of the discharge current and its self-induced magnetic field. A number of flight systems have been built and flown for precise stationkeeping (TIP/NOVA 1964-1982), with average thrust levels ranging from micro to millinewtons. Typical Isp's range from 1200-1500 sec. Primex, NASA Lewis, and the AFRL Electric Propulsion Laboratory have been investigating PPT's for small satellite application. Even though the PPT has a very high Isp, the added mass from the capacitor and low thrust efficiency are limiting factors for small satellite stationkeeping missions. Research has looked at increasing the thrust with higher input power PPT's, but lifetime issues have been a problem that have kept these under research and development [Stuttgart, 98] [Spanjers, 98] [NASA Lewis, 98].

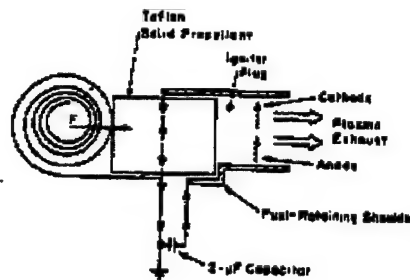


Figure 2-7: PPT from [NASA Lewis, 98]

2.1.3. Cold Gas Propulsion Systems

Cold-gas thrusters have seen a variety of spacecraft applications going back to the early 1960s. TRW used them on more than 40 different missions [Greco 71]. Their inherent safety is underscored by their use on Space Shuttle astronaut's Manned Manoeuvring Unit (MMU). The energy for a cold-gas thruster comes from energy of the high-pressure gas. Onboard a spacecraft, the operating principle is not much more complex. A working fluid, e.g. compressed nitrogen, is stored at high pressure (normally >200 bar). It is then regulated down to some operating pressure (around 10 bar). The nozzle is normally integral to the control valve. Opening the valve releases the gas to expand out of the nozzle producing thrust [Sellers, 96].

Any compressible gas can be used for cold gas applications. Table 2-3 shows the *specific impulse* for various gases.

| Gas | Molecular Weight | Specific Impulse (sec) |
|----------------|------------------|------------------------|
| Air | 28.9 | 74 |
| Argon | 39.9 | 57 |
| Carbon Dioxide | 44.0 | 67 |
| Helium | 4.0 | 179 |
| Hydrogen | 2.0 | 296 |
| Nitrogen | 28.0 | 80 |
| Methane | 16.0 | 114 |

Table 2-3: Specific impulse performance for various gases [Sutton, 92]

After studying Table 2-3, helium would seem to be a good choice for small satellite stationkeeping applications based upon its *specific impulse*. However, Equation 2-5 shows that volume is also important for small satellites. Table 2-4 presents a comparison of two extreme cases, nitrogen and helium. Even though the nitrogen system has more propellant mass, it delivers higher total impulse. Thus, for cold-gas thruster applications on volume-limited missions, nitrogen will deliver more total impulse than helium for a given volume. Furthermore, for a given propellant mass, this analysis does not take into account the additional tank mass needed to store the larger volume of the less dense helium. When this is considered, the nitrogen system is even more advantageous overall. Therefore, all cold-gas thruster applications analysed subsequently will assume nitrogen as the propellant. Thrust levels for cold-gas systems are practically limited by the maximum operating pressure of the control valves. Typical thrusters operate at < 1 N. Their power usage is relatively low as it takes little power to hold open a single, small valve (~ 1-5 W). The disadvantage of a nitrogen cold gas system for small satellite stationkeeping missions is the low performance [Sellers, 96].

| Parameter | Nitrogen | Helium |
|--|------------------------|------------------------|
| Molecular Weight | 28.014 kg/kmole | 4.003 kg/kmole |
| Ratio of specific heat, γ | 1.397 | 1.66 |
| Tank Volume | 6.57 litre | 6.57 litre |
| Tank Pressure | 240 bar | 240 bar |
| Temperature | 293 K | 293 K |
| Density | 276 kg/m ³ | 60 kg/m ³ |
| Total initial mass | 1.81 kg | 0.394 kg |
| Characteristic Exhaust Velocity, C^* | 431 m/sec | 1076 m/sec |
| Throat radius | 0.5 mm | 0.5 mm |
| Optimum expansion ratio | 100 | 30 |
| Nozzle exit radius | 5 mm | 3 mm |
| Thrust | 3.25 N | 3 N |
| I_{sp} | 75.6 sec | 172.6 sec |
| Mass flow rate | 4.4 gm/sec | 1.7 gm/sec |
| Total impulse available | 1344 N-sec | 667.8 N-sec |
| Density I_{sp} | 2.09×10^4 sec | 1.04×10^4 sec |

Table 2-4: Performance parameters for nitrogen vs. helium cold-gas thruster options from [Sellers, 96]

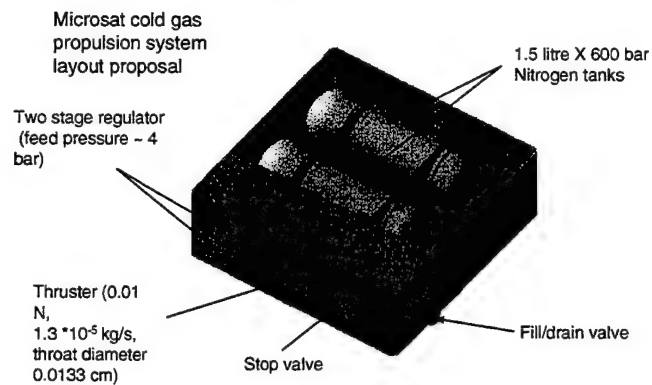
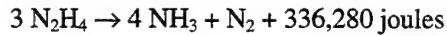


Figure 2-8: Prototypic nitrogen cold gas system for small satellite application

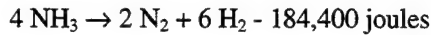
2.1.4. Chemical Propulsion Systems

Chemical propulsion systems use the energy inherent in chemical bonds released through catalytic action or combustion to produce high temperature exhaust products that are then expanded out a nozzle to high velocity. Chemical systems can be classified into cryogenic liquid, storable liquid, hybrid, and solid systems. The storable liquid monopropellant system will only be presented since it is the industry standard for low cost (simplicity) stationkeeping missions.

Monopropellant rockets rely on a single propellant. The release of energy within the chemical bonds of the propellant is initiated by the presence of a catalyst. The most widely used monopropellant systems uses hydrazine as the working fluid. Chemically, hydrazine decomposes with an exothermic reaction into ammonia and nitrogen when exposed to a catalyst as follows:



Unfortunately, if the reaction is allowed to continue, the ammonia further decomposes in an endothermic reaction as follows:



Therefore, the art of hydrazine catalyst bed design is aimed at minimising the effect of this second reaction which lowers operating temperature, reducing overall engine efficiency [Sellers,96].

Hydrazine catalyst material normally consists of iridium or cobalt deposited on a porous ceramic such as aluminium oxide. These compounds are commercially available going by the trade names Shell-405 or LCH. The chief limitation on thruster lifetime is catalytic attrition caused by a variety of effects, including mechanical breakdown from thermal and pressure cycling as well as chemical poisoning by trace contaminants in the propellant. To avoid this last effect, strict requirements on the chemical purity of the hydrazine are typically imposed [Sellers,96].

Thrust levels for hydrazine systems range from 0.1 - 400 N. Table 2-5 shows the performance for the Primex MR-106E thruster. The power requirements for the system are for the opening of valves and heating of the propellant tanks and catalyst pack (freezing point is 275.16 K). The low power and performance (*Isp* and *Density Isp*) of the hydrazine system make it attractive for small satellite missions. The issue is the expense required in handling the problems associated with hydrazine mentioned previously.

| Parameter | Value |
|----------------------------------|-----------------------|
| Catalyst | LCH 227/202 |
| Steady-state thrust (N) | 11.1 - 31.2 |
| <i>Isp</i> (sec) | 228 - 235 |
| Propellant specific gravity | 1.023 |
| Average Density <i>Isp</i> (sec) | 236.8 |
| Rated total impulse (Nsec) | 124,700 |
| Total pulses | 12,405 |
| Minimum impulse bit (Nsec) | 0.56 |
| Feed pressure (bar) | 6.7 - 24.1 |
| Chamber pressure (bar) | 4.5 - 12.4 |
| Nozzle expansion ratio | 61:1 |
| Mass flow rate (gm/sec) | 5.0 - 13.1 |
| Valve power | 27 W maximum @ 28 VDC |
| Thruster mass (kg) | 0.52 |

Table 2-5: MR-106E hydrazine mono-propellant thruster performance data [Sellers, 96]

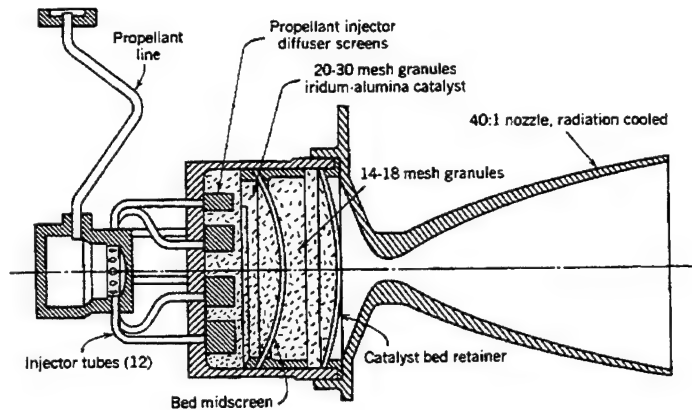


Figure 2-9: Cut away view of a hydrazine mono-propellant thruster from [Sutton, 92]

2.1.5. Analysis

Now that all of the potential systems have been introduced, an analysis is needed to determine which is best for small satellite stationkeeping missions. Using the equations presented in Section 2.1.1 for the 6 parameters, an analysis will be conducted for two types of missions:

- 3 year stationkeeping mission for a 300 kg platform in a 750 km sunsynchronous circular orbit, $i = 98.39^\circ$, $\sim \Delta V$ 200 m/s (from Equation 2-9)
- Experimental volume constrained mission for a 200 km circular orbit (Space Shuttle), $\sim \Delta V$ 5 m/s (complete system volume limited to 300 mm x 300 mm x 110 mm). ΔV derived for a nitrogen cold gas system, since its performance requires the most volume.

The other assumption for this analysis is that the spacecraft bus is available to provide 100 W continuous power (valid based upon UoSAT-12 and MightySatII.1 spacecraft).

| System, Thrust, Isp, Power, Supplier | Propellant Mass/ Mass of Spacecraft (~300 kg) (%) | Propellant Volume/ Volume of Spacecraft (0.8m ³) (%) | Trip Time for ΔV (hours) | Thrust Disturbance Torque (Nm) | Power Consumed /Power Available (%) | Acceleration over drag (m/s ²) | Integration* | Cost*** |
|--|---|--|----------------------------------|--------------------------------|-------------------------------------|--|--------------|----------------------|
| N ₂ Cold Gas, 100 mN, 75 sec, 5 W, EG&G | 24 | 83 | 146 | 0.007 | 1 | 0.0003 | Low | OTS £3,500 |
| N ₂ H ₄ Mono-Prop, 100 mN, 220 sec, 10 W, Primex | 9 | 3 | 159 | 0.007 | 1 | 0.0003 | High | OTS £25,000 |
| N ₂ O Resistojet, 500 mN, 150 sec, 300 W, None | 13 | 7 | 30 | 0.04 | 5 | 0.002 | Low | Not OTS or under R&D |
| H ₂ O Resistojet, 270 mN, 182 sec, 600 W, None | 11 | 4 | 68 | 0.02 | 39 | 0.0008 | Medium | Not OTS or under R&D |

| | | | | | | | | |
|--|-----|------|-------|---------|-----|----------|--------|--|
| N ₂ H ₄ Resistojet, 360 mN, 300 sec, 610 W, Primex | 7 | 2 | 45 | 0.03 | 25 | 0.001 | High | OTS £100,000 |
| NH ₃ Resistojet, 30mN, 296 sec, 100 W, NIIEM- ELKOS | 7 | 3 | 537 | 0.002 | 49 | 0.0001 | High | OTS Cost not available (Russian) |
| N ₂ H ₄ Arcjet, 200mN, 500 sec, 1.8 kW, Primex | 4 | 1 | 82 | 0.01 | 134 | 0.0007 | High | OTS £125,000 |
| NH ₃ Arcjet, 115 mN, 483 sec, 750 W, U of Stuttgart | 4 | 2 | 142 | 0.008 | 97 | 0.0004 | High | OTS £33,000 |
| NH ₃ Microwave, 300 mN, 550 sec, 1.1 kW, PSU | 4 | 2 | 55 | 0.02 | 57 | 0.001 | High | Not OTS Under R&D |
| Xe Ion, 17 mN, 2585 sec, 440 W, TRW | 1 | 1 | 977 | 0.001 | 392 | 0.00006 | Medium | OTS £1,000,000 |
| Xe Hall, 30 mN, 1200 sec, 700 W, MAI | 2 | 2 | 551 | 0.002 | 352 | 0.0001 | Medium | OTS £625,000 |
| Cs FEED, 1 mN, 6000 sec, 60 W, Centrosazio | 0.3 | 0.07 | 16655 | 0.00007 | 913 | 0.000003 | Medium | Not OTS Under R&D |
| NH ₃ MPD, 23 mN, 600 sec, 430 W, ISAS (Japan) | 3 | 2 | 722 | 0.002 | 283 | 0.00008 | Medium | Not OTS Flown as experiment |
| PPT, 4.5 mN, 1500 sec, 120 W, Primex | 1 | 0.4 | 3679 | 0.0003 | 403 | 0.00002 | Medium | Developed in 1970's Under R&D expected cost £130,000 |

Table 2-6: Comparison of Various Systems for a 3-year small satellite stationkeeping mission

*-- Assumes the spacecraft can provide 100 W of continuous power for 1 hour each day for 3 years

**-- High - system uses a toxic propellant; Medium - system may cause some integration problems with the spacecraft, electromagnetic interference, plume impingement, charging, thermal, etc. ; Low - little or no integration issues

***. "One-off" price quotes obtained from [Cassidy, 95], [Fleming, 95], [Clauss, 95], [Riehle, 98], and [Bromaghim, 98]

Table 2-6 shows some interesting results for a 3-year stationkeeping mission. Several of the systems are not attractive for the following reasons:

- Cold Gas : consumes 83 % of the spacecraft volume
- Arcjets, Ion, Hall, FEEP, MPD, and PPT: have very good performance (< 2% of spacecraft volume consumed), but power requirements are excessive
- Microwave: higher power requirement compared to resistojets and mono-propellant

The remaining choices are the hydrazine monopropellant, ammonia, hydrazine, nitrous oxide, or water resistojet systems. Table 2- 6 shows for this mission class, adding a resistojet to a hydrazine system only increases the volume performance by 1 %, and increases the power required by 24 %. An ammonia resistojet offers the same volume performance, but requires a 48 % increase in power. That leaves a hydrazine monopropellant system and two unconventional systems, a nitrous oxide and water resistojet. The hydrazine system out performs the water and nitrous oxide resistojets by 1 % and 3 % respectively in volume, and by 4% and 38 % respectively in power. All of the thrust disturbance torques are low enough to be countered with reaction or momentum wheels. However, since the hydrazine is toxic, the integration and thruster costs are high. The cost presented in Table 2-6 is just the thruster cost and does not include the expulsion system, hydrazine itself (£90 per litre), and supporting infrastructure. The slight performance penalty (especially with the nitrous system) of the resistojets may be countered by lower total system cost.

Studying Table 2-2 can also reinforce this argument. An in-house research programme using easy to handle propellants will increase the “corporate knowledge” of the University and allow greater control for the mission requirements. At the start of the research programme, the University purchased an off the shelf nitrogen cold gas system from Arde for UoSAT-12 attitude control (11 thrusters - 10 flight and 1 spare). Unfortunately, performance measurements of the system revealed that each thruster was operating at a thrust level of 400 % over its specification. The thruster was redesigned internally (quicker then relying on vendor) to correct this problem with extra hardware costs and man-hours. As Table 2-6 shows the various thruster costs, the other more complex systems may be difficult/impossible to modify, especially since most small satellites require a short lead time.

Chapter 2: Resistojet Technology Options

| System, Thrust, Isp, Power, Supplier | Propellant Mass/ Mass of Spacecraft (~300 kg) (%) | Propellant Volume/ Volume of Spacecraft (0.8m ³) (%) | Trip Time for ΔV (hours) | Thrust Disturbance Torque (Nm) | Power Consumed (W) | Acceleration over orbit drag (m/s ²) | Integration | Cost |
|--|---|--|--------------------------|--------------------------------|--------------------|--|-------------------|-------------------|
| N ₂ Cold Gas, 100 mN, 75 sec, 5 W, EG&G | 1 | 2 | 4 | 0.007 | 21 | 0.0002 | Same as Table 2-6 | Same as Table 2-6 |
| N ₂ H ₄ Mono-Prop, 100 mN, 220 sec, 10 W, Primex | 0.2 | 0.09 | 4 | 0.007 | 42 | 0.0002 | " | " |
| N ₂ O Resistojet, 500 mN, 150 sec, 300 W, None | 0.3 | 0.2 | 1 | 0.04 | 137 | 0.002 | " | " |
| H ₂ O Resistojet, 270 mN, 182 sec, 600 W, None | 0.3 | 0.1 | 2 | 0.02 | 1127 | 0.0007 | " | " |
| N ₂ H ₄ Resistojet, 360 mN, 300 sec, 610 W, Primex | 0.2 | 0.06 | 1 | 0.03 | 705 | 0.001 | " | " |
| NH ₃ Resistojet, 30mN, 296 sec, 100 W, NIEM-ELKOS | 0.2 | 0.08 | 14 | 0.002 | 1388 | 0.00002 | " | " |
| N ₂ H ₄ Arcjet, 200mN, 500 sec, 1.8 kW, Primex | 0.1 | 0.04 | 2 | 0.01 | 3748 | 0.0006 | " | " |
| NH ₃ Arcjet, 115 mN, 483 sec, 750 W, U of Stuttgart | 0.1 | 0.05 | 4 | 0.008 | 2715 | 0.0003 | " | " |
| NH ₃ Microwave, 300 mN, 550 sec, 1.1 kW, PSU | 0.1 | 0.05 | 1 | 0.02 | 1574 | 0.0009 | " | " |
| Xe Ion, 17 mN, 2585 sec, 440 W, TRW | 0.02 | 0.02 | 25 | 0.001 | 10783 | <u>-0.00003</u> | " | " |
| Xe Hall, 30 mN, 1200 sec, 700 W, MAI | 0.04 | 0.05 | 14 | 0.002 | 9720 | .000002 | " | " |

| | | | | | | | | |
|--|-------|-------|-----|---------|-------|------------------|---|---|
| Cs FEED, 1 mN, 6000 sec, 60 W, Centropazizo | 0.008 | 0.002 | 417 | 0.00007 | 25024 | <u>-0.00008</u> | “ | “ |
| NH ₃ MPD, 23 mN, 600 sec, 430 W, ISAS (Japan) | 0.1 | 0.04 | 18 | 0.002 | 7789 | <u>-0.000008</u> | “ | “ |
| PPT, 4.5 mN, 1500 sec, 120 W, Primex | 0.03 | 0.01 | 93 | 0.0003 | 11109 | <u>-0.00007</u> | “ | “ |

Table 2-7: Comparison of various systems for a high drag (Space Shuttle) experimental volume constrained mission

Table 2-7 shows the results of a volume constrained, high drag orbit mission (200 km). Some of the systems achieve very high performance (e.g. FEED), but they will not be able to move the spacecraft due to their low thrust! The results produced in Table 2- 6 and 2-7 give supporting evidence that a water and nitrous resistojets offer attractive options for small satellite stationkeeping missions if they can be designed at the performance level presented. Thus, a research programme was started for the first time investigation of these systems for low cost small satellite stationkeeping applications.

2.2. *Resistojet History*

This section gives a brief history of resistojets systems. It is a result of a detailed literature survey conducted on past and present resistojets systems. The motivation for the detailed survey is to study past and present systems to help formulate a research plan and system “trade tree” for a new resistojets. The section first discusses past systems that have flown in space and the need for a newer system. A history of water resistojets systems and the problems associated with their research programmes are presented. The section concludes with a discussion of existing flight qualified resistojets systems and their potential problems for small satellite applications.

2.2.1. Past Flight Systems

The first space operation of an electrothermal unit of any kind took place on September 19, 1965, when a tiny resistojets was fired successfully for 30 minutes to slightly adjust the position of the *Vela* nuclear -detection satellite. The design features of this TRW built spacecraft shown in Table 2-8. Figure 2-10 shows a picture of the *Vela* spacecraft.

This section will briefly present the history of flight qualified resistojets systems. Table 2-9 summarises these various systems.

| Spacecraft | Dimensions (mm) | Weight (kg) | Power (W) | Heater | Chamber Temperature (K) | Isp (sec) |
|------------|--------------------|----------------|--------------|---------------------------|-------------------------------|--------------|
| Vela | 50 (o.d.) x 154 | 1.32 | 90 | helical resistance rod | 811 | 123 |

Table 2-8: Specifications of 1st Resistojet –90 W TRW Resistojet for Vela Spacecraft [TRW,98]

| Satellite | 1 st Flight | Flights | Propellant | Power W | Country | Producer | Use |
|----------------------|------------------------|---------|------------------|---------|---------|----------|---|
| Vela | 1965 | 2 | Nitrogen | 90 | USA | TRW | orbit adjustment |
| Advanced Vela | 1967 | 4 | Nitrogen | 30 | USA | TRW | orbit adjustment, attitude control |
| US Navy satellite | 1965 | 5 | Ammonia | 30 | USA | GE | orbit control, attitude control |
| ATS - A,C | 1966 | 2 | Ammonia | 10 | USA | AVCO | experiment |
| ATS-D,E | 1968 | 2 | Ammonia | 30 | USA | AVCO | attitude control |
| Meteor, Resurs | 1970 | ? | Ammonia | ? | USSR | ? | attitude control |
| US Navy satellite | 1971 | 4 | Ammonia | 10 | USA | AVCO | orbit adjustment |
| US Navy Satellite | 1971 | 1 | Hydrazine | ? | USA | AVCO | experiment |
| Sol Rad-10 | 1971 | ? | Hydrazine | 10 | USA | AVCO | ? |
| INTELSA T V | 1981 | 13 | Hydrazine | 350 | USA | TRW | NS stationkeep ing |
| SATCOM IR... | 1983 | 25 | Hydrazine | 600 | USA | Primex | NS stationkeep ing |
| UoSAT-12 | 1998 | 1 | Nitrous oxide | 100 | UK | SSTL | experiment for stationkeep ing |

Table 2-9: Flight Qualified Resistojet Systems [Stuttgart, 98]

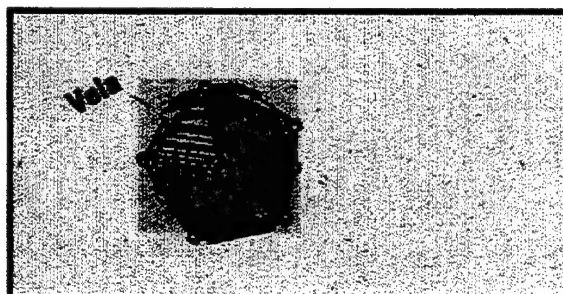


Figure 2-10: Picture of Vela spacecraft from [TRW, 98]

Table 2-8 shows the evolution of resistojets that have flown in space. Nitrogen, due to its ease of handling and thermal characteristics (no evaporation required) was chosen for use on these first spacecraft. Performance and storage density eventually led designers to pursue ammonia (Isp - 300 sec, density - 747 kg/m^3).

Figure 2-11 shows a picture of a 50 W ammonia system built by AVCO Corporation. It uses a molybdenum duct heater. These type of thrusters are used primarily for attitude control since they have to be operated in a pulsed mode.

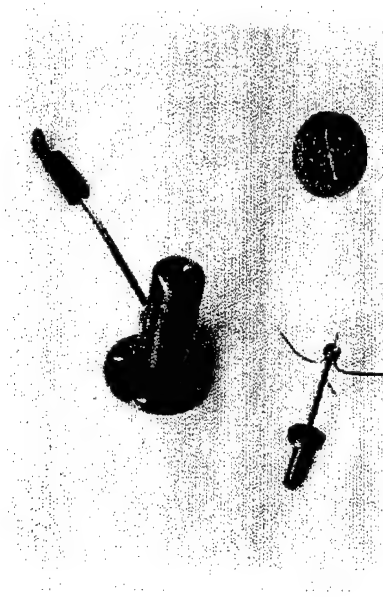


Figure 2-11: Picture of 50 W pulsed resistojet from [Jahn, 77]

Resistojets then evolved to use hydrazine. Hydrazine became quite popular as a chemical mono-propellant due to its capability of decomposing after interacting with a catalyst. Mono-propellant hydrazine systems produce an Isp of ~ 220 sec. If a resistojet is added to increase the chamber temperature and resultant energy of the exhaust stream, the Isp increases to ~ 300 sec with a storage density of 1.01 kg/m^3 . With these performance numbers, hydrazine resistojets have been primarily used for stationkeeping.

Resistojets have also been designed for other working fluids including: methane, hydrogen, water, carbon dioxide, helium, oxygen, air, argon, and combinations of fluids. All of these have initially been tested in some form (laboratory, vacuum, and microgravity conditions), but only nitrogen, ammonia, and hydrazine systems have flown in space. Water was of great interest to NASA for space station applications. Recently it has gained attention by Dornier for a mission to Mercury. Since the ambient spacecraft temperature is on the order of 500 K as the spacecraft gets near Mercury, chemical systems start to decompose making water an attractive propellant. Unfortunately, no flight qualified

systems were ever produced which is discussed in the next section. [Greco, 71], [Zafran, 83], [Morren, 87], [Humble, 95], and [Faulks, 98].

2.2.2. Water Resistojet Systems

Resistojets using water as a working propellant have been considered for stationkeeping several times during the past three decades. Biowaste resistojets, for which water was a candidate propellant, were baselined on the Manned Orbital Research Laboratory (MORL) during the late 1960's, and water resistojets were baselined for orbit maintenance on the Industrial Space Facility (ISF) during the late 1980's. Water was also a candidate propellant for multipropellant resistojets baselined for growth versions of Space Station Freedom (SSF) due to the possibility of reducing life cycle costs. This led NASA Lewis to investigate water resistojets in a programme that lasted from 1987 - 1993. Many hours of test data were obtained on engineering models and prototype thrusters for all of these programmes. Unfortunately, design problems and difficulties, as well as outside political factors caused the programmes to be terminated. A flight qualified system was never developed or flown [Morren, 93A]. Table 2-10 shows all of the design data for these systems. Each of these systems will be briefly discusses in chronological order.

| Designer | Type of Chamber | Dimensions/ Mass | Input Power | Mass Flow Rate/Chamber Pressure | Thrust | Chamber Temp/ Isp |
|----------------------------|---|--|--|---------------------------------------|---------------|----------------------|
| Stone (NASA Lewis) | Straight tube surrounded by heater | L: 113 cm D: 1.09 cm | 70 - 270 kW | 5.7 - 65 g/sec | Not measured | 377 K |
| Stone (NASA Lewis) | Straight tube with helical wire inserts (0.16 mm o.d. with 2 cm pitch) | L: 154 cm D: 1.11 cm | 70 - 270 kW | 7.4 - 13 g/sec | Not measured | 378 K |
| Marquardt Company | Series of concentric tubes- 3 pass heat exchanger using Pt-20 Ir alloy heater. Needed water evaporator for steam operation, cartridge heater surrounded by packed bed of copper | L: 7.62 cm D: 0.95 cm cavity surrounded by 6.35 cm of insulation Water evaporator: L: 5.7 cm D: 2.54 cm | Heat exchanger: 0 - 50 W Water evaporator: 0 - 150 W | 0.5 g/sec 2.5 Bar | 0.044 N | 220 s |
| Rocketdyne and Technion | Grain-stabilised platinum central | 36 channels: 0.05 cm wide, | Heat exchanger : 73 - 602 W | 1.76 - 2.77g/sec 2 Bar | 0.22 - 0.24 N | 115 - 172 s |

| | | | | | | |
|--|--|---|--------------------------------------|--------------------------------------|-----------------|-------------|
| decoupled system | cylindrical heat exchanger inside a platinum sheathed heater No dimensional data given for water evaporator | 0.13 cm deep, 18.8 cm long | Water evaporator: 708 - 470 W | | | |
| Rocketdyne and Technion coupled system | same as above, but no water evaporator | same as above | 198 - 505 W | 0.684 - 1.15 g/sec 2 Bar | 0.078 - .122 N | 117 - 159 s |
| Morren at NASA Lewis | Stainless steel heat exchanger configured to use vortical flow for phase separation | L: 8.4 cm D: 2.3 cm Inconel sheathed heater | 445 - 904 W | 0.104 - .191 g/sec 7 - 22 Bar | 0.170 - 0.360 N | 167 - 192 s |
| Morren at NASA Lewis | Three packed bed heat exchangers - Inconel sheathed centrally located cartridge heater surrounded by sand, 10 μ m sintered 304L stainless steel, and 60 μ m sintered stainless steel | Heater: L: 10.2 cm D: 1.27 cm Chamber: L: 10.2 cm O.D. 2.54 cm Wall thickness: 0.0165 cm | 750 W | .203 - .209 g/sec 4 - 5 Bar | Not measured | 400 - 600 K |

**Table 2-10: History of Water Resistojet Systems [Stone,75], [Halbach,71], [Zafran, 83]
[Morren,93B]**

2.2.2.1. Space Power Research at NASA Lewis

From 1961 - 1971 James R Stone investigated forced-flow once-through boilers for space power applications [Stone, 1975]. His space application was for metallic fluids that could be used for cooling of space reactors, but used water due to ease of testing. This research was very useful in understanding the fundamental operation of forced flow boilers: change in heat transfer rates, flow instabilities, pressure drop across the thrust chamber, and changes in exit steam quality as a function of thrust chamber configuration. Due to the high power levels (kW), the design obviously would not work for small satellite resistojet application.

2.2.2.2. MORL Programme

In the early 1970's the Marquardt Company conducted research on a 44 mN biowaste resistojet. The thruster configuration consisted of an electric resistance-heated 3-pass heat exchanger and a nozzle for accelerating the heated gas. An electrically heated, packed-bed, heat exchanger was used to serve as an evaporator in the tests for water, since the thruster cavity could only function with a gas inlet. Operation of the vaporiser alone and integrated with the thruster was stable in various orientations with respect to gravity, which was believed by the author to indicate compatibility with a low gravity environment. The entire system was tested in vacuum and demonstrated a thrust of ~ 0.1 N and a specific impulse of 220 s. The author lists the following advantages of the system relative to a single tube type resistojet:

- high thermal efficiency for low power consumption
- final gas temperature close to maximum wall temperature for high specific impulse
- minimised stresses in the hottest inner element for long life
- a higher voltage lower current power characteristic.

The disadvantages of the system are:

- some means of automatic power control was required to couple the water vaporiser to the thruster cavity itself
- the thruster requires evaporated steam at the inlet
- the concentric tube design is complex, requires an expansion bellows to maintain cavity geometry
- the thruster cavity itself is made of platinum (expensive)
- no data evaluating gravity sensitivity were reported.

Unfortunately, no lifetime tests and system demonstration tests were conducted (just proof of concept), since the programme was terminated at the cancellation of the MORL programme [Halbach, 70], [Halbach, 71], and [Morren, 93B].

2.2.2.3. NASA Industrial Space Facility and Advanced Development Programme for the Space Station

In the 1980's, water resistojets were investigated again for the Industrial Space Facility and in support of the Advanced Development Programme for the Space Station. NASA Lewis sponsored research with the Rocket Research Company, TRW, Rocketdyne Division of Rockwell International, and Technion. The Rocket Research Company and TRW tested ammonia, nitrogen, and hydrogen using their existing augmented hydrazine thrusters. They did not consider water as a working fluid [Zafran, 83].

Rocketdyne and Technion started a programme with the objective of evaluating the operating characteristics of an engineering model multipropellant resistojet operating on hydrogen, helium, methane, water, steam, nitrogen, air, argon, and carbon dioxide. The design consisted of a central cylindrical heat exchanger inside a coiled sheathed heater (used by the commercial glass industry).

The design life goal was for a minimum of 10,000 hours. Data were obtained for steam operation at a variety of power levels for each of two conditions: steam supplied to the thruster from a water vaporiser and liquid fed directly to the thruster.

The decoupled system (separate boiler) appeared to operate in a manner very similar to the seven gaseous propellant systems since the fluid entering the heat exchanger was already a vapour and required only superheating. Since the range of operating capabilities of the boiler was limited, only one inlet pressure setting was tested (2 bar), although four total power levels ranging from 780 to 1160 W were examined. The system demonstrated a maximum Isp of 184 s at a thrust level of 230 mN, while consuming 466 W in the water vaporiser and 692 W in the thruster. The heater temperature near the nozzle under these conditions was measured to be about 1400 K.

The coupled system required the thruster to act as a boiler and superheater. Therefore, the thruster operated at high temperatures to perform the superheating, causing a large temperature difference between the incoming liquid and the heat exchanger walls. This was an undesirable condition, which calls for a thin layer of liquid in contact with the heat exchanger wall. Such a condition would require a liquid to wall temperature difference on the order of 320 K. However, the room temperature liquid fed directly into the thruster encountered wall temperatures as high as 970 K, which caused the incoming liquid stream to flash to a mixture of superheated vapour and liquid droplets.

The range of stable operation was narrower for the coupled system than for the decoupled system, so the power levels and the thrust levels were highly interdependent. Four power levels ranging from 200 to 500 W, each at a different thrust level, were tested. The coupled system demonstrated a maximum Isp of 159 sec at a thrust level of 84 mN while consuming 289 W. The heater temperature near the nozzle under these condition was approximately 870 K.

The large variations in the data obtained from the coupled system as compared to the decoupled system are due to the relatively low flow rates experienced from the coupled system. These were typically only 1/3 of the flow rates of the decoupled system, so the resulting uncertainty in mass flow rate was much larger for the coupled system. No significant performance advantages were demonstrated for either water feeding scheme over its alternative. Typical times required to reach equilibrium from cold start up were on the order of 90 minutes. Shut down transient response showed similar time constants with cool down to 470 K or less requiring more than 90 minutes without flow through the heat exchanger. Since this data only represented an engineering model thruster, a

programme was developed at NASA Lewis to define the design characteristics of a flight model water resistojets [Morren, 87].

NASA Lewis used the engineering model results from the Rocketdyne / Technion thruster to build their own. They developed a laboratory model to study the concept of a forced-flow, once-through water vaporiser for application to resistojets thrusters. The vaporiser design concept employs flow swirling to attach the liquid flow to the boiler chamber wall, providing for separation of the two fluid phases. This vaporiser was modified with a nozzle and a centrally-located heater to facilitate vaporisation, superheating, and expansion of the propellant, allowing it to function as a resistojets. All of the components, including boiler chamber, superheater, end cap, and nozzle were fabricated from stainless steel. The heater cable consisted of a nichrome centre conductor wire, a layer of magnesium insulation, and an Inconel sheath that was swaged to compact the magnesia insulation around the heater wire. The heater operated at temperatures of ~ 1000 K. Performance was measured at thrust levels ranging from 170 to 360 mN and at power levels ranging from 443 to 904 W. Isp's ranged from 167 to 192 s [Morren, 88]. Further tests revealed the vaporiser to be highly sensitive with respect to gravity. This result stopped work on the design since it would not function in microgravity [Morren, 93A].

2.2.2.4. Space Station Freedom

In 1993, NASA Lewis continued their in-house investigation of water resistojets for drag compensation on Space Station Freedom. They realised that life evaluations of resistojets water vaporisers had not been conducted and therefore started a programme to investigate cyclic endurance tests (up to several thousands of hours) of three packed-bed water vaporisers. The first concept, a sand-filled vaporiser, consisted of a centrally-located cartridge heater surrounded by an annular heat exchanger filled with sand. The heater was rated at 750 W at 120 V, and comprised a nickel-chromium alloy filament, ceramic insulation, and Inconel sheath. Superheated vapour exited the heat exchanger through an outlet tube 41 mm long with a 12.7 mm outer diameter and a 7.95 mm inner diameter.

The other two vaporisers were porous metal-filled. The metal-filled heat exchangers were packed with sintered type 304L stainless steel with packing pore sizes of 10 μm and 60 μm .

The vaporisers were tested for periods of up to 500 hours and 250 thermal cycles. The pressure drop across the sand-filled version increased by 147 percent in 38 hours and 19 thermal cycles. Bonding of the sand granules in the downstream end of the heat exchanger was the suspected cause of failure of

this vaporiser. Pressure drops across two sintered stainless steel-filled versions were more gradual. The 60 μm pore size showed an 80 percent increase in 500 hours and 250 thermal cycles and the 10 μm pore size showed a 20 percent increase in 350 hours and 175 thermal cycles. Two problems occurred with the porous metal-filled vaporisers: corrosion-red-orange powder covered the inlet face and the heater surface. These deposits indicated that rust was formed by reaction of the sintered metal packing with oxygen dissolved in the water. Inadequate thermal contact between the heater and porous heat exchanger packing was believed to have caused an excessive heater-to-heat exchanger temperature drop. This was substantiated by post-test disassembly of one of the vaporisers. NASA Lewis recommended further work to fix these problems and conduct more tests, but unfortunately the programme was not continued [Morren, 93B].

2.2.2.5. Conclusions

There have been several approaches to water resistojet design. None of these research programmes resulted in a flight qualified system. As shown in Table 2-11, there has been considerable work done which has created a number of unanswered theoretical and practical questions.

| Programme | Unresolved Theoretical Issues | Unresolved Practical Issues |
|---|---|---|
| Space Power Research at NASA Lewis | Vapour at the exit (wanted pure steam) | Very high power input (kW), Chamber temperature very low (377K) |
| MORL Programme | No data evaluating gravity sensitivity | Separate evaporator required Only engineering model system developed |
| NASA Industrial Space Facility and Advanced Development Programme for the Space Station | Did not work under microgravity conditions - flow problems Flow stability problems at low flow rates | Only engineering model developed |
| NASA Space Station Freedom | Sand bed sintered together after 10 hours of operation causing the pressure drop across the thruster to become too severe | Low chamber temperature ~350 K Gaps formed between heater and sintered stainless steel Only engineering model developed |

Table 2-11: Unresolved Theoretical and Practical Problems in Past Programmes

2.2.3. Existing Flight Qualified Resistojet Systems

There are two resistojet systems that are flown in space today, a Primex hydrazine system and a NIEM-ELKOS ammonia system. Primex Aerospace Company markets different kinds of hydrazine resistojets that are operational on satellites for various missions. Figure 2-12 shows the MR-502 A resistojet in detail. The specifics of the system are shown in Table 2-12.

| MR-502 A Thruster | Specifications |
|---------------------------|---|
| Thrust | 0.8-0.36 N |
| Pressure | 26.5 - 6.2 bar |
| Isp | 299 sec |
| Minimum Impulse Bit | 88.96 mNs |
| Total Impulse | 524.9 kNs |
| Mass | 0.871 kg |
| Valve power | 8.25 W |
| Valve heater power | 1.54 W |
| Cat bed heater power | 3.93 W |
| Augmentation heater power | 885 - 610 W |
| Steady state firing | 2 hours single firing 370 hours cumulative |

Table 2-12: Primex MR-502 Hydrazine Resistojet Specifications from [Cassidy, 95]

Primex also makes a 350 W resistojet (177 mN) which is the lowest power hydrazine system currently available off-the-shelf [Stuttgart, 98].

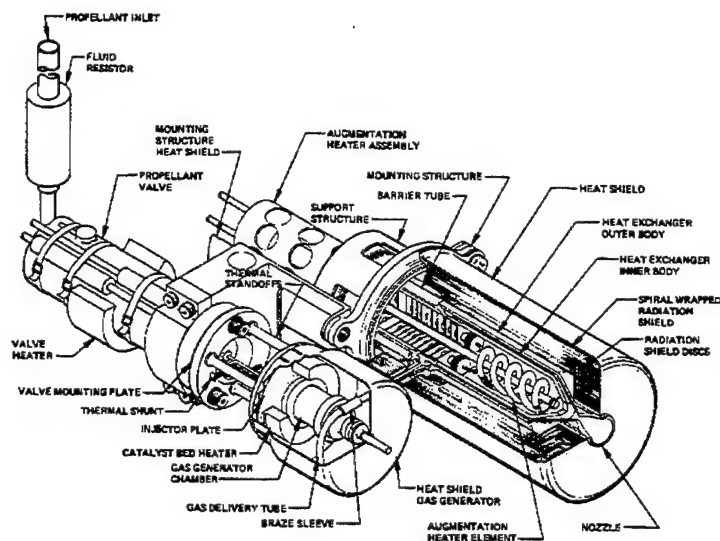


Figure 4. Augmented Catalytic Thruster

Figure 2-12: Primex Resistojet from [Stuttgart, 98]

Several Russian satellites have flown ammonia EHT-15 thrusters. This multi-pass thruster, shown in Figure 2-13, was developed at NIEM-ELKOS. The “cold” propellant can be regulated as it flows through the supply line into the jet and from there is conveyed into the outer chamber. Next the “cold” propellant flows over an insulating powder layer through the porous heating element into the inner chamber. The propellant heated in this way is then released into the nozzle. During operation the electrical resistors reach 2300 K, the insulators and insulating powder reach approximately 2100

K and the heating element 1900 K. The performance specifics for this system are shown in Table 2-13.

| EHT - 15 Thruster | Specifications |
|-------------------|----------------|
| Thrust | 0.05 - 0.03 N |
| Entrance Power | 100 - 450 W |
| Specific Impulse | 296 sec |
| Specific Power | 3300 W/N |
| Total Impulse | 500000Ns |
| Mass | 0.49 kg |

Table 2-13: EHT-15 Specifications from [Stuttgart, 98]

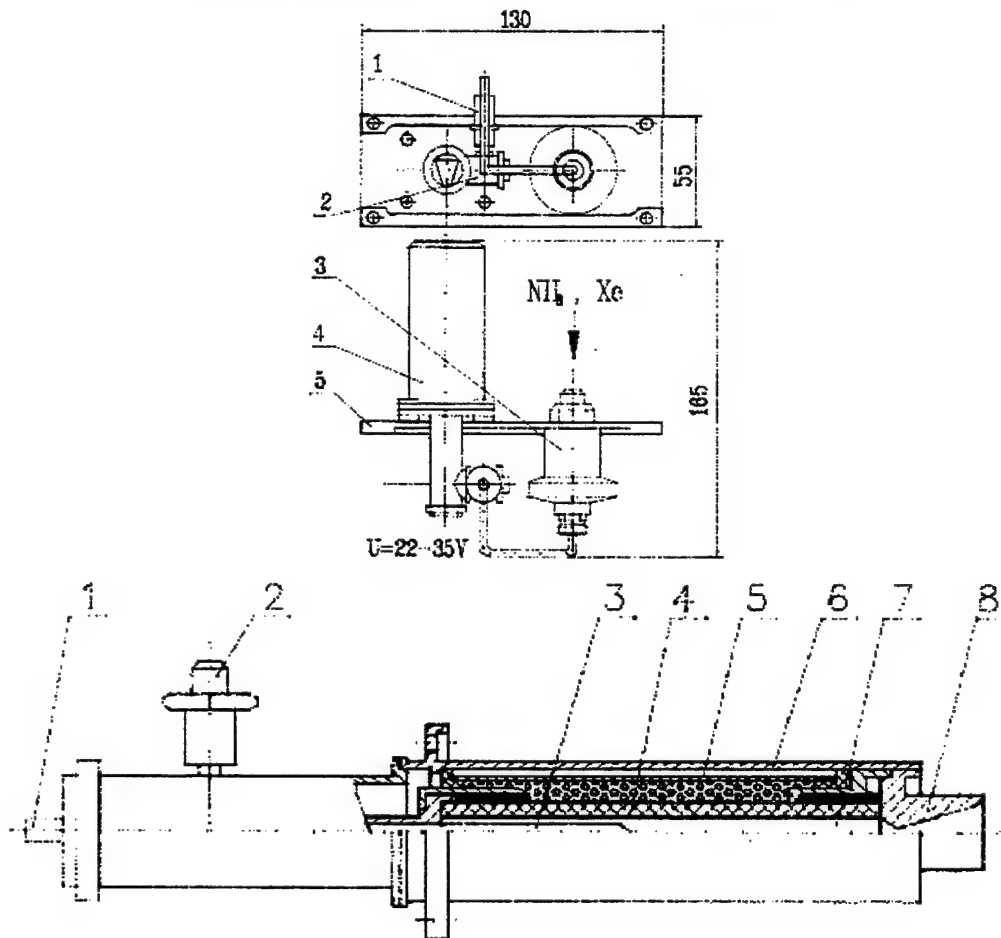


Figure 2-13: EHT-15 Ammonia Thruster from [Stuttgart, 98]

Tables 2-12 and 2-13 show two off-the shelf systems that offer high specific impulse. Due to these performance numbers, they have seen extensive service in the United States and Russia (flown on 75 spacecraft) [CPIA, 98]. However, as shown in Tables 2-6 and 2-7, due to their power requirement and toxic propellant, they may not be best suited for low cost small satellite stationkeeping missions compared to a nitrous oxide or water resistojet system. As described in the last section, there are no off-the-shelf water resistojet systems. There has been no research on nitrous oxide resistojet systems.

Thus, at the start of this research programme, a water and nitrous oxide resistojet looked very attractive as far as cost and safety, if a flight qualified system could be built with comparative performance to the above systems. To develop these systems, a theoretical design approach is needed. A survey of existing models for resistojet design is described in the next section.

2.3. **Resistojet Design Approach**

This section discusses the current state-of-the-art approach to resistojet design. This approach relies on a one dimensional thermodynamic model coupled with empirical data obtained from engine testing. A short discussion on the recent computational models to resistojet nozzle design is also presented.

The current approach to resistojet design and performance assumes a one dimensional adiabatic constant specific heat expansion through the nozzle. This assumption allows the attainable exhaust speed u_e to be solved through a simple energy balance using the first law of thermodynamics :

$$\frac{1}{2} u_e^2 = \frac{1}{2} u_c^2 + C_p (T_c - T_e) \approx C_p T_c \quad (2-18)$$

where:

U_e = exit velocity (m/s)

U_c = chamber velocity (m/s)

C_p = specific heat (J/kg K)

T_c = chamber temp (K)

T_e = exit temperature (K)

The reason Equation 2-18 can be reduced is that the flow speed in the chamber, U_c , and the exit temperature, T_e , are usually negligible in a first approximation. The constant pressure specific heat of the propellant gas per unit mass C_p is seen to be a particularly critical quantity, since it defines the stagnation enthalpy which can be imparted to the gas at a given temperature, and thereby limits the attainable exhaust speed. At first guess, hydrogen seems to be an attractive propellant from this standpoint, since its molecular degrees of freedom and its low molecular weight give it a very high C_p in the temperature range of interest. For example, if we had a chamber temperature of 3000 K, hydrogen has a C_p of 2×10^4 J/kg K at 1 bar pressure. Using Equation 2-18 this gives an exhaust speed, U_e , of 10000 m/s or an I_{sp} of 1000 sec [Jahn, 77].

The thrust that a resistojet can achieve depends on the mass flow that can be efficiently heated and expanded. This mass flow rate scales with the size and chamber pressure of the resistojet. From Equation 2-6, the power is also an important factor. If a resistojet is operating on 30 kW power at 3000 K, the system would produce 6 N of thrust, assuming perfect conversion of the electric power to heat.

However, this system might not be the best first order solution for a small satellite. Table 2-14 presents a comparison of a hydrogen, water, and nitrous oxide systems operating at 100 W. Figure 2-14 shows the density and specific impulse for various working fluids assuming a resistojet chamber temperature of 1000 K.

| Working Fluid | Thrust (mN) | Isp (sec) | Power (W) | Cp (kJ/kg K) | Tc (K) |
|---------------|-------------|-----------|-----------|--------------|--------|
| hydrogen | 37 | 546 | 100 | 14.32 | 1000 |
| water | 93 | 219 | 100 | 2.3 | 1000 |
| nitrous oxide | 141 | 144 | 100 | 1.0 | 1000 |

Table 2-14: Comparison of various working fluids @ 100 W input power (100 % power conversion efficiency) and 1000 K

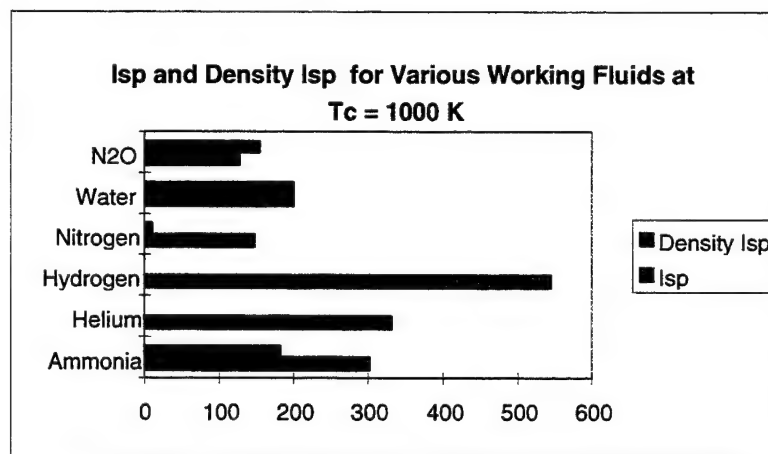


Figure 2-14: Isp and Density Isp for a Resistojet with a Chamber Temperature of 1000 K

Figure and Table 2-14 show the attractiveness of a water and nitrous oxide system. For the same given input power, the water and nitrous oxide systems produce more thrust. Even though their Isp is less than hydrogen, their density Isp is much greater. Since small satellites are volume constrained (i.e. propulsion system must fit in a 300 mm x 300 mm x 110 mm box), a water system would provide double the ΔV for this volume, even though its Isp is 3 times less.

These calculations are good for an initial estimate at performance, but all practical resistojet thrusters depart from the ideal model used in several important respects:

- Flow is not one dimensional
- Temperature, pressure and density gradients in chamber and nozzle which can result in 2 phase flow for some working fluids
- Viscous and thermal boundary layers develop in nozzle
- Power efficiency not 100 %

In previous models, due to the surface heating found in resistojets, the two dimensional effects can usually be handled by semi-empirical fashion and will manifest themselves in relatively small nozzle

inefficiencies or jet profile losses, which detract by approximately 10 % from the ideal exhaust speed. However, if there are severe gas property gradients, then a more rigorous approach is needed to characterise these first order effects.

The second practical departure from ideal performance involves heat loss, mainly by radiation, from the thruster body or jet. This can be regarded as a loss of some fraction of the input electric to thermal radiation, but the actual conversion may occur in several ways:

- heater element transfers some of its input energy to surrounding elements of the thruster which radiate it to space
- hot propellant stream may radiate or conduct heat to the cooler nozzle walls
- viscous dissipation in the nozzle boundary layers heat the nozzle which then radiates to space - discussed in detail in Chapters 4 and 5
- some of the radiant energy in the hot gas flow may escape axially out to the exhaust nozzle

Reduction of such losses to small levels has been handled by intuitive or semi-empirical analysis. Previous designs have used insulation, baffling, and re-entrant gas flow passages to try to increase the heat transfer efficiency [Jahn, 77].

The last and most serious departure of resistojets from the ideal model represented by Equation 2-18, arises from the strong temperature dependence of the specific heats of the propellant gases and the inability of these gases to maintain internal energy equilibrium during their rapid expansion through the nozzle. This effect is defined as frozen flow. Frozen flow occurs in the portions of the flow where the temperature is changing on the local particle time scale compared to the slower internal modes (e.g. vibration, dissociation, ionisation, or recombination). This temperature change may lag significantly behind its equilibrium level, and consequently the enthalpy, and hence the flow velocity, will depart from the equilibrium values.

Since different gases have different properties, it is important to consider the propellant properties and the operating conditions to reduce these losses. There are three possibilities for doing this:

- extend the nozzle length to provide more time for molecular recombination
- operate at a higher pressure level to increase the recombination rate
- use other propellants with less tendency for frozen flow losses

Previous investigators have addressed these frozen flow problems. From practical experience, it has been determined that protraction of the nozzle normally reduces frozen flow losses less than it increases viscous thermal losses. However, nozzle throat size is important in this trade which is discussed in detail in Chapters 4 and 5. High-pressure operation is a more attractive solution, and may improve performance in other respects. Increasing the chamber pressure lowers the dissociation level in the chamber and increases recombination rates in the nozzle. In addition, it improves heat

transfer to the flow from the heater surfaces, reduces radiation losses by increasing the optical depth of the hot gas, and permits a smaller chamber and nozzle for a given flow. The negative impacts of a higher chamber pressure are a bigger expulsion system is required and higher mechanical stresses on the chamber walls [Jahn, 77].

The last and obvious way to improve frozen flow losses is in the choice of propellant. As shown in Figure 2-15, frozen flow losses, and resultant impact on I_{sp} , depends on the working fluid. This is another important factor to consider in the system design process.

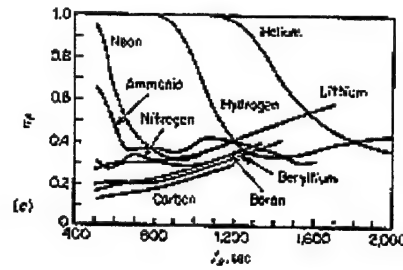


Figure 2-15: Frozen flow efficiency versus I_{sp} for various working fluids from [Jahn, 77]

In conclusion, the basic problems that need to be addressed in the analytical phase of resistojet development are:

- heat transfer from the resistance element to the gas stream - there are various means of heat transfer which will be addressed in Section 2.5
- radiation losses from the complete assembly (viscous induced)
- high temperature materials technology - higher T_c gives better performance from Equation 2-18, but is limited to the thermal properties of the chamber material
- frozen flow losses

Unfortunately, there has not been much research conducted in the theoretical analysis of resistojets. Analyses become cumbersome in the geometry and temperature ranges of interest for different resistojets. Since the flow in the chamber is usually laminar, the heat transfer to the fluid stream is primarily by conduction, and closed-form solutions for simple geometries would be possible if the gas flow were calorically ideal. Unfortunately, the specific heat, thermal conductivity, and gas density all vary substantially with temperature. This requires iterative procedures to achieve self-consistent solutions. Thus the current state-of-the-art analytical approach has been to assume that the detailed solution of the gas dynamic heat transfer is not critical to implementation of a particular resistojet concept. Generally, a few experimental surveys using the desired propellants with various heater and chamber dimensions will lead directly to an adequate optimisation of the geometry and bulk flow parameters for a given system. A similar situation prevails with respect to thermal radiation losses from the resistojet design [Jahn, 77].

There are three examples of this empirical based approach to resistojet design (There are other electric propulsion system models in [Humble, 95], but they do not go to the detail of these models). Zafran presents the first in 1985. Zafran used the TRW flight qualified HiPEHT hydrazine thruster (augmentation heat exchanger after catalytic decomposition of the hydrazine) to characterise the performance of other propellants. This design used a double helix heater with a vortex heat exchanger. He tested nitrogen, ammonia, and hydrogen at varying mass flow rates whilst holding the input power to ~ 500 W. Table 2-15 shows equations Zafran derived from the empirical test results.

| Working Fluid | Equation where: P= Power (W) F= Thrust (mN) Isp = Specific Impulse (sec) | Error bar (%) | Overall Heat Transfer Efficiency (%) Output Energy / Input Energy |
|---------------|--|------------------|--|
| Nitrogen | $I_{sp} = 80 + 20(P/F)$ | 13.9 | 73 |
| Ammonia | $I_{sp} = 110 + 15(P/F)$ | 8 | 51.5 |
| Hydrogen | $I_{sp} = 294 + 15(P/F)$ | 6.1 | 61 |

**Table 2-15: Performance prediction for HiPEHT Resistojet based upon empirical results
[Zafran, 85]**

These empirical curve fits work well for most of the possible operating regimes of the thruster. There were problems operating the thrusters at low flow rates for all of the propellants (sharp reduction in efficiency). Zafran attributed this to flow separation, viscous losses in the low mass flow rate nozzle, or poor heat transfer in a low-density vortex flow field. He did not investigate this further and omitted all of the low flow rate data in his analysis. His recommendations for further design improvement were to add a preheater at the inlet to raise the exhaust gas temperature at high flow rates [Zafran, 85].

Even though Zafran's thrusters achieved high performance, efficiency, and produced performance prediction equations, there are several issues with just using empirical data for explanation of thruster operation. Zafran was not able to characterise the performance at low flow rates (applicable to small satellites due to low input power). Therefore, his curve fits do not explain or predict the decrease in performance if the thruster was operating in this low flow region. Zafran did not specify operating pressure or exact input power with each run, which could also be factors in changing the performance prediction equations produced.

Aston of the Electric Propulsion Laboratory, Monument, Colorado, USA, presented a semi-empirical model that describes the operating characteristics of resistojet engines. He only considered hydrogen

as the propellant due to its high specific impulse. He derived specific engine design and performance correlations from 7 different resistojet engineering model systems. One was designed at 30 kW, two at 3 kW, one at 16 kW, and 3 at a 44 mN thrust level. From this Aston was able to formulate the design enthalpy as:

$$\frac{Pe}{\dot{m}} = 1.183367 \times 10^7 e^{(1.4668 \times 10^{-3} I_{sp})} \quad (2-19)$$

where:

Pe = input power (W)

\dot{m} = mass flow rate (kg/s)

I_{sp} = specific impulse (sec)

From this, a relationship was developed to determine the nozzle gas temperature at the design operating condition:

$$T_g = \left(\frac{Pe}{\dot{m}} + 1.69266 \times 10^7 \right) / 2.2685 \times 10^4 \quad (2-20)$$

where:

T_g = Gas temperature (K)

Pe = input power (W)

\dot{m} = mass flow rate (kg/s)

Gas viscosity at the throat was determined from curve fitting hydrogen properties and using the throat gas temperature:

$$u = 1.69808 \times 10^{-7} \times T_g^{0.69488} \quad (2-21)$$

where:

T_g = gas temperature (K)

u = gas viscosity (Pas)

The viscosity can then be used to determine the Reynolds number for hydrogen:

$$Re = \frac{(4.0\dot{m})}{\pi d_{th} u} \quad (2-22)$$

where:

\dot{m} = mass flow rate (kg/s)

d_{th} = nozzle throat diameter (m)

μ = viscosity (Pas)

Re = Reynolds number (no dimensions)

Aston then determined the nozzle specific impulse efficiency as a function of the Reynolds number and nozzle area ratio:

$$\eta_{Isp} = Re / ((\epsilon / 8.144 \times 10^{-2} + \epsilon 8.818 \times 10^{-3}) + 1.107 Re) \quad (2-23)$$

where:

ϵ = nozzle expansion ratio (exit area/throat area, no dimensions)

Re = Reynolds number (no dimensions)

η_{Isp} = nozzle specific impulse efficiency (no dimensions)

He finally determined the thermal efficiency by correlating experimental measurements on the thrusters and averaging the results for the different power levels:

$$\eta_{th} = 0.9297 + 1.269 \times 10^{-6} P_e \quad (2-24)$$

where:

η_{th} = input power/output power (no dimensions)

P_e = input power (W)

Aston's model correlated well with an engineering model Space Station thruster. The results are shown in Table 2-16.

| Model | Thruster |
|-----------------------------|----------------------------|
| Thrust 0.09943 N | Thrust 0.0979 N |
| Efficiency 0.43357 | Efficiency 0.4318 |
| Mass flow rate 0.02029 kg/s | Mass flow rate 0.0202 kg/s |

Table 2-16 Comparison of Aston's Model vs Engineering Model Thruster [Aston,89]

However, there are still problems with Aston's more detailed approach. If Zafran's test data is applied for hydrogen to Aston's model, the results are off by a factor of 2 - 6 with respect to specific impulse, using input power and mass flow rate as the input variables (Equation 2-19). This shows the crutch of relying heavily on empirical data for performance prediction. If a case is discovered that was not used in the model, there is a potential for erroneous results.

The last approach to modelling performance is the use of detailed numerical models. Boyd has looked at this work at the University of Cornell. He has used the direct simulation Monte Carlo (DSMC) method to model gas flow through small nozzles. The computational method captures the nonequilibrium effects in the nozzle flow field. He used the Primex hydrazine resistojets for experimental data. Data are taken along the axis and the exit plane of the resistojets nozzle. Comparison of the numerical and experimental results give good agreement, the model consistently over predicts specific impulse by 10 %. For the complex flow fields involved, predicting performance within 10% is considered a good result [Boyd, 96].

Boyd's approach is unique in that it characterises the nozzle performance purely from the physics, there is no reliance on empirical data, except for model comparison purposes. The model has also been used for predicting plume impingement. Since the data does not rely on empirical data, it has the potential to be expanded to other systems. The limitations of the method is that it can only be used for nozzle flow, and not resistojets chamber design.

In summary, the existing resistojets models have produced good results for their specific systems, but with the limitations as discussed above. Thus, none of these models could be used for a new resistojets satellite application. Based upon these results, a new model is needed for resistojets conceptual design.

Earlier discussions showed that there is some merit in water and nitrous oxide resistojets for small satellite application. Since water resistojets operate in an unique environment (2-phase flow, change in heat transfer characteristics through the boiling phase, flow stability), a survey is needed to study the boiling and heat transfer relationships in a water system. This survey will allow a better understanding of these unique heat transfer relationships and is needed before a detailed model can be developed.

2.4. Boiling / Heat Transfer

The use of water (or any other liquid) as a resistojets propellant differs significantly from gas, primarily due to the requirement that the fluid undergoes a phase change before useful thrust can be obtained. This is especially true for water due to its low vapour pressure. Steam table data show [Morren, 88] that ~0.52 MJ/kg are required to bring water from a storage temperature of 290 K to saturation temperature at a boiler chamber pressure of 4 bar. Vaporisation of liquid water at that pressure requires an additional 2.13 MJ/kg. Although the energy requirements for preheating and vaporisation are individually insensitive to ambient pressure, their sum is highly sensitive to pressure.

The water resistojet must expend a large quantity of power for vaporising the propellant over its entire operating range. Still more power must be expended to superheat the vapour, since expansion of saturated vapour to a hard vacuum would likely result in condensation in the nozzle. A typical breakdown of the power input in previous designs is shown in Figure 2-16.

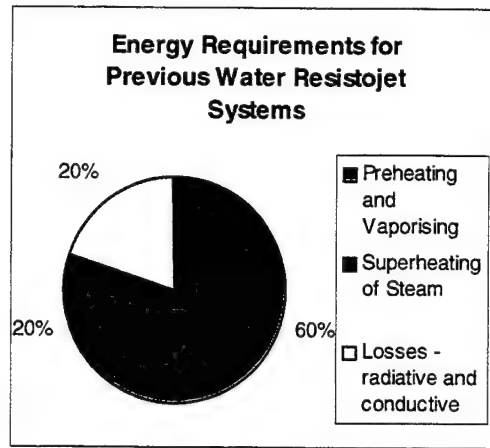


Figure 2-16: Energy Break Down for Previous Water Resistojet Systems [Morren, 88]

Therefore, the heat transfer efficiency for water resistojet systems will be lower compared to other systems due to the vaporisation energy requirement. To design for the highest efficiency, it is first important to understand the theory behind water resistojet operation. Most of the theory can be derived from fundamental boiler theory.

The boiler required for application to water resistojets is the forced-flow, once-through type, in contrast to the simpler and more common pot type boilers you have at home. To integrate with a continuous-flow propulsion system, the liquid is converted into superheated vapour in a single pass through the boiler. In this process, the following information is important:

- two-phase heat transfer and pressure drop
- definitions of various boiling regimes
- predictions of critical heat transfer conditions such as the "boiling crisis" and critical flows
- requirements for thermal and hydraulic stability

Liquid boiling research was conducted in the 1960's and early 1970's for space power applications and is summarised by [Stone, 75]. A brief description of the basic considerations important to the design of a forced flow, once-through boiler is addressed below.

During the boiling of a fluid flowing through a channel, several heat-transfer regimes are encountered. A typical case is illustrated in Figure 2-17. The liquid water enters the channel and is heated in the liquid phase to the point where bubble nucleation first occurs. Nucleate boiling continues until enough vapour is generated such that the resulting increase in velocity is sufficient to suppress

nucleation. Beyond this point, heat is added to a thin liquid film and vaporisation occurs at the liquid-vapour interface. Throughout these boiling regimes, liquid is being entrained in the vapour core. In spite of any redeposition of liquid from the core to the film, at some point there is no longer sufficient liquid to wet the wall, and the liquid film breaks down. This results in a large reduction in heat transfer coefficient, often more than an order of magnitude. This transition has been termed “boiling crisis”, “departure from nucleate boiling”, “onset of dry wall boiling”, and “burnout”. This film breakdown is generally followed by a transitional regime wherein a considerable amount of liquid remains on the wall. Eventually, only a few droplets remain on the wall, and most of the heat added through the wall goes into heating the vapour. It then becomes difficult to vaporise the remaining droplets.

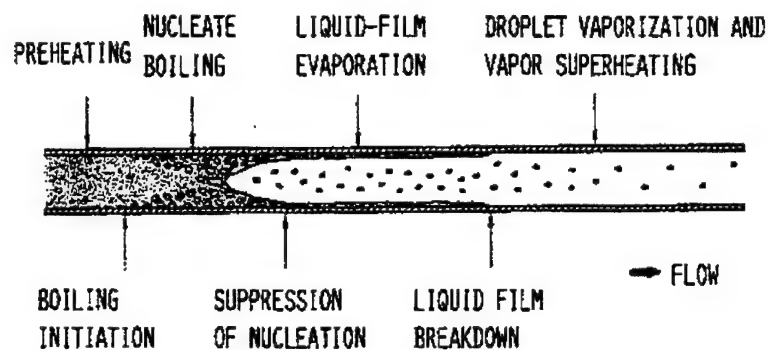


Figure 2-17 Typical Heat -Transfer Regimes for Boiling in Flow Channel from [Stone, 75]

To design a forced-flow boiler, it is necessary to be able to predict the heat-transfer and pressure-drop characteristics in each of these regimes. This problem is complicated by the wide variety of possible two-phase flow regimes and by various thermodynamic nonequilibria such as *subcooled boiling*, *liquid bulk superheat*, and liquid droplets in superheated vapour. These terms are described later in this section. It is also very important that the boiler not interact with other components of the flow system to produce instabilities.

The problem of boiler instabilities is quite serious in systems using forced flow, once-through boilers. Such instabilities lead to poor performance of the system, flow oscillations, and can even cause failure. Lowdermilk, Lanzo, and Siegel [Stone, 75] found that flow oscillations can cause a large decrease in the heat flux at the boiling crisis. This instability can be prevented by restricting the flow upstream, thereby decoupling or isolating the boiler from the upstream liquid, which can also contain vapour or gas voids. Stone also discovered that changing the nozzle geometry has an impact on the instabilities. Thus, the boiler feed system, inlet, and exit geometry are all-important to instabilities.

To initiate vaporisation in a liquid, either the pressure must be lowered below saturation pressure or the temperature raised above the saturation temperature. Surface boiling with the liquid bulk temperature less than saturation is termed *subcooled boiling*. When vaporisation is achieved by lowering the pressure of the liquid below saturation, the term *liquid tension* is usually used to describe the non-equilibrium condition before vaporisation occurs. If the liquid bulk temperature is considerably above saturation temperature it is called *bulk superheat*. These regions are shown in Figure 2-18.

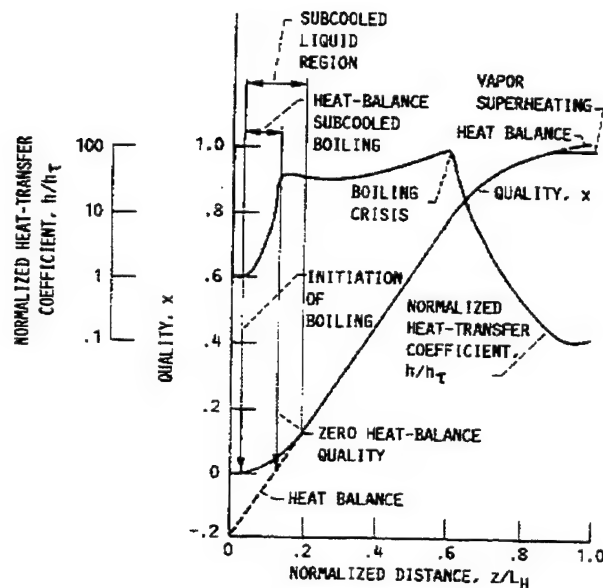


Figure 2-18 - Typical Boiling Heat-Transfer Performance from [Stone, 75]

Although there have been numerous studies of boiling heat transfer, there is still no generally applicable means of prediction available, especially for high-density-ratio fluids such as low pressure water. This is especially true of the subcooled boiling regime, where non-equilibrium effects are important [Morren, 88]. Seventeen different boiling heat transfer correlations have been studied in this survey. None of them are applicable to resistojet design either due to the wrong thermodynamic conditions (pressure, mass flow rate, temperature, and power) or geometry of the boiler [Tong, 65]. Typical variations of the boiling heat transfer coefficient and quality with axial distance through a boiler are also shown in Figure 2-18. The heat transfer coefficient is normalised to the all-liquid value. Boiling heat transfer coefficients are much higher than the liquid values prior to the boiling crisis and then decrease rapidly with distance, eventually reaching a value on the order of the gas heat transfer coefficient. Three heat transfer regimes are defined in Figure 2-18:

- the subcooled regime, from the inception of boiling to zero heat-balance quality
- net-quality boiling prior to the crisis

- the post-crisis regime.

A multitude of flow patterns is conceivable for two phases flowing concurrently, as is the case in a boiler tube. This makes it difficult to develop reliable correlations of two-phase pressure drop, heat transfer coefficient, and boiling crisis. Each depends on the geometry and flow characteristics of the individual system. "Bubbly", "slug", "stratified", "annular flow" are all examples of these types of flow and is shown in Figure 2-19.

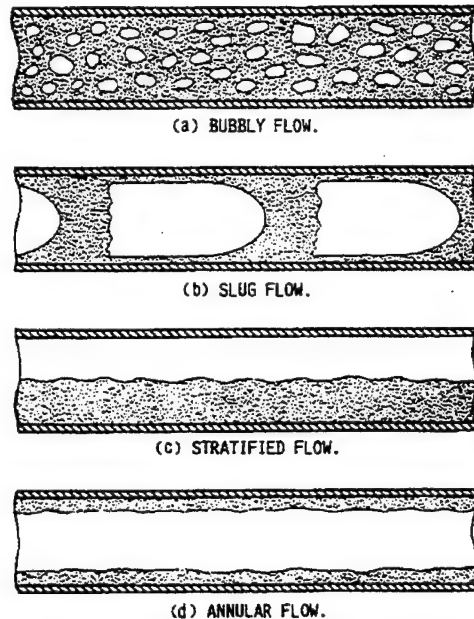


Figure 2-19 Typical Two-phase Flow Patterns from [Stone, 75]

The longer the boiling crisis heat transfer phase is postponed, the better for the system based upon the increased heat transfer. The importance of postponing boiling crisis poses special problems for operation in low-gravity environments, since insuring liquid-solid adhesion requires some local application of an attractive force (i.e. acceleration or liquid surface tension). The need to maintain proper solid-liquid contact can be avoided, if the liquid is heated radiatively. [Morren, 88] revealed that nearly all of the incident radiation not reflected at the liquid-vapour interaction will be absorbed by a thin film of liquid for source temperatures on the order of 1000 K.

The last fundamental concept to address is drying of the vapour. In space applications, the flow through the exit needs to be completely vaporised due to sublimation when it reaches the vacuum of space. In order to dry the vapour, the two-phase mixture is often swirled within the boiler, thus centrifuging the liquid to the heated wall, where it can be vaporised. Swirling or vortexing the flow has also shown to increase the critical heat flux by 2.5 times more than for straight flow [Tong, 65].

This swirl has generally been obtained by means of inserts in the chamber (materials whose configuration cause the fluid/steam mixture to swirl). There are several examples of this inserts:

1. helical wire placed in the middle of a tube
2. by coiling the tube that the fluid/steam flows through
3. by a combination of inserts and tube coiling
4. rotating the boiler
5. the cyclone boiler concept.

Tube coiling and inserts increase vapour drying, but they can increase pressure drop significantly and tend to promote *rivulet flow* (vapour superheat with liquid still present), which is an unsteady flow condition. Rotating boilers are advantageous due to their insensitivity to gravity field and orientation. However, they require moving parts and rotating seals. The cyclone boiler concept represents an attempt to exploit the benefits of the rotating boiler without the need for moving parts. The liquid or two-phase feed mixture flows into the boiler chamber tangentially in such a manner that a vortex flow pattern is established, and vaporises due to the pressure drop across the inlet as well as heat applied through the chamber wall. The liquid is centrifuged to the wall, and is then driven toward the apex of the cone by secondary flow effects augmented by surface tension. NASA Lewis Research Centre tried this concept and ran into problems with the liquid film not adhering to the wall, thus wall temperatures tended to rise several hundred degrees above saturation level, reducing the heat transfer efficiency [Morren, 88]. A final (and more obvious) approach is to design a thruster that has enough heat transfer efficiency or swirling built into the heater, giving the water enough energy to completely vaporise.

Now that all of the relevant background theory has been introduced, the next section will address the new design approach followed in this research programme. This approach is used for the first thruster design and is then improved with subsequent empirical test results to improve the thruster design and model.

2.5. New Design Approach

As introduced in Section 2.1, a nitrous oxide and water resistojet are attractive options for small satellite stationkeeping missions. This section discusses the design approach to develop these thrusters. The first design item was the theoretical performance of the system as a function of different thermodynamic conditions in the chamber. While this describes the theoretical result from the standpoint of pure chemistry, achieving these conditions with high efficiency is the engineering challenge.

A good approximation for calculating theoretical performance is the Isp code developed by Curt Selph [Selph, 92] at the Air Force Research Laboratory Rocket Propulsion Directorate. This is a

thermochemistry equilibrium code that allows the user to enter working fluid thermodynamic conditions in the chamber and it will calculate the performance through the nozzle. Table 2-17 summarises initial performance for various working fluid conditions. These conditions were analysed for the following reasons:

- 10 bar is the available feed pressure from UoSAT-12
- material considerations: stainless steel represents a low-cost option and it starts to degrade rapidly in stress properties if its temperature is above 1200 K
- Past resistojet programmes have had heater temperatures from 1000 - 1700 K
- heat transfer efficiency varies from 25 - 50 %

All of the calculations assumed a nozzle expansion ratio (exit area : throat area) of 100:1 and an ambient pressure of 8×10^{-5} Bar.

| Working Fluid Conditions; Tc - Chamber temperature (K) Pc -Chamber pressure (Bar) | Tc 700 Pc 2.5 | Tc 700 Pc 10 | Tc 800 Pc 2.5 | Tc 800 Pc 10 | Tc 900 Pc 2.5 | Tc 900 Pc 10 |
|---|------------------|-----------------|------------------|-----------------|------------------|-----------------|
| Water Isp (sec) | 166 | 168 | 175 | 177 | 185 | 185 |
| Nitrous Oxide Isp (sec) | 117 | 117 | 126 | 126 | 134 | 134 |

Table 2-17: Initial Performance Calculations

The next issue to address is the power and mass flow required to produce the chamber conditions shown in Table 2-17. From Equation 2-6, if it is assumed the input electrical powers range from 10 W - 560 W (at 100 % heat transfer efficiency), a thrust in the range of 10 mN - 1 N is achieved for the conditions in Table 2-17. To relate input power to mass flow rate and temperature, the first order power requirement can be obtained from a simplification of the First Law of Thermodynamics:

$$Q = \dot{m} \times C_p \times \Delta T \quad (2-25)$$

where Q = Power (W)

\dot{m} = mass flow rate (kg/s)

C_p = gas heat capacity (J/kg K)

ΔT = Final gas temperature - initial temperature (K)

This is not a straightforward calculation based upon the changes in heat transfer rate as the water evaporates (two phase flow). Nitrous oxide enters the chamber as a gas due to controlling the flow conditions as it is expelled from the tank at its 48 bar vapour pressure (function of temperature) to the

10 bar chamber. The heat capacity for water is obtained by averaging the heat capacities over the entire temperature and pressure operating range- 2060 J/(kg K). This approach is discussed more thoroughly in [Todreas, 90]. It served as the best approximation and can be compared to the experimental results obtained. The heat capacity for nitrous oxide is 1000 J/kg K. Using Equation 2-25, Figure 2-20 shows the mass flow rate required as a function of power for a 100 % efficient operating engine operating from powers of 10 - 560 W and a chamber temperature of 900 K.

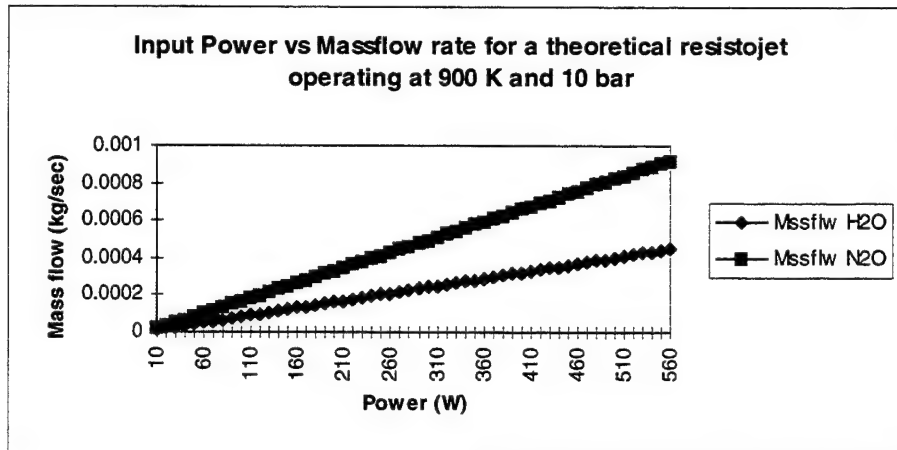


Figure 2-20: First-order Resistojet Massflow Requirements as a Function of Power

The mass flow rate generated from Equation 2-25 is used to design the nozzle in the C^* equation. C^* is a function of the propellant characteristics and chamber design. There are two ways it is expressed:

$$C^*_{measured} = \frac{P_c A_t}{\dot{m}} \quad (2-26)$$

$$C^*_{theoretical} = \frac{\sqrt{\gamma R T}}{\gamma \sqrt{\left[\frac{2}{\gamma+1}\right]^{\frac{\gamma-1}{\gamma+1}}}} \quad (2-27)$$

where:

C^* = characteristic exhaust velocity (m/s)

P_c = chamber pressure (Pa)

A_t = throat area (m^2)

\dot{m} = mass flow rate (kg/s)

γ = ratio of specific heats

R = specific gas constant (J/kgK)

T = chamber temperature (K)

The theoretical C^* is calculated based upon the working fluid thermochemistry and chamber temperature. It is used in Equation 2-26, along with the mass flow rate and chamber pressure, to calculate the nozzle throat area. For the conditions shown in Figure 2-20, the C^* equations predict that nozzle throat diameter varies as a function of mass flow rate from 0.1 mm to 0.8 mm. These equations show the “exit orifice” needed to support the desired chamber conditions.

Once the nozzle throat is determined, a relation is needed to determine the exit diameter. Equation 2-28 shows the expansion ratio of the nozzle.

$$\varepsilon = \frac{A_e}{A_t} \quad (2-28)$$

where:

A_e = nozzle exit area (m^2)

A_t = nozzle throat area (m^2)

The exit area is determined by the expansion ratio. Figure 2-21 shows the area ratio versus the specific impulse for a water resistojet operating at a chamber temperature of 900 K, chamber pressure of 4 bar, and an ambient pressure of vacuum. This analysis also used the Isp code developed by [Selph, 92]. Figure 2-21, shows that the Isp increases as a function of the area ratio. It also shows that after a ratio of 100:1, the increase changes from exponential to linear. A 100:1 to ratio also is a realistic manufacturing limit based upon the small throat diameters. Varying the chamber temperature and pressure predict similar theoretical results to Figure 2-21.

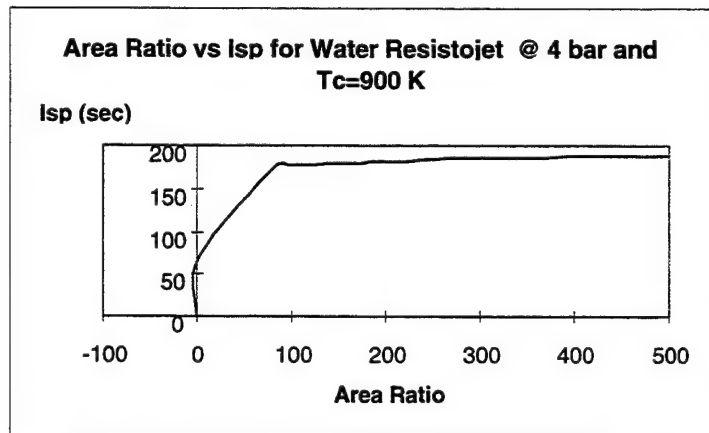


Figure 2-21: Isp vs Area Ratio for a Water Resistojet Operating @ 4 bar and a Chamber Temperature of 900 K

Now that the thrust, I_{sp} , and nozzle size have been predicted based upon the input power, mass flow rate, temperature, and pressure for the nitrous oxide and water working fluids, the optimum heat exchanger to produce these conditions is needed.

Based upon the literature survey, there have two approaches to thruster configuration:

1. A decoupled system where two separate units provide for the evaporation of the fluid and the superheating of gas.
2. A coupled system where a single unit provides the evaporation and produces high temperature gas for a high temperature rocket exhaust.

It is deduced that a coupled system would be the best design to pursue first to meet small satellite applications due to the following reasons:

- Power: lowest total power system to date is 781 W, evaporator has operated at 466 W or higher [Morren, 87]
- Volume: small satellites have tight constraints, e.g. mounting area for MightySatII.1 is 100 mm x 180 mm
- Stability: past designs have experienced flow problems with the evaporator causing feedback problems to the super heating chamber [Morren, 87]

There are several approaches to coupled system design. Table 2-18 presents these various options. If the heat exchanger is designed properly, the propellant temperature will closely approach the temperature of the heater element prior to expulsion through the nozzle. This is accomplished by placing the heater element in a flow field where the radial and axial velocities are much smaller than the tangential velocities. This phenomenon can also be described as “stay time”. High gas velocities across the heater surface are maintained while residence times of the gases contacting the heater are extended, both factors increase heat exchanger efficiency. The term used to define this type of flow, is called *vortical flow*.

There are several ways to induce a *vortical flow* field. The engineering challenge is to induce the field without a high ΔP (pressure drop). A large ΔP effects heat transfer, flow instability, and consequently overall performance. Table 2-18 shows the various approaches to meet this design challenge.



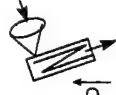
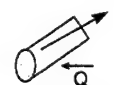
| System | Advantages | Disadvantages |
|--|--|--|
| Tube with helical inserts  | Simple | Low efficiency Pressure drop - UoSAT 12 has low pressure system: ☹️ |
| Heated Tube  | Simple | Very low efficiency - needs high power (kW) or very high volume: ☹️ |
| Flow swirling Induced by Geometry  | Engineering model systems have been successful | Complex, Have had flow problems under microgravity conditions: ☹️ |
| Packed Beds  | high performance, low complexity, flexibility | hot spots, material problems, thermal cycling, flow instabilities: ☹️ |

Table 2-18: Initial Design Trades

Previous designs have had problems producing *vortical flow*. Straight tubes have low efficiency. Previous designs by [Stone, 75] required kW of power. Helical inserts have had flow problems. Experimental data collected by [Stone, 75] produced a ΔP of 2.4 bar at a mass flow rate of 10 g/s @ 300 K. They also demonstrated flow instabilities due to *rivulet* flow. Self-induced flow swirling due to the geometry of the thruster (cyclone concept) worked well in engineering model tests, but failed under microgravity conditions. Packed beds have worked well in microgravity, but have had flow instability problems at low flow rates and material interaction problems [Morren, 93B].

Based upon Table 2-18, packed beds look like a resistojet concept worth further study for small satellite application. The advantages of packed beds are:

- high surface area for high heat transfer
- high power density
- low complexity
- packing density can determine pressure drop

Unfortunately, beds also have several disadvantages:

- high heat transfer can cause material problems (melting)
- has potential for non-uniform heat transfer (hot spots)

- thermal cycling can cause voids in the bed producing hot spots
- choice of bed material may lead to *channelling*
- low flow rates can produce flow instabilities due to friction losses or viscosity

Even though past work on past bed concepts for resistojet application encountered some problems, the high performance potential at low cost made them worth further study. To prove the hypothesis that bed concepts offer the best solution to small satellite application, a thermal model had to be developed to compare the potential of the new design with other concepts. The packed bed model was developed first. Several correlations were needed for the bed model.

The *Ergun Pressure Drop Correlation* is an expression for the flow pressure loss in a packed bed.

$$\frac{dP}{dr} = 150 \frac{(1-\epsilon)^2}{D_p^2 \epsilon^3} \mu u_s + 1.75 \frac{1}{\sqrt{150 \epsilon^3}} \times \sqrt{150 \frac{(1-\epsilon)^2}{D_p^2 \epsilon^3}} \times \rho u_s^2 \quad (2-29)$$

where:

μ = fluid viscosity (Ns/m²)

D_p = particle diameter (m)

u_s = superficial or free stream fluid velocity (m/s)

ρ = fluid density (kg/m³)

ϵ = gas volume/total volume (packed bed porosity-no units)

P = pressure (Pa)

r = bed radius (m) [Witter, 93]

Equation 2- 29 is a combination of viscous and kinetic energy loss terms. It was derived with consideration given to

- rate of fluid flow
- viscosity and density of the fluid
- closeness and orientation of the packing
- size, shape, and surface of the particles.

There are multiple equations for the heat transfer in packed beds that could be used, but the correlation developed by Achenbach has become the most widely used relation for high power density and small particle sized beds which is best for the volume and power constrained small satellite application. The heat transfer coefficient from the solid bed surface to the bulk gas can be expressed by:

$$\begin{aligned}
 h_i &= Nu \frac{k_b}{D_p} \\
 Nu &= \frac{1-\varepsilon}{\varepsilon} \left[0.622926 \left(\frac{Re}{1-\varepsilon} \right)^{2.32} + 6.44603 \times 10^{-4} \left(\frac{Re}{1-\varepsilon} \right)^3 \right] Pr^{0.33} \\
 Re &= \frac{\rho D_p u_s}{\mu} \\
 Pr &= \frac{\mu C_p}{k_b}
 \end{aligned} \tag{2-30}$$

where:

D_p = particle diameter (m)

C_p = heat capacity of the fluid (J/kgK)

ε = bed porosity (no dimensions)

ρ = fluid density (kg/m³)

μ = fluid viscosity (Ns/m²)

u_s = superficial or free stream fluid velocity (m/s)

k_b = bulk gas conductivity (W/mK) [Witter, 93]

These equations are used for preliminary sizing of the bed, once the energy input is determined.

There are several approaches for energy input into the bed :

- mount a high temperature resistive heater in the centre of the chamber and surround it with the bed material
- use highly conductive bed materials and a geometrical configuration that allow the electrical energy to be directly input into the bed.

From [Lawrence, 93] the latter method has been tried using a rolled screen wire mesh. This design showed high heat transfer efficiency, but had overheating problems and short life span. Similar concepts tried by [Maize, 93] also had short life spans. The first approach is also simple and uses readily available materials. Thus, it was chosen for the energy input for the bed material model.

The steady state equations and material temperatures are found from an energy balance across the entire control volume (heater and bed):

$$\ddot{q}_s V_s - U_T A_h (T_s - T_b) = Q_s - U_s A_h (T_s - T_w) - h_t A_h (T_w - T_b) = 0.0 \tag{2-31}$$

where:

\ddot{q}_s = power density in solid material (GW/m³)

V_s = solid material volume (m^3)

U_T = overall heat transfer coefficient based on mean temperature of solid (W/m^2K)

A_h = heat interface area (m^2)

T_s = solid material average temperature (K)

T_b = temperature of the bulk fluid (K)

Q_s = effective volume heat deposition per particle surface area (GW/m^2)

U_s = heat transfer coefficient for solid material (W/m^2K)

T_w = temperature of the fluid at the wall (K)

h_t = bed heat transfer coefficient (W/m^2K) [Witter, 93]

To solve these equations over time, a computer model was developed. The model was developed by modifying the one - dimensional TRITRAN computer code used to model nuclear reactors to resistojet application [Witter, 93]. The source code along with a properties routine for water / steam is included in Appendix A. The properties routine was based upon data found in [Todreas, 90]. The computer model of the thruster allows the user to vary:

- power
- working fluid
- mass flow rate
- inlet pressure
- bed materials
- bed particle size
- thruster geometry
- time transients.

A model is also needed to compare packed beds with other systems. Due to the simpler geometry, the heat transfer rate in a straight tube can be approximated from Equation 2-32. Reducing the First Law of Thermodynamics since conditions in a resistojet chamber present no external work, and the changes in kinetic and potential energy are small derives the final equation.

$$\begin{aligned}\dot{Q} - \dot{W} &= \dot{m}(\Delta h + \Delta ke + \Delta pe) \\ \dot{Q} &= \dot{m}(h_e - h_i)\end{aligned}\tag{2-32}$$

where:

\dot{Q} = power input (W)

\dot{m} = mass flow rate (kg/s)

h_e = static enthalpy at exit (J/kg)

h_i = static enthalpy at intake (J/kg)

The computer model presented in Appendix A was modified to also simulate a straight tube. Equation 2-32 could then be used as a benchmark for the transient results produced by this computer model.

Figure 2-22 shows the design approach used for the initial design of resistojets in this research programme.

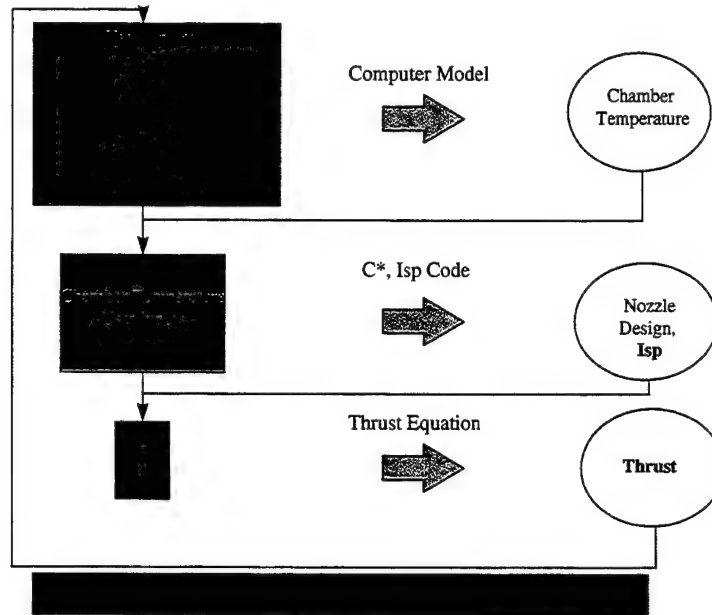


Figure 2-22: Design Approach Flow Chart

For the initial model, the results are compared to past resistojet designs to evaluate performance. Figure 2-22 shows that based upon these results, the model can be varied to produce the optimum design. Once testing starts, the experimental results are used to improve the model that is used to increase the performance in future designs.

For the initial simulation, a heated tube and various bed designs were run using helium as the working fluid. Helium is used as the working fluid due to its easy equation of state properties (ideal gas, no two-phase flow, and constant specific heat with temperature). There are also adequate test results from other programmes for design comparison. Due to the reasons discussed in Section 2.4, a higher efficient design is needed compared to past designs. The assumptions for the initial model:

- Working fluid: helium
- Power: 400 W
- Pressure: 10 bar
- Mass flow rate: 0.1 g/s
- Simulation time: 5 minutes, total firing duration is 10 minutes. This constraint is based upon the power requirements of UoSAT-12.

- Bed material: 350 μm silicon carbide
- Bed porosity: 42 %
- Thruster geometry: varied.

The simulation results are shown in Table 2-19 for various geometry options for the above conditions with comparisons to “multi-pass” engineering model thrusters tested by NASA Lewis.

| System / Dimensions | Chamber Temperature (K) | Nozzle Throat Diameter with 100:1 expansion ratio to vacuum (mm) | Isp (sec) | Thrust (mN) F = 2P/c |
|---------------------------------|----------------------------|---|-----------|-----------------------------|
| Straight Tube 60 mm x 180 mm | 401 | 0.40 | 203 | 402 |
| Packed Bed 60 mm x 180 mm | 544 | 0.43 | 238 | 342 |
| Packed Bed 25 mm x 300 mm | 537 | 0.43 | 236 | 346 |
| Packed Bed 20 mm x 400 mm | 512 | 0.43 | 231 | 353 |
| Packed Bed 20 mm x 360 mm | 512 | 0.43 | 231 | 353 |
| Packed Bed 15 mm x 500 mm | 492 | 0.42 | 226 | 361 |
| Packed Bed 15 mm x 180 mm | 506 | 0.42 | 229 | 356 |
| Packed Bed 90 mm x 90 mm | 404 | 0.40 | 204 | 400 |
| Packed Bed 60 mm x 90 mm | 457 | 0.41 | 217 | 376 |
| Packed Bed 60 mm x 60 mm | 475 | 0.42 | 222 | 367 |
| Packed Bed 360 mm x 360 mm | 293 | 0.37 | 172 | 474 |
| Packed Bed 30 mm x 30 mm | 507 | 0.42 | 229 | 356 |
| Packed Bed 180 mm x 180 mm | 293 | 0.37 | 172 | 474 |
| Packed Bed 15 mm x 400 mm | 497 | 0.42 | 227 | 359 |
| Packed Bed 15 mm x 15 mm | 521 | 0.43 | 233 | 350 |

| | | | | |
|--|-------|---------|-----|-----|
| Packed Bed 10 mm x 500 mm | 523 | 0.43 | 233 | 350 |
| Packed Bed 10 mm x 400 mm | 531 | 0.43 | 235 | 347 |
| Packed Bed 10 mm x 180 mm | 439 | 0.41 | 213 | 383 |
| 1987 NASA Lewis Engineering Model @ 322 W | _____ | _____ | 247 | 285 |
| 1987 NASA Lewis Space Station Engineering Model @ 167 W | _____ | _____ | 204 | 287 |
| 1986 NASA Lewis Space Station Engineering Model @ 200 W | _____ | 0.84 mm | 325 | 240 |

Table 2-19: Comparison of Various Resistojet Designs past thruster design from [Morren, 87], [Morren, 88]

The various configurations presented show the impact of thruster geometry on performance. The optimum configuration is a 30 mm x 180 mm cylinder for the input conditions. Less diameter, but longer designs ("pencils"), suffers due to less bed material from the heater dimensions (smallest available 6 mm in diameter). Higher diameter and shorter length designs ("pancakes"), suffer due to heat transfer losses. Chambers with an equal diameter and equal length suffer a combination of these effects.

Comparing the simulation results to past designs produces an interesting conclusion for helium. Thruster efficiency for electric propulsion systems always compares the total output power / total input power. This relation is shown in Equation 2-33.

$$Efficiency = \frac{FxIspg_o}{2xP_{input}} \quad (2-33)$$

where:

F= thrust (N)

Isp = specific impulse (sec)

$g_o = 9.81 \text{ m/s}^2$

P_{input} = input power (W)

Using the NASA Lewis results in this equation, the efficiencies are 107 %, 172 %, and 191 % respectively. Since other working fluids (nitrogen, water, carbon dioxide, etc) were tested, this efficiency analysis was applied to those test results and more “reasonable” efficiencies were achieved, e.g. 53 % for nitrogen. The Isp or thrust reported in these helium test reports must be incorrect. The 60 mm x 180 mm packed bed system efficiency works out to 50 - 68 % (4 % better than the NASA multi-pass system in a direct comparison with nitrogen). This depends on how the thrust is calculated (mass flow and exit velocity, power, or C^*) since these are theoretical results. A full discussion of efficiency comparison is discussed in Chapter 5. However, the simulation results show there is value in investigating packed beds further.

The results presented in Table 2-19 used silicon carbide as the bed material. There are thousands of choices of possible bed materials. In selecting a bed material, the material heat transfer properties are important. Their properties are:

- density
- heat capacity
- thermal conductivity

Due to price, availability, compatibility, and balance of the properties shown above, stainless steel, boron carbide, silicon carbide, copper, sintered alumina, and sand were investigated. Table 2-20 summarises their properties. More background information behind the selection of these materials is presented in Chapter 3.

Varying particle diameters were chosen to study the impact on packing density (through the *Ergun Correlation*) and resultant impact on heat transfer performance as shown in the *Achenbach Correlation* discussed above. The modelling results shown in Table 2-19 were changed for operation with water. The new state equations were developed (Appendix A) for water. The power was increased to 500 W due to the extra energy required to vaporise the water from Figure 2-19 and still meet the power requirements of UoSAT-12 for 10 minutes of operation. The results of the model for water operation using the various heat transfer material are shown in Figure 2-23. Figure 2-24 shows a transient run for the initial helium analysis (Table 2-19). The time to reach steady state increases for water due to the vaporisation requirements. The higher chamber temperatures achieved are due to the mass flow rate was decreased by 30 % for the water simulations. This water simulation led to the sizing of the proof of concept thruster.

| Material | Particle Diameter | Cp (heat capacity) | k (thermal conductivity) | ρ (density) |
|------------------|-------------------------|--------------------|--------------------------|------------------------|
| Stainless steel | 450 μm | 460 J/kgK | 19 W/mk | 8000 kg/m ³ |
| Boron carbide | 500 - 710 μm | 466 J/kgK | 18 W/mK | 2500 kg/m ³ |
| Silicon carbide | 500 μm | 687 J/kgK | 1.046 W/mK | 2970 kg/m ³ |
| Copper | 50 μm | 385 J/kgK | 46.2 W/mK | 8930 kg/m ³ |
| Sintered alumina | 20 μm | 1050 J/kgK | 4 W/mK | 3960 kg/m ³ |
| Sand | 500 μm | 444.28 J/kgK | 0.5 W/mK | 1800 kg/m ³ |

Table 2-20: Bed Materials Investigated

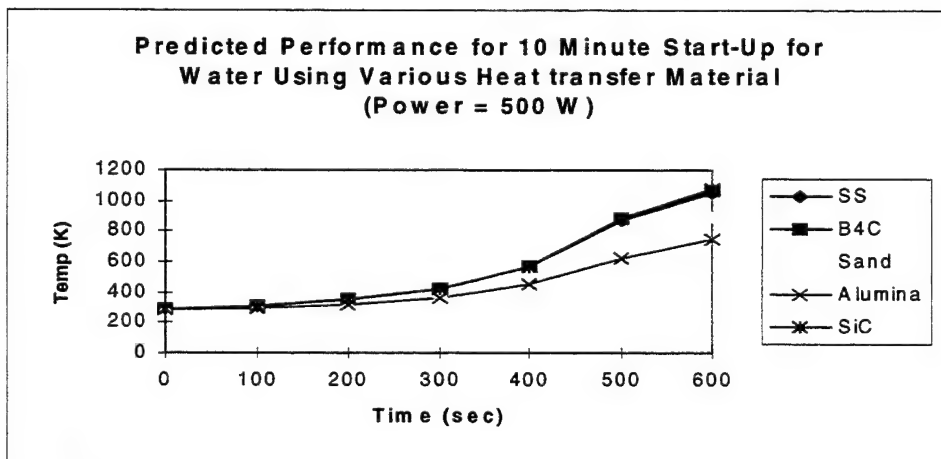


Figure 2-23: Predicted performance for a water resistojet with various bed materials (SS = stainless steel, B₄C = boron carbide, SiC = silicon carbide)

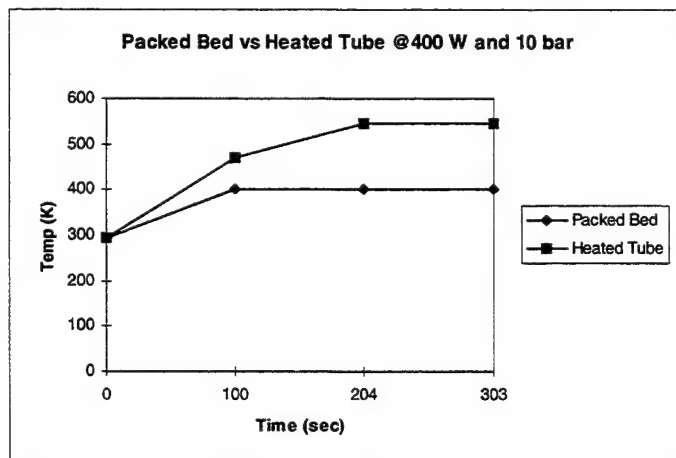


Figure 2-24: Packed Bed vs Heated Tube Resistojet Thrusters. Dimensions: 60 mm x 180 mm @ 400 W and 10 bar pressure

As shown in Figure 2-22, as the test hardware is fabricated, the empirical results obtained in each phase of the research programme will help validate the thermal model and better understand the physics of operation for future design.

2.6. Conclusions

This chapter provided details on past systems and gave motivation for development of a novel resistojets for small satellite application. It also discussed the reasons for a new simulation tool in predicting performance and enhancing future design. The next chapter describes in greater detail the proof of concept thruster and presents initial results as the research programme entered the testing phase.

2.7. References

- [Aston, 89] “ A Detailed Model of Electrothermal Propulsion Systems”, AIAA 25th Joint Propulsion Conference, 1989.
- [Beattie, 98] “XIPS Keeps Satellites on Track”, *The Industrial Physicist*, pages 24 - 26, American Institute of Physics, June 1998.
- [Boyd, 96] “ Computational and Experimental Investigations of Rarefield Flows in Small Nozzles”, *AIAA Journal*, Vol. 34, 1996.
- [Bromaghim, 98] Email received from Mr Daron Bromaghim, AFRL Electric Propulsion Laboratory, 29 August 1998.
- [Cassidy, 95] Personal phone conversation with Mr Joe Cassidy, Primex, December, 1995.

- [Centrosazio, 98] Centrosazio Web Page, 1998.
- [Clauss, 95] Personal phone conversation with Mr Craig Clauss, Atlantic Research Company, December, 1995.
- [CPIA, 98] John Hopkins Chemical Propulsion Information Association Web Page, 1998.
- [ESTEC, 97] 2nd ESA Spacecraft Propulsion Conference, Electric Propulsion Sessions, May, 1997.
- [Fleming, 95] Personal phone conversation with Mr Alan Fleming, Arde, December, 1995.
- [Faulks, 98] Personal phone conversation from Mr Faulks of DASA, August 1998.
- [Greco, 72] and Bliss, J.R., "Design and Operational Characteristics of an Integrated Biowaste Resistojet System", AIAA 7th Propulsion Specialist Conference, AIAA 71-686, Salt Lake City, Utah, USA, June 1972.
- [Halbach, 70] "10 mlb Biowaste Resistojet Performance", NASA Langley Contract NAS1-9474, 1970.
- [Halbach, 71] "10 mlb Biowaste Resistojet Performance", AIAA 7th Propulsion Joint Specialist Conference, Salt Lake City, Utah, June 14 - 18, 1971.
- [Humble, 95] Henry, Gary, N., and Larson, Wiley J., *Space Propulsion Analysis and Design*, New York: McGraw-Hill, Inc., 1995.
- [Jahn, 77] *Physics of Electric Propulsion*, McGraw-Hill Book Company, New York, 1977.
- [Larson, 92] Wertz, J.R. (ed.), *Space Mission Analysis and Design*, 2 ed., Microcosm, Inc. Torrance, California and Kluwer Academic Publishers, Dordrecht, The Netherlands, 1992.
- [Lawrence, 93] *Flow Instability Tests in a Particle Bed Reactor Nuclear Thermal Rocket Fuel Element*, MIT Master's Thesis, MIT, Cambridge MA USA, June 1993.
- [Maize, 93] Personal conversation with Dr George Maize of Brookhaven National Laboratory, June 1993.
- [Micci, 96] Email received from Dr Michael Micci of Pennsylvania State University, 12 December 1996.
- [Micci, 98] Personal conversation with Dr Michael Micci, at Edwards AFB California, December 1997.
- [Morren, 87] Jones, R.E., Louviere A J and Sovey J.S., "Water Propellant Resistojets for Man-tended Platforms", 38th Astronautical Federation Congress, Brighton UK, October 10-17 1987.

- [Morren, 88] Stone, J.R., "Development of a Liquid-Fed Water Resistojet," AIAA-88-3288, AIAA/ASME/SAE/ASEE 24th Joint Propulsion Conference, Boston, Massachusetts, 11 - 13 July 1988.
- [Morren, 93A] "Gravity Sensitivity of a Resistojet Water Vaporiser," NASA Technical Memorandum 106220, AIAA-93-2402, 29th Joint Propulsion Conference, Monterey, California, June 28-30, 1993.
- [Morren, 93B] MacRae, G.S., "Preliminary Endurance Tests of Water Vaporizers for Resistojet Applications," AIAA-93-2403, 29th Joint Propulsion Conference, Monterey, California, June 28-30, 1993.
- [NASA Lewis, 98] NASA Lewis Research Centre Electric Propulsion Web Page, 1998.
- [Paul, 98] Personal interview with Mr Malcolm Paul, retired Royal Ordnance propulsion engineer, August 1998.
- [Riehle, 98] Email received from Dr Martin Riehle of University of Stuttgart, 28 August 1998.
- [Sellers, J.J.] "Investigation into Low-Cost Propulsion Systems for Small Satellite Missions", Ph.D. Thesis, Department of Electrical Engineering, CSER, University of Surrey, Guildford, UK June, 1996.
- [Selph, 92] *ISP Computational Computer Code*, AFRL, 1992.
- [Spanjers, 98] Personal conversation with Dr Greg Spanjers, AFRL Electric Propulsion Laboratory, January 1998.
- [Spores, 98] Personal conversation with Dr Ron Spores, AFRL Electric Propulsion Laboratory, January 1998.
- [Stone, 75] Gray V.H., and Gutierrez, O.A., "Forced-Flow Once-Through Boilers", NASA SP-369, 1975.
- [Stuttgart, 98] University of Stuttgart Electric Propulsion Web Page, 1998.
- [Sutton, 92] *Rocket Propulsion Elements An Introduction to the Engineering of Rockets*, 6th Edition, New York: John Wiley & Sons, Inc., 1992.
- [Todreas, 90] and Kazimi M.S., *Nuclear Systems I Thermal Hydraulic Fundamentals*, New York: Hemisphere Publishing Organisation, 1990.
- [Tong, 65] *Boiling Heat Transfer and Two-Phase Flow*, John Wiley and Sons, New York, 1965.
- [TRW, 98] TRW Web Page, 1998.
- [Witter, 93] "Modelling for the Simulation and Control of Nuclear Reactor Rocket Systems", Ph.D. Thesis, Department of Nuclear Engineering, Massachusetts Institute of Technology, June, 1993.

Chapter 2: *Resistojet Technology Options*

[Zafran, 83] and Jackson B., "Electrothermal Thruster Diagnostics Volume 1: Executive Summary",
NASA CR - 168174-Vol-1, NASA Lewis, March 1983.

[Zafran, 85] "Resistojet Operation with Various Propellants", AIAA 21st Joint Propulsion Conference,
Monterey, California, July 8- 10, 1985.

Chapter 3

Proof of Concept Research Phase

3. PROOF OF CONCEPT RESEARCH PHASE

3.1. GOALS AND OBJECTIVES

3.2. THRUSTER DESIGN AND EXPERIMENTAL APPARATUS

3.3. EXPERIMENTAL RESULTS

3.4. MODELLING RESULTS

3.5. CONCLUSIONS

3.6. REFERENCES

This chapter summarises the design, experimental set-up, and test results of the proof of concept thruster. The test results are analysed for rocket performance prediction and compared to the thermal model. These results, coupled with experimental observation, are compared to the 6 constraints mentioned in Chapter 2:

- mass
- volume
- power
- thrust
- integration
- cost

If the constraints are not satisfied, another phase of research is required. These constraints were not satisfied for the proof of concept thruster. The chapter concludes by suggesting design improvements for the next research phase.

3. Proof of Concept Research Phase

3.1. Goals and Objectives

As discussed in Chapter 2, there are six important parameters to consider in resistojet design for small satellite application. These are:

- mass
- volume
- power
- thrust
- integration
- cost.

As the design trades and analysis showed in Chapter 2, a packed bed approach using nitrous oxide and water as the working fluids looked the most attractive for small satellite application. The analysis approach presented in Chapter 2 also identified a methodology for designing the thruster. This methodology led to the proof of concept thruster.

The goals of the proof of concept research phase were:

- collect data and observe fluid flow
- observe behaviour of various bed materials
- characterise endurance
- determine rocket performance (thrust, Isp)

The data obtained from this system would hopefully show that the thruster functioned at an acceptable performance for small satellite application under various operating conditions. The data would also be used to evaluate performance and provide feedback to the thermal model. Realistically, it was thought that the proof of concept would not become the flight model, but a model to prove the concept and theory mentioned in Chapter 2. These results could then be used to design a flight thruster in the next phase of the research programme.

3.2. Thruster Design and Experimental Apparatus

3.2.1. Thruster and Water Experimental Apparatus

The proof of concept test programme began in Dec 1995 and terminated in November 1996. The proof of concept thrust chamber is 30 mm by 120 mm with a 10 mm by 110 mm commercial cartridge heater installed in the centre provided by Hedin in Essex, UK. Figure 3-1 shows a drawing of the heater. Figure 3-2 shows a cut-away drawing of the proof of concept thruster.

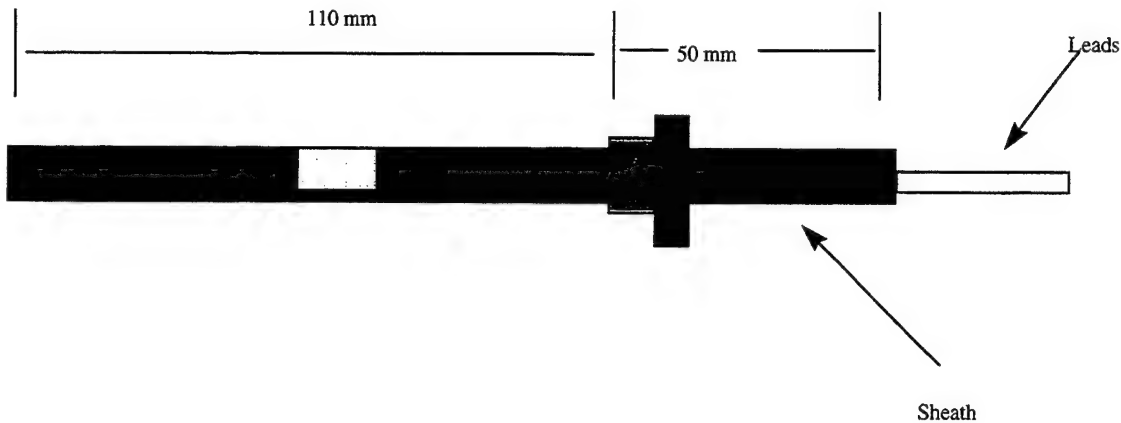


Figure 3-1: Hedin 560 W @28 V cartridge heater

The chamber is made of 304 stainless steel due to its ease of manufacturing and low cost. The heater is composed of nickel-chromium alloy filament, Magnesium oxide insulation, and an Inconel sheath. At 28 V input voltage, it is designed to produce 560 W at a watt density of 24 W/cm^2 . The 28 V input voltage is the same as the voltage provided on UoSAT-12 and MightySATII.1. Thus no power conditioning is required for thruster operation. Around the heater, the chamber is packed with the various heat transfer material. The heater and all connections to the chamber use screwed fittings. This approach allows quick replacement of the various bed materials.

In this design, the flow rates for the two working fluids varies from :

- water: 0.05 - 0.1 g/s @ 10 bar with nitrogen pressurent @ 10 bar
- nitrous oxide: 0.1 - 0.35 g/s @ 10 bar, no pressurent since vapour pressure is 48 bar.

An injector with six 500 μm diameter holes provides an uniform flow to the bed for the above flow rates. For the water tests, a 2 mm sintered disk (65% porosity) is added just after the injector (inner diameter just slightly larger then heater diameter) which provides a pressure drop to decouple the inlet pressure from the chamber pressure. Otherwise flow oscillations from chamber boiling can regulate the inlet flow as mentioned in Chapter 2. The working fluid then flows across the bed, is heated, and passes out through the 0.5 mm throat diameter nozzle (expansion ratio is 25:1) as super-heated steam or nitrous oxide.

Since the proof of concept tests were tested at sea level pressure (University of Surrey Hut-10 for water and Royal Ordnance Wescott for nitrous oxide), the expansion ratio should have been 3.34:1. However, due to a miss-communication with the mechanical design team, a 25:1 nozzle was fabricated. This error produced an *overexpanding nozzle* where the fluid was expanded to a lower pressure than the external pressure since the exit area is too large. According to [Sutton, 1992], for nozzles in which the exit pressure was very close in value to the inlet pressure, subsonic flow prevails

throughout the nozzle. This represents a decrease in performance, but should not effect the conditions in the chamber, which was the primary goal of the proof of concept tests. Therefore, the 25:1 nozzle could be used without effecting the results.

One of the other concerns in designing the thrust chamber was the interaction of the bed heat transfer material with the nozzle. A sintered disk (only used for very small bed material sizes due to its pressure drop of $\sim 1-2$ bar) or a 50 mesh stainless steel screen were used at the aft end to contain the heat transfer material. The instrumentation in the thrust chamber consisted of three pressure gauges and 12 thermocouples.

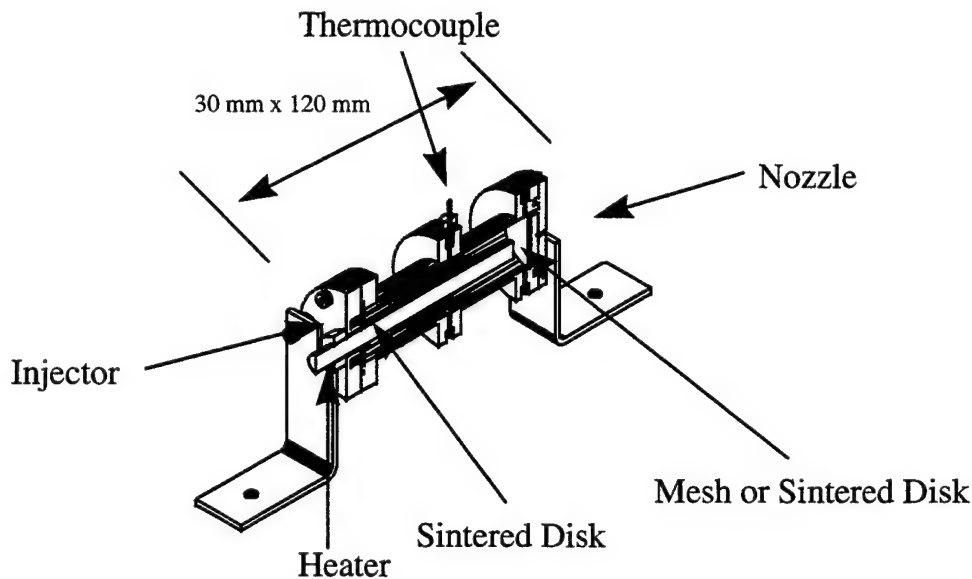


Figure 3-2: Cut-away diagram of proof of concept thruster

Figure 3-3 shows a schematic of the experimental apparatus for the water trials. Figure 3-4 shows pictures of the apparatus fully assembled for the water trials conducted in Hut-10 at the University of Surrey. The power supply is a Farnell H Series 3kW DC power supply unit (0-60 V DC, 0-50 A). The power is adjusted by control knobs for voltage and current on the console. The power supply console displays voltage and current via a needle display. A standard BOC nitrogen cylinder is used to supply nitrogen gas to pressurise the water. The gas is stored at 200 bar but has a 12 bar regulator to regulate pressure to the water tank between 0 - 12 bar. The volume of the cylinder is 7278.24 L which is adequate for completing several runs. The water is stored in a 2 L tank which has been proof tested up to 100 bar. De-ionised water supplied by the University of Surrey Chemical Engineering Department is used for the water trials.

There are 4 valves in the system. Valve 1 is used to open pressure from the nitrogen cylinder to the water tank; valve 2 is a system relief valve; valve 3 is aft of the tank to open flow to the flow meter; and valve 4 (needle valve) is used at the flow meter to regulate flow into the thruster. One filter is located aft of the water tank. Standard 6.4 mm outer diameter stainless steel and copper pipe is used for the system plumbing.

Proof System to 100 Bar

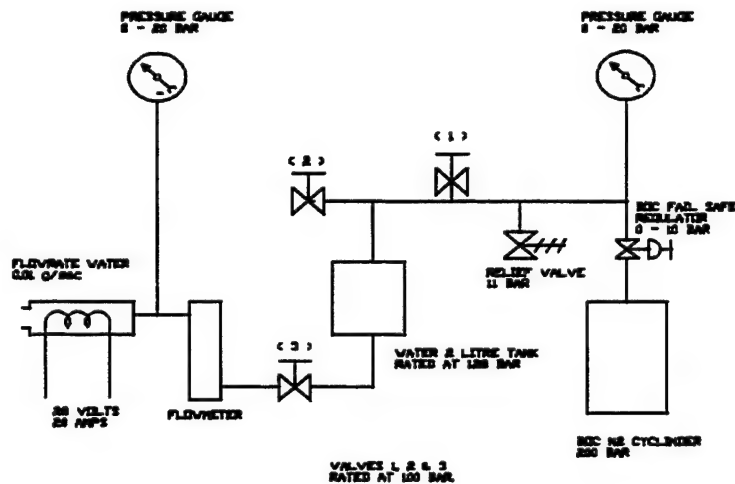


Figure 3-3 - Schematic of Experimental Apparatus

The flow meter used is a Fischer and Porter linear flowmeter rated for water. It has a linear scale with a red sphere used to read flow between the scales. A “catch and weigh” is performed at the start of the programme for calibration. The catch and weigh procedure takes several readings at fixed points on the linear scale and compares them to an actual weighed quantity after a fixed period of time. A linear regression of the flow meter readings to weighed flow rate is then performed. Figure 3-5 shows a plot of this regression.

There are five pressure gauges in the system:

- one with the regulator to the nitrogen bottle
- gauge 2 at the inlet to the water tank
- gauge 3 at the inlet to the injector
- gauge 4 in the thrust chamber prior to the aft screen mesh or sintered disk
- gauge 5 aft of that gauge just before the nozzle to measure exit pressure of the chamber.

Originally, there were twelve thermocouple locations, six in the middle of the chamber and six at the aft end of the chamber. These thermocouples were placed at various depths inside the bed. After initial tests, the number of thermocouples was reduced to only two, one in the middle of the chamber buried close to the heater, and one at the aft end near the chamber wall. This change was due to leak problems that occurred during the initial tests and will be discussed in the next section.

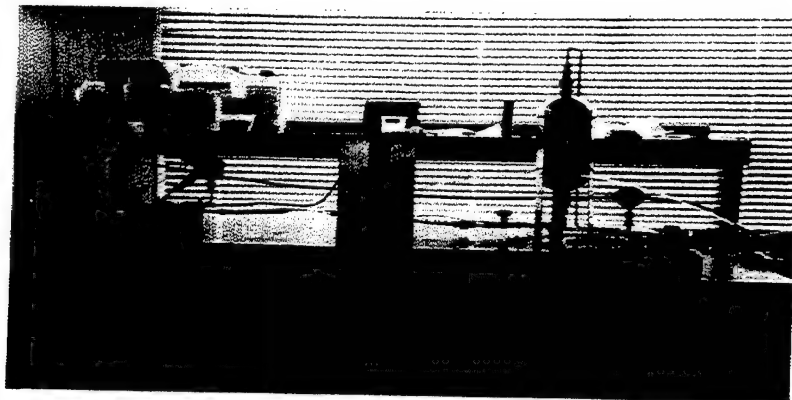


Figure 3-4 - Picture of the Experimental Apparatus

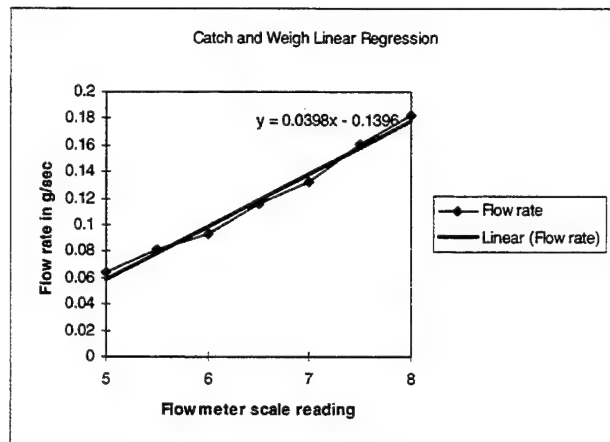


Figure 3-5 - Flowmeter Regression for Calibration

The experiments are conducted using the following test procedure.

RESISTOJET TEST PROCEDURE

1. Insure V1, V2, V3, and V4 are fully closed N₂ regulator fully closed.
2. Insure all pipe connections made, leak tight
3. Insure power supply off
4. Insure water tank full
5. Have test data sheet on-hand
6. Turn on thermocouple and pressure transducer power supply
7. Turn N₂ regulator knob to 10 bar
8. Open V2 to pressurise tank
9. Check pressure tank gauge
10. Open V3 (tank isolator)
11. Turn on power supply
12. Check thermocouple readings-preheat until bed temperatures are high enough to start the water flow
13. Slowly turn V4 to desired flow rate
14. Monitor test article pressure and temperature until end of test (10 minutes maximum)
15. End test
16. Turn off V4 (monitor temps)
17. Turn off power supply
18. Close V3
19. Close V2
20. Open V1. Check tank pressure (make sure it equals 0)
21. Turn back regulator knob on N₂ bottle to 0

EMERGENCY PROCEDURE

1. Turn off power supply
2. Close V3 or V4
3. Close V2
4. Open V1

The bed assembly procedure was as follows (see Figure 3-2):

- attach the heater to the injector plate (threaded in) and add washers and Silcoset (silicon sealant which keeps properties with increasing temperature) for extra sealing
- attach sintered disk to the injector with Silcoset around the perimeter
- attach heater and injector plate to thrust chamber with 6 M5 screws and bolts (add Silcoset also)
- attach thermocouples and seal off area where thermocouples are not used
- add heat transfer material- slowly pour bed material into thrust chamber. Occasionally shake thrust chamber to insure even distribution of the bed for a good packing density (30 - 40 %)
- add screen mesh or sintered disk; attach nozzle to back flange with 6 M5 screws and bolts and Silcoset
- attach the assembled thruster to the bench mounts

Each test was monitored by at least two people. The response time of the system allowed two people to record the data by hand. Power, all three pressure gauge readings, thermocouple, flowmeter readings, time via a stop watch, and observations (time to reach steady state, leaks, material degradation, liquid at nozzle exit, etc.) were recorded at each minute of thruster operation. Most run durations were from 30 minutes to 1 hour.

3.2.2. Nitrous Oxide Experimental Apparatus

The experimental set up for the nitrous oxide systems has some minor differences. All of the tests were conducted at RO Wescott at the J-4 test site due to safety concerns at the University. Figure 3-6 shows the thrust chamber and experimental set up.

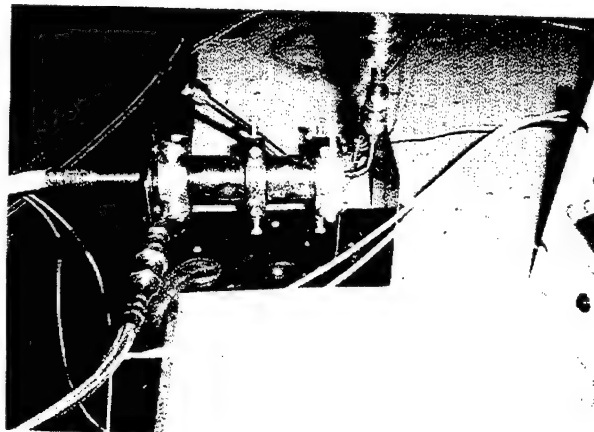
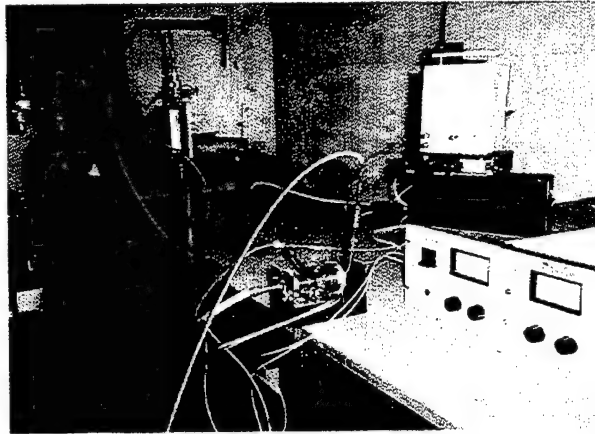


Figure 3-6: Nitrous oxide apparatus for proof of concept thruster

A standard BOC nitrous oxide cylinder is used to supply nitrous gas to the system. The gas is stored at 48 bar but has a regulator to regulate pressure between 0 - 12 bar.

There are 2 valves in the system. Valve 1 is a needle valve used to open pressure from the cylinder to the system and regulates flow through the flow meter. Valve 2 is a stop valve used for safety. Standard 6.4 mm outer diameter stainless steel piping is used for the system plumbing.

The flow meter used is a Fischer and Porter linear variable area gas flowmeter rated for nitrous oxide at 10 bar within 3 % error.

There are four pressure gauges in the system:

- one at the regulator
- gauge 2 at the inlet to the injector
- gauge 3 in the thrust chamber prior to the aft screen mesh or sintered disk

- gauge 4 aft of that gauge just before the nozzle to measure exit pressure of the chamber

The sintered disk was not added at the injector due to flow stability is a small concern with the nitrous system since it enters the chamber as a gas.

There are 2 thermocouple locations, 1 in the middle of the chamber and 1 at the aft end of the chamber. These thermocouples are both located at depths of approximately 5 mm from the chamber wall.

The proof of concept thruster programme went from start to first test in only 3 months. The cost for the thruster (all heat transfer material included) and complete test infrastructure was £2700.

3.3. Experimental Results

This section addresses the test campaign of the proof of concept thruster from the initial test on 18 March 1996 through the end of the campaign on 22 Nov 96. The total cumulative test time is just over 27 hours with stainless steel, boron carbide, silicon carbide, copper, sand, and a mixture of sand and copper as the bed materials.

3.3.1. Water Experimental Test Observations

The following sub sections summarise specific results for each of the materials tested using water as the working fluid. These materials were chosen for the following reasons:

- good thermal characteristics— combination of material density, thermal conductivity, and heat capacity
- cost— each bed material < £20 per kg
- material compatibility—resistant to material degradation
- quick availability—<3 weeks

3.3.1.1. Stainless Steel

The first series of tests investigated stainless steel spheres as the heat transfer material. Stainless steel was chosen due to its good heat capacity and thermal conductivity properties, its compatibility to the thrust chamber (same material) since thermal expansion can be a problem in beds, and its low cost, £50 for 20 kg. A total of thirty-eight tests were conducted on this material. This number exceeds the other materials tested due to problems discovered in the early tests.

The first problem encountered was leaks in the following areas:

- at the heater attachment to the injector
- the aft flange
- and sporadically around the 12 thermocouples

These leak areas are shown in Figure 3-7. These problems were solved by:

- adding a Dowty washer (washer with rubber seal), and a fibre washer coated with Silcoset around the attachment bolt at the thread of the heater attachment to the injector
- ensuring the bed was not over packed and adding Silcoset to both the aft flange and nozzle plate
- replacing 10 of the thermocouple locations with M5 screws

The thermocouple locations had to be replaced since there were leaks occurring at most of the thermocouple locations. These leaks caused problems with the chamber pressure and mass flow rate. The experimental trade-off was monitoring multiple bed temperatures versus not being able to have a performance measurement since the chamber pressure and mass flow rate measurements would not be accurate.

The second problem was a pressure drop of 2 bar across the aft sintered disk. The disk was replaced with a 50 mesh stainless steel screen. The resultant pressure readings from the two aft pressure gauges were nearly identical in subsequent tests. The sintered disk was only used for bed material with particle diameters smaller than the mesh to prevent the bed material from depositing in the nozzle.

After the problems were alleviated, a total of 17 hours of tests were conducted on the stainless steel bed.

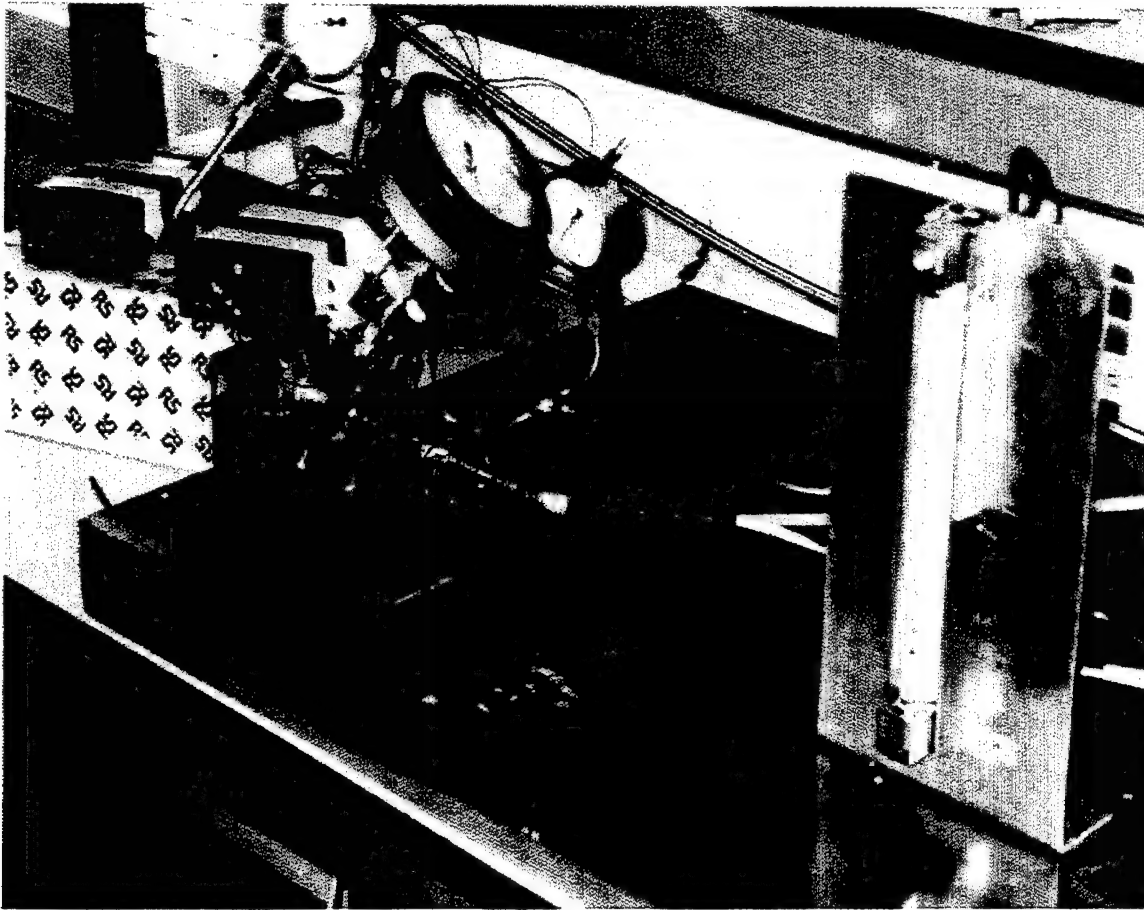


Figure 3-7: Picture of leak areas on resistojet

There were several interesting observations noted from the stainless steel campaign:

- it took a very long time to reach steady state. On the order of 15 minutes to produce an exit plume with no liquid water droplets, 45-60 minutes for steady state. This time delay is due to the high density of the bed material (takes a long time to heat up compared to less dense materials)
- inspection of the bed after runs showed that the stainless steel became discoloured in the middle of the bed and sintered itself to the heater. Sometimes the sintered material would be 2-3 mm thick. Even though this phenomena occurred, no drastic changes in performance were noticed
- the bed was tested horizontally and vertically with no changes in performance indicating the bed should function with respect to changes in gravity (microgravity) [Morren, 93]
- the bed was tested continuously for 5 hours indicating it has potential for meeting the lifetime requirements of an experimental mission

3.3.1.2. Boron Carbide

Boron carbide was next tested due to its heat transfer characteristics (highest thermal conductivity and heat capacity) and low density shown in the thermal model results in Chapter 2. About 1 hour of test

data was collected. Unfortunately the results were very poor due to a white pasty substance that was produced near the nozzle 3- 4 minutes into each run. This substance eventually clogged the nozzle.

After repeated performance, the bed was disassembled and the substance was all over the bed, causing it to become a solid block. After consulting with several chemists, I learned from [Seville, 96], that at temperatures above 570 K the boron carbide reacts with steam to form boron oxide (a white pasty substance which solidifies to a crystalline). Unfortunately, this chemical reaction was not published in the literature when the bed material investigation was started. Based upon these results, the boron carbide was discarded as a candidate substance.

3.3.1.3. Silicon Carbide

Silicon carbide (SiC) was next tested due to its good thermal characteristics (slightly less than boron carbide), low density (compared to stainless steel), low cost (£ 2 per kg), and material compatibility (will not react with steam up to 2300 K). Just under 4 hours of test data were collected on SiC. The SiC reached steady state operation with no water droplets out the exit much more quickly than stainless steel (in about 4 to 5 minutes). Inspecting the apparatus after tests, the bed material had not sintered or discoloured in any form.

Heater life became an issue during the SiC phase of the programme. Only one heater was used for the entire stainless steel campaign (17 hours of operation). Two heaters failed in a row after only operating for just over an hour in the silicon carbide phase. Even though the performance was at a higher temperature than the stainless steel phase, it was not significantly higher (20 K higher @ 500 W, instead of 560 W for stainless steel). After consultation with Hedin (the manufacturer), the heaters were not rated for "long endurance" at the high current @ (28 V, 20 amps). Unfortunately, "long endurance" was defined by the manufacturer to be a "relative" term. The lifetime was estimated to be one year for currents operating at 2 amps (220 V). This failure was not unexpected due to the low cost of the cartridge heater (£17 each). After inspecting one of the burned out heaters, severe degradation was discovered on the heater wires just before the wires entered the metal sheath (Figure 3-1). "Thermal soak back" from the thrust chamber was causing the inlet leads of the heater to get too hot causing the wires to melt. This problem was solved by adding an additional nitrogen line to flow gas directly over the input leads before they entered the metal sheath. This cooling solution worked, but limited the length of a single run due to the extra nitrogen required. However, based upon the similarity of the results for 4 hours of test data, there was enough data to compare it to similar runs made with stainless steel.

3.3.1.4. Copper

Copper powder was selected next to test due to its very high thermal conductivity (2.5 times better than stainless steel which had been the highest tested to date). A smaller particle diameter was also selected (50 μm) to test for the impact of particle size on performance. This particle size was also chosen due to the cost of 500 μm copper was £1500 per kg which was far above the £20 per kg programme goal. The bed heated up very rapidly (due to high thermal conductivity) and reached operation with no water droplets in only 3 - 5 minutes. A total of approximately 2 hours of test data was recorded for copper. After each run, the bed cooled down quite rapidly once the power supply was shut off. Water almost instantly started coming out of the apparatus due to poor heat transfer. Again, this could be attributed to the high thermal conductivity of the copper.

Another phenomenon observed during one of the copper tests was that the middle thermocouple decreased in temperature after about 10 minutes of operation (in previous tests both thermocouples raised continuously until reaching steady state as long as none of the parameters were changed: power, flow, etc). The middle thermocouple reached a lower temperature than the aft thermocouple after another 8 minutes into the test (see R2896.xls in Attached CD for complete test history). This was a very interesting result, as the middle thermocouple was in the middle of the thrust chamber located next to the heater and the aft thermocouple is right next to the exit and is almost touching the outer wall of the chamber. This phenomena can be described as *channelling*. *Channelling* is an effect that can occur in beds with poor packing densities. Poor packing densities can create movement of the particles in the bed causing voids that allow the fluid flow in one straight path (or "channels"). Channelling is not a good effect, the heat transfer changes manifest themselves by a decrease in temperature in the bed.

After disassembly of the copper bed, it was noticed that the copper completely sintered itself around the heater. It was practically in one solid block. The copper had to be scraped out with a scalpel. Oxidation was also starting to occur, there was white powder mixed in the bed.

3.3.1.5. Foundry Sand

Foundry sand was tested next because it had been tested before at NASA Lewis allowing for a good comparison. Four tests were conducted for a total of 2 hours of test data. The thruster reached operation with no water droplets after 8 minutes. It also had the highest heat retention after power shut down compared to the other bed materials. The efficiency (output energy/input energy) of the thruster was 4 % higher compared to the NASA Lewis system.

3.3.1.6. Foundry Sand / Copper

The last bed configuration was a mixture of the foundry sand and copper. A metal insert was fabricated that allowed half of the chamber to be filled with copper and sand. The copper was first inserted around the heater with the sand going from the middle of the bed to the outer wall. The insert was removed and the materials settled with little mixing. This approach was tried to increase the heat transfer. Having a material of high conductivity around the heater should quickly transfer the heat out to the less conductive, but higher heat capacity sand. This method would allow the total temperature in the thrust chamber from the heater to the outer wall to decline more linearly, instead of exponentially decreasing.

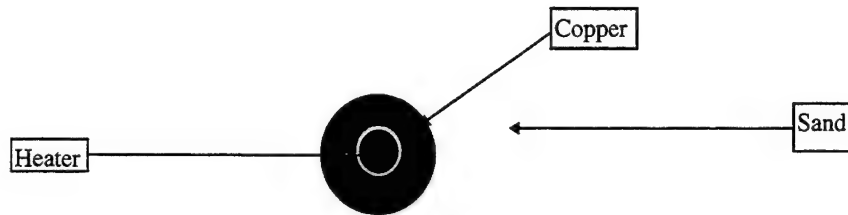


Figure 3-8: Drawing of copper/sand system

Two tests were conducted, with disappointing results. Channelling was noticed again due to dissimilar bed materials with different coefficients of thermal expansion. When heated, this expansion mismatch created voids in the bed which allowed the flow to find a direct path. The combined system took longer to reach steady state than the thruster that only operated on sand.

Table 3-1 shows the summary of the test observations for the various bed materials tested using water as the working fluid. Figure 3-9 presents photographs taken during this phase of testing. Several lessons were learned with the experimental observations:

- heater lifetime and temperature - need a higher temperature longer life heater (better “off the shelf” option)
- leak prevention - will use welded fittings instead of screws and Silcoset
- start-up transient length - the time to reach pure steam operation (no vapour or drips of water) and maximum temperature is too long. Analysis of the data should lead to some solutions to alleviate this problem.
- need a more sensitive needle valve- the current valve brings in an initial flow rate that is too high (valve is not very sensitive). This has an impact on system behaviour (too high of a mass flow rate causes water droplets out the exit nozzle).
- silicon carbide showed no material degradation and a good response time to reach steady state

The next section addresses the calculations performed to assess the performance of these experiments.

| Material | Advantage | Disadvantage |
|------------------------|--|--|
| Stainless steel | High temperatures achieved | <ul style="list-style-type: none"> • Sintering • Long start-up |
| Boron carbide | None | Boron oxide produced clogged nozzle |
| <i>Silicon carbide</i> | <ul style="list-style-type: none"> • <i>Fast start-up</i> • <i>No material degradation</i> | <i>Less temperature achieved than stainless steel</i> |
| Copper | Very fast start-up | <ul style="list-style-type: none"> • Channeling • Most of bed sintered to heater |
| Sand | High heat capacity | <ul style="list-style-type: none"> • Long start-up • Some sintering to heater |
| Copper / sand | None | <ul style="list-style-type: none"> • Long start-up • Channeling • Sintering |

Table 3-1: Summary of Test Observations

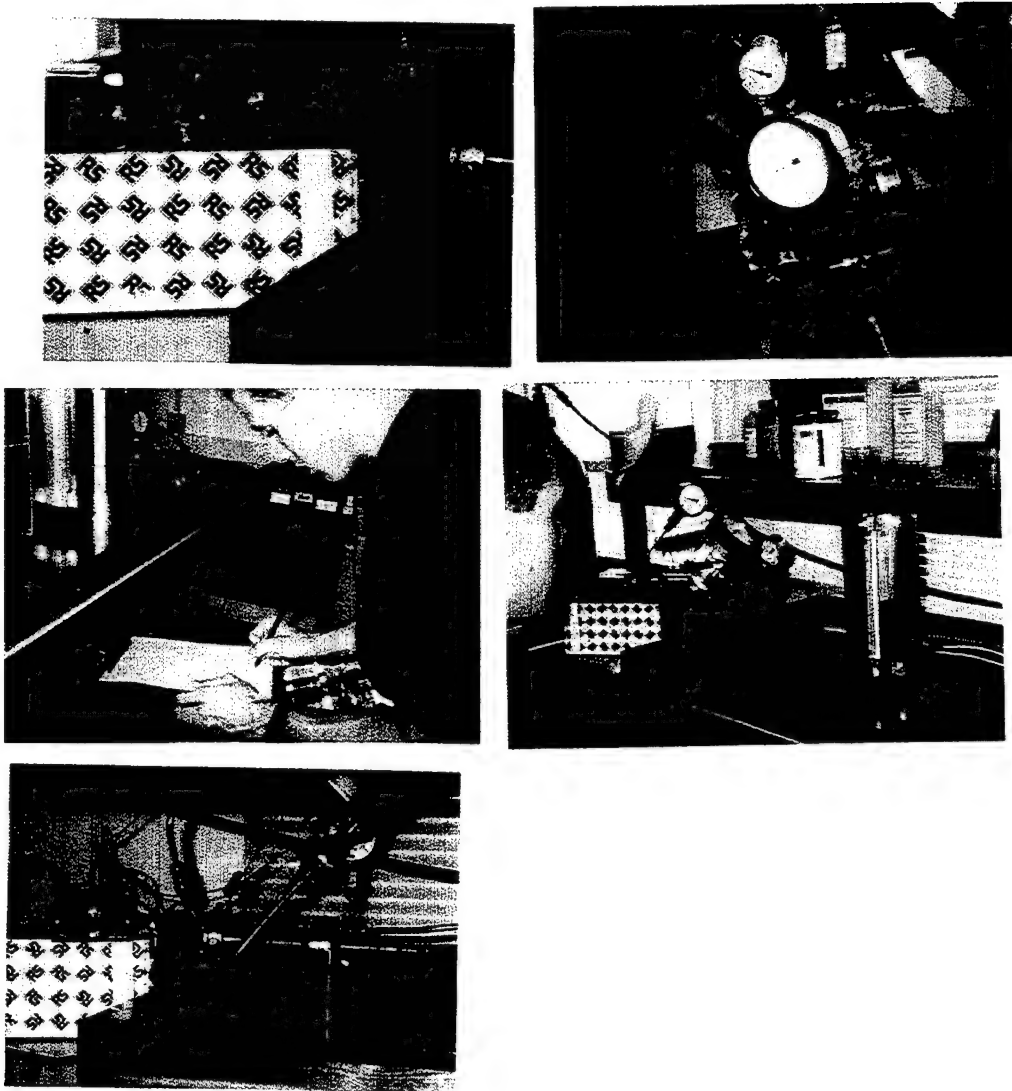


Figure 3-9: Pictures During Testing

3.3.2. Water Experimental Results

This section briefly discusses the results for the water tests for the proof of concept phase. All of the experimental results can be found on the attached CD ROM.

Figure 3-10 shows the result of chamber temperature (middle of the bed thermocouple) and input power versus time with no flow for stainless steel, copper, and sand at almost equal power levels. The only variable is that the Hedin heater life was different for the three materials:

- stainless steel - beginning of life
- copper - five hours
- sand - 10 hours

Figure 3-10 also shows that bed temperatures close to 1000 K should be achievable with the system (no shielding or insulation). Unfortunately, it also shows it takes ~ 20 minutes to reach steady state temperature.

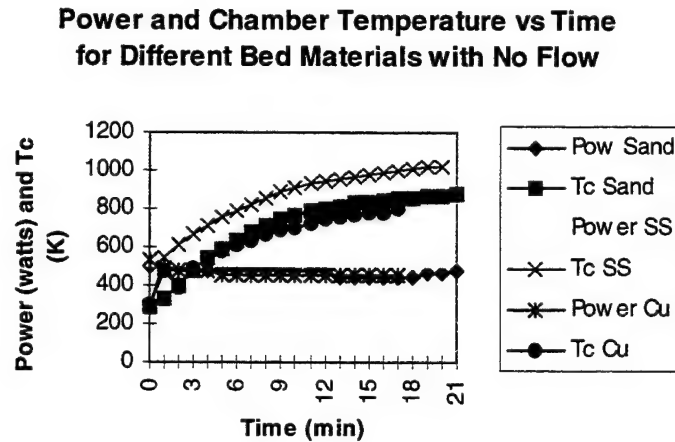


Figure 3-10 Bed test with no flow

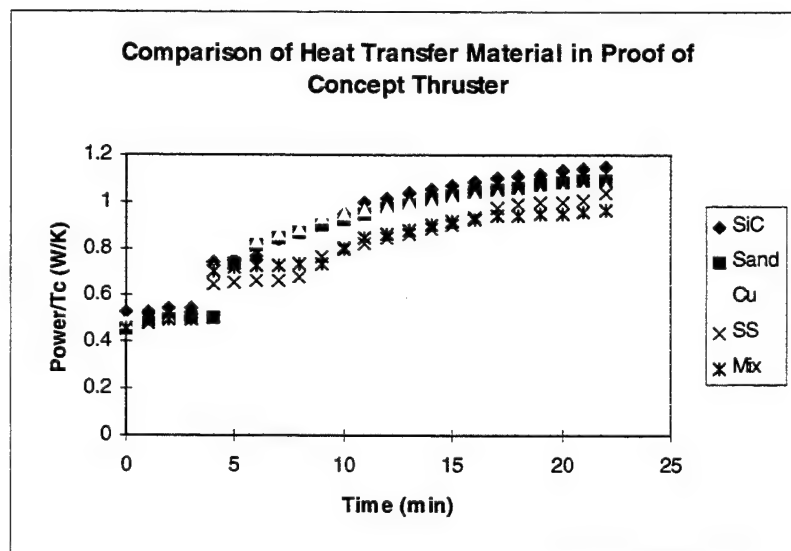


Figure 3-11: Comparison of Various Bed Materials

Figure 3-11 presents a comparison of each of the materials tested. Stainless steel obtained the highest exit temperature of the materials tested, but took the longest time to reach steady state (15 minutes). The sand and SiC reached steady state quicker, (~ 6 - 8 minutes) obtained high chamber temperatures, and did not show much fluctuation in temperature. The copper had a fast start-up (3 minutes), but did not reach as high a temperature at steady state. This plot does not show the entire picture for all of the test data, but does show the general trends.

Figure 3-11, along with the experimental observations, showed that silicon carbide represented the best material for the proof of concept phase.

Figures 3-12 - 3-15 shows the general behaviour of the water proof of concept tests. These results show data collected from a test conducted on 13 June 1996. Figure 3-12 and 3-14 show the mass flow rate versus and temperature versus time for a silicon carbide water test with a constant power input. There is an initial surge of mass flow rate at start-up due to the sensitivity of the flowmeter valve. According to the First Law of Thermodynamics, the mass flow then gradually decreases over time as the chamber temperature increases, until the thruster reaches steady state. This trend shows the heat transfer efficiency (output energy/input energy) is increasing until the system reaches steady state.

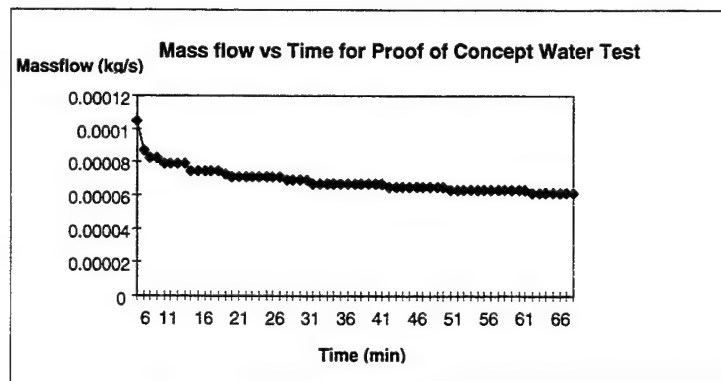


Figure 3-12: Mass flow vs Time for SiC Water Proof of Concept Test (13/6/96)

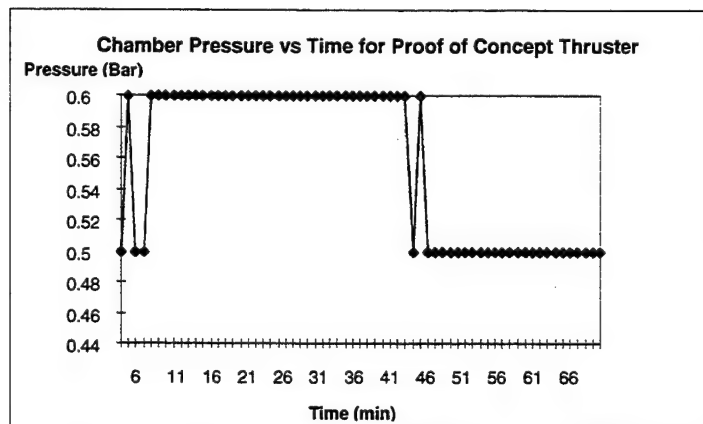


Figure 3-13: Chamber Pressure vs Time for SiC Water Proof of Concept Test (13/6/96)

Figure 3-13 shows the chamber pressure (gauge pressure) versus time. This shows that the pressure showed little variation over time (0.1 Bar). The inlet pressure to the chamber is 1 bar. The chamber pressure is regulated by the mass flow rate, nozzle diameter, and exit pressure. Since the test is conducted at sea level and the nozzle size (as stated earlier, large for sea level), the chamber pressure

is low for the given mass flow rate. It is also a function of heat transfer efficiency which is discussed in Section 3.4.

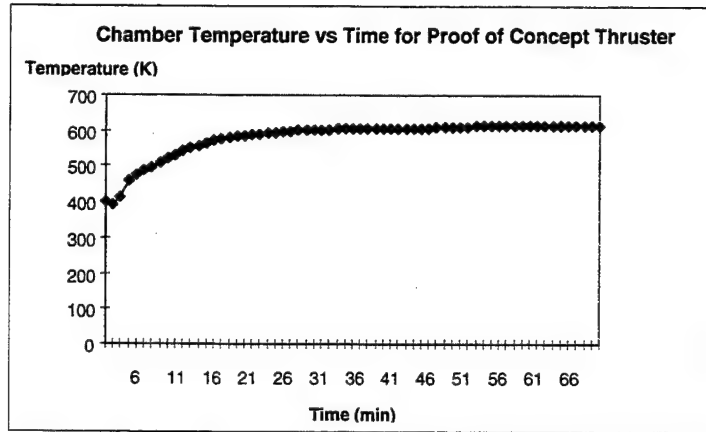


Figure 3-14: Chamber Temperature vs Time for SiC Water Proof of Concept Test (13/6/96)

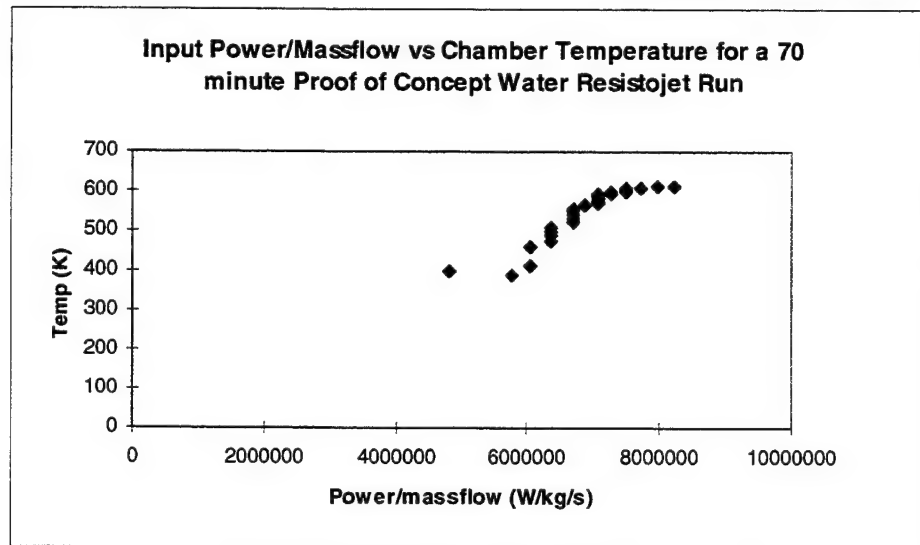


Figure 3-15: Power/mass flow rate vs Chamber Temp. over Time for SiC Water Test (13/6/96)

Figure 3-15 shows the ratio of the input power (500 W) over mass flow rate versus chamber temperature. This expression is derived for comparing the efficiency of the system to other concepts that operate at different flow conditions and analysing scaling of the system for different powers. The equation for this ratio is:

$$y = 7E - 05x + 51.597 \quad (3-1)$$

where:

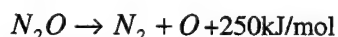
x= Power / mass flow rate (W/kg/s)

y = Temperature (K)

3.3.3. Nitrous Oxide Experimental Test Observations

The nitrous oxide test phase started after the water tests. Water was tested first due to its better performance. The test observations from the water phase were applied in choosing the nitrous oxide configuration. Thus, silicon carbide was the only bed material used. The operating parameters were also different due to the following reasons:

- No vaporization required—lower power, higher mass flow rate and chamber pressure compared to water
- Hybrid application—the funding to start this development effort was provided by the United States Air Force Academy and the United States Air Force European Office of Aerospace Research and Development. They were interested in using the resistojet as a start up mechanism for a nitrous oxide / HTPB hybrid rocket. A hybrid rocket needs the nitrous oxide to reach 850 K to start combustion in the chamber. The state of the art devices use “one off” start up mechanisms (solids, electrical). For space propulsion application, a restartable system is attractive. Thus the resistojet was worth investigating further for this option. Since hybrids function at 10 - 100's N thrust, the proof of concept thruster was run at the highest flow possible to achieve the 600 C temperature.
- Decomposition—nitrous oxide starts decomposing at temperatures above 700 K. This exothermic reaction is:



The 100 % decomposition temperature is 1900 K. If the resistojet reaches temperatures where decomposition occurs, the extra heat produced can replace the power needed from the heater or increase the chamber temperature with constant power input. Since nitrous oxide has not been used before for resistojet application, it will be important to characterise these decomposition effects.

The proof of concept resistojet was tested for a total of 7 hours using nitrous oxide as the propellant. The silicon carbide bed material did not see any material degradation for the life of these tests. The heater reliability became even more of an issue in this test phase compared to the water tests. Since water entered the chamber as a liquid, it acted as a much better coolant to the heater compared to nitrous oxide. The input power was lowered to 500 to 200 W to decrease the heater temperature for the flow rate chamber temperature, but maintain a chamber temperature above 700 K. The heaters still failed after 1 – 3 hours of operation, even with the nitrogen cooling added as discussed in the water testing section. A new heater design was needed for the next research phase.

3.3.4. Nitrous Oxide Experimental Results

This section presents the experimental results for one of the nitrous oxide resistojet runs. This run, conducted on 26/3/98, is prototypic of the other 6 runs conducted during this research phase. All of the experimental results can be found in the attached CD-ROM.

Figures 3-16 through 3-19 show the results for the nitrous oxide run conducted on 26 March 1998.

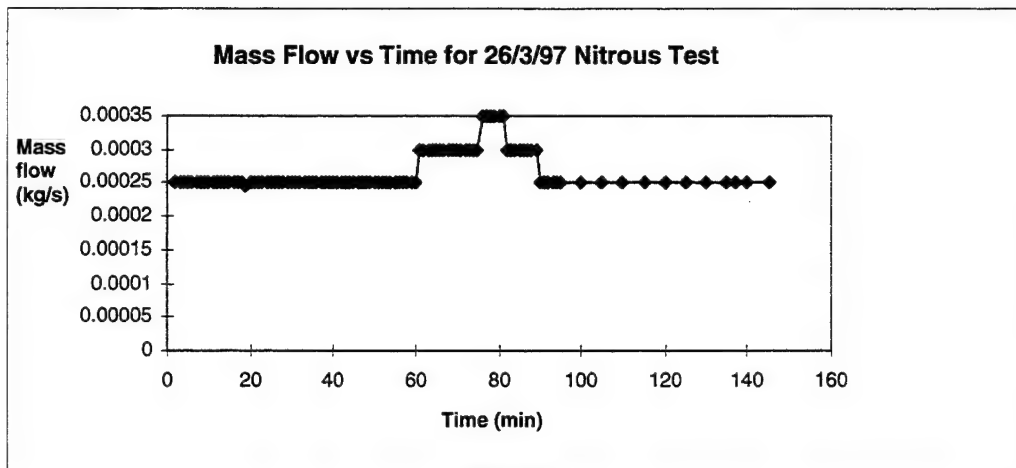


Figure 3-16: Mass flow vs Time for Proof of Concept Nitrous Oxide Resistojet

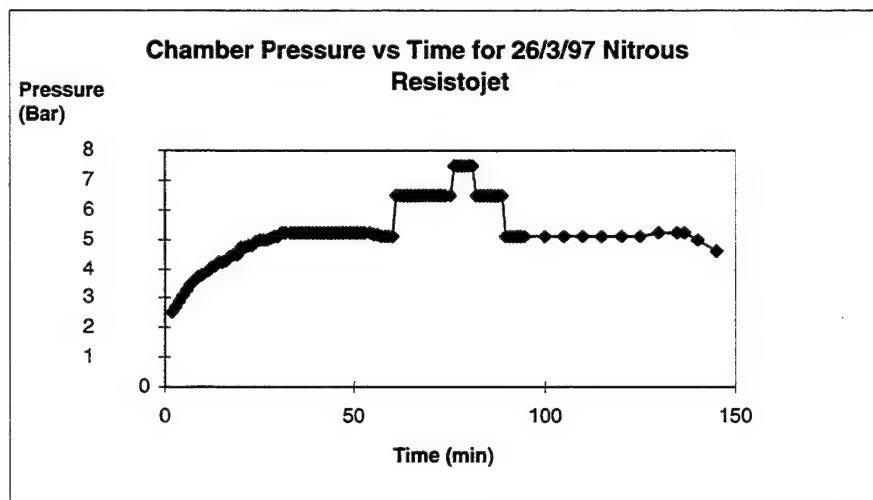


Figure 3-17: Chamber Pressure vs Time for Proof of Concept Nitrous Oxide Resistojet

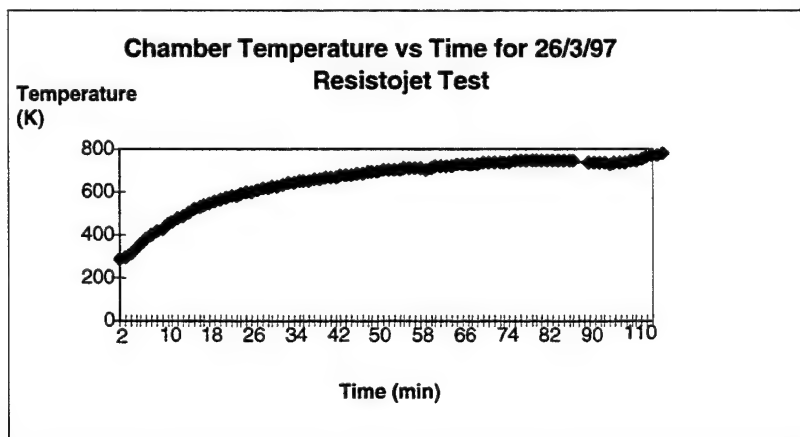


Figure 3-18: Chamber Temperature vs Time for Proof of Concept Nitrous Oxide Resistojet

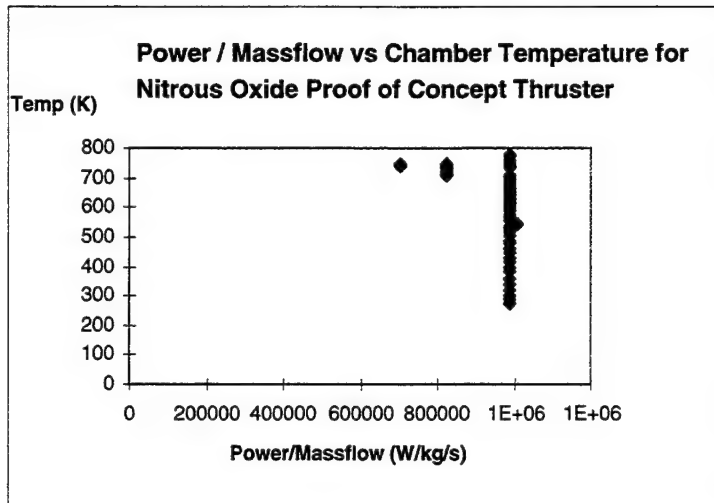


Figure 3-19: Efficiency versus Time for Proof of Concept Nitrous Oxide Resistojet @ 200 W

Looking at the results over time for the experiment, the mass flow and power remain steady (changes in Figure 3-16 were from a manual increase in mass flow) whilst the chamber temperature and chamber pressure gradually rise. This behaviour over time is due to the conduction heat transfer from the heater to the bed, the convection heat transfer of the bed to the working fluid, and then radiation losses to the outside.

Equation 3-2 shows the power divided by mass flow rate versus chamber temperature results for nitrous oxide. This is similar to Equation 3-1 and is an empirically derived relation from the nitrous oxide test results for evaluating heat transfer.

$$y = -0.0006x + 1222.4 \quad (3-2)$$

where:

x = Power/mass flow (W/kg/s)

y = Temperature (K)

Nitrous oxide is more power efficient than water. At approximately half of the input power, and 3 times the mass flow rate, it is able to produce the same chamber temperature as the water run. This result supports the earlier argument that nitrous oxide would be more efficient due to the exothermic reaction and no vaporisation of the working fluid. Evaluation of the heat transfer efficiency is discussed in the next section.

3.4. Modelling Results

This section discusses the analytical results obtained for the proof of concept research phase. The experimental results are analysed to predict performance and compared with the theoretical predictions presented in Section 2.5.

The experimental results can be expressed in terms of heat transfer efficiency. Figures 3-20 and 3-21 represent an energy balance calculation for the proof of concept thruster. It is a division of the output energy in the exhaust (kinetic energy of the exhaust) over the input energy (just electrical power since kinetic energy is negligible due to low input flow rate). The key term in this equation is the calculation of the exit velocity based upon measured results of the chamber temperature, chamber pressure and assumption of ratio of specific heats. This is the same equation that was introduced in Chapter 2.

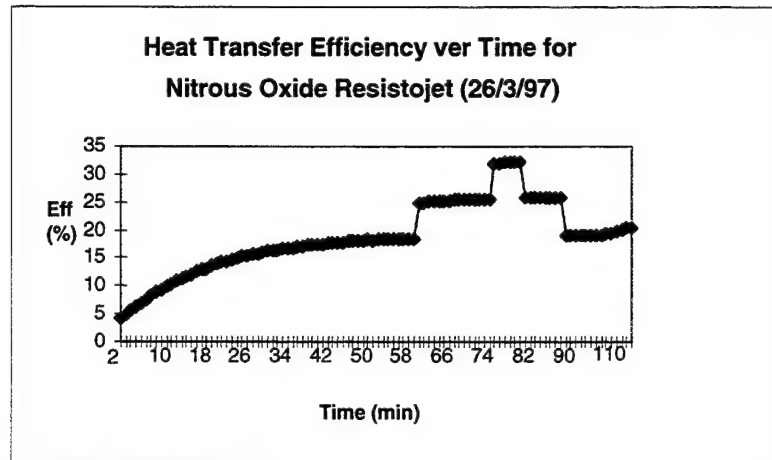


Figure 3-20: Heat Transfer Efficiency Based Upon Kinetic Energy for Proof of Concept Thruster

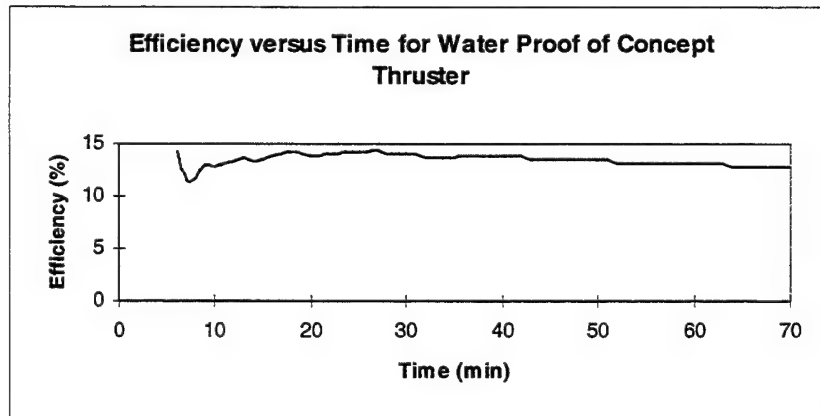


Figure 3-21: Heat Transfer Efficiency Based Upon Kinetic Energy for Proof of Concept Thruster (13/6/96)

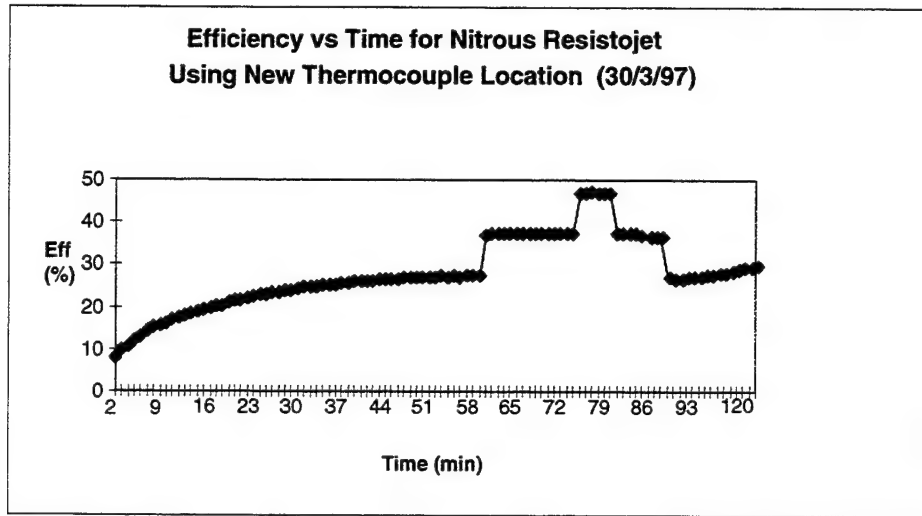


Figure 3-22: Heat transfer efficiency using new thermocouple location for Nitrous Oxide experiment (30/3/97)

$$Efficiency = \frac{\frac{1}{2} \dot{m} V_e^2}{InputPower} \quad (3-3)$$

where:

$$V_{exit} = \sqrt{\frac{2 \cdot \gamma \cdot R_u \cdot T_0}{(\gamma - 1) \cdot M} \cdot \left[1 - \left(\frac{P_e}{P_0} \right)^{\gamma-1/\gamma} \right]}$$

V_{exit} = nozzle exit velocity (m/s)

R_u = universal gas constant (8314.41 J/kmol*K)

T_0 = chamber temperature (K)

P_e = exit pressure (Bar-Pa)

P_0 = chamber pressure (Bar-Pa)

M = molecular mass of gas (kg/kmol)

γ = ratio of specific heats (unit less)

Input power = heater power (W)

\dot{m} = mass flow rate (kg/s)

These results show that the heat transfer efficiency was low for this thruster compared to off the shelf systems and the predicted results presented in Chapter 2 (50-75%). This was first attributed to the thermocouple location. The thermocouple used in Equation 3-3 was located 5 mm from the chamber wall and 5 mm from the nozzle exit. The efficiency increased if the middle thermocouple located 60

mm from the exit and 10 mm from the chamber wall was used. The results are shown in Figure 3-22. Even though this is an improvement, the efficiency is still low (48 % instead of 75 %).

This heat transfer analysis also shows the difference between the two working fluids. Nitrous oxide is a factor of 4 times higher compared to water. This is due to the vaporisation energy requirement for water.

There are other heat transfer approaches for calculations of efficiency using only thermodynamic data for analysis:

- performance based on C^*
- performance based on an energy balance using convective heat transfer

The C^* approach is similar to evaluating chemical rocket performance. The equations used for this approach are:

$$C^*_{\text{measured}} = \frac{P_c A_t}{\dot{m}} \quad (3-4)$$

$$C^*_{\text{theoretical}} = \frac{\sqrt{\gamma RT}}{\gamma \sqrt{\left[\frac{2}{\gamma+1}\right]^{\frac{(\gamma-1)}{(\gamma+1)}}}} \quad (3-5)$$

where:

P_c = chamber pressure (Pa)

A_t - throat area (m^2)

\dot{m} = mass flow rate (kg/s)

γ = ratio of specific heats

R = universal gas constant (8314.4 J/kmol K)

T = chamber temperature (K)

These equations are derived in [Sutton, 1992]. C^* is a function of the propellant characteristics and chamber design. It is independent of the nozzle characteristics, such as the area ratio or the nozzle pressure ratio. In chemical rockets, it is a figure of merit used in comparing propellant combinations and combustion chamber design. The theoretical value is obtained by first using thermochemistry data to obtain a combustion chamber temperature. Thermocouples are not used in the chemical rocket combustion chamber because the temperature is very high (3000 K). However, in the proof of

concept chamber, temperature is measured. This temperature and the values of γ and R for water are used to calculate the theoretical C^* and compare this with the measured pressure and mass flow rate.

This analytical approach showed that SiC had the highest heat transfer efficiency of all the materials tested which ties up with the real observations. This approach also predicted slightly higher efficiencies than the input energy/output energy approach.

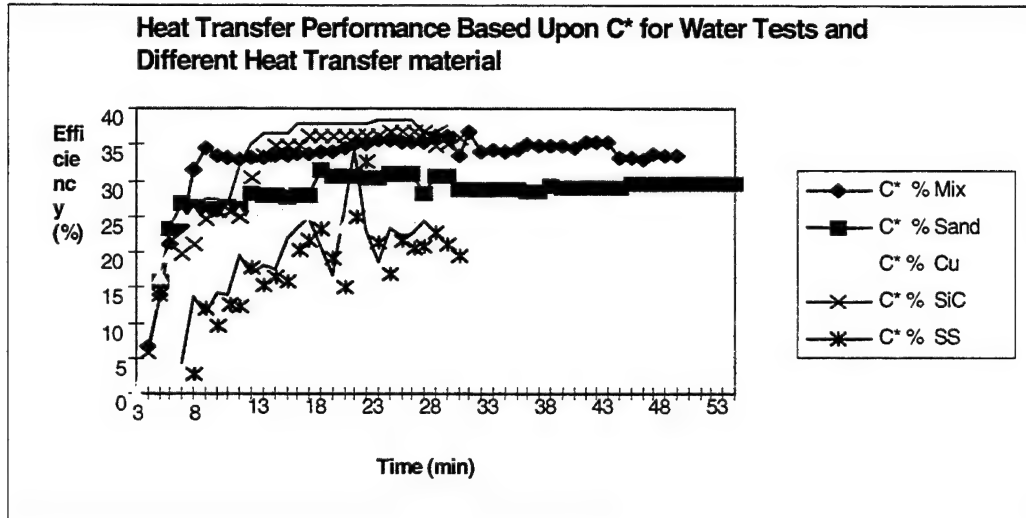


Figure 3-23 Comparison of C^* Efficiencies for the Various Heat Transfer Material. The test parameters (power, flow, pressure) were very similar for these experiments

The next approach used is convective heat transfer. The First Law of Thermodynamics shows:

$$Q = \dot{m}C_p(T_{final} - T_{initial}) \quad (3-6)$$

The key assumption in this equation is the fluid heat capacity. It changes by a factor of 5 in the steam to water transition and is also a function of pressure. As discussed previously, these values are averaged across the entire operating range as a function of temperature and pressure. This approach determined that 2060 J/kg K is the C_p value needed for this calculation. This approach is discussed in greater detail in [Todreas,90]. It is valid for water and steam two phase flow mixtures where the proportion of water to steam vapour is approximately equal. If the system is primarily liquid water, the C_p is 4187 J/kg K. The power calculated is compared with the power supply power to determine the efficiency. The initial chemical energy of the fluid (for total power = electrical energy + chemical energy) is zero since the inlet enthalpy times the mass flow rate equals approximately 0.1 Watts. Figure 3-24 shows the result of this approach for one of the proof of concept tests. The convective heat transfer process predicts efficiencies between 8 - 18 %.

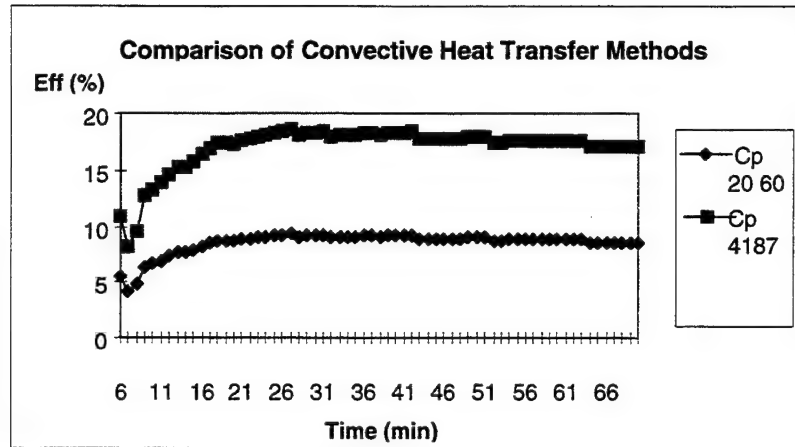


Figure 3-24: Convective Heat Transfer Efficiency Results assuming a Cp of 4187 J/kg K and 2060 J/kg K.

Figure 3-25 is a comparison of the convective heat transfer efficiency (assuming Cp of 4187 J/kg K) and C* heat transfer efficiency for one of the stainless steel tests. The results look encouraging—within 10% of each other for most of the test duration. Some thrust stands have shown variations up to 25% [Sutton, 96].

The heat transfer analysis also matched the observed experimental results for the two working fluids. In the water tests, silicon carbide had the highest heat transfer efficiency. The efficiency was also lower than predicted in Chapter 2. This can be attributed to radiation losses out through the chamber wall.

Equation 3-7 shows the expression for radiation losses.

$$Q = \epsilon \sigma A T^4 \quad (3-7)$$

where:

ϵ = material emissivity

σ = Stephen Boltzman constant $5.67 \times 10^{-8} \text{ Wm}^{-2}\text{K}^{-4}$

A = surface area (m^2)

T = wall temperature (K)

Equation 3-7 shows that if the wall temperature is lowered from 500 K to 320 K, the radiation losses can be reduced by a factor of 4. The wall temperature and lower thermal mass (extra 30 mm wall thickness needed for thermocouples) will have to be improved for the next phase.

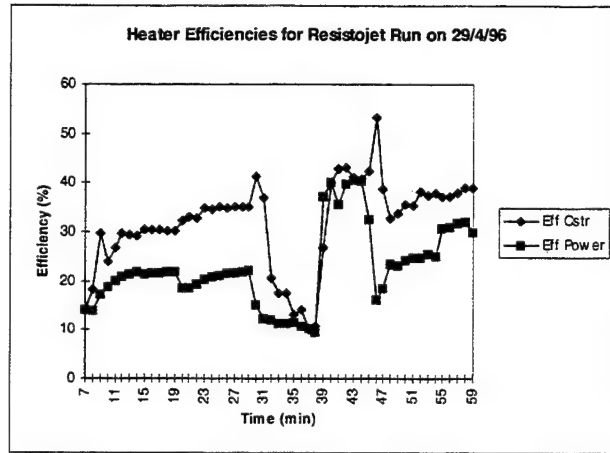


Figure 3-25: Comparison of Thermodynamic Efficiencies for the Two Heat Transfer Methods for One Stainless Steel Test

The rocket performance for the proof of concept thruster was purely based on measured temperature and pressure readings in the chamber. These experiments used mass flow, C^* , V_e , T_c , γ , P_c , and the Isp code discussed in Chapter 2 for performance measurement. Isp and thrust were not critical at this point, since at this stage of the test programme the goal was to reach the maximum chamber temperature for the input power level. Measured temperature and pressure with the nozzle expansion ratio (25:1) were used to generate thrust, Isp, and heat transfer efficiency. There were several thermodynamic approaches for this which are discussed below.

The first uses the exit velocity equation (from Equation 3-3). Using the exit velocity equation (ideal rocket assumptions) and assuming perfect expansion, the thrust and Isp can be expressed as:

$$Isp = V_{exit}/g_0 \quad (3-8)$$

$$F = \dot{m}V_{exit}\eta \quad (3-9)$$

where:

\dot{m} = measured mass flow rate (kg/s)

η = nozzle efficiency (0.92 for 15° half-angle nozzle)

V_{exit} = expressed in Equation 3-3 (m/s)

The next method used the Isp thermochemistry code developed by Curt Self. The input parameters were:

- measured chamber pressure (Bar - psi)
- measured ambient pressure (Bar - psi)
- measured chamber temperature (K)
- expansion ratio

- working fluid

The code then calculates the performance for these chamber conditions. It assumes that the flow in the nozzle is :

- isentropic
- 1-dimensional
- allows chemical reactions to occur in nozzle

The last series of performance calculations is based upon C^* . The measured C^* (Equation 3-4) is used to estimate performance through the following equations:

$$I_{sp} = ((2 \cdot \gamma^2) / (\gamma - 1) \cdot (2 / (\gamma + 1))^{\gamma+1/\gamma-1} \cdot (1 - (P_e/P_c)^{\gamma-1/\gamma}))^{0.5} \cdot \eta \cdot C^* / g_o \quad (3-10)$$

where:

γ = ratio of specific heats (C_p/C_v - no dimensions)

P_e = exit pressure (bar)

P_c = chamber pressure (bar)

C^* = characteristic exhaust velocity (m/s)

η = nozzle efficiency

g_o = gravitational constant (m/s^2)

$$F = A_t \cdot P_c \cdot \gamma \cdot ((2 / (\gamma - 1) \cdot (2 / (\gamma + 1))^{\gamma+1/\gamma-1} \cdot (1 - (P_e/P_c)^{\gamma-1/\gamma}))^{0.5} \cdot \eta \quad (3-11)$$

where (everything same as above except for new variables):

A_t = throat area (m^2)

$$I_{sp} = C^* / g_o \cdot \gamma \cdot ((2 / (\gamma - 1) \cdot (2 / (\gamma + 1))^{\gamma+1/\gamma-1} \cdot (1 - (P_e/P_c)^{\gamma-1/\gamma}))^{0.5} \quad (3-12)$$

where: all the same variables used in the above equations.

$$F = C^* \cdot m \cdot \gamma \cdot (2 / (\gamma - 1) \cdot (2 / (\gamma + 1))^{\gamma+1/\gamma-1})^{0.5} \quad (3-13)$$

where: all the same variables used in the above equations.

All the equations are based upon C^* . They are derived in [Humble, 1995]. The assumptions behind their derivation are as follows:

- Isentropic flow
- 1- dimensional
- products of combustion constitute a perfect gas
- Frozen flow

- Steady flow

The performance results for these various approaches is shown in Table 3-2 for a proof of concept resistojet run (13/6/96) using water as the working fluid.

This thruster was tested at sea level using silicon carbide as the bed material. The steady state measurements were:

Power: 504 W

Propellant: Water

Mass flow rate: 6.14 E-05 kg/s

Chamber pressure: 150,000 Pa

Chamber Temperature: 616.16 K

| | | |
|---------------|------|----|
| Isp Code | 29 | 48 |
| Eq 3-8, 3-9 | 21 | 36 |
| Eq 3-10, 3-13 | 56 | 21 |
| Eq 3-11, 3-12 | 12.8 | 22 |

Table 3-2: Summary of performance for proof of concept thruster

Table 3-2 shows there was a variation in the predicted performance of the resistojet. This variation is the result of the simplifying assumptions associated with these equations. The assumptions used to derive these equations required that the flow was steady, a perfect gas, and 1-dimensional. Since the Isp thermochemistry code did not have as many simplifying assumptions as the other equations, it is the best approach for predicting future performance of the resistojet. Even though this approach still has simplifying assumptions, it did serve as a first order metric for an efficient resistojet design - high chamber temperature for the input fluid mass flow rate, power, and pressure.

The variation in results also showed to get the most accurate performance figure for the resistojet, a thrust stand would be needed. The thrust stand result could then be compared to the performance predicted in the Isp code.

The predicted thermal model temperature versus measured chamber temperature is shown in Figure 3-26. The predicted temperature is 14 % higher than the measured chamber temperature. The model

predicted this result based upon the water working fluid (derived equations of state in Appendix A), mass flow rate, pressure, inlet temperature, thruster geometry, heater size, and power. This result gave good confidence for the next thruster design. There were no models that were of the shelf that could be applied for this design.

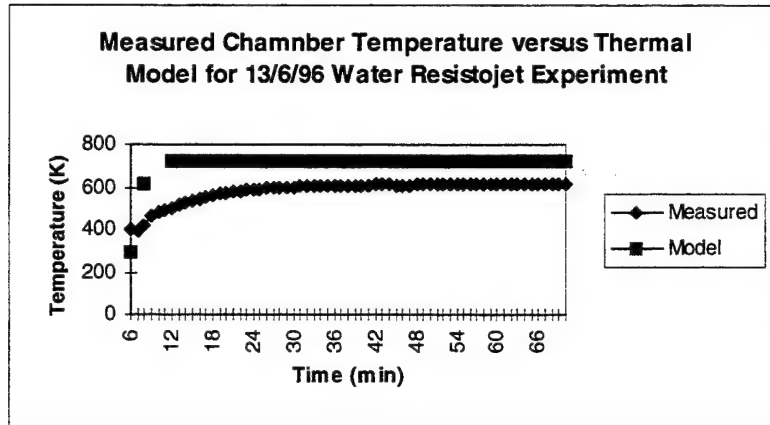


Figure 3-26: Comparison of thermal model to measured chamber temperature for the proof of concept thruster experiment (13/6/96)

3.5. Conclusions

This research phase was successful in proving a packed bed using silicon carbide as the bed heat transfer material is feasible for resistojet application. However, to meet the small satellite mission constraints several improvements are needed in another phase of research. The constraints that are not satisfied are:

- Power: The time to reach steady state was on the order of 30 minutes, which @ 560 W of input power, does not meet the power constraint.
- Mass/Volume: The heat transfer efficiency was lower than projected due to radiation losses
- Integration: heater lifetime was unreliable, ~1 - 2 hours and at least 7 hours is needed for the experimental mission presented in Chapter 2.

The approach to solve these problems is presented in the next chapter.

3.6. References

- [Humble, 95] Henry, Gary, N., and Larson, Wiley J., *Space Propulsion Analysis and Design*, New York: McGraw-Hill, Inc., 1995.
- [Morren, 93] "Gravity Sensitivity of a Resistojet Water Vaporiser," NASA Technical Memorandum 106220, AIAA-93-2402, 29th Joint Propulsion Conference, Monterey, California, June 28-30, 1993.
- [Seville, 96] Phone conversation with Mr Allan Seville of New Metals and Chemists, UK, June, 1996.
- [Sutton, 92] *Rocket Propulsion Elements An Introduction to the Engineering of Rockets*, 6th Edition, New York: John Wiley & Sons, Inc., 1992.
- [Sutton, 96] Phone conversation with Mr Alan Sutton, Air Force Research Laboratory, Electric Propulsion Laboratory, Jan, 96.
- [Todreas, 90] and Kazimi M.S., *Nuclear Systems I Thermal Hydraulic Fundamentals*, New York: Hemisphere Publishing Organisation, 1990.

Chapter 4

Prototype Research Phase

4. PROTOTYPE RESEARCH PHASE

4.1. GOALS AND OBJECTIVES

4.2. THRUSTER DESIGN AND EXPERIMENTAL APPARATUS

4.3. EXPERIMENTAL RESULTS

4.4. MODELLING RESULTS

4.5. CONCLUSIONS

4.6. REFERENCES

This chapter summarises the design, experimental set-up, and test results of the prototype thruster. The results from the proof of concept phase are used for a change in the system design: lower power and mass flow, and use of insulation for the best total impulse and performance. Relationships are derived that show optimum performance for the working fluid and power level. The test results are also compared with the thermal model for future design applications. The key result in this research phase is that friction losses in the nozzle presented performance losses (thrust and specific impulse) for the optimum chamber conditions. The chapter concludes explaining this result and the requirement for another phase of research.

4. Prototype Research Phase

4.1. Goals and Objectives

Based upon the proof of concept results, the prototype thruster was developed next in the research programme. With the knowledge gained from the proof of concept thruster, it was planned that the prototype thruster would satisfy the 6 small satellite stationkeeping constraints and produce a flight qualified system.

The first goal was to improve the poor results from the last research phase. Improvements were needed in :

- heater temperature and lifetime—fails integration metric
- time to reach steady state—fails power metric
- heat transfer efficiency—fails mass metric
- performance—fails mass metric

If these results are improved, then the thruster would be ready for the flight qualification phase. Thus the second goal of this phase was to produce a flight qualified thruster and the associated design tools.

4.2. Thruster Design and Experimental Apparatus

One of the problems in the first phase was the heater performance. It was deduced that a better heater (greater than 1 hour lifetime, high temperature @ low input power) must be found to improve performance. After a detailed survey (www, literature search, catalogues, and personal contacts) a new heater was discovered through the ISE Inc. company located in Cleveland Ohio, USA. This heater cost 5 times as much (£100), but had a lifetime of one year of continuous operation @ 980 C internal heater temperature. The Hedin heater used in the last research phase had no specification for lifetime as a function of temperature. It was decided to conduct an experiment by placing a thermocouple on the outer sheath of the heaters and evaluating their temperature at the same input power. The results are shown in Figure 4-1.

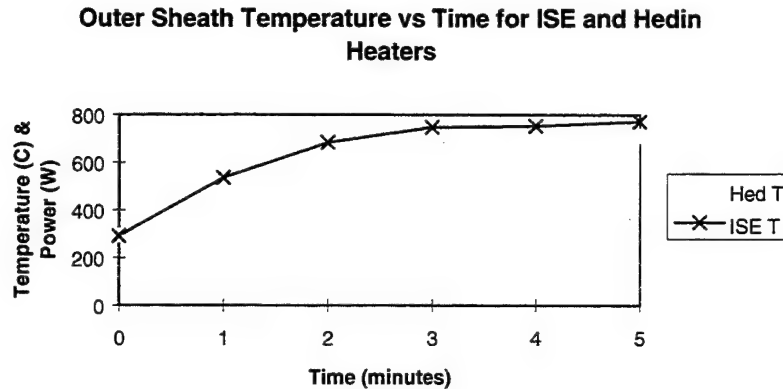


Figure 4-1: Heater comparison sea level test @ 225 W power

The ISE heater had a faster increase in sheath temperature and reached a higher temperature than the Hedin heater @ 225 W input power. Based upon the lifetime published from the vendor and the demonstrated unreliability of the Hedin heaters, the ISE heater was a good replacement for improving the test results and moving the thruster closer to meeting the research constraints.

The second problem addressed was time to reach steady state. Depending on the start-up conditions - power and mass flow rate, the time to reach steady state varied from 30 - 60 minutes for the two working fluids in the last phase. Since most of the experiments were at 560 W, this would only allow 20 minutes of operation on UoSAT-12 (on-orbit power average of 140 W) and would produce unacceptable performance. This type of transient has been witnessed in other systems. Past resistojets did not reach steady state until 90 minutes of operation [Zafran, 83] and arcjets take between 30 - 90 minutes [Stuttgart, 97]. Thus, for this phase of research it would be better to lower the power to support a longer run time. Thus, the prototype thruster was designed for 200 W to support 1 hour of operation on UoSAT-12.

The third issue to address was the performance of the test rig due to instrumentation. The proof of concept thruster had 12 thermocouple locations. This led to extra thermal mass (15 mm of stainless steel fitting support material) and leaks. The reason for having the 12 thermocouples in the last research phase was for bed material characterisation. As mentioned in Chapter 2, hot spots have occurred previously in beds, and more thermocouple locations would help determine if such flow conditions exist. However, since the various thermocouple locations were leading to leaks, the performance of the system could not be properly evaluated.

For this phase of research, 2 thermocouples and 2 pressure transducers were used for performance characterisation. One thermocouple was fabricated in the middle of the heater to monitor heater temperature. Since the manufacturer's guaranteed lifetime was 1 year at 980 C, it was important to insure that this temperature limit was not exceeded. The second thermocouple was located at the chamber exit, slightly below the nozzle exit (Figure 4-2). A tube was welded to the back nozzle plate, surrounding a 1 mm hole to allow access of the thermocouple to the chamber. This thermocouple was used to monitor chamber temperature. From the performance analysis presented in Chapter 3, chamber temperature was used to derive several ways of evaluating performance. The empirical results presented in Chapter 3 also showed that one chamber thermocouple served as a good metric for evaluating performance and flow conditions in the chamber even though some of the effects may be localised.

There were two pressure transducers. One was located in the aft tube at the same location of the thermocouple (Figure 4-2). The other was located at the inlet to the chamber. Welded fittings were used instead of screwed fittings since the screwed fittings lead to leaks in some of the proof of concept tests.

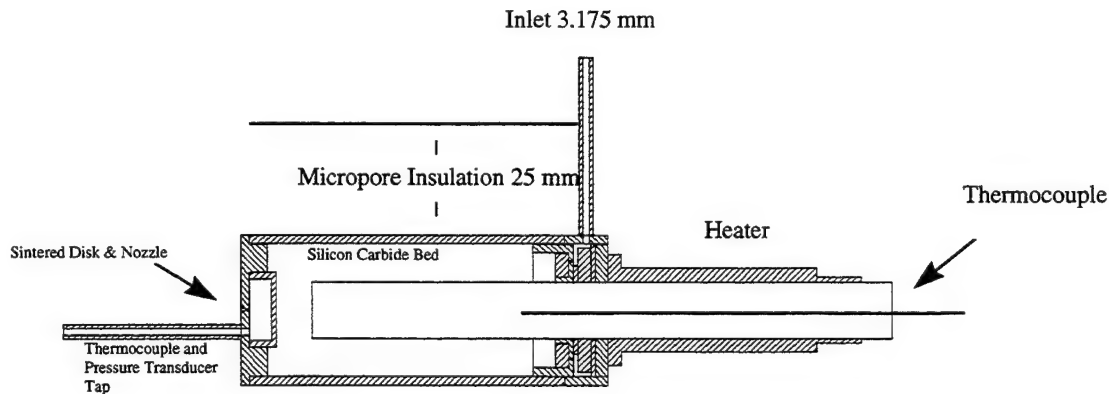


Figure 4-2: Prototype Thruster

Figure 4-2 and Table 4-1 show the prototype thruster design. The thrust chamber dimensions and nozzle are reduced to accommodate the lower energy input. The nozzle dimensions require the throat to be spark eroded. These dimensions and flow conditions were analysed using the thermal model to produce the optimum design @ 200 W. The simulation results for the above dimensions and proof of concept test results are shown in Figure 4-3. These results show that the smaller dimensions and use of insulation should improve the heat transfer of the system over time. Two thrusters were fabricated, an engineering model and a flight model.

| System | Specification |
|---------------------------|---|
| Thrust Chamber Dimensions | 30 mm (o.d.) x 120 mm |
| Power | 200 W |
| Bed Material | Silicon carbide (42 % packing density - measured through volume displacement) |
| Thruster Mass | 270 g |
| Insulation | Micropore, thermal conductivity of 0.006 W/m ² in vacuum, 25 mm thick |
| Nozzle | 0.12 and 0.128 mm throat diameter, sized to support lower mass flow rate in chamber due to lower power input, 100:1 expansion ratio |

Table 4-1: Prototype Thruster Specifications

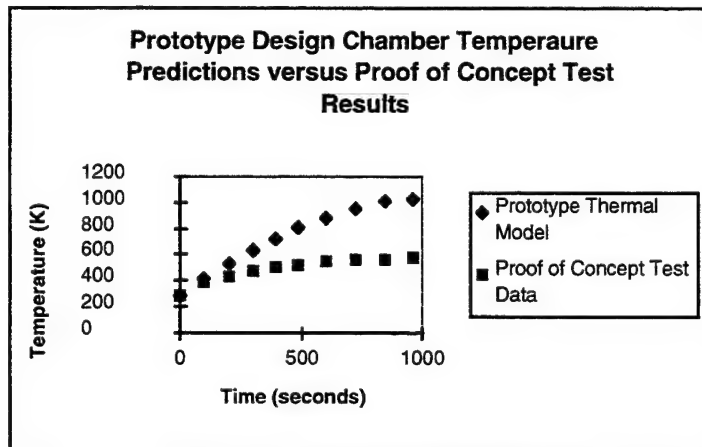


Figure 4-3: Prototype Chamber Temperature Prediction using the Thermal Model versus Proof of Concept Test Results

In this research phase, multiple working fluids were tested. There were two reasons for this approach:

- Ideal gases (N₂, He) have easy state properties (perfect gas law). These gases will enable easier validation of the thermal model compared to water (phase change) and nitrous oxide (decomposition reaction).
- use of methanol and isopropyl alcohol mixtures with water. At the beginning of this research phase, the initial thermal models of UoSAT-12 showed the spacecraft would function for periods of time at temperatures ~ - 20 C. Adding these solvents to water has the propensity to lower the freezing point of the mixture (creating anti-freeze).

The amount of solvent to add can be calculated by:

$$\Delta T = nmF \quad (4-1)$$

where:

ΔT = freezing point solvent - freezing point solution (K)

$n = \text{ion factor} = 1 \text{ (ions)}$

$m = \text{moles of solution (mol)}$

$F = -1.86 \text{ (correlation factor for water) (ions mol/K)}$

The amount of solvent added to the water solution does impact the specific impulse since isopropyl alcohol ($\text{HOCH}_2\text{CH}_2\text{OH}$) - IPA and methanol (CH_3OH) are heavier molecules. Figure 4-4 shows the decrease in Isp as more IPA is added to the water solution.

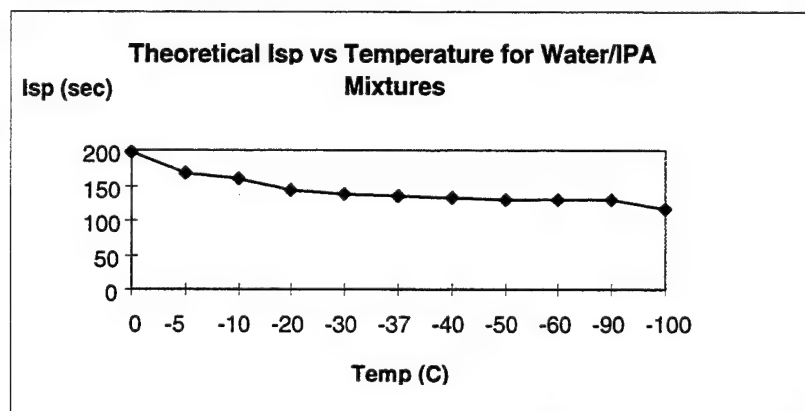


Figure 4-4: Change of performance with addition of IPA (0 - 90 % mixtures by mass) Each point shows the optimal water to isopropyl mixture for that temperature.

The programme started testing in April 1997 and was conducted in 2 phases - April through October 1997, and Dec 97 through Jan 98. The first phase was conducted at approximately sea level at the University of Surrey and at the Royal Ordnance facility. The Royal Ordnance facility allowed vacuum testing to 0.3 mBar. The second phase was conducted at Edwards AFB using the NASA Jet Propulsion Laboratory inverted pendulum thrust stand at the Air Force Research Laboratory Electric Propulsion Laboratory.

4.3. Experimental Results

Figure 4-5 shows pictures of the prototype thrusters in the vacuum facility at Royal Ordnance. Over 150 hours of data were collected using the two thrusters. Table 4-2 summarizes the test parameters for the two thrusters. As stated in the last section, two thrusters were built to represent an engineering model and flight system. Unfortunately, as test data was collected, problems occurred that caused one of the thrusters to fail. As this thruster was repaired, the flight thruster was used to conduct more tests since it became evident that this phase was not going to produce a thruster ready for the flight qualification phase. These specific problems will be described later in this section.

| Test Parameter | Result |
|---------------------|---|
| Power | 10 - 220 W |
| Massflow rate | 0.000005 - 0.00001 kg/s |
| Pressure | 4 - 17 bar |
| Working fluids | Helium, Nitrogen, Water, Water/Isopropyl Alcohol, and Nitrous Oxide |
| Bed Material | SiC, SiC/MgO (discussed later in section) |
| Chamber Temperature | 450-1100 K |
| Thrust | 5 - 20 mN |

Table 4-2: Test Parameters for Prototype Thruster Tests

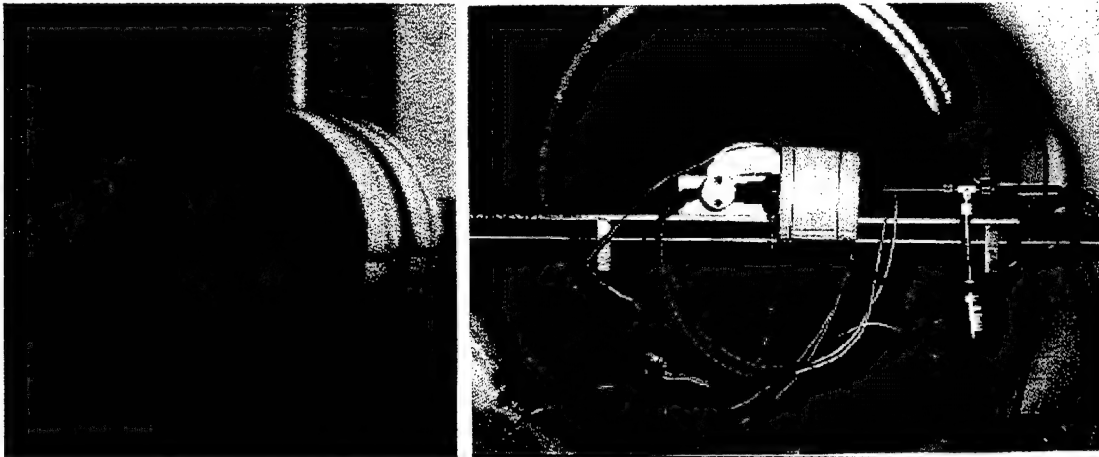


Figure 4-5: Pictures of Prototype Resistojet First picture shows thruster glowing at steady state temperature of 900 K. The second shows the thruster in the Royal Ordnance vacuum right before conducting a test.

The initial results showed an improvement in the prototype phase. Figure 4-6 shows the difference in performance for the two research phases at sea level.

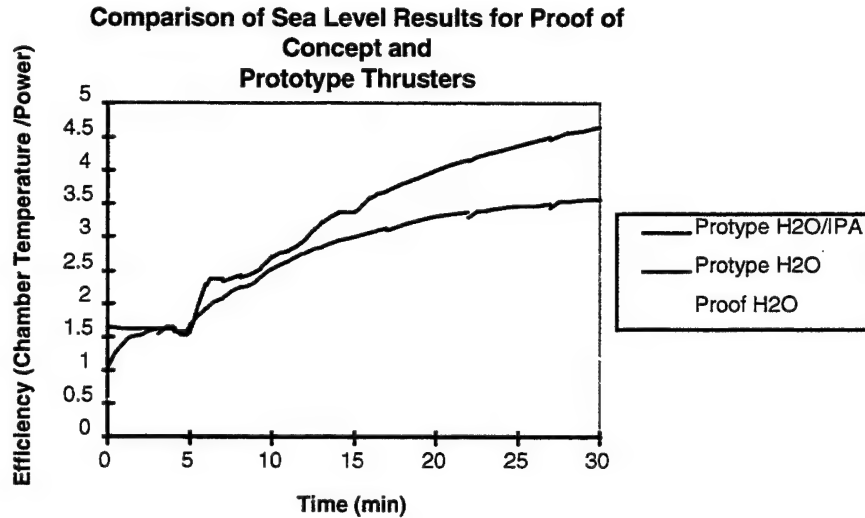


Figure 4-6: Comparison of Proof of Concept and Prototype Resistojets @ sea level: Notice the Chamber Temperature to Input Power ratio is a factor of 3 better for the prototype thruster using water as the working fluid.

Further observations of the prototype test results were also encouraging:

- heater lifetime: up to 150 hours of operation without a failure (compared to several hours with the proof of concept heater)
- heat transfer: factor of 3 higher chamber temperature at a lower input power as predicted by thermal model (Figure 4-6)
- faster start-up (reached steady state 15 minutes sooner than proof of concept thruster)
- no variation in performance with respect to gravity (Figure 4-7)
- no ice observed in exhaust plume under vacuum @ 30 mTorr

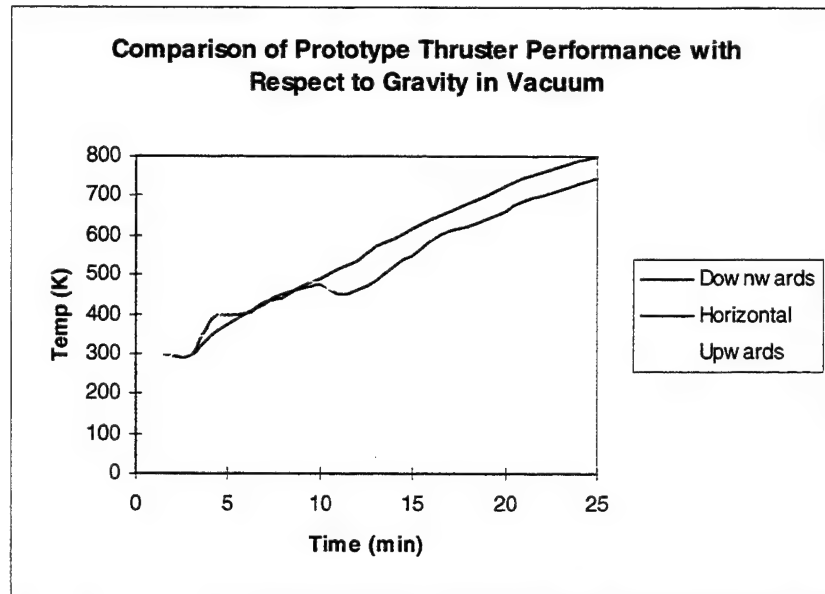


Figure 4-7: Comparison of Thruster Performance with Respect to Gravity in Vacuum using Water as the working fluid @ 200 W. The Downwards, Horizontal, and Upwards legend represent the thruster orientation [Morren, 93].

However, problems occurred whilst observing the 75 tests during this phase of the research programme. As shown in Figure 4-8, there were flow oscillations observed at start-up as the thruster was reaching steady state. This was due to the coupling of the inlet pressure to the chamber pressure as the water evaporated. A stainless steel sintered disk was added just aft of the injector to give a pressure drop to prevent the flow oscillations regulating the inlet flow. The disk did not decouple the flow, so a Lee Visco Jet flow restrictor was added to the inlet. This worked very well in preventing the oscillations and a smoother start-up was observed.

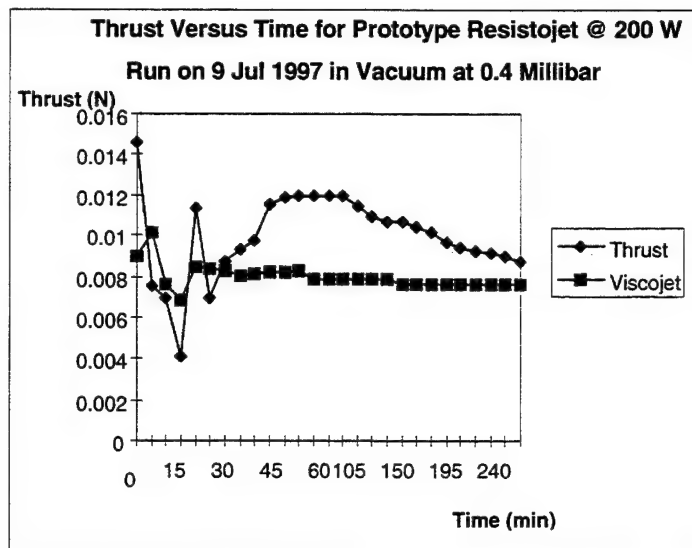


Figure 4-8: Thrust versus time for one of the Prototype trials. Notice the variation at start-up. This was due to flow oscillations in the chamber as the thruster was reaching steady state. This was corrected by adding a flow restrictor (Lee Visco jet) at the inlet.

The next problem encountered is clogging of the nozzle. Figure 4-9 shows the thrust versus time for the two thrusters. It is postulated that the clogging is caused by oxidation of the stainless steel. Figure 4-10 shows the oxidation rate of steel as a function of temperature. The prototype thrusters operate at temperatures close to 1000 K for long durations during the test programme. Since the nozzle was only ~0.1mm in diameter at the throat, the oxidation of the stainless causes flaking which gradually clogs the nozzle over time. Figure 4-11 shows the results of an electron microscope analysis of the nozzle. The picture shows the exit area of the nozzle- entire exit area covered with particulate. The Scanning Electron Microscope also analyses the surface material composition. The results show high concentrations of oxygen in the clogged area.

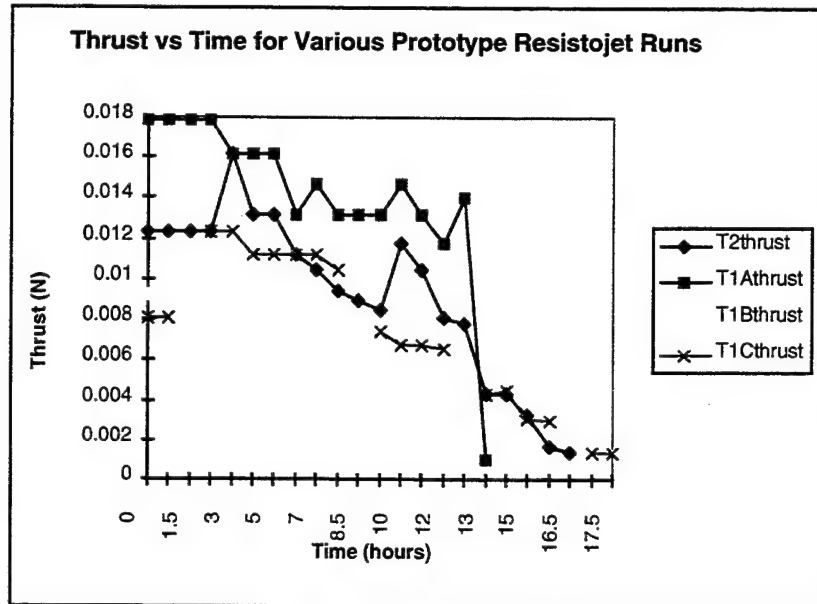


Figure 4-9: Thrust versus time for the two resistojets used in the Prototype programme.
Thruster 1A 1 B 1C, represents the same thruster, just that the clog in the nozzle had been opened by various means (0.1 mm drill bit, vibration, cleaning) and the test was started over again.

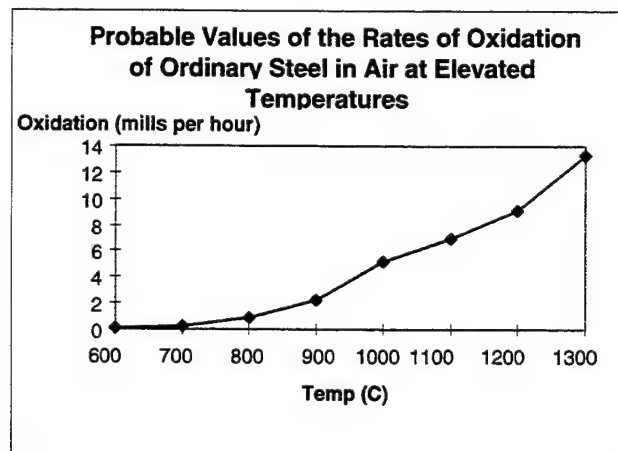


Figure 4-10: Oxidation rates of ordinary steel as a function of temperature from [Haynes Alloy, 97]

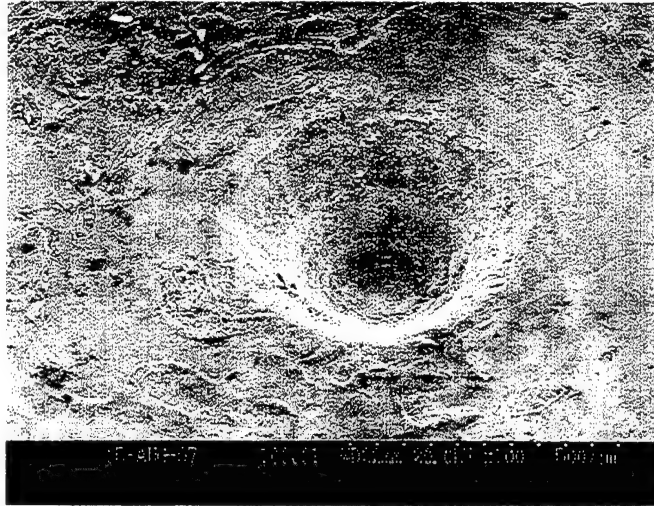


Figure 4-11: Scanning electron microscope view of the nozzle exit area showing the clogged nozzle

Since the nozzle and thrust chamber used in the programme were low grade stainless (316 or less - the chambers were made from scrap material), a more oxidant resistant material is needed to increase lifetime. Per discussions with several vendors, low cost materials are available (e.g. Hastelloy) that are oxidant resistant up to temperatures above 1000 C.

Haynes Alloy (Hastelloy) was purchased and re-welded onto the thrusters shown in Figure 4-9. This improved the performance compared to Figure 4-9, but a slight thrust decay was still observed. This result will be described in greater detail in Chapter 5.

The bed material in one of the re-welded materials was replaced with a homogenous mixture of silicon carbide (350 μm) and magnesium oxide (5 mm). It was suggested that magnesium oxide could act as a catalyst for nitrous oxide and allow decomposition to start at 250 C instead of 600 C [Drum, 97]. This bed mixture material is shown below:



Figure 4-12: SiC and MgO Catalyst

It would have been ideal to find a 350 μm powder of MgO. Unfortunately this was found to be cost prohibitive (£1000). The thermodynamic properties of MgO also show it is a very good insulator ($k=13 \text{ W/mK}$), so a complete MgO bed would have been difficult to heat up. Unfortunately, the catalyst material did not work. It performed worse than the nitrous oxide tests just using silicon carbide as the bed material. It was deduced that any added decomposition that was gained at lower temperature was lost due to the poor heat transfer characteristics of MgO. These results are discussed further in Chapter 5.

The isopropyl alcoholic test results were also poor. Since IPA contains carbon, coking occurred in the chamber. Under a high concentration experiment (60 % water, 40 % IPA by mass), one of the thrusters completely clogged the injector with carbon deposits. The deposits could not be cleaned through an ultrasonic bath or nitric acid. The thruster had to be cut open and the injector replaced. IPA tests were then ruled out.

The last problem observed in all of the tests was friction losses in the nozzle. This dramatically decreased the efficiency of the thruster. An analysis of these losses will be presented in Chapter 5.

4.4. *Modelling Results*

Figure 4-13 through 16 shows the mass flow rate, chamber temperature, chamber pressure, and efficiency as a function of time for a 100 W water experiment. These results were similar to other runs at higher powers for this research phase since the mass flow was altered to keep the heater temperature at its design limit of 980 C. For lower power runs, mass flow was maintained or slightly lowered with a resultant decrease in chamber temperature. All of the test results are attached in the enclosed CD-ROM. A summary of the significant test results is discussed in Chapter 5.

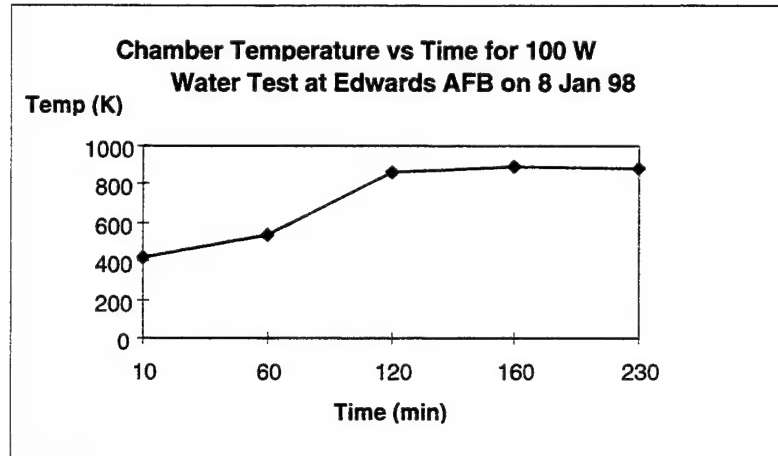


Figure 4-13: Chamber Temperature vs Time for Prototype Water Resistojet

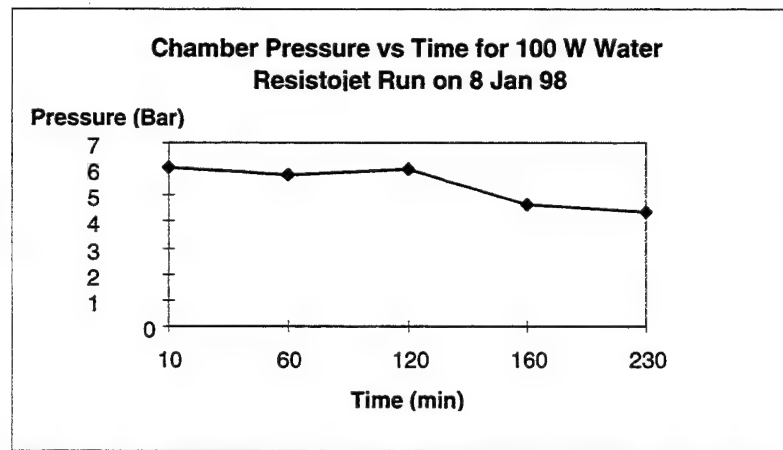


Figure 4-14: Chamber Pressure vs Time for Prototype Water Resistojet

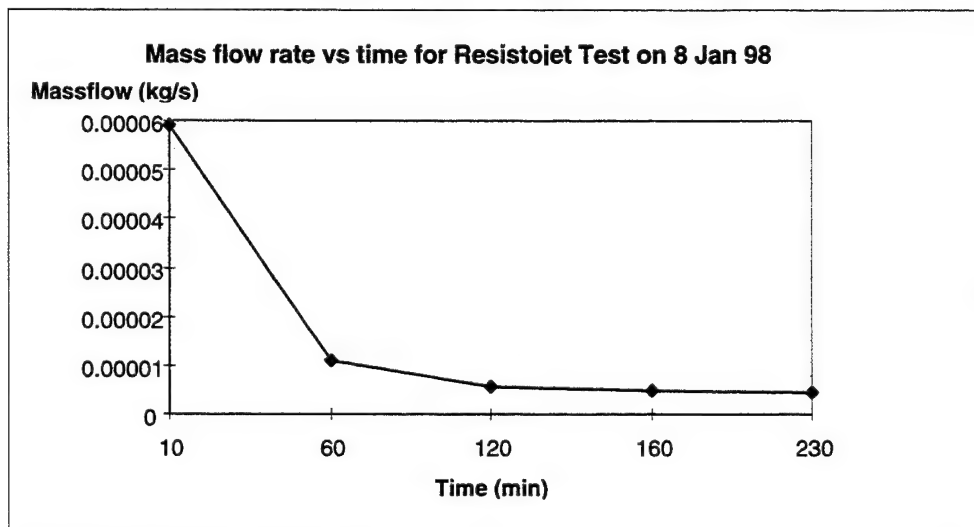


Figure 4-15: Mass Flow Rate vs Time for Prototype Water Resistojet

Figures 4-13 - 4-15 show similar trends to the proof of concept results. At a constant input power, pressure slightly drops / remains constant as the chamber temperature increases and the mass flow

rate decreases. These observations match the First Law of Thermodynamics (energy is proportional to the mass flow rate and temperature) and C^* (efficiency is inversely proportional to the mass flow rate) equations presented in Chapter 3 to show the heat transfer rate is increasing with time.

Figure 4-16 shows the relationship of input power, mass flow rate, and chamber temperature as a function of time for the prototype water thruster. The equation predicts the input power/mass flow rate ratio as a function of chamber temperature. This will be important in analysing scaling and is discussed in Chapter 6.

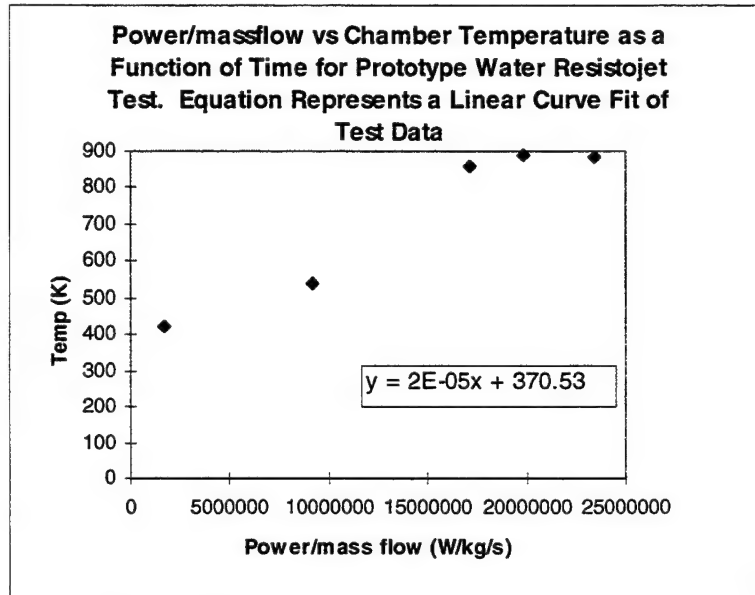


Figure 4-16: Chamber efficiency vs time for Water Prototype Experiment

Figure 4-17 through 4-20 show the prototype results for a 100 W nitrous oxide prototype experiment. The results were similar over varied power levels and mass flow rates for this thruster geometry due to the heater constraint.

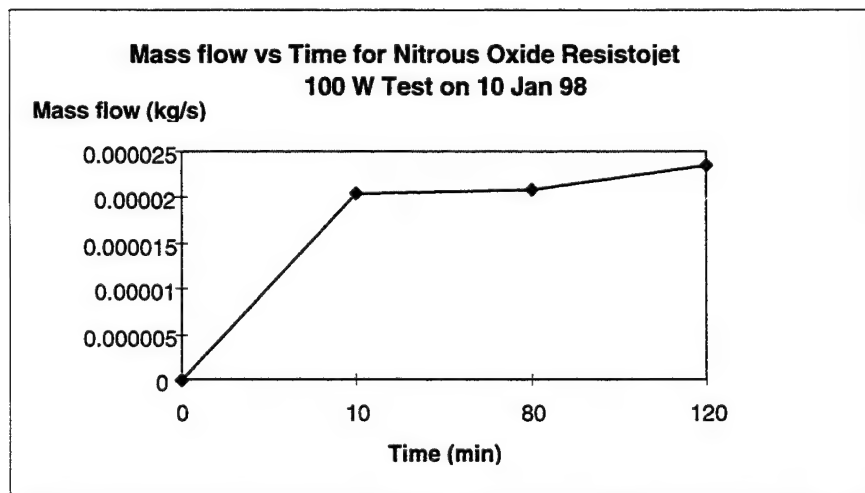


Figure 4-17: Mass flow vs time for 100 W Prototype Resistojet Test

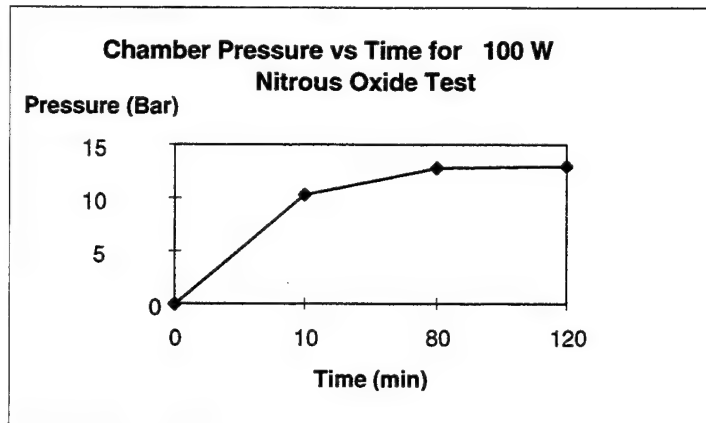


Figure 4-18: Chamber Pressure vs Time for Nitrous Experiment

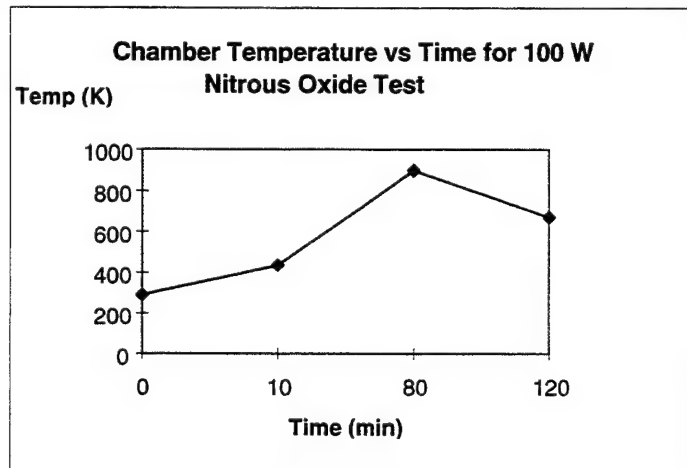


Figure 4-19: Chamber Temperature vs Time for the Same Experiment, power shut off with mass flow rate continuous at 110 Minutes

These results also show an increase in heat transfer over time (until the power is cut off). Since C^* is directly proportional to chamber pressure, it is increasing with time while mass flow rate remains constant. For the First Law of Thermodynamics equation, chamber temperature is increasing while mass flow rate remains constant.

Figure 4-20 shows the chamber efficiency. The equation generated is useful for empirical scaling comparisons for nitrous oxide.

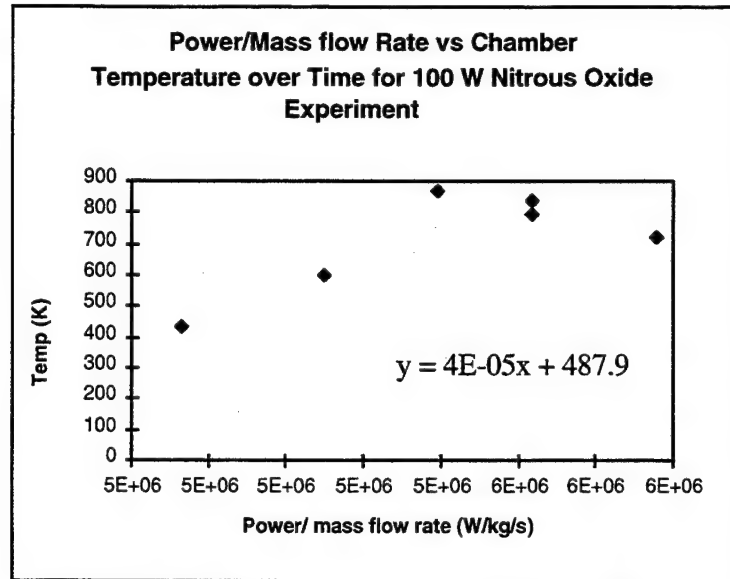


Figure 4-20: Chamber efficiency for 100 W Nitrous Oxide Experiment - power to mass flow rate ratio pretty constant through out experiment. Equation shows curve fit over time.

Since the second phase of tests (Dec 97 - Jan 98) were conducted on a thrust stand at the Air Force Research Laboratory's Electric Propulsion Laboratory, there is another source of calculating heat transfer efficiency besides the methods discussed in Chapter 3. The thrust stand and its capabilities are discussed in the next Chapter. The heat transfer efficiency can be calculated in a different way since there is a measured thrust. The measured Isp and thrust from the thrust stand can be used to calculate the exit jet power. The new relation becomes:

$$\text{Efficiency} = \frac{F I_{sp} g}{2 P_{\text{input}}} \quad (4-2)$$

where:

F= Thrust (N)

Isp = specific impulse (sec)

Pinput = input power (W)

Figure 4-21 and 4-22 show a comparison of using Equations 4-2 and 3-3 for analysing heat transfer. Figure 4-21 shows a comparison of the two methods for a 100 W nitrogen experiment. The two methods are very close, within 2 % of each other for the length of the experiment. Figure 4-22 presents a different story. After the first 60 minutes, the methods are within 2 % of each other, but as time goes on, the methods diverge. The thrust efficiency decreases over time. At 3 hours, the thrust efficiency is just below 1 %. There are three explanations for this result:

- decay in thrust due to nozzle clogging - unlikely since thruster passed a nitrogen flow test after the experiment - good flow out the exit end.
- error bar in thrust stand - since the thrust for this experiment was measured between 3- 9 mN and the error bar on the thrust stand was ± 3 mN, this is producing a source of error in the thrust measurement. The nitrogen experiment ran between 14 - 17 mN

producing less error in the thrust measurement. The thrust stand will be discussed in greater detail in Chapter 5.

- friction losses - even though the water measurement is at the lower end of the error bar in the thrust stand measurement, friction losses offer an explanation. As the chamber temperature increases, viscosity of the fluids increases, and the mass flow rate drops, thus increasing the overall friction losses. The heat transfer performance of the two methods is very low. More than 90 % of the energy is not being transferred to the fluid.

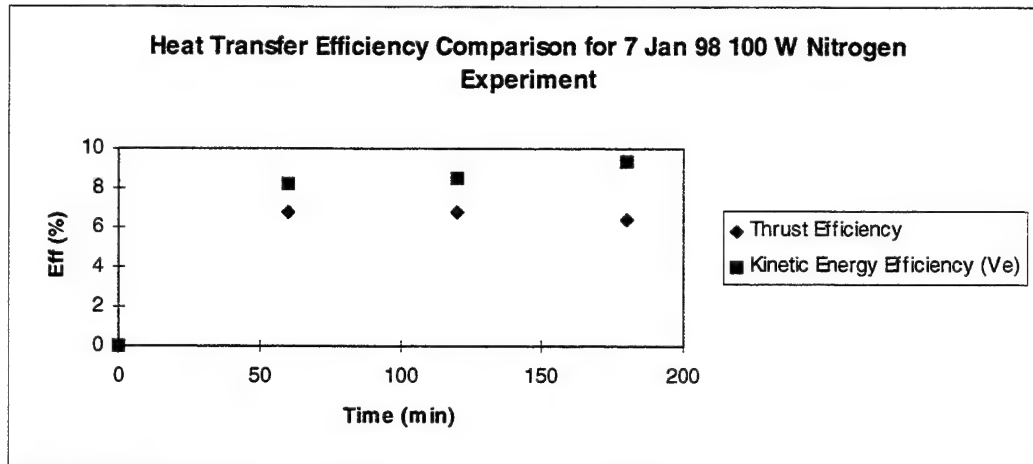


Figure 4-21 Comparison of heat transfer efficiency for prototype nitrogen experiment

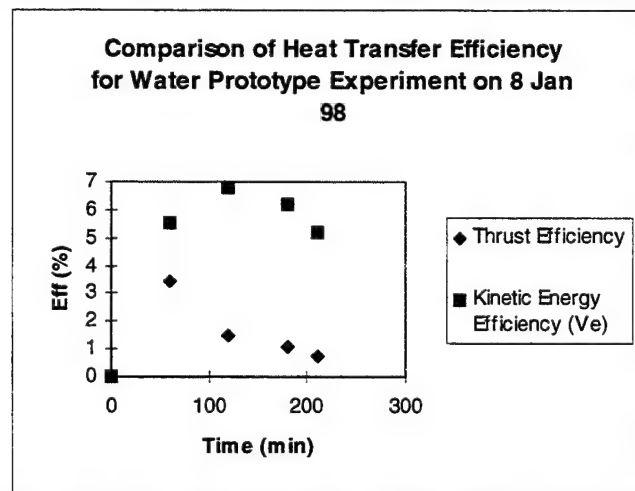


Figure 4-22: Comparison of Heat transfer efficiency for prototype water experiment

Figure 4-23 shows the heat transfer comparison for nitrous oxide. This experiment was conducted at 10 mN which is in between the thrust levels of the previous two experiments. It also shows a decrease in efficiency over time. The decrease in the kinetic energy efficiency occurs when the power increases from 105 - 120 W. This trend shows that something else is going on besides friction losses. If the power input is too high for the input mass flow, radiation losses dominate and the energy is transferred to the outside before it can heat the fluid. Use of insulation can lower the outer wall temperature to decrease these losses, but there is an energy limit for a given mass flow rate. This relation, error bars on thrust measurements, and friction losses all need to be addressed in the next research phase.

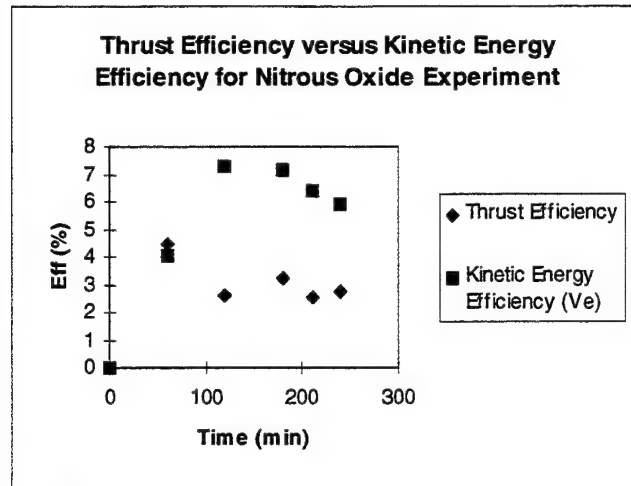


Figure 4-23: Comparison of heat transfer efficiency for prototype nitrous oxide experiment

Table 4-3 shows a comparison of specific impulse and heat transfer results for the working fluids tested for the prototype research phase. All of the results for the thrust stand measurements are presented in the next Chapter.

| Gas | Isp (sec) | Qeff (%) |
|---------|-----------|----------|
| N2O | 101.3127 | 9.608175 |
| N2O Cat | 99.40499 | 9.517179 |
| N2 | 102.7614 | 9.757975 |
| H2O | 110.1974 | 10.96853 |
| He | 116 | 16 |

Table 4-3: Comparison of Prototype Experiment Propellant Performance

Figure 4-24 shows a comparison of the thermal model simulation results to one of the prototype helium experiments. The results were improved compared to the proof of concept phase. This is attributed to:

- Helium state properties are easier to generate (perfect gas)
- Error detected in bed to heater geometry after Dr Parkinson visit in April 98.

This is an important achievement, since as the tests results from this research phase showed, another phase of research was required before flight qualification of the thruster can begin.

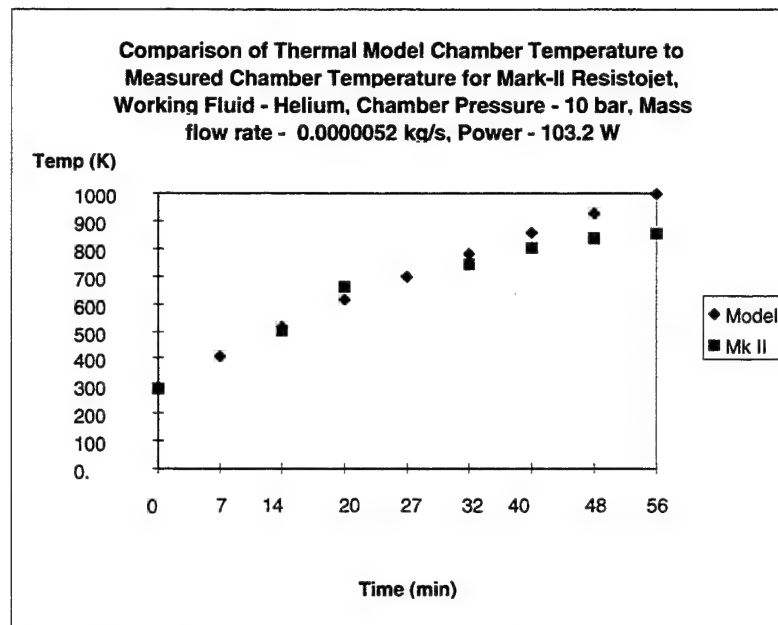


Figure 4-24: Comparison of Thermal Model to Measured Temperature for Prototype Thruster

4.5. Conclusions

Another phase of research is required due to the thruster not meeting the following constraints:

- Mass - performance is just slightly higher than a cold gas system, current system is not worthy of using spacecraft power for a slight gain in specific impulse
- Integration - nozzle clogging could reduce lifetime for flight system

A new system is needed that improves upon the results obtained in this phase. A higher mass flow rate system is needed to decrease radiation and friction losses. A new thermal design is needed to accommodate this and a study is also required to better characterise the friction losses. A more detailed material analysis is also required to insure the thruster can meet the satellite lifetime constraints.

4.6. References

[Haynes Alloy, 97] Haynes Alloy Company Brochure, 1997.

[Morren, 93] "Gravity Sensitivity of a Resistojet Water Vaporiser," NASA Technical Memorandum 106220, AIAA-93-2402, 29th Joint Propulsion Conference, Monterey, California, June 28-30, 1993.

[Stuttgart, 98] University of Stuttgart Electric Propulsion Web Page, 1998.

[Zafran, 83] Zafran S., and Jackson B., "Electrothermal Thruster Diagnostics Volume 1: Executive Summary", NASA CR - 168174-Vol-1, NASA Lewis, March 1983.

[Drum, 97] Personnel discussion with Cadet Jenn Drum, June, 1997.

Chapter 5

Protoflight Research Phase

5. PROTOFLIGHT RESEARCH PHASE

5.1. GOALS AND OBJECTIVES

5.2. THRUSTER DESIGN AND EXPERIMENTAL APPARATUS

5.3. EXPERIMENTAL RESULTS

5.4. MODELLING RESULTS

5.5. CONCLUSIONS

5.6. REFERENCES

This chapter summarises the design, analysis and test results for the protoflight thruster research phase. Results from the prototype research phase demonstrated that the heat transfer and endurance results were unacceptable to satisfy the small satellite mission constraints. The thrust stand results and heat transfer analysis show that friction and radiation losses are very dominant in the performance of the prototype thruster. This chapter presents an independent flow analysis that predicts this behaviour. From this analysis and the thermal model, the protoflight thruster is designed. The experimental apparatus, test results, and analysis of the test results are presented. The results of this phase show that a flight qualified resistojet thruster can meet the small satellite stationkeeping constraints.

5. Protoflight Research Phase

5.1. Goals and Objectives

The protoflight programme was started in October 1997 for testing at Edwards AFB in Dec 1997 - Jan 1998. There were several goals for this phase of the programme:

- solve material problems encountered in the prototype phase
- demonstrate performance and endurance that could lead to a flight qualified system
- develop analytical tools to support this design phase

The protoflight system used the two thrusters from the prototype programme and 4 new thrusters. A total of 450 hours of data was generated.

5.2. Thruster Design and Experimental Apparatus

The approach in the design of the protoflight system compared to the prototype system was to scale up the design. There were several reasons for this approach:

- higher power operation was decided to ease integration onto the Edwards AFB thrust stand. The thrust stand had previously tested a 30 kW arcjet and a 175 mN nitrogen resistojet. Thus three of the thrusters were designed for 300 W and one was designed for 700 W.
- There was outside interest expressed by Martin Lang of ESA/ESTEC in using the resistojet on the ATV or European module of the Space Station Freedom. A proposal was submitted to ESA for partial funding of this research.
- higher power operation should reduce the heat transfer and friction losses in the nozzle due to the higher mass flow rate.

Before the thermal model can be used for the design of the protoflight thruster, an analysis is needed to investigate the friction losses discovered in the prototype phase. There are several tools to analyse these losses. The first is to look at the discharge coefficient. The discharge coefficient can be defined as:

$$C_D = \frac{\dot{m}_{actual}}{\dot{m}_{ideal}} \quad (5-1)$$

where:

\dot{m}_{actual} = mass flow rate (kg/s)

\dot{m}_{ideal} = mass flow rate (kg/s)

It represents the measured flow rate over the ideal flow rate for the given nozzle design. If this ratio is less than 1, boundary layers exist.

The next approach is the thrust coefficient. The thrust coefficient is defined as:

$$C_F = \frac{F}{A_T P_o} \quad (5-2)$$

where:

F= thrust (N)

A_t = throat area (m²)

P_o = chamber pressure (Pa)

This expression shows the measured thrust over the throat area and chamber pressure. It is a metric to evaluate the given nozzle expansion efficiency to ideal conditions. The ideal expression is:

$$C_F = \sqrt{\frac{2k^2}{k-1} \left(\frac{2}{k+1}\right)^{(k+1)/(k-1)} \left\{1 - \left(\frac{p_2}{p_1}\right)^{(k-1)/k}\right\} + \frac{p_2 - p_3}{p_1} \frac{A_2}{A_1}} \quad (5-3)$$

where:

k = ratio of specific heats (no dimensions)

p₂= nozzle exit pressure (Pa)

p₃= ambient pressure (Pa)

p₁= chamber pressure (Pa)

A₂ = exit area (m²)

A₁= throat area (m²)

The last approach is to compare the specific impulse. From Chapter 2, the measured specific impulse is expressed as:

$$Isp = \frac{F}{\dot{m} g_o} \quad (5-4)$$

where:

F= thrust (N)

\dot{m} = mass flow rate (kg/s)

g_o = gravitational constant (9.81 m/s²)

The ideal or theoretical specific impulse is obtained from the Isp code. It calculates Isp based upon the theoretical C* and C_F:

$$Isp = \frac{c}{g_o}$$

$$c = C^* C_F$$

$$C^*_{theoretical} = \frac{\sqrt{\gamma R T}}{\gamma \sqrt{\left[\frac{2}{\gamma+1}\right]^{\frac{(\gamma+1)}{(\gamma-1)}}}} \quad (5-5)$$

where:

Isp = specific impulse (sec)

c = effective exhaust velocity (m/s)

g_o = gravitational constant (9.81 m/s^2)

γ = ratio of specific heats (no dimensions)

C_F = thrust coefficient (no dimensions) Equation 5-3

C^* = characteristic exhaust velocity (m/s)

R = specific gas constant (J/kgK)

T = chamber temperature (K)

If the measured thrust coefficient and specific impulse differ significantly from ideal, losses in the nozzle are occurring. Table 5 -1 shows that the performance is degraded in the prototype nozzles for both the water and nitrous oxide experiments. Figure 5-1 shows the ideal Isp versus expansion ratio for the nitrous oxide and water prototype test conditions.

| Nozzle throat (mm) | Exp. Ratio | Ideal Isp (sec) | Actual Isp (sec) | % of Ideal Isp | C_D | C_F | C_F Ideal | C_F (%) |
|--------------------------|------------|-----------------|------------------|----------------|-------|-------|-------------|-----------|
| 0.12 (Nitrous Oxide) | 100:1 | 131 | 70 | 53 | .73 | .83 | 1.8 | 46 |
| 0.128 (Nitrous Oxide) | 100:1 | 131 | 83 | 64 | .77 | 1.03 | 1.8 | 57 |
| 0.128 (Water) | 100:1 | 175 | 72 | 41 | 0.72 | 0.54 | 1.7 | 32 |

Table 5-1: Nozzle Performance of Prototype Thruster

Table 5-1 shows that boundary layers exist in the nozzle due to the discharge coefficient being below 1. These boundary layers lead to friction losses, hence the significant drop in specific impulse from ideal conditions. Since this is a significant contribution to poor performance, a more detailed study is needed.

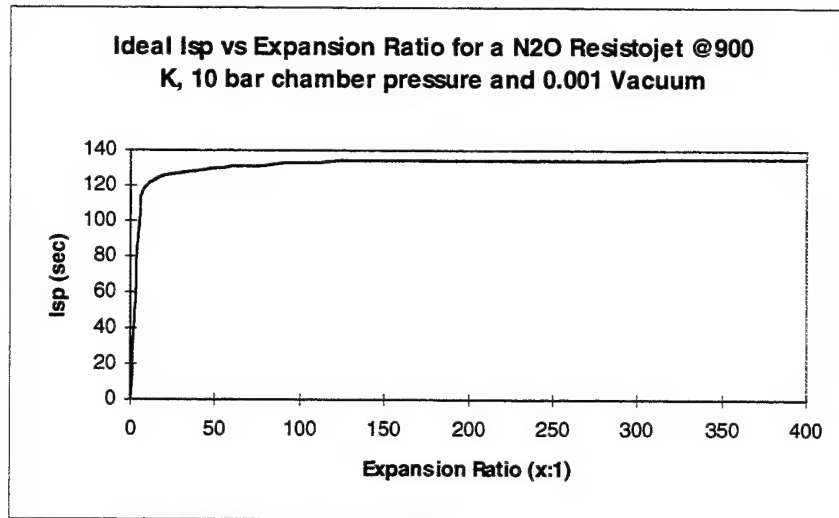
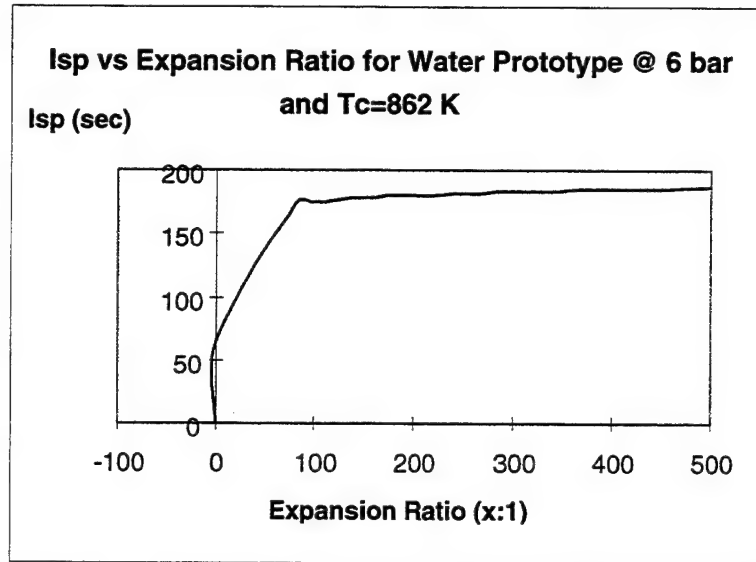


Figure 5-1: Expansion Ratio vs Isp for Ideal Water and Nitrous Oxide Prototype Test Conditions

According to *Fluid Mechanics* [White, 1986] Reynolds numbers in the few 1000's or less show the flow is dominated by viscous effects or boundary layers. The Reynolds number equals:

$$Re = \rho U d / V \quad (5-6)$$

where:

ρ = gas density (kg/m³)

U = local velocity (m/s)

d = local diameter (m)

V = gas viscosity (kg/ms)

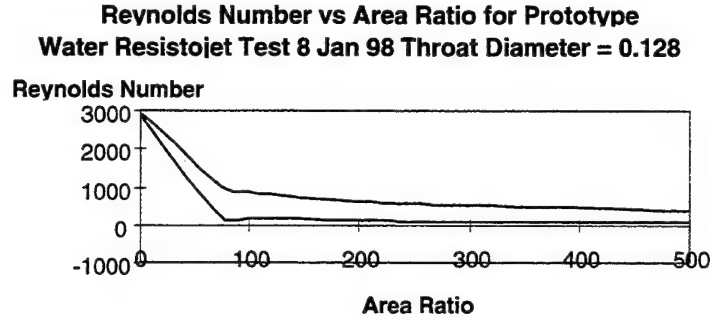


Figure 5-2: Reynolds Number versus Area Ratio for Water Prototype Test

The Reynolds analysis demonstrates that the nozzle is important in resistojet design. Even though the thruster had a high chamber temperature (~ 900 K), the geometry of the nozzle became the driver in the flow behavior. Even though the gas velocity and diameter increases with an increase in the nozzle area, they are not enough to compensate for the change in density. The gas viscosity decreases by a factor of 3 compared to a factor of 200 change in density. The Reynolds number analysis thus shows that the boundary layer effects are becoming worse due to the expansion. These results clearly show a bigger nozzle is needed for better performance.

The Knudsen Number is defined as the ratio of the mean free path of molecular collisions divided by the geometric diameter. The mean free path of molecular collisions equals:

$$\lambda = \frac{1}{\sqrt{2}\pi N \xi^2} \quad (5-7)$$

where:

N = local number density (molecules/cm³)

ξ = average molecular diameter (cm)

The Knudsen number equals:

$$Kn = \frac{\lambda}{D} \quad (5-8)$$

where:

D = local diameter (cm)

If this number is significantly less than 1, then the continuum flow calculations can be used. If it gets greater than 0.01, then the flow starts to break down. As Figure 5-3 shows, this is a problem in the prototype thruster. The flow is breaking down as it expands (increasing Knudsen) number. This also

predicts shocks are probably developing in the nozzle as the flow breaks down, adding to the boundary layer losses.

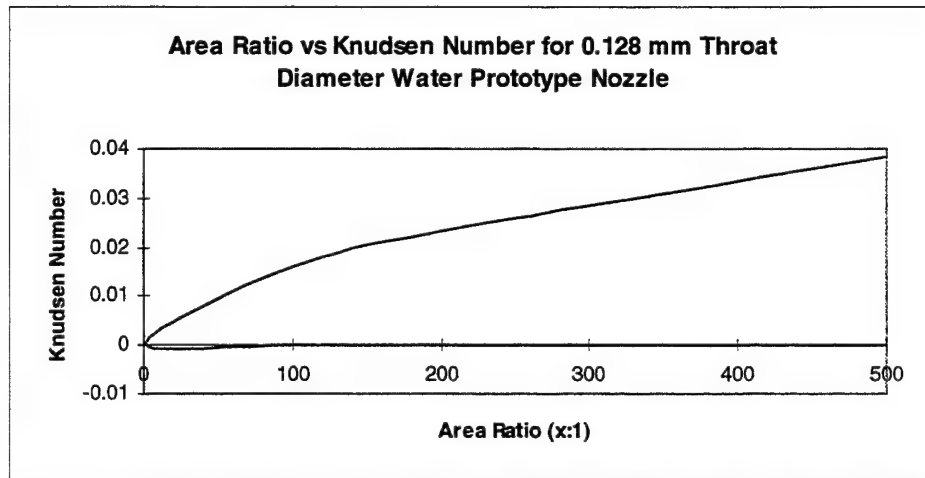


Figure 5-3: Area Ratio vs Knudsen Number for Water Prototype Thruster. Similar results were observed for the prototype nitrous experiments at 0.128 mm and water and nitrous experiments at 0.12 mm

These results are important to the small satellite community. As far as the literature survey to date, the 0.12 mm throat diameter data is the lowest recorded [Janson, 96]. Janson reports specific impulse losses of 17 - 37 % in nozzles ranging from throat diameters of 0.2 mm - 0.7 mm under nitrogen flow. Even with advances in micro-machining technology, throat size and impact on flow rate and boundary layers are important parameters to consider.

For the design of the protoflight thruster, a bigger nozzle is needed. However, there is a delicate balance between power, mass flow rate, and temperature based upon rocket science and verified in the last two programme phases. Bigger nozzles require higher mass flow rates which require higher input power to maintain the chamber temperatures achieved in the prototype research phase. However, with heat transfer efficiencies around 10%, radiation and friction losses were dominating input power consumption. Additionally, the thrust stand at Edwards AFB is only qualified for an error bar of $\pm 3\text{mN}$. These inputs require a higher power and higher thrust system (higher mass flow rate) to pursue qualification of the protoflight thruster. The thermal model is used to find the optimum design for these requirements.

Figure 5-4 shows a comparison of two thruster designs from the protoflight phase and test results from the prototype phase. Table 5-2 shows the assumptions for the simulation compared with the test data.

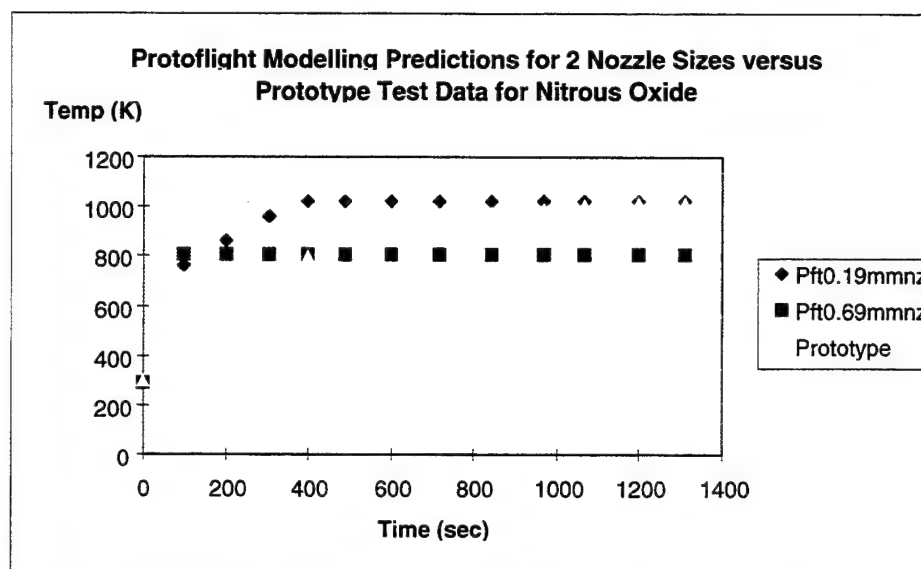


Figure 5-4: Protoflight Simulations versus Prototype Test Data for Nitrous Oxide

| Specification | Protoflight 0.19 mm nozzle throat | Protoflight 0.69 mm nozzle throat | Prototype 0.128 mm nozzle Test Data throat |
|--------------------------------------|-----------------------------------|-----------------------------------|--|
| Dimensions diameter then length (mm) | 60 x 220 | 60 x 220 | 30 x 120 |
| All have expansion ratio of 100:1 | | | |
| Working fluid | Nitrous Oxide | Nitrous Oxide | Nitrous Oxide |
| Nozzle throat size (mm) | 0.19 | 0.69 | 0.128 |
| Mass flow rate (kg/s) | 0.00004 | 0.0004 | 0.000017 |
| Pressure (Bar) | 10 | 10 | 10 |
| Power (W) | 400 | 300 | 130 |

Table 5-2: Specifications for Simulation and Test Data

The dimensions for the protoflight simulations were determined in a similar manner to the cases presented in Chapter 2, Table 2-19. Figure 5-4 shows the trade-offs in nozzle design. For the 0.18 mm case, a slight increase in nozzle size will allow a high chamber temperature at a slightly higher power. The impact on performance will be friction losses will still exist, but not to the extent of the 0.128 mm throat diameter case. As Figure 5-5 shows, the Reynolds Number is double for the 0.19 mm nozzle compared to the 0.128 mm case. The 0.694 mm nozzle should produce very little losses, since the Reynolds Number is much higher (Figure 5-6) and the Knudsen number is much less compared to the other two cases (Figure 5-7). The primary issue with the higher mass flow rate nozzle, is the extra power required.

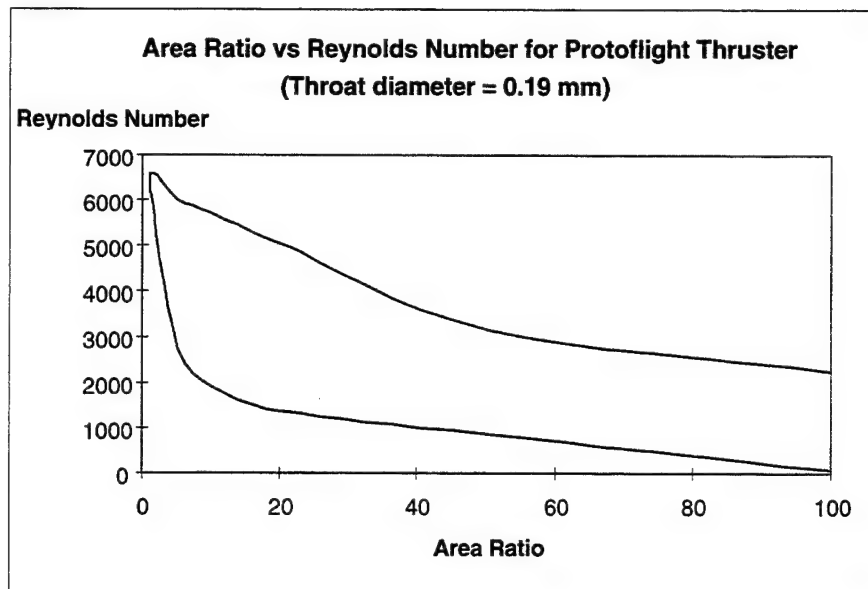


Figure 5-5: Reynolds number versus Area Ratio for 0.19mm throat diameter Protoflight Nozzle Simulation

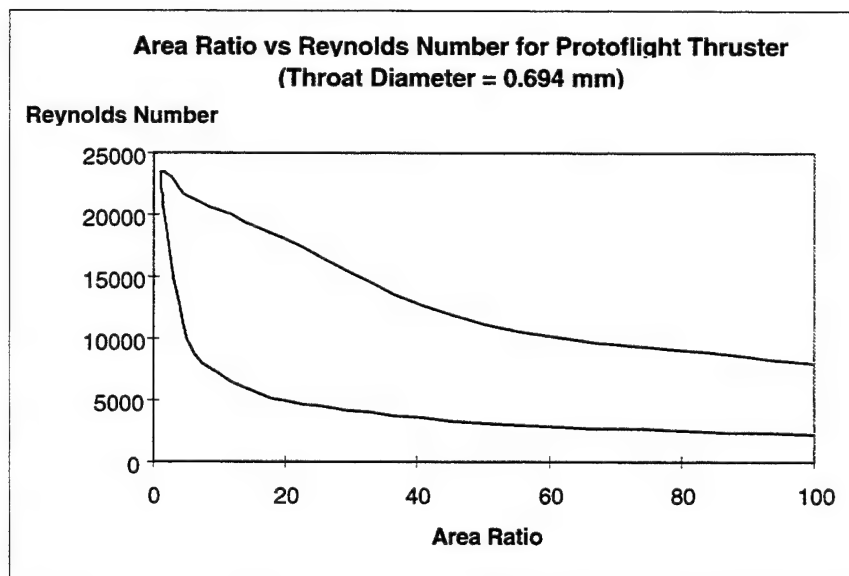


Figure 5-6: Reynolds Number versus Area Ratio for 0.69 mm Protoflight Nozzle

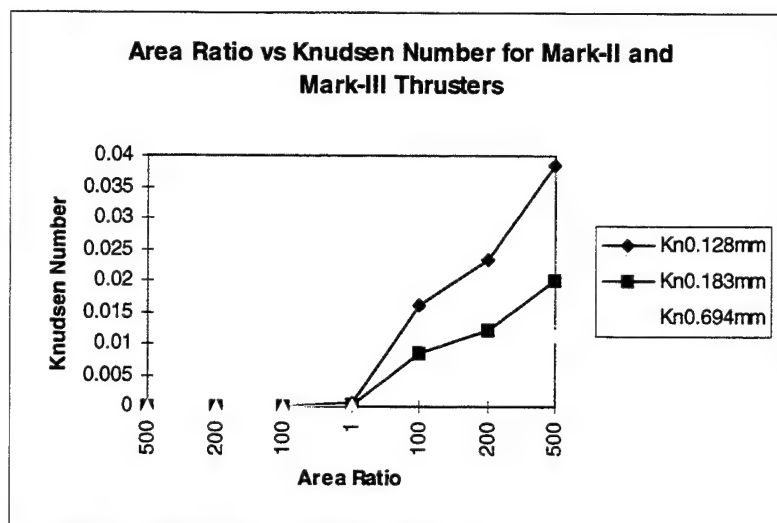


Figure 5-7: Comparison of Knudsen Numbers for Prototype and Protoflight Thrusters. At an expansion ratio of 100:1, 0.694 mm nozzle is the only one where the flow is not breaking down.

Thus, the total thrusters and working fluids used in this phase of the research programme are (the prototype thrusters were used for a comparison to the protoflight thrusters):

- Prototype #1 (0.12 mm nozzle): nitrogen, water, helium
- Prototype #2 (0.128 mm nozzle with MgO catalyst): nitrous oxide
- Protoflight #1 (0.183 mm nozzle): water, nitrogen, nitrous oxide, water/methanol
- Protoflight #2 (0.183 mm nozzle): water - long endurance test
- Protoflight #3 (0.194 mm nozzle with MgO catalyst): nitrous oxide
- Protoflight #4 (0.694 mm nozzle): water, water methanol, nitrous oxide, nitrogen, helium

The nozzle specifications to the spark erosion vendor were 0.12 mm for the prototype, and 0.18 and 0.7 mm for the protoflight. The exact dimensions were determined via scanning electron microscope.

Table 5-3 lists the specifications of the protoflight thrust chamber for the 0.18 and 0.694 mm throat diameter nozzles. Figure 5-8 shows a drawing and picture of the Protoflight thrust chamber.

| Protoflight Specifications |
|---|
| Thruster: 60 mm o.d. x 220 mm long |
| Micropore insulation - 25 mm thickness covering thrust chamber |
| Power: 0 - 600 W |
| Pressure: 3 - 100 bar |
| Massflow rate: 0.00001 - 0.0005 kg/s |
| Isp: 70 - 334 sec |
| Thrust: 9 mN - 0.5 N |
| Chamber Temperature: 850 K - 1200 K |
| 2 thermocouples & transducers for thermodynamic instrumentation |
| test conditions: @ vacuum & thrust stand |
| mass: 1.2 kg |
| electron beam welded connections |
| 60µm stainless steel filtered mesh at aft end of bed |
| 350 µm SiC or SiC/MgO bed material |
| 4 different nozzles (2 @ 0.183 mm, 0.194 mm, 0.694 mm) all made of Haynes alloy to reduce oxidation |
| Chamber 316 stainless steel (oxidation only occurring in nozzle in tests to date) |

Table 5-3: Protoflight specifications

Cutaway of Protoflight Thruster

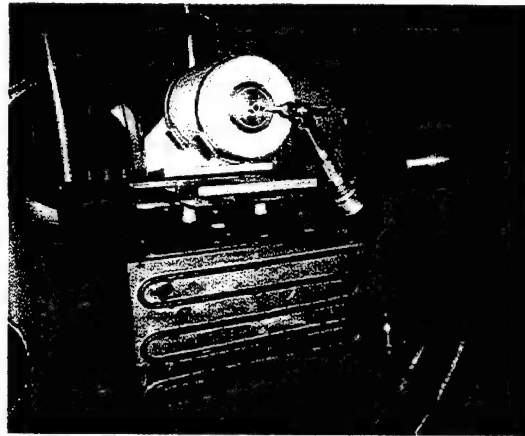
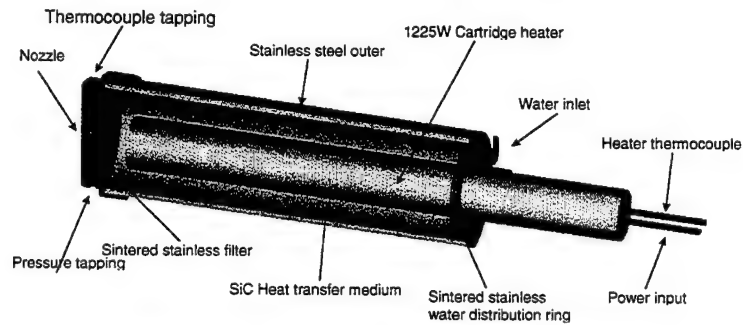


Figure 5-8: Drawing and picture of Protoflight thruster. Picture shows Protoflight #4 on thrust stand at Edwards AFB.

Figure 5-9 shows the NASA Jet Propulsion Laboratory (JPL) inverted pendulum thrust stand inside an Edwards AFB vacuum (~ 30 mTorr turn down). This thrust stand is recognized in the electric propulsion community as state-of the art (+-3mN error bar). Variations in performance as high as 25 % have been observed on other thrust stands. Thus the reason for testing at Edwards AFB.

This thrust stand is classified as a calibrated displacement type- see drawing in Figure 5-9. The thruster was mounted to a platform (phenolic plate 300 mm x 300 mm) which was in turn supported by an upright flexure arrangement. An interchangeable load spring could be adjusted to match the sensitivity requirements of the tests. Thrust induced displacements of up to 5 mm were measured using a linear variable differential transformer (LVDT).

Because flexures provided a frictionless means of thrust stand movement, hysteresis effects were negligible. Propellant was supplied through the thrust stand by means of an internal propellant flexure. The flexure was a 1/8" stainless steel tube bent into a rectangular shape and anchored to the thrust stand base at its lower end. The upper end was anchored to the mounting platform of the thrust stand so the entire tube could flex during displacements with relatively little stiffness.

Current was sent through the thrust stand using internal electrical flexures - wires dangling from the top of the thrust stand. A pressure transducer was mounted at the inlet side well before the piping entered the thrust stand (on the base). The heater thermocouple was attached in the same location as the power leads. The chamber transducer and thermocouple were mounted at the aft end and were tied to the inlet pipe to allow full motion of the thrust stand. A water cooled copper enclosure surrounded the entire thrust stand to prevent radiant heat from impinging on the flexures and structural components.

In-situ calibration of the thrust stand was performed using two strings of masses - 5 masses up to 5 g and 3 masses up to 15 g. The masses could be lowered in succession, and would engage the thrust stand through a monofilament nylon line which passed over a precision pulley. A rotary vacuum feedthrough was used to manually lower each mass, which could be done at any time during a series of tests.

A ± 5 volt analogue signal was output by the LVDT readout and used as a thrust signal. This was routed to LABVIEW and a strip chart recorder to provide a permanent record of test operations.

Due to the low thrust to weight ratio of the resistojet, thrust measurements were very sensitive to angular tilting and distortions of the vacuum facility. Thermal radiation absorbed by the test port walls resulted in deviations and would manifest itself in the form of thermal drift. Such deviations were compensated for with an angular inclinometer mounted on the thrust stand base and adjusted by using a leveling mechanism. Remote control leveling of the thrust stand to a resolution of 10 seconds of arc was possible [Haag, 91].

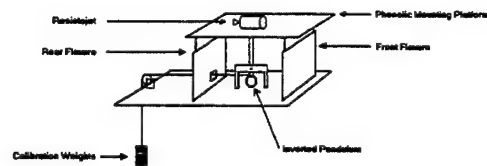
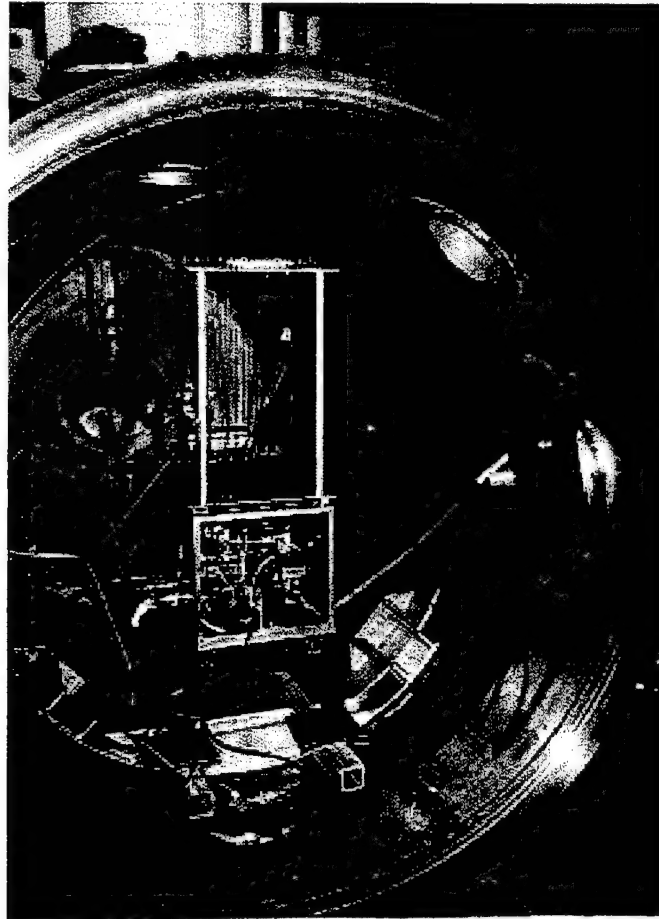


Figure 5-9: NASA JPL Inverted Pendulum Thrust Stand and Drawing of core elements of the thrust stand

The thrust stand was VERY sensitive in operation. Outside disturbances such as wind blowing on the vacuum ducting, sonic booms, people touching the vacuum vessel, walking near it, or working in an adjacent vacuum. Slamming of doors and thermal drift were the main sources of error. Errors were

corrected by bolting the thrust stand to the floor, keeping people away from the rig, and not testing in high wind conditions. The toughest problem was thermal drift. The problem was discovered to be a cooling cycle of 3 degrees C in the cooling lines (creating a thermal temperature difference in 30 minute cycles). Once the cooling lines were shut off this problem was reduced. Thrust was also measured to a zero reference point. A ball valve was added just outside the vacuum vessel that could cut off the flow to get a zero thrust measurement on the LVDT. The flow could then be put back on and a thrust measurement taken. The total time to do this was 10 minutes, temperature change in the thruster was negligible, so the readings were accurate. The error bar analysis is discussed later in this section.

Figure 5-10 shows the test procedure and a picture of the entire testing facility.



| Test Procedure |
|--|
| Set up thruster - insure no interference with thrust stand movement |
| Turn down vacuum |
| Calibrate thrust stand - using weight set appropriate for test (0 - 30 mN, 30 mN - 600 mN) |
| Conduct Test |
| Power on, flow on, thrust, thermocouple, pressure, vacuum readings |
| Zero Thrust Test - flow off/on |
| Recalibrate and compare to original |
| ERROR BAR : ± 3 mN |

Figure 5-10: Picture of test facility and procedure

The thrust stand was vital in determining the performance of the system. It has already been mentioned that the error bar on the thrust stand was ± 3 mN. This was determined by analysis on all of the sources of errors:

Error in Chart Recorder:

Precision/Data Scatter:

$$\text{Hash width} = 0.045'' \quad u_{01} = 1/2(0.045'') \times 50 \text{mN} / 0.745'' = 1.51 \text{mN}$$

$$= 1/2(0.045'') \times 1.5 \text{V} / 3.919'' = 8.61 \text{E-3V}$$

Instrument itself:

$$\text{T1C-9000: } e_1 = 2.5 \text{E-3V}$$

$$\text{Recorder: } e_2 = (0.25\%)(1.5) = 3.75 \text{E-3V linearity}$$

$$e_3 = (1\%)(1.5) = 1.5 \text{E-2 V accuracy}$$

Thus:

$$U_c = \sqrt{((2.5 \text{E-3})^2 + (3.75 \text{E-3})^2 + (1.5 \text{E-2})^2)}$$

$$= 1.56 \text{E-2V}$$

Overall Uncertainty:

$$U_d = \pm \sqrt{(u_0^2 + u_c^2)} = \pm \sqrt{((8.61 \text{E-3})^2 + (1.56 \text{E-2})^2)}$$

$$= \pm 1.79 \text{E-2V or}$$

$$= \pm 3.13 \text{mN}$$

Error in Weight Uncertainty ** Negligible Compared to Other Uncertainty.

$$\text{Readability} = 0.1 \text{ mg}$$

$$\text{Reproducibility} = 0.1 \text{ mg}$$

$$\text{Linearity} = 0.1 \text{ mg}$$

$$U_c = \pm \sqrt{((0.1)^2 \times 3)} = 0.173 \text{ mg} = 1.73 \text{E-4 g}$$

$$= 1.697 \text{E-3mN}$$

Error in Labview:

$$\text{Zero order: } U_0 = 1/2(305.18 \mu\text{V}) = 152.59 \text{E-6V (resolution of card)}$$

1st order: scatter in data precision error

$$P = S_x / N^{1/2} = 0.01177 / (2436)^{1/2} = 2.38E-4$$

Instrument errors:

$$T1C - 9000 : e_1 = 0.05\% (@5V) = 2.5E-3V$$

AT-M10: Linear error

$$e_2 = (.0000305)(5V) + 3\mu V + 76\mu V = 1.604E-3V$$

Nonlinearity / relative accuracy

$$e_3 = 228.89E-6 V$$

$$U_c = +2.98E-3V$$

Overall uncertainty:

$$U_d = + \sqrt{(U_0^2 + P^2 + U_c^2)} = 2.99E-3V @ 175 mN/V = 0.52mN$$

** Less error than chart recorder

Background Information for calculations:

Chart recorder:

$$P = 0.045'' - +1.51mN \text{ (from finite, non-zero hash width)}$$

$$F = 50 mN / 0.745'' \quad 67.11 mN/in$$

$$1.5V / 3.919'' \quad 175 mN/V$$

Labview:

$$T_o = 1.1681 V$$

$$\text{Weight 1: Point 1653 } 1.4502V \text{ } W_1 = 4.9994 g$$

$$\text{Weight 2: Point 1654 } 1.7285 V \text{ } W_2 = 5.0025 g$$

Bad Points: Due to venting 2439 and beyond

Point 1: $(1.4502-1.1681)/((4.9994\text{g}) \times (9.81/\text{m/s}^2))=5.7520 \text{ e-3 V/mN}$
 $=173.85\text{mN/V}$

Point 2: $(1.7285-1.4502)/((5.0025)(9.81)) = 5.6716\text{e-3V/mN} = 176.34 \text{ mN/V}$

Using both weights: $5.7115\text{e-3V/mN} = 175.09\text{mN/V}$

AT-M10-16X:

Gain error

After calibration $\pm 0.00305 \%$

Temp: $\pm 0.0008\% / \text{C}$

Pregain offset error

After calibration : $\pm 3\mu\text{V}$

Temp: $\pm 5\mu\text{V/C}$

Postgain offset error

After calibration $\pm 76\mu\text{V}$

Temp: $\pm 120\mu\text{V/C}$

Relative accuracy: $\pm 0.75 \text{ LSB } (\pm 228.89\mu\text{V})$

System noise: $0.6 \text{ LSB } (183.11 \mu\text{V})$

From manual, 1 LSB at a gain of 1 $\pm 10\text{V}$ range = $305.18 \mu\text{V}$

Measurement precision ($\pm 10\text{V}$, gain = 1) = $305.18 \mu\text{V}$

T1C-9000:

Non-linearity $\pm 0.05\%$

Omega Chart Recorder:

linearity: $\pm 0.25 \%$

accuracy: 1%

Thermal drift (no thruster on the stand)

$+0.074'' - +4.97\text{mN}$

+0.111" - +7.45mN Peak value

-0.053" - -3.56mN mN

4 p.m. - 9:30 p.m. : drift between 0 and -3.56mN

9:30 p.m. - 7:30 a.m. : no distinguishable drift (cooling lines not on)

7:30 a.m. - 8:50 a.m. : monotonically increasing to a peak of 7.45 mN at 8:50 a.m.

8:50 a.m. - 4 p.m.: drift between 0 and 4.97 mN

This thermal drift was a source of error. Figure 5-11 shows a performance measurement for the prototype resistojet using nitrogen as the working fluid. The peaks correspond to the thermal drift.

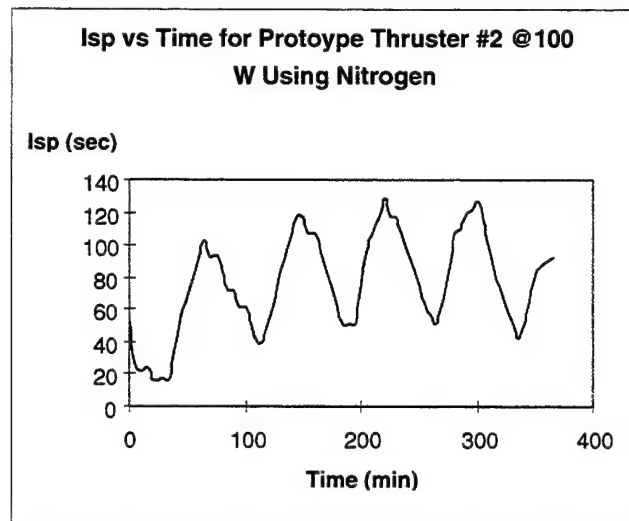


Figure 5-11: Thermal Drift in Prototype Thrust Measurement

The cooling lines were turned on for this run to mitigate the thermal drift that might be induced from the thruster. Unfortunately, it was discovered that the cooling lines had a 3 degree Celsius temperature change over a 30 minute period (placed thermocouple on feed lines). This corresponds to the above change in measurement - 30 minute period. The cooling lines were shut off and the drift was mitigated. There was some drift, but much less than the above measurement, a couple of mN over a 9 hour cycle. To improve accuracy further, it was decided to take zero thrust measurements through-out the run. A ball valve was added to the outside of the vacuum vessel to cut down the blow down in the line from the flowmeter to the stand (cuts out 2 m of feed line) The flow was cut off several times during the run. It would take 3 minutes to have all of the flow decay and the thrust reach zero, the flow would then be turned on and in another 7 minutes it would reach a steady value (10 minutes total time). These type of measurements allowed the drift to go to 0 and the $\pm 3\text{mN}$ value discussed above could be used for the error bar calculation. There were other sources of error:

- high wind (vibrated vacuum ducting - if winds too strong did not test)
- doors slamming (put up signs that testing was going on to mitigate this)
- people walking / working near stand (kept them away during 10 minute period, bolted down vacuum chamber for further away more discreet disturbances)
- sonic booms from aeroplanes (did not use data if it occurred during thrust measurement)

Besides the thrust stand, the other sources of error could come from the power supply and mass flowmeter for impact on efficiency (Isp - flowmeter and heat transfer - input power) calculations. The power supply has a published error bar of $\pm 2\%$ from the manual. The flowmeter had a guaranteed calibration of $\pm 3\%$. Since Isp is an important measurement, the mass flow rate calibration could be verified by performing a catch and weigh test. The linear variable area flowmeter could be set at various settings along the scale, measured to a volume over time, and then weighed. Figure 5-12 shows a comparison of the flowmeter calibration vs the catch and weigh. This curve could also be directly used for determination of the mass flow.

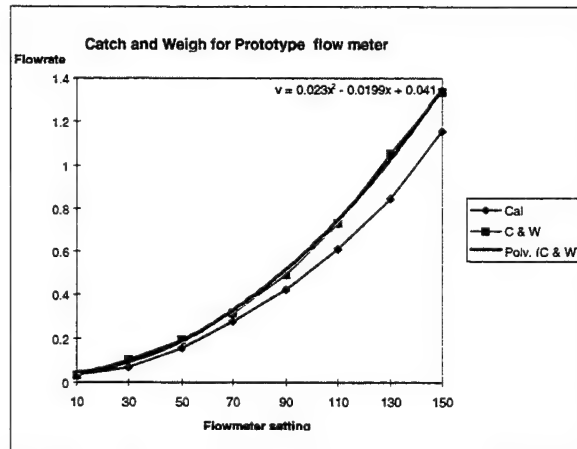


Figure 5-12: Catch and Weigh for Prototype Flow meter. Similar experiments were done for the protoflight flow meter for liquids. For gases, the 3 % error bar was assumed due to the catch and weigh for liquids was under the 3 % error. In testing the flight expulsion system (Chapter 6), the entire expulsion system was placed on a scale and the mass flow rate was verified over time. This test also verified the 3 % error bar prediction from the vendor.

These total error bar results give high accuracy - $<5\%$, for the Protoflight #4 (0.694 mm throat), good accuracy for the Protoflight #1 - #3 (0.183 - 0.194 mm throat) - 15% , and an average accuracy for the Prototype (0.12 - 0.128 mm throat) - 30% . Even though the potential error was highest for the prototype system, the low performance numbers were confirmed with the heat transfer, flow analysis, and performance of Protoflight #1 - #3 (explained in next section).

5.3. Experimental Results

The protoflight test campaign was very successful in regard to test results. The best result was a 354 hour continuous test using water as the working fluid in the protoflight thruster #2. Figure 5-13

shows the thrust over time for this test. The drastic decreases in the thrust were due to power shut downs at the Laboratory or an accidental cut off (5 times). Since this could represent thermal cycling in space, these results were included on the plot. The thruster was off for approximately 12 hours during the first 4 outages, and for 3 hours on the 5th. The thrust decayed from 18mN to 12 mN over the whole test period. This was due to silicon oxide deposits in the nozzle which will be discussed later in this section. This endurance test was the longest ever recorded water resistojet trial [Morren, 93]. This test result showed the uniqueness of the system and impressed the USAF AFRL personnel so much that they decided to fund the University and SSTL to fly the resistojet on the MightySATII.1 mission. This will be discussed in further detail in Chapter 6.

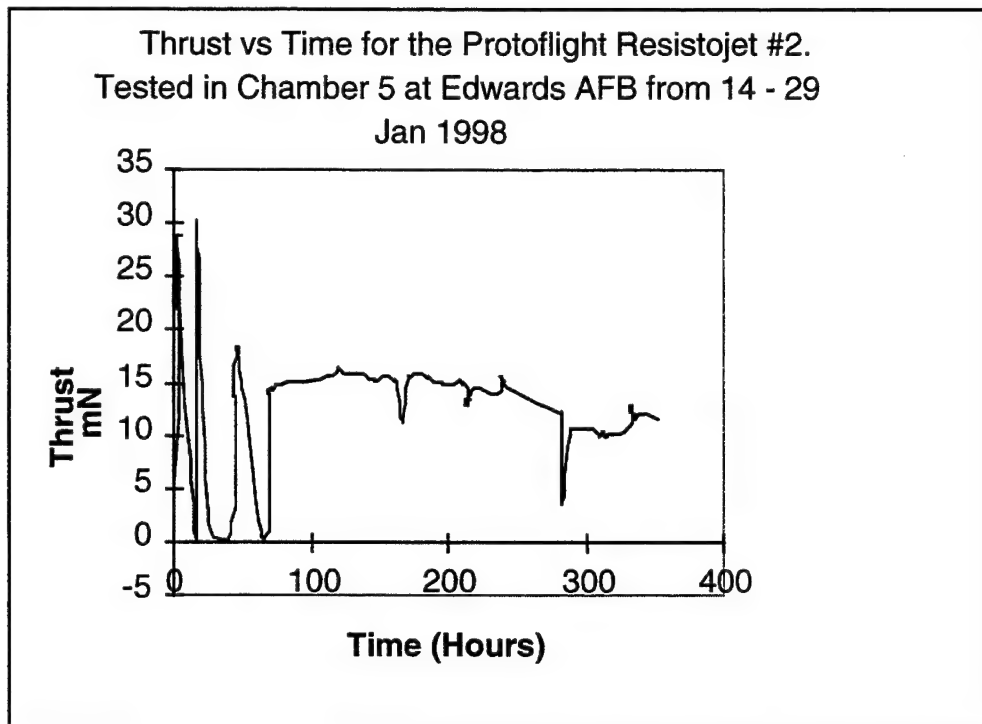


Figure 5-13: Thrust versus time for the Protoflight #2 thruster. This thrust value was calculated from Equation 3-9 since the thrust stand was concurrently in use for performance characterisation of other protoflight thrusters. Compared to thrust measurements on the thrust stand with other protoflight thrusters at the same mass flow rate, the thrust figures are accurate. Thrust decay was monitored by flow meter mass flow rate decay.

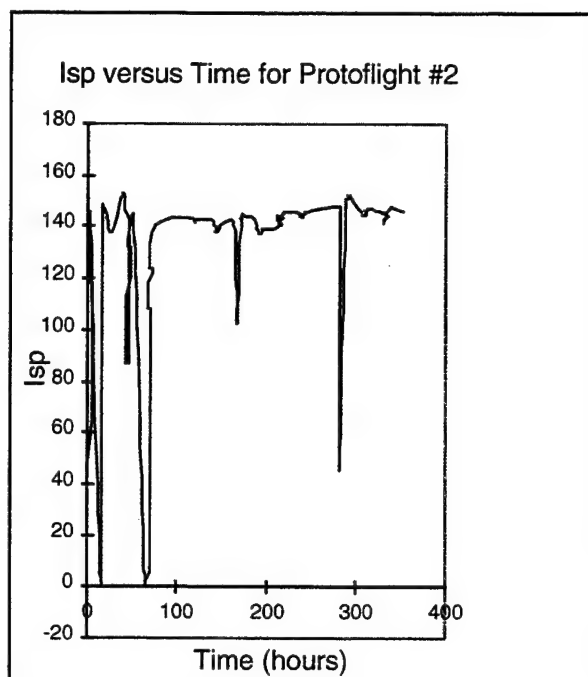


Figure 5-14: Isp versus Time for Long Endurance Test Using Protoflight Thruster #2.

Calculated from chamber temperature and pressure using Isp Code.

Another outstanding result was the first-ever self sustained nitrous oxide decomposition reaction for resistojet applications in the Protoflight #4 thruster. Figure 5-15 shows the chamber temperature over time for the experiment (left it run over night). Figure 5-16 shows the thruster glowing in vacuum.

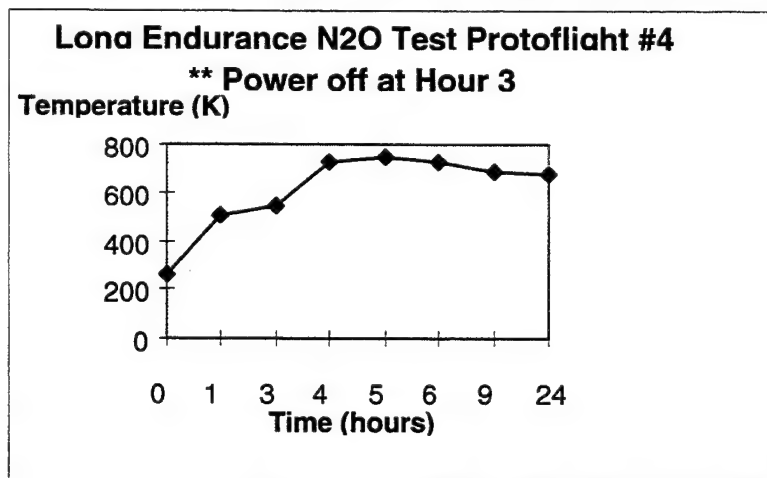


Figure 5-15: Temperature versus Time for Protoflight #4 Thruster

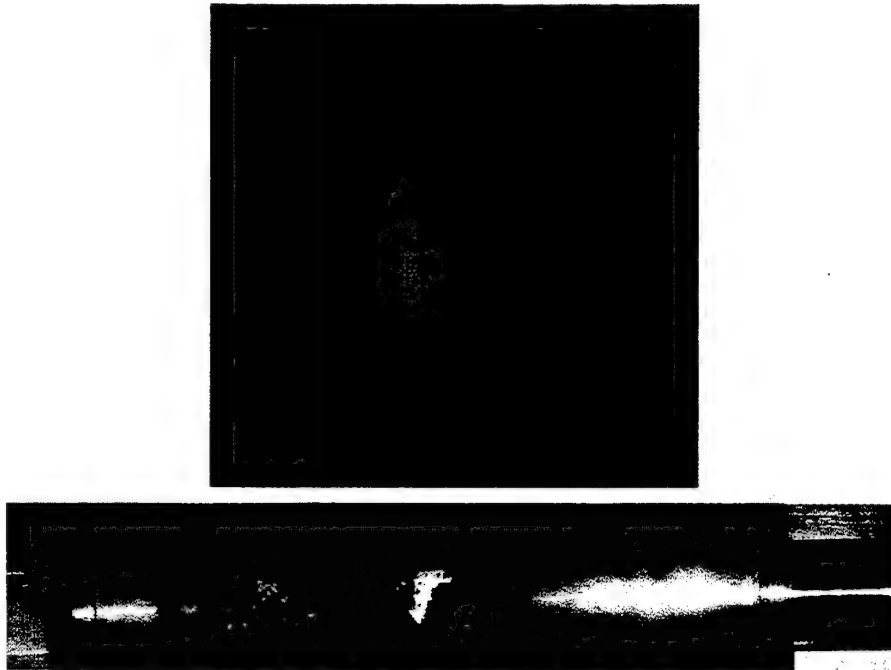


Figure 5-16: Protoflight #4 thruster glowing and picture of thruster after test (charring from insulation)

This test campaign also demonstrated the need of the Micropore Insulation in reducing the thruster outer wall temperature to reduce radiation losses. Figure 5-17 shows the temperature difference with and without the insulation for the same thruster (Protoflight #3) @ 300 W.

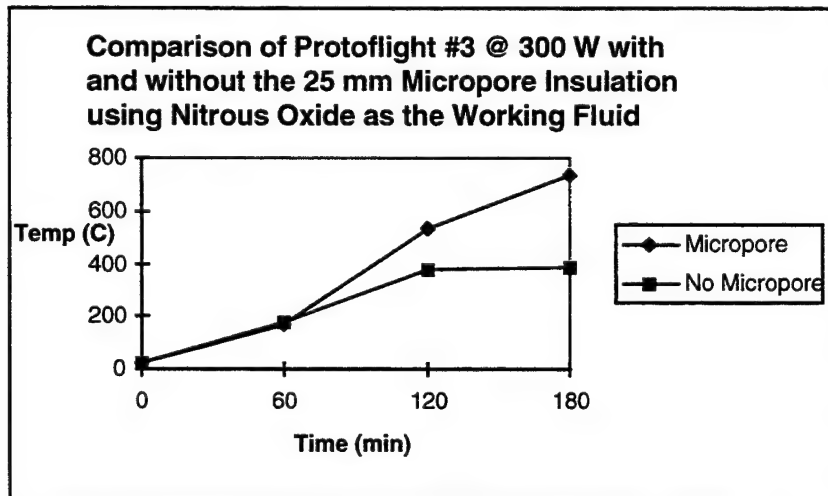


Figure 5-17: Validation for Using the Micropore Insulation

There were some problems encountered in the protoflight programme. The first was friction losses. Friction losses dramatically reduced performance in 5 of the 6 thrusters. This was expected for the prototype thrusters, but was not expected for protoflight #1 - #3. Tables 5-4 and 5-5 show the results for the water and nitrous oxide tests.

| Nozzle Throat (mm) | Exp Ratio | Ideal Isp for testing condition (sec) | Actual Isp (sec) | % of Ideal Isp | C_D | C_F | C_F Ideal | % of C_F Ideal |
|--------------------|-----------|---------------------------------------|------------------|----------------|-------|-------|-------------|------------------|
| 0.128 | 100:1 | 175 | 72 | 41 | 0.72 | 0.54 | 1.7 | 32 |
| 0.183 | 100:1 | 181 | 110 | 61 | 0.97 | 1.06 | 1.8 | 59 |
| 0.694 | 100:1 | 179 | 179 | 100 | 0.86 | 1.55 | 1.8 | 86 |

Table 5-4: Comparison of Performance for Prototype and Protoflight thruster for the Water Experiments

| Nozzle throat (mm) | Exp. Ratio | Ideal Isp (sec) | Actual Isp (sec) | % of Ideal Isp | C_D | C_F | C_F Ideal | C_F (%) |
|--------------------|------------|-----------------|------------------|----------------|-------|-------|-------------|-----------|
| 0.12 | 100:1 | 131 | 70 | 53 | .73 | .83 | 1.8 | 46 |
| 0.128 | 100:1 | 131 | 83 | 64 | .77 | 1.03 | 1.8 | 57 |
| 0.183 | 100:1 | 135 | 101 | 75 | .62 | .88 | 1.8 | 49 |
| 0.194 | 100:1 | 139 | 99 | 72 | .67 | .95 | 1.8 | 53 |
| 0.694 | 100:1 | 140 | 134 | 96 | .87 | 1.76 | 1.82 | 97 |

Table 5-5: Comparison of Performance for Prototype and Protoflight thrusters for the Nitrous Oxide Experiments

These results showed, that even though a higher chamber temperature was obtained with the smaller nozzles at a lower power, the flow was still too low to overcome the friction losses. The results from protoflight thrusters #1 - #3 were improved compared to the prototype thrusters, but still showed a significant drop in Isp. Figure 5-7 showed that the Knudsen number was above 0.01 for these cases, however this is the point where the flow starts to break down, so a test result was useful in determining to what extent the flow rate had on performance. The performance achieved from the 0.694 mm nozzle was quite promising and showed the system can meet acceptable performance levels. Flow rate and power will have to be traded for the flight design. This was a useful conclusion and will be vital in the sizing of the flight thruster.

The MgO catalyst discussed in Chapter 4 had little impact in the prototype and protoflight thrusters. Figure 5-18 shows the results for the prototype#1 and prototype#2 tested @ 100 W. Since these thrusters were the same dimensions, just different bed material, the catalyst had no impact on the chamber temperature.

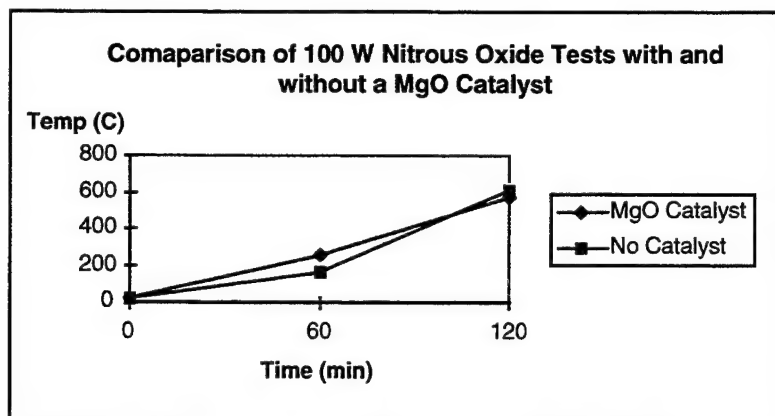


Figure 5-18: Prototype Comparison Test - Catalyst not much impact on performance

Material interaction was still an issue with the protoflight thruster. The key scientific fact discovered was that the oxidation deposits observed in the prototype programme were not solely due to the stainless steel nozzle material. More detailed scanning electron microscope nozzle analysis (on the long endurance run since that had the most build-up; as previously discussed all of the prototype water thrusters had nozzle problems) showed that the particulate observed in the nozzle was silicon oxide. Silicon oxide was also discovered on the bed particles themselves. This proved that the deposits were coming from inside of the chamber. Figure 5-19 shows a before and after firing of the bed material.



Figure 5-19: Before and after pictures of the SiC bed material. Notice the tiny spots on the bed material in the after photograph on right.



Figure 5-20: Silicon Oxide deposits in nozzle throat - amorphous deposition

After the bed material was removed, a white pasty substance was discovered on the downstream end of the thrust chamber. An electron microscope picture of the substance is shown in Figure 5-21. The microscope material analysis revealed that the substance was silicon oxide. As Figure 5-20 showed, there was silicon carbide in the nozzle, but not as much crystal growth. This can be attributed to the screen mesh that was electron beam welded in at the aft end (Figure 5-8). Figure 5-22 showed some of the silicon oxide that was filtered from the nozzle.

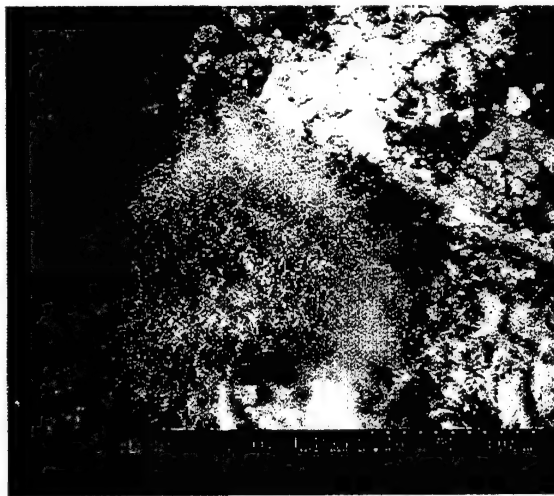


Figure 5-21: Dendritic crystal growth - slow growth, atom by atom along an axis



Figure 5-22: Silicon Oxide deposits on inner wall of screen mesh

These type of deposits were also observed in the nitrous oxide tests, which meant it was not purely steam induced. After discussions with the bed material vendor and more electron microscope analysis, the deposits were coming from silicon oxide already in the bed material. Since the melting point is 500 C, it was boiling off of the silicon carbide and mixing in the fluid stream and attaching itself on the small nozzle throat (for the first 5 thrusters, none in the larger throat of thruster #6). After discussions with the vendor (Universal abrasives), it was discovered that the bed was made of at least 0.5 % (not much material needed for a small nozzle) silicon oxide in each particle. This is shown in Figure 5-23, the amount of oxygen and silicon before and after a firing.

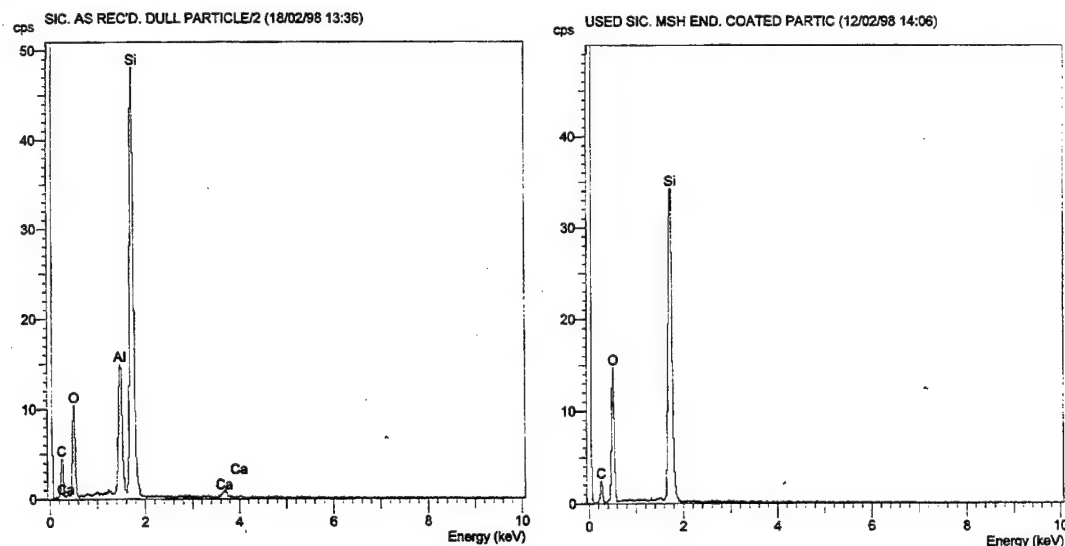


Figure 5-23: Amount of Silicon and Oxygen in the bed Material before and after a firing- counts per second of material versus energy of the electron.

The water was analysed to make sure it was not compounding this effect. Figure 5-24 showed the particulate discovered in the water using an ICP analysis. It was also thought that the water might have had a low pH, thus leeching out some of the silicon carbide. The measured pH was 6.5, thus this

was not a factor. The water analysis turned out to be low in material content except for calcium. For future tests, the water will be analysed and make sure the levels are as low as possible (all should be at ppb level according to a conversation with a chemist, [Rusek, 98]).

| Element | Value |
|-----------------|-------|
| Sodium (ppm) | 3.49 |
| Magnesium (ppm) | 0.35 |
| Calcium (ppm) | 4.56 |
| Silicon (ppb) | 1.8 |
| Vanadium (ppb) | 3.66 |
| Chromium (ppb) | 2.1 |
| Manganese (ppb) | 12.7 |
| Iron (ppb) | 0.21 |
| Cobalt (ppb) | 1.19 |
| Nickel (ppb) | 0.13 |
| Copper (ppb) | 6.8 |
| Zinc (ppb) | 22.6 |
| Cadmium (ppb) | 2.8 |
| Antimony (ppb) | 7.7 |

Figure 5-24: ICP analysis of water from [Ward, 98]

The next issue to address was to how to get rid of the silicon oxide before firing ? There were two solutions, try to cook it out under thermal vacuum testing or get higher enriched silicon carbide. The results are shown in Figure 5-25. Advanced Furnace Technology took 2 kg of silicon carbide for treatment. They washed the bed material with IPA and a ultrasonic bath and then baked it in vacuum at 1500 C for 4 hours. This did reduce the oxygen levels as per Figure 5-25. They also weighed the material and discovered they had lost 10 grams of material after the treatment. The second plot shows "green silicon carbide" which is higher enriched. Universal Abrasives says this material has a 0.25 % of Silicon oxide. It was also noticed that some of the baked particles became green after the process - showing it is purer, Figure 5-25 shows hardly any oxygen.

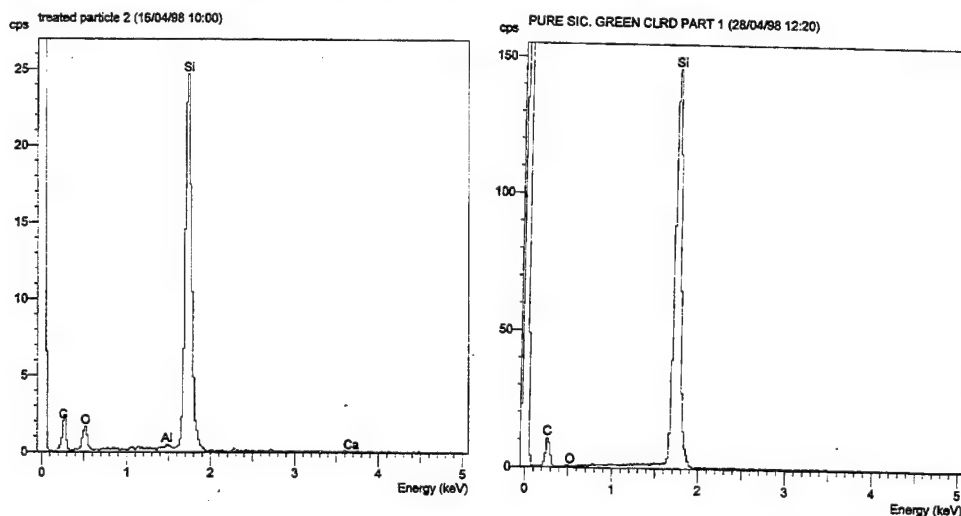


Figure 5-25: Treated and Green Silicon carbide SEM oxygen content

There are a number of solutions to solving this material interaction problem. Since the Protoflight #4 nozzle did not have any blockages in its 50 hours of operation on nitrous oxide and water, a bigger nozzle also looks like an attractive option. Since the silicon oxide was joining the gas stream, a

bigger nozzle would prevent adhesion through the converging / diverging section. The disadvantage of this approach is that a bigger nozzle demands higher flow rate and hence power. A tighter mesh size might filter more of the silicon oxide out, but too tight of a mesh can cause pressure drop or flow problems. It seems if the silicon oxide is removed before firing, there should be no deposits. Thus, the best solution would be to vacuum treat the green silicon carbide and use this material in future tests with a bigger nozzle (also reduces friction losses). Results of the vacuum bake of the green silicon carbide showed that 1 g of material was lost - matched with predictions that less silicon oxide is in the material.

5.4. Modelling Results

The protoflight #4 system achieved better performance. The system was designed for a thrust level of approximately 0.5 N (0.694 mm throat diameter). Figures 5-26 through 5-30 show the mass flow, chamber temperature, chamber pressure, thrust and efficiency for a nitrous oxide run on 22 Jan 98. The system performed as expected, chamber pressure remained somewhat steady with a decrease in mass flow rate and increase in chamber temperature over time. The exciting result was the time length with constant temperature and no energy input (self-sustaining).

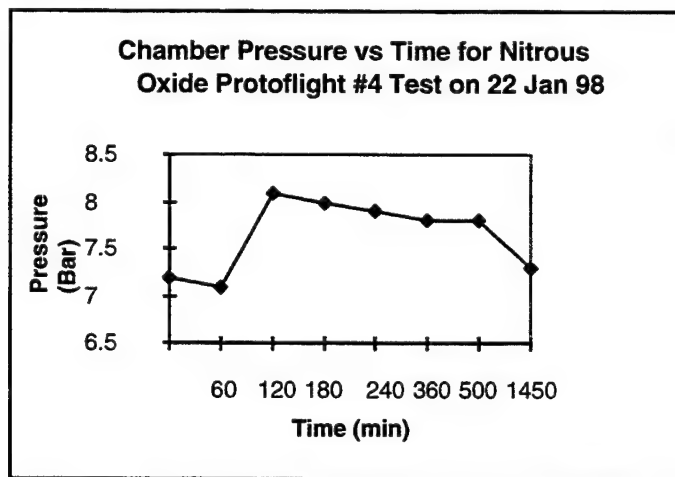


Figure 5-26: Chamber pressure vs time for Protoflight Thruster

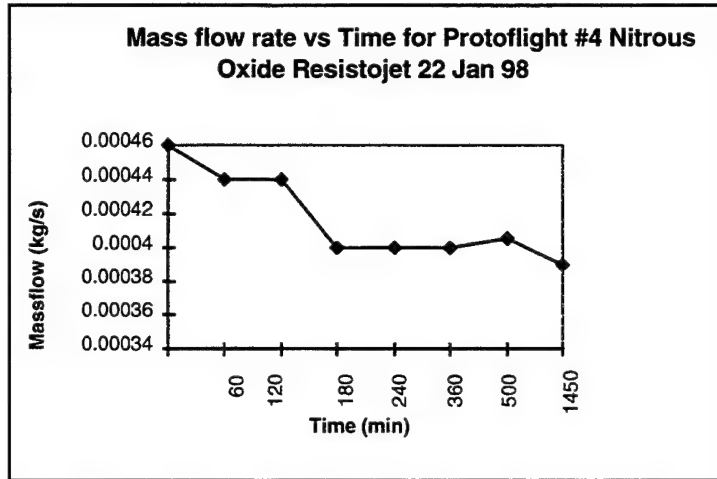


Figure 5-27: Massflow rate vs time for Protoflight Thruster

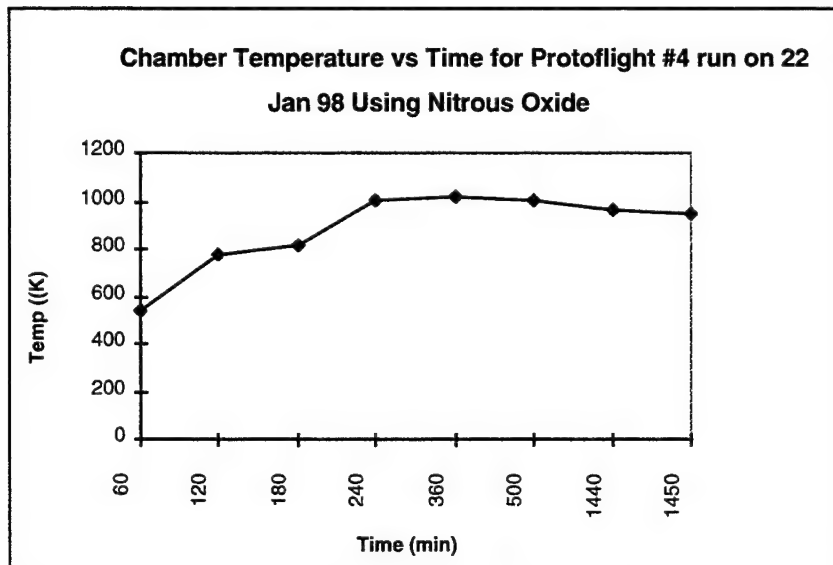


Figure 5-28: Chamber Temperature vs Time for Protoflight #4

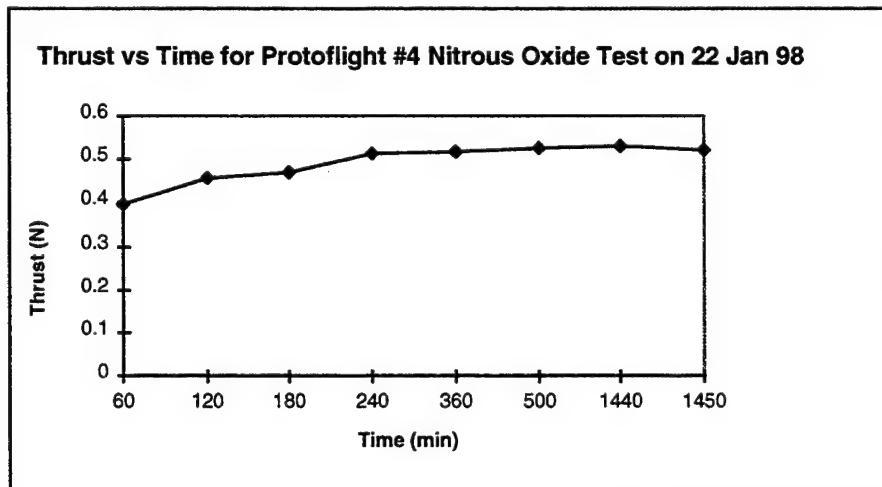


Figure 5-29: Thrust vs Time for Protoflight #4.

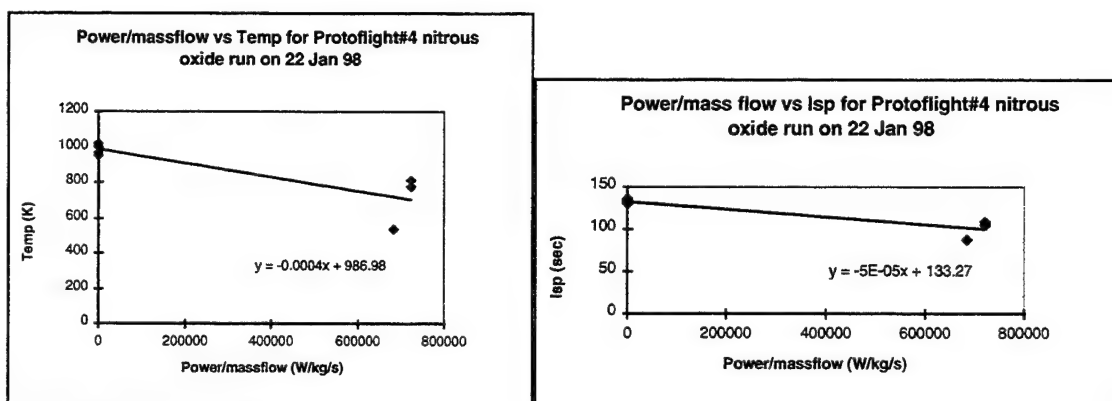


Figure 5-30: Efficiency vs time for Protoflight #4. Equations can be used for empirical scaling which is discussed in Chapter 6. Lines represent these equations over time.

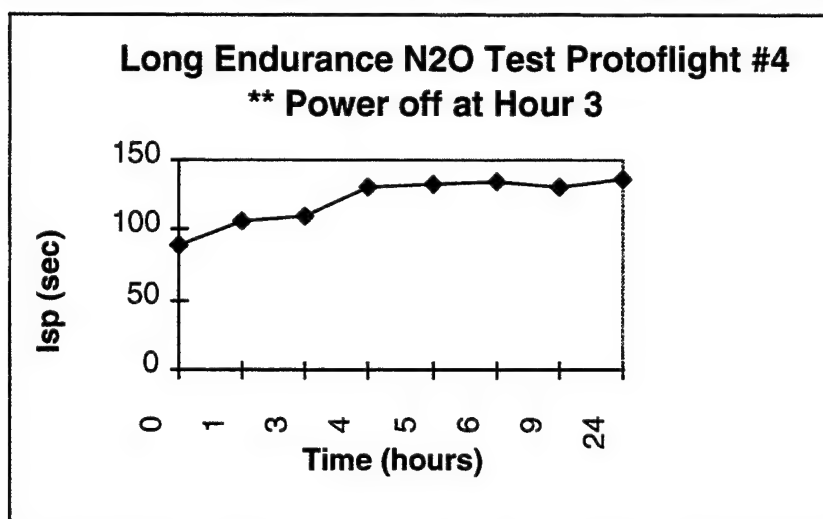


Figure 5-31: Isp versus Time for Protoflight#4

The heat transfer efficiency calculations vs time are shown in Figure 5-32. The 100 % efficiency was due to the self sustaining nitrous oxide decomposition reaction. This reaction was discovered during the “zero thrust measurements”. When the mass flow rate was turned to zero out the thrust stand due to the slight thermal drift, the bed was left with no flow and no power due to keeping the heater temperature close to 980 C. The short time required to let the stand settle from abruptly bringing the thrust to zero was 2 minutes. Since at hour 3, the temperature was above the start of decomposition temperature for the reaction, it was decided to leave the power off when the flow was brought back on. The pressure, flow rate, and power (0 W) were left at the same settings for 21 hours. The slight decay was due to the nitrous oxide feed cylinder getting near its end of life. The explanation for this result is that the prototype thruster achieved the highest heat transfer rate of any of the thrusters (above 75 % with power on).

Another experiment was run the day before (20 Jan 98) and during one of the zero thrust tests the temperature shot up to 1400 K when the flow was turned on. The chamber temperature decayed back

down to 1000 K. This change of temperature can be attributed to the reaction trying to reach its full decomposition temperature (1900 K), but radiation losses reduced the temperature to 1000 K. Since this occurred near the end of the day, it was decided to wait until the next day to try a longer test with no power.

The very intriguing result of these reactions are the ability of nitrous oxide to sustain itself for long periods of time at temperatures under its full decomposition temperature. Since the 22 Jan 98 test used the supply of nitrous oxide, and the test campaign was near the end, with a need to test other working fluids, there was only one experiment confirming this reaction.

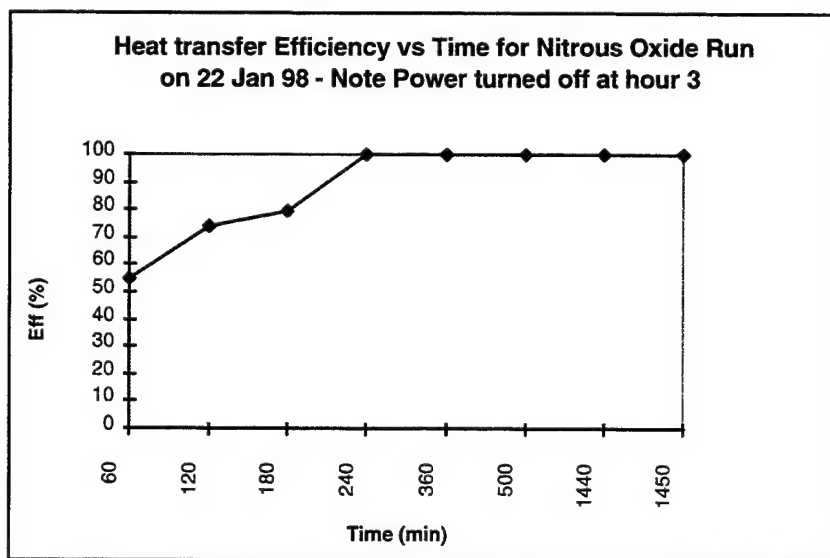


Figure 5-32: Heat transfer efficiency versus time for the Protoflight #4

The Protoflight water test results are shown in Figure 5-33 - 5-37.

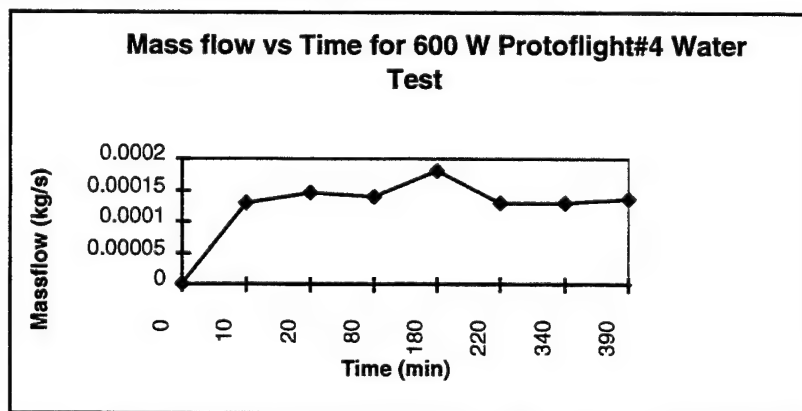


Figure 5-33: Massflow vs Time for Protoflight#4 Water Test

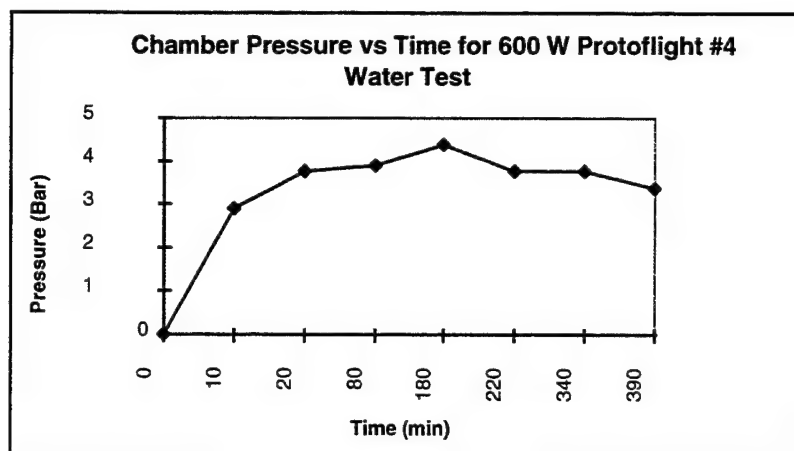


Figure 5-34: Pressure vs Time for the same water experiment

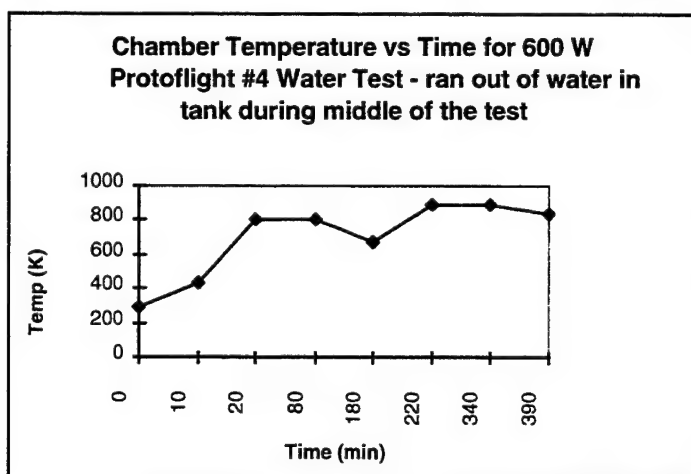


Figure 5-35: Chamber Temperature vs Time for same water experiment

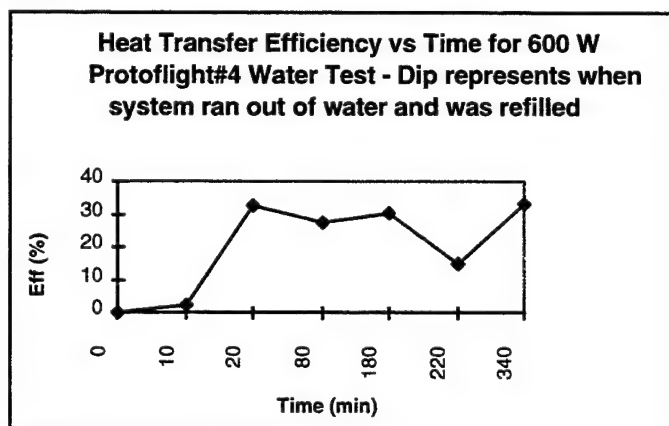


Figure 5-36: Heat Transfer Efficiency vs time for Prototflight#4 600 W Water Test

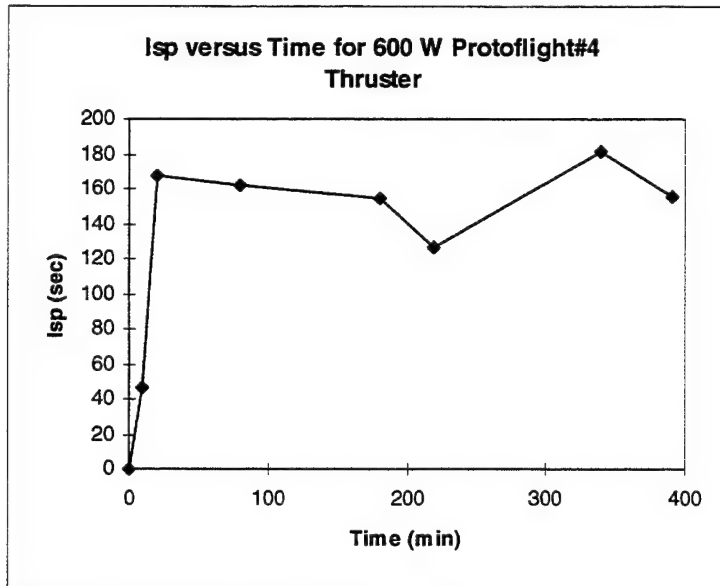


Figure 5-37: Isp versus Time for 600 W Protoflight Thruster. Dip in performance is due to filling water tank (2 litres capacity). Long time intervals due to “zeroing out” thrust measurement for thermal drift and are representative of performance over the interval.

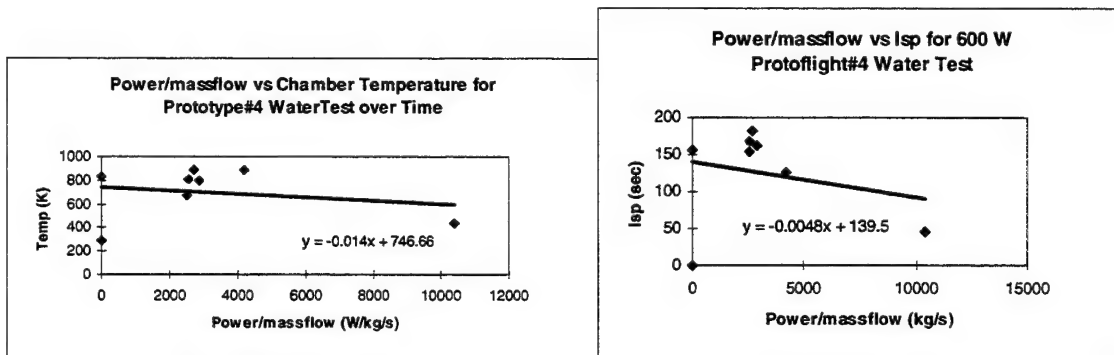


Figure 5-38: Efficiency vs Time for Protoflight Water Test. Equations can be used for empirical scaling. The lines represent these equations.

The water protoflight#4 test results followed similar heat transfer trends. The massflow rate remained constant whilst the chamber pressure and chamber temperature slightly increased. The heat transfer efficiency is less than nitrous oxide due to the extra energy required to vaporise the water. This thruster offered the best performance compared to all of the water systems. Since the total error bar is less than 4 %, there is high confidence in these numbers. This thruster showed that the friction losses are the number one design item to address for scaled down design (which is discussed in the next Chapter). Table 5-6 shows all of the steady state prototype and protoflight test results. The calculated values are from the tests that did not use the thrust stand. All of the test programme results are shown in the attached CD-ROM.

Chapter 5: Protoflight Research Phase

| Thrust Comments | Date/ Test Duration | Working Fluid | F (mN) | Isp (sec) | Q _{eff} (%) | Power (W) | T _c (C) | P _c (bar) | Mdot (kg/s) | Vacuum (mTorr) |
|---|-------------------------|------------------|---------------|--------------|-------------------------|--------------|--------------------|----------------------|----------------|---------------------------------|
| MarkII#1 Thrust on torsion stand - problem with flexures | 18/12/97 5 hr 10 min | nitrogen | 4.8-calc | 94-calc | 7.4-calc | 10 | 447 | 2.9 | 5.24E-06 | 29 |
| MarkII#1 thrust too high for torsion stand | 17/12/97 5 hr | nitrogen | 4.78- calc | 134-calc | 2.25- calc | 100 | 618 | 10.2 | 3.63E-06 | 31 |
| Mark-III#1 repeat run of 15/12/97 | 16/12/97 7 hr 40 min | nitrogen | 30 | 103 | 7.8 | 193.6 | 635.9 | 10.2 | 2.96E-05 | 50 |
| Mark-III#3 ran off decay heat from N2O run | 15/1/98 1 hr 20 min | nitrogen | 32 | 79 | N/A (no power) | 0 | 329 | 10.7 | 4.2E-05 | 38 |
| Mark-III#1 repeat test of 12 Dec | 15/12/97 7 hr | nitrogen | 27 | 89 | 5.5 | 213 | 563.5 | 10.1 | 3.1E-05 | 59 |
| Mark-III#1 first test at RO Wescott no stand | 26/11/97 2 hr | nitrogen | 50 (calc) | 99 (calc) | 13 | 292 | 607 | 10.8 | 5E-05 | .3 millibar only at RO |
| Mark-II#1 first thrust recording - drift 100% of thrust value | 9/12/97 1 hr 20 min | nitrogen | 9.3 | 65 | 2.1 | 143 | 689.1 | 9.8 | 1.47E-05 | 66 |
| Mark-II#1 still have drift in thrust reading | 10/12/97 7 hr 35 min | nitrogen | 12.2 | 85 | 5.1 | 100 | 642.6 | 8.9 | 1.47E-05 | 66.5 |
| Mark-III#1 first no drift thrust reading - shut off flow to zero out stand, only 2 points | 11/12/97 2 hr | nitrogen | 28 | 89 | 6.1 | 200 | 554.4 | 10.4 | 3.21E-05 | 66.4 |
| Mark-III#1 first no drift reading over operating range | 12/12/97 3 hr 5 min | nitrogen | 27 | 94 | 5.6 | 221 | 682.4 | 10.2 | 2.96E-05 | 68 |

Chapter 5: Protoflight Research Phase

| Thruster Comments | Date/ Test Duration | Working Fluid | F (mN) | Isp (sec) | Qeff (%) | Power (W) | Tc (C) | Pc (bar) | Mdot (kg/s) | Vacuum (mTorr) |
|--|-------------------------------|------------------|--------|-----------|--|--------------|--------|----------|----------------|--|
| Mark-III#4 first test with big nozzle | 17/1/98 3 hr 10 min | nitrogen | 445 | 134 | 75 | 389 | 657.1 | 7.5 | .00034 | 104 |
| Mark-III#1 n2 endurance test | 26-28/1/98 43 hr 35 min | nitrogen | 24.7 | 93 | 6.25 | 180 | 600.7 | 8.4 | 2.71E- 05 | 32.5 |
| Mark-II#1 higher pressure | 7/1/98 2 hr 40 min | nitrogen | 14 | 94 | 6.36 | 101 | 621 | 11.3 | 1.52E- 05 | 45.7 |
| Mark-III #4 ran after n2 test | 17/1/98 30 min | helium | 314 | 249 | 76.12 | 504 | 559.5 | 5.9 | .000128 | 123 |
| Mark-III#4 ran after N2O test | 22/1/98 1 hr 40 min | helium | 357 | 303 | 133 - too much decay heat from N2O run | 398 | 409 | 5.7 | .00012 | 84.2 |
| Mark-II #1 first he run | 7/1/98 3 hr 20 min | helium | 6.1 | 101 | 3 | 101 | 618.1 | 7.7 | 5.31E- 06 | 44.3 |
| Mark-II#1 100W perf. | 19/12/97 4 hr 37 min | water | 4.1 | 74 | 1.5 | 100 | 623.1 | 4.3 | 5.64E- 06 | 48.7 |
| Mark-III#2 long endurance test for MightySA TII.1 | 14/1/98- 29/1/98 354 hr | water | 14.5 | 146 | 5.4 | 192 | 584 | 5.91 | 1.01E- 06 | 54 |
| Mark-III#1 repeat test of 17/12/98 | 18/12/97 6 hr 30 min | water | 9.7 | 88 | 2.1 | 203 | 632.8 | 4.8 | 1.12E- 05 | 52.9 |
| Mark-II#1 first water test with good thrust measureme nt | 17/12/97 4 hr | water | 10.5 | 85 | 2.2 | 203 | 658.4 | 4.6 | 1.26E- 05 | 67.4 |
| Mark-III#1 first test on water @RO Wescott | 26/11/97 1 hr 45 min | water | 13.4 | 171 | 3 | 382 | 588 | 5.1 | .000008 | .3 milli bar |
| Mark-II#1 first attempted thrust measureme nt - not accurate | 9/12/97 40 min | water | 2.1 mN | 37 | 0.3 | 143 | 593.2 | 4.4 | 5.92E- 06 | 159 (found leak afterward s) |

Chapter 5: Protoflight Research Phase

| Thruster Comments | Date/ Test Duration | Working Fluid | F (mN) | Isp (sec) | Qeff (%) | Power (W) | Tc (C) | Pc (bar) | Mdot (kg/s) | Vacuum (mTorr) |
|---|--|--------------------|--------|-----------|-------------|--------------|--------|----------|----------------|-------------------|
| Mark-III#4 First water test with big thruster - clogged nozzle with ice up to 100 bar, cleared and thruster kept running | 19/1/98 4 hr 27 min | water | 250 | 155 | 31.23 | 609 | 340.8 | 3.8 | .000165 | 76.4 |
| Mark-III#4 second water test | 20/1/98 7 hr 10 min | water | 233 | 182 | 33 | 631.4 | 618.7 | 3.8 | .00013 | 71.3 |
| Mark-III#4 repeat water test | 23/1/98 2 hr 37 min | water | 243 | 177 | 33 | 640.14 | 490.9 | 3.8 | .00014 | 73.6 |
| Mark-III#1 repeat water test of #1 done with smaller weight set and no viscojet | 24/1/98 5 hr 50 min | water | 24 | 110 | 4.85 | 266.96 | 652.4 | 8.7 | 2.25E-05 | 45.2 |
| Mark-III#2 thrust measureme nt after 354 test | 29/1/98 1 hr 40 min after 354 hr | water | 1.55 | 20 | .07 | 220 | 272.7 | 10.3 | 7.78E-06 | 34.5 |
| Mark-II#1 100W test for performanc e again | 8/1/98 5 hr 15 min | water | 4 | 72 | 1.5 | 102 | 587.9 | 6 | 5.92E-06 | 48.9 |
| Mark-III#4 60% water 40% Methanol by weight, used to lower freezing point of water to - 20 C | 23/1/98 2 hr 50 min | water/meth anol | 196 | 169 | 25.6 | 635.6 | 609.6 | 3.3 | .000119 | 63.7 |
| Mark-III#1 poor performanc e due to nozzle clog in middle of run | 26/1/98 3 hr 15 min | water/meth anol | 2.1 | 31 | .15 | 219.3 | 637.4 | 7.3 | 7.13E-06 | 30.9 |
| | | | | | | | | | | |
| | | | | | | | | | | |

| Thruster Comments | Date/ Test Duration | Working Fluid | F (mN) | Isp (sec) | Qeff (%) | Power (W) | Tc (C) | Pc (bar) | Mdot (kg/s) | Vacuum (mTorr) |
|--|------------------------|------------------|--------|-----------|---|--------------|--------|----------|----------------|-------------------|
| Mark-III#3 test with MgO catalyst and insulation on | 15/1/98 6 hr 12 min | N2O | 28.8 | 96 | 4.5 | 302 | 734 | 10.8 | 3.07E-05 | 39.6 |
| Mark-III#1 no catalyst | 12/1/98 7 hr 34 min | N2O | 26.2 | 101 | 8.7 | 149 | 641.7 | 11.2 | 2.63E-05 | 43.2 |
| Mark-III#3 catalyst test and no insulation for its impact on performanc e | 14/1/98 6 hr 20 min | N2O | 33.4 | 75 | 4.1 | 297 | 377.7 | 11 | 4.52E-05 | 39.9 |
| Mark-III#3 catalyst test with insulation on | 13/1/98 6 hr 26 min | N2O | 29.9 | 99 | 4.8 | 301 | 743.5 | 10.8 | 3.07E-05 | 44.1 |
| Mark-II#1 comparativ e test to 9 Jan 98 which had the MgO catalyst | 10/1/98 2 hr 5 min | N2O | 17 | 83 | 6.7 | 103 | 626.1 | 12.9 | 2.09E-05 | 46.6 |
| Mark-II#2 test with catalyst | 9/1/98 5 hr 45 min | N2O | 9.2 | 74 | 2.8 | 121 | 654.54 | 10.7 | 1.28E-05 | 44.1 |
| Mark-III#4 first test with big nozzle, no catalyst | 21/1/98 5 hr | N2O | 524 | 148 | 110% - decomp osition occurin g | 345 | 916.8 | 8.8 | .00036 | 56.3 |
| Mark-III#4 Repeat test of yesterday, shut power off at hour 3, ran for 20 hours with no power | 22/1/98 23 hours | N2O | 524 | 137 | N/A - no power on | 0 | 678.2 | 7.3 | .00039 | 60.2 |

Table 5-6: Summary of Prototype and Protoflight Test Results. The Prototype series of thrusters were referred to sometimes as the Mark-II and the Protoflight series were referred as the Mark-III.

The thermal model was developed throughout the test programme. Figure 5-39 shows a simulation versus test data for the Protoflight#4 600 W and 300 W nitrous oxide experiment. The improvement in the model in this phase was due to discovering a paper by [Rao, 84] at the 1984 International Heat Transfer Conference, Niagara Falls, NY stating that the transient heating time between a similar sized

bed of spheres is 2- 4 times the continuum value. Hence, the longer time to reach steady state in the model.

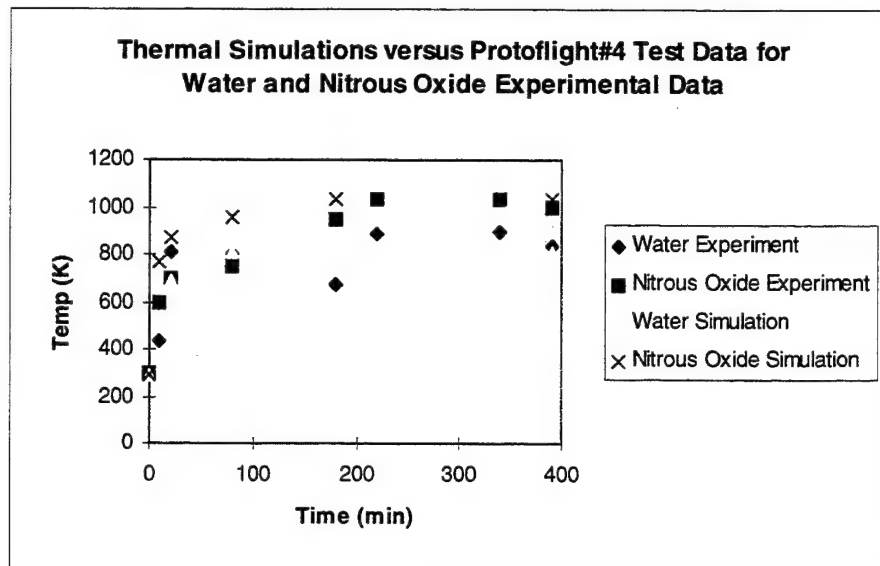


Figure 5-39: Comparison of thermal model simulations to test data. Dip in water data is due to refilling the 2 litre tank.

5.5. Conclusions

The protoflight test programme was successful. For the first time in the research programme, enough data was generated that proved a resistojet system could be designed to meet the 6 small satellite constraints discussed in Chapter 2. These constraints are:

- Mass : Isp's of 150 - 180 sec in Protoflight #4
- Power: 0 - 600 W, even though the Protoflight#4 system was at 300 W, the self-sustaining decomposition reaction will lower the power constraint. However, an investigation through the use of the design tools is needed for the design of the flight system.
- Integration: 354 hour lifetime using water is 5 times the lifetime required for a 200 m/s mission (Chapter 2).
- Thrust: Protoflight#4 was at 0.5 N @ 300 W power for nitrous oxide. Well above LEO gravity losses and would require a firing time of only 5 % of allocated power budget from Chapter 2.
- Volume: Both liquid systems have high density Isp's 75 sec for nitrous oxide and 182 sec for water
- Cost: prototype#4 costs £5000 (recurring cost only)

The issues with using this data and design tools developed for a flight qualified system will be discussed in the next Chapter.

5.6. References

- [AFT, 98] Meeting with Dr Paul Tolkien at Advanced Furnace Technology, Cambridge, UK, March, 1998.
- [Haag, 91] Haag, Thomas W., Curran, Francis, "High Power Hydrogen Arcjet Performance", NASA Technical Memorandum 105143, 27th Joint Propulsion Conference, Sacramento, CA, June 24- 27, 1991.
- [Janson, 96] Janson, S.W., Helvajian, H., "Batch- fabricated Microthrusters: Initial Results", 32nd AIAA Joint Propulsion Conference, Lake Buena Vista, Florida, July 1-3, 1996.
- [Lang, 97] Personal phone conversation with Martin Lang, ESA/ESTEC, September, 1997.
- [Morren 93] "Gravity Sensitivity of a Resistojet Water Vaporiser," NASA Technical Memorandum 106220, AIAA-93-2402, 29th Joint Propulsion Conference, Monterey, California, June 28-30, 1993.
- [Rao, 84] Rao, S. Mohan, Toor, H.L., "Heat Transfer Between Particles", International Heat Transfer Conference, Niagara Falls, 1984.
- [Rusek, 98] Personal interview with Dr John Rusek, China Lake Naval Weapons Centre, Edwards AFB , California, January, 1998.
- [Self, 92] *ISP Computational Computer Code*, AFRL, 1992.
- [Sutton, 92] *Rocket Propulsion Elements An Introduction to the Engineering of Rockets, 6th Edition*, New York: John Wiley & Sons, Inc., 1992.
- [Tagnarelli, 98] Personal phone conversation with Fisher Porter flow meter representative, January, 1998.
- [Universal Abrasives, 98] Personal phone conversation with Universal Abrasives technical sales representative, April, 1998.
- [Ward, 98] Personal interview with Dr Nigel Ward, University of Surrey Chemical Engineering Department, April, 1998.
- [White, 86] *Fluid Mechanics, 2nd Edition*, New York: Mc-Graw Hill, Inc., 1986.

Chapter 6

Flight Systems

6. FLIGHT SYSTEMS

6.1. FLIGHT DESIGN

6.2. UoSAT-12

6.3. MIGHTYSATII.1

6.4. REFERENCES

The preceding chapters showed the design analysis and test results of all of the resistojets test experiments conducted to date. After analysing the data, consulting with U.S. Air Force and University of Surrey spacecraft personnel, and re-analysis of the 6 small satellite constraints, it was determined that a 100 W system using nitrous oxide and water as the working fluids was attractive for small satellite stationkeeping missions. This approach led to the design of two flight systems. The first, was a 100 W nitrous oxide system for the University of Surrey's UoSAT-12. The second, was a 100 W water system for the United States Air Force MightySATII.1 mission. In this Chapter, the spacecraft (bus and subsystems), mission, resistojet design, and application to the mission were presented.

6. Flight Systems

6.1. Flight Design

This section describes the mission trades and analysis conducted to determine the flight configuration for future small satellite missions. Applying the test data to the 6 small satellite constraints, the following conclusions are drawn:

- Mass—Isp's of 136 - 182 sec for nitrous oxide and water can meet 3 year stationkeeping constraint.
- Volume—Water storage density of 1000 kg/m³ and nitrous oxide density of 710 kg/m³ @ 48 bar give good density Isp's compared to gases
- Power—With UoSAT-12 having an on-orbit average power of 140 W and MightySATII.1 allocating 100 W available to the thruster per orbit (~90 minutes with eclipse periods), 100 W is the best choice of power to maximise thruster operation per orbit BUT must produce enough heat to the working fluid at the highest flow rate due to friction losses. Thus the bed must be designed for the highest heat transfer efficiency to reduce flow losses. The results from the protoflight#4 test suggest that high heat transfer efficiency is achievable (10 % better when compared to NASA Lewis nitrogen and water multi-pass thrusters in a comparable test [Morren, 87]). If the bed has a high heat transfer efficiency for nitrous oxide, the self-sustaining reaction may begin and it will reduce this power requirement even more. However, the analysis must show that the proper flow conditions can exit at the lower power.
- Integration—Both working fluids are non-toxic and have produced long run times (up to 354 hours). Nitrous oxide has the added benefit of running off of its vapour pressure so no expulsion system is required.
- Thrust—The protoflight#4 had a specific thrust of 1.7W/mN for nitrous oxide and 0.38 W/mN for water. This compares with 60W/mN for a FEEP system.
- Cost—Cost details are explained in Chapter 7, but the recurring cost for the flight thruster is £5000.

Using these constraints, a 100 W system looks feasible for small satellite application if the heat transfer is optimised for 100 W.

6.1.1. Design Approach

Assuming an input power of 100 W, the thermal code is applied to determine the thruster geometry, mass flow rate, and pressure. Figure 6-1 shows the results for a 30 mm o.d. x 109 mm chamber with a 25 mm Micropore insulation layer and an outer stainless steel jacket to encapsulate the Micropore insulation. This is required due to the Micropore is a very "chalky" substance, and something will be required to protect it from interacting with the spacecraft in flight. Rigid coatings were explored, but to handle the rigors of space (thermal cycling, vacuum, vibration) a 1.5 mm outer sleeve of stainless steel is the best option. The flow conditions optimised for this geometry are shown in Table 6-1.

| Flow Conditions | Nitrous Oxide | Water |
|---|---|---------------------|
| Power (W) | 100 | 100 |
| Chamber Size (mm) | 30 mm o.d. x 109 mm | 30 mm o.d. x 109 mm |
| Mass flow rate (kg/s) | 0.0001 | 0.00003 |
| Chamber Pressure (Bar) | 10 | 5 |
| Nozzle Throat Diameter (mm) (rounded at the throat exit and polished to further reduce friction losses) | 0.4 | 0.3 |
| Bed Material | SiC | SiC |
| Chamber Temperature (per Figure 6-1) | 812 K (decomposition can start at ~700 K) | 520 K |
| Isp (sec) (ideal - due to Knudsen number) | 127 | 152 |
| Thrust (calculated from Isp and mass flow rate Eq 2-1) | 125 mN | 45 mN |
| Efficiency (Eq 2-33) | 78 % | 34 % |

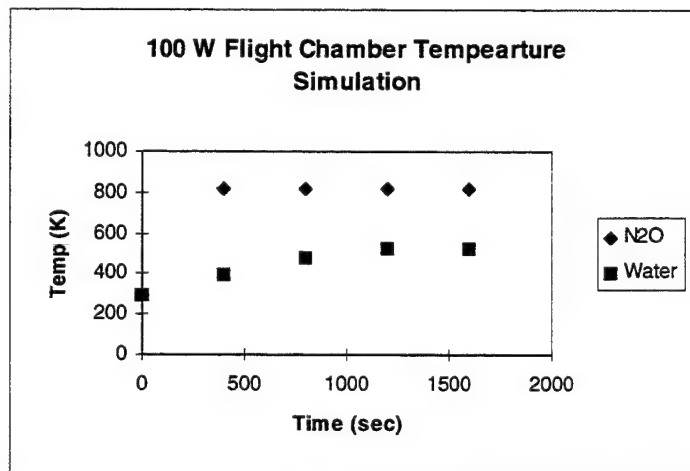
Table 6-1: Flow Conditions for Thermal Simulations**Figure 6-1: 100 W Thermal Simulation for Both Working Fluids**

Table 6-1 presents the flow rates obtained from the thermal model for water and nitrous oxide. These flow rates represent a trade off with the chamber temperature, input power, chamber pressure, and chamber bed geometry for the two systems. Based upon the previous empirical test results, the mass flow rate is increased (at the sacrifice of the chamber temperature) to compensate for flow losses. The next process in the design approach is evaluate the Knudsen number to determine the flow characteristics for these flow rates. Figure 6-2 shows the Knudsen Number for the 0.3 mm nozzle versus the 0.69 mm nozzle from the last research phase (lower flow rate presented since it has the propensity to produce higher flow losses).

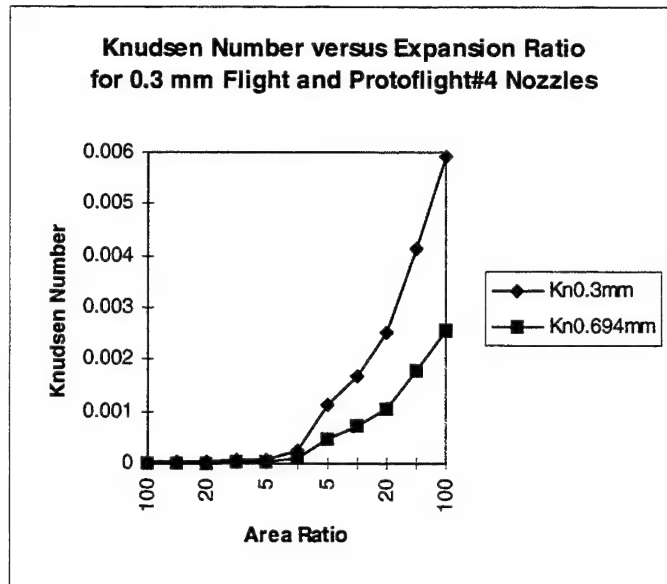


Figure 6-2: Knudsen Numbers for Protoflight#4 and 0.3mm Flight Nozzle. Notice Knudsen Number is not higher than 0.01 so flow will not break down.

Figure 6-2 shows the new flow rate is well below the 0.01 flow break down point, even at the end of the 100:1 expansion ratio. This result is also confirmed by the Reynolds Number analysis shown in Figure 6-3. The higher mass flow rate has reduced the chamber temperature from 900 K to 520 K. However, since the friction losses in the nozzles in Chapter 5 were ~40 % for the higher chamber temperature, but low mass flow rate, the Isp will still be higher (150 sec compared to 100 sec) at the lower chamber temperature. The flow rate should produce an Isp near ideal (5 %) as per the results in Chapter 5.

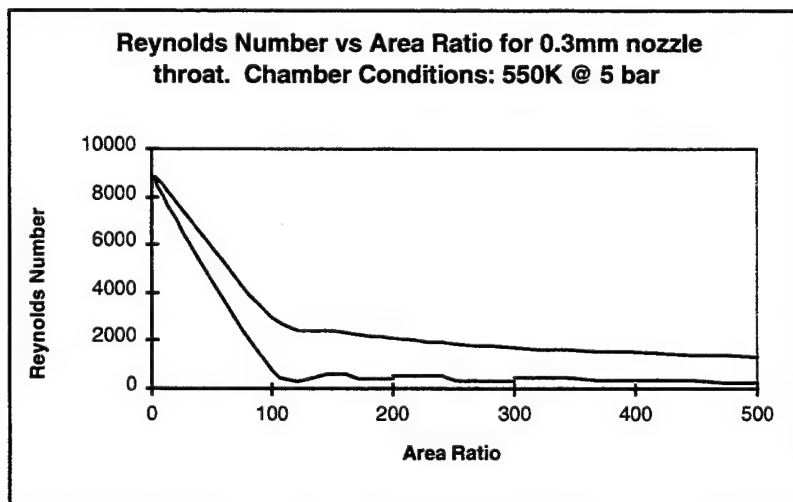


Figure 6-3: Reynolds Number for 0.3mm throat diameter. Indicates getting above boundary layer range (Re = several thousand)

6.1.2. Other Approaches

There are other approaches for the flight design. The first approach uses the off-the-shelf SINDA/3D code for thermal analysis [Gomes, 98]. From the thermal point of view, the resistojet is mainly a dissipating element, with a cooling fluid. This is, nevertheless, a very big simplification of the real problem that is far more complex. It is more complex due to the large number of interactions between the different components of the engine. The code does an energy balance across the entire control volume (resistojet body) and makes assumptions of the amount of heat that is transferred into the fluid (heat transfer efficiency) and densities and thermal properties of the materials involved. This heat transfer efficiency input was determined from the empirical test results or resistojet thermal code already developed. A schematic of the flight thruster with a temperature profile using this approach is shown in Figure 6-4.

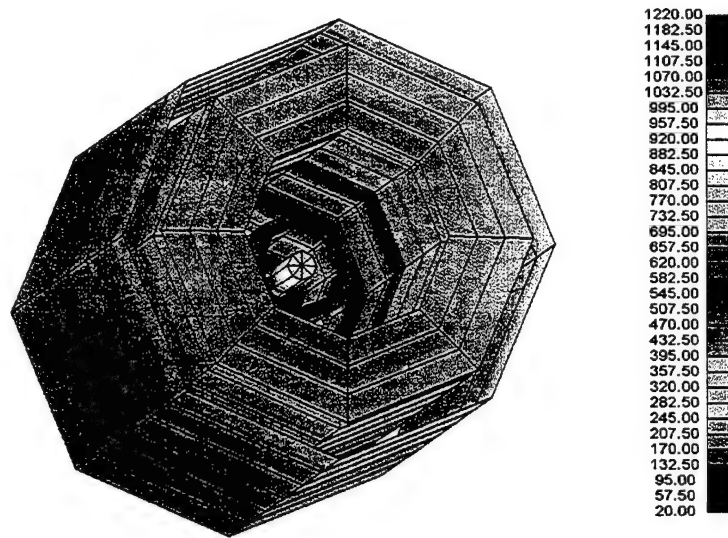


Figure 6-4: SINDA-3D Simulation of the Flight Resistojet (from inlet end in Celsius) [Gomes, 98]

The model predicted temperatures in the chamber to vary up to 473 K higher than the measured results obtained in the earlier test programme. This error was due to inaccuracies in the exact material configuration of the heater. It was hoped that more empirical data or using the resistojet thruster thermal model above as a plug in module could improve the thermal accuracy of the system.

The other approach is to use empirical data itself. Equations 6- 1 and 6-2 show the specific impulse as a function of the input power divided by the mass flow rate. These equations were generated from all of the test data in the last two phases (using measured power and thrust and resultant measured Isp) for each working fluid.

$$y = -7E - 10x^3 + 9E - 06x^2 - 0.0381x + 123.57 \quad (6-1)$$

where:

x= nitrous oxide input power / thrust (W/N)

$$y = I_{sp} \text{ (sec)}$$

$$y = -1E - 11x^3 + 8E - 07x^2 - 0.0182x + 183.48 \quad (6-2)$$

where:

x =water input power/thrust (W/N)

$$y = I_{sp} \text{ (sec)}$$

These equations should represent a reasonable performance assumption since it covers the entire operating range of all 6 thrusters tested with similar geometries and takes into account scaling losses for the smaller prototype thrusters and the good performance of the protoflight#4. The equations are cubic due to they represent the “tightest fit” for all of the test data. Table 6-2 shows these results for powers from 50 - 300 W, and thrust levels from 12 - 500 mN using the nitrous oxide equation.

| Power (W) | Thrust (mN) | Isp (sec) |
|-----------|-------------|-----------|
| 300 | 500 | 104 |
| 300 | 300 | 94 |
| 300 | 200 | 84 |
| 300 | 100 | 71 |
| 300 | 50 | 68 |
| 300 | 20 | -785 |
| 300 | 15 | -2638 |
| 300 | 12 | -6141 |
| 200 | 100 | 71 |
| 200 | 50 | 68 |
| 200 | 20 | -57 |
| 200 | 15 | -444 |
| 200 | 12 | -1252 |
| 100 | 100 | 94 |
| 100 | 50 | 78 |
| 100 | 20 | 71 |
| 100 | 15 | 62 |
| 100 | 12 | 26 |
| 50 | 100 | 104 |
| 50 | 50 | 94 |
| 50 | 20 | 84 |
| 50 | 15 | 71 |
| 50 | 12 | 68 |

Table 6-2: Use of empirical data to generate performance data for the design of nitrous oxide resistojets.

Table 6-2 shows the perils of solely relying on empirical data for design. The 300 W, 500 mN had a demonstrated Isp of 137 sec, but the empirical analysis predicts 104 sec. In some cases, the data is useless (- Isp's). Thus the thermal model developed in support of this research programme and performance equations with comparisons to empirical data is the best approach. It is also more scientific, since it allows the user to vary parameters and study the impact on performance (see Appendix A).

6.2. UoSAT-12

6.2.1. Spacecraft & Mission

The UoSAT-12 spacecraft is described in Chapter 1. This spacecraft is the motivation for starting research into resistojet application. UoSAT-12 is the first SSTL mini-satellite (300 kg) and as such it is a research and development funded marketing mission. It carries a communications payload (Merlion) developed in collaboration with Nanyang Technical University, Singapore, a GPS experiment jointly funded with ESA and SSTL, and an imaging payload.

The mission objectives are to demonstrate a capability for a high payload-to-bus mass/volume ratios at a low cost per kilogram. High bus performance, failure resilience, and modularity to support a wide range of payloads are SSTL hallmarks.

There are several payloads:

1. **Merlion High Speed Data Link** - analogue transparent and regenerative digital L - S-Band transponders using circularly polarised antennas operating with DSP at 9k6, 1Mbps on the uplink, 9k6 and up to 2Mbps on the downlink.
2. **GPS** - an experimental GPS receiver for position, orbit determination, and time-transfer. The receiver has multiple antennas for experimentation and attitude determination through Interferometric techniques.
3. **Imaging System** - 10 metre panchromatic and 30 metre multi-spectral imagers are backed by a low resolution wide angle camera. The imaging system is supported by four transputers and data is transferred to the OBC386 via the ethernet.

The bus systems are as follows:

1. **Power**- the spacecraft is powered by nine Gallium Arsenide Solar Panels giving 140 Watts orbital average power. Three separate power systems with Nickel-Cadmium batteries provide a 28 Volt failure-resilient system.
2. **On-Board Data Handling**- two 386 computers each provide 4Mbytes of programme memory and 120 Mbytes of ramdisk. One 186 computer provides 786 Kbytes of memory and 16Mbytes of Ramdisk with CAN data network. An ethernet supports high data transfer.
3. **RF Systems** - The RF uplink comprises two redundant VHF payload receivers and one TTC receiver for initial spacecraft acquisition. The downlink comprises two redundant UHF 10 W transmitters and a UHF high power amplifier which can raise the nominal 10

Watt output to 40 Watts for pager style receivers. Data rates from 300 bps to 76.8 kbps are expected to be achieved.

4. **Attitude and Orbit Determination and Control System** - three axis stabilisation for high resolution imaging is achieved by reaction wheels. The nitrogen cold gas system will be used for three axis control, spin up / down, momentum wheel desaturation, and orbital manoeuvring. The nitrous oxide resistojet is used solely for orbital manoeuvring. Other control elements comprise magnet - torquers and a gravity gradient boom. Attitude determination is by magnetometers, sun sensors, horizon sensors, star cameras, and a GPS receiver. [Ward, 98]

Figure 6 - 1 shows a picture of the entire propulsion system for UoSAT-12.

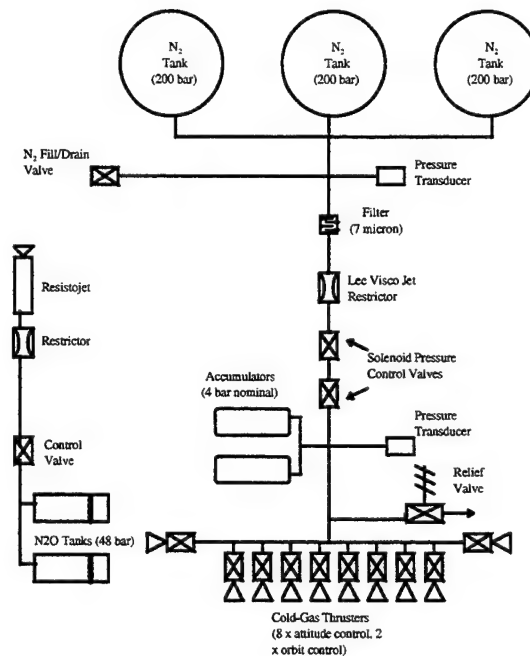


Figure 6-5: UoSAT-12 Propulsion System Architecture

The research into cold gas systems started with the requirement for attitude control and orbit maneuvering for the upcoming UoSAT-12 mission. The system is discussed in greater detail in [Sellers 96]. The baseline assumptions used in the configuration of this system are as follows:

- total volume of $\text{GN}_2 = 27$ liters (to meet spacecraft volume constraints) .
- placement of tanks relative to spacecraft CG is important
- 100 mN thrust from each thruster
- use flight proven hardware to minimize integration tests required
- rely on suppliers own certification (which turned out to be a bad assumption for this system, as stated in Chapter 2)
- build the propulsion system (or large part of it) as a module

- protoflight only (except for breadboard model using dynamic single components)
- cost is the number one driver

Figure 6-6 shows pictures of the cold gas hardware for the proposed UoSAT-12 mission. The 200 bar “bang-bang” pressure control system offers ease of implementation and testing, flight heritage demonstrated by the Oscar P3 spacecraft, and cost savings. Tables 6-3 and 6-4 show the mass break down and performance for the UoSAT-12 mission.

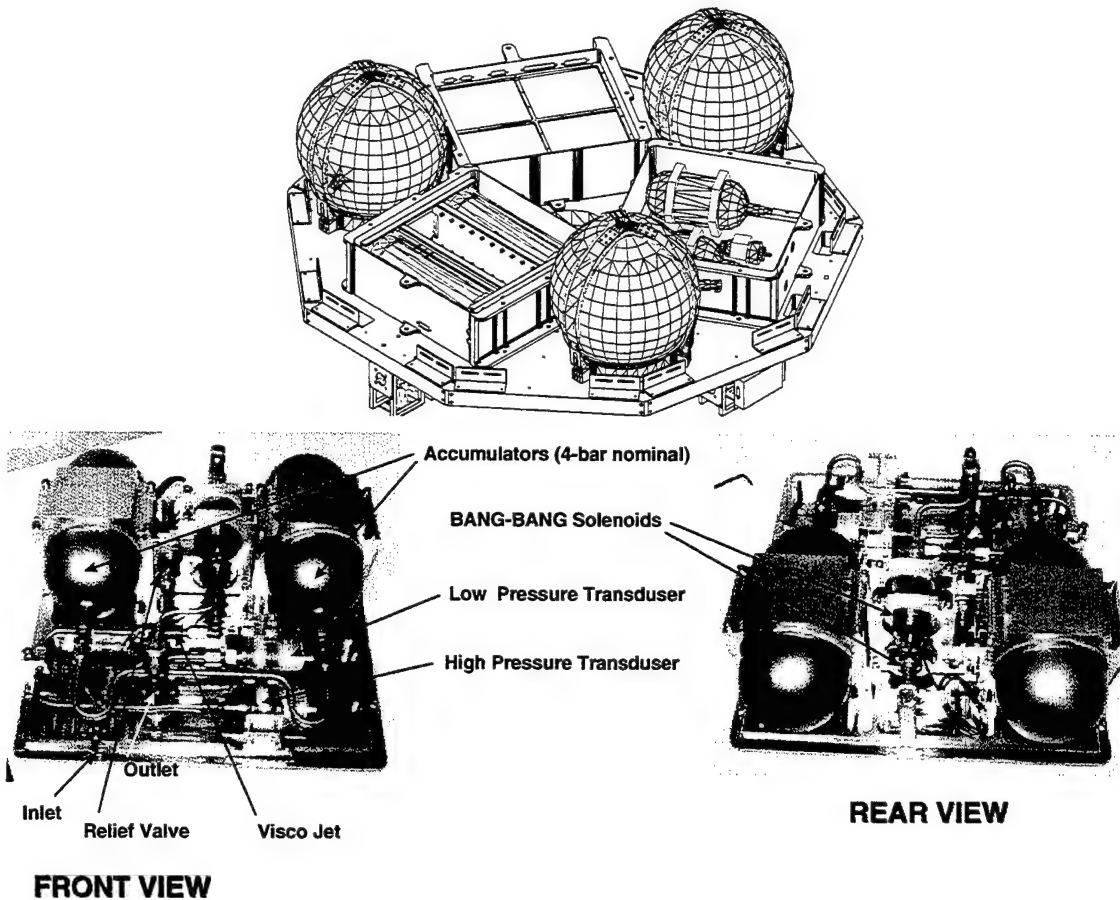


Figure 6-6: UoSAT-12 Propulsion System Pictures

| | | | |
|---|-----|-------|-------|
| Nitrogen tanks (spherical, 10.291 litre, flight qualified, O.D.: 0.274m max dome to boss 0.295 m) | 3 | 4.354 | 13.1 |
| Accumulator (cylindrical, 1.3 litre, flight qualified, 0.089 O.D., 0.29 m length) | 2 | 1.1 | 2.2 |
| Nitrogen filter | 1 | 0.05 | 0.05 |
| Lee Visco Jet | 1 | 0.05 | 0.05 |
| Nitrogen fill/drain valve | 1 | 0.045 | 0.045 |
| Bang-bang valve | 2 | 0.54 | 1.08 |
| Pressure relief valve | 1 | 0.2 | 0.2 |
| Pressure transducer | 2 | 0.35 | 0.7 |
| Cold-gas thrusters | 10 | 0.32 | 3.2 |
| Pipe work / bracketry | n/a | 5 | 5 |
| Total | | | 25.6 |

Table 6-3 : Mass break down for UoSAT-12 cold gas system

| Performance Parameter | Value |
|-----------------------|---------------------------|
| Mass N ₂ | 7.1 kg |
| Total Impulse | 4.389×10^3 Nsec |
| Total Angular Impulse | 2.085×10^3 Nmsec |
| ΔV | 16.4 m/s |

Table 6-4: Cold Gas System Performance

There are three main 200 bar nitrogen tanks which provide propellant for the cold-gas thrusters. Pressure is regulated via the pulsing of two high pressure valves which will be controlled using feedback from a downstream transducer. Low pressure gas will be stored in two accumulators at a nominal 4 bar for use by the thrusters. Eight cold-gas thrusters will be used for the attitude control experiment. Two thrusters will be used for the orbit control experiment.

Preliminary tests of the system performance have been characterized using an engineering model of the cold gas system. The results of these tests were used to write the software which will be used in integration tests to be conducted in the Fall of 98. The preliminary results show that the cold gas system can handle minimum thrust variation for firings at a minimum impulse bit of 20 msec (with new 0.5 mm throat diameter nozzle inserts designed by SSTL since the vendor nozzles were twice the required size). Once assembled, integrated and tested, the system will be used for the following flight experiments on UoSAT-12:

1. Fundamental Test of Cold Gas Attitude Control:

+x, +y, +z

Try to dump out momentum (assumed random 15 deg/stumble)

If works, use CGJ to put satellite into Thompson equilibrium

Force required to do this **10 Nms**

Then use boom, magnet torquers, and wheel

Desaturate Wheels (+/-1000 rpm)

Assuming wheel is designed for 2000 rpm

Need **0.8 Nms** for each firing

SMAD assumes once per day (worst case)

882 Nms for 3 yr lifetime

Spin Up / Spin Down (10 deg/s)

Requires 5 Nms

2. Orbital Manoeuvring :

Can move satellite 4.5 km using **750 Ns** of gas

When ? Function of:

Initial orbit keps

Demonstration only

Fire at apogee / perigee ?

early firing and later firing (6 months later)

3. Total Budget:

Attitude Control: 902 Nms (45 %)

Orbital Manoeuvring: 750 Ns (17 %)

These tests will leave 38 % of the ΔV capability for emergency or other uses. Pending these results, more experiments will be planned.

6.2.2. Resistojet Application

The nitrous oxide resistojet for UoSAT-12 will be used for an orbital maneuvering experiment to demonstrate the stationkeeping applications for a platform of the configuration of UoSAT-12. This system was selected due to its density Isp, self-pressurisation (does not require integration into the cold gas system which was useful since the resistojet was qualified at the late stage of UoSAT-12 development), ease of handling, and performance. The first requirement was to determine where the thruster could be located on the platform and what impact its operation would have on the rest of the spacecraft. This work was started during the proof of concept test campaign. It was important for feedback in the design / operation of the proof of concept thruster and design of the thruster for the next phase. These types of simulations helped support the choice of a 100 W nitrous oxide resistojet.

To be able to integrate the thruster onto the spacecraft and allow operation with the attitude control systems, an on-orbit simulator was required. With the help of Mr. Yoshi Hashida, these integration issues were studied [Hashida, 96].

Mr Hashida of SSTL wrote the on-orbit simulator code (the source code and input variables are attached in Appendix C). The code uses the spacecraft dimensions, centre of gravity location, mass, initial orbit, attitude actuators (deployable boom, magnet torquers, momentum wheel, and 10 cold gas thrusters), and nitrous oxide resistojets location to model the attitude of the spacecraft over time while firing the nitrous oxide resistojets. This simulation studied the impact of resistojets location, thrust level, firing duration, and use of other actuators (boom, momentum wheel, magnet torquers, and cold gas jets) on the spacecraft attitude and orbit as a function of time.

At the start of each simulation, the spacecraft is in a perfect attitude state- three-axis control with no disturbances in orientation at an altitude of 720 km. The simulation does not assume there are any outside forces that could cause disturbance torques. It then allows the nitrous oxide resistojets location to be entered with thrust level and firing duration with respect to the spacecraft centre of gravity. Other attitude actuators can be programmed (by themselves or in combination, or none at all-except for the deployed gravity gradient boom, which is a fixed parameter) - momentum wheel (dimensions and rpm), magnet torquer firings (on or off), and the cold gas jets (8 locations, all at 0.1 N thrust) to assist in the attitude of the spacecraft while the resistojets are in operation. With these variables set, the simulation then monitors the spacecraft attitude in three axes as a function of time.

The first analysis trade-off investigated was thrust level as a function of location. Based upon integration requirements with the cold gas system, and other spacecraft instruments, the resistojets can not be located at the spacecraft centre of gravity. Unfortunately, this means that the thruster will create disturbance torques when it is fired. The closest the resistojets can be located to the spacecraft centre of gravity is on the space facet approximately 0.400 m away in the x, 0.110 m away in the y, and 0.005 m away in the z. This location is shown in Figure 6-7.

The order of the disturbance torque is influenced by the thrust level, firing duration, and compensation acquired from the other actuators previously mentioned. The optimised solution is finding the right mixture of these three variables. A possible solution can also be to cant the nozzle in the direction of the centre of gravity, but there will be a slight offset for the entire mission life since the centre of gravity will change (mass will change as propellant is expelled).

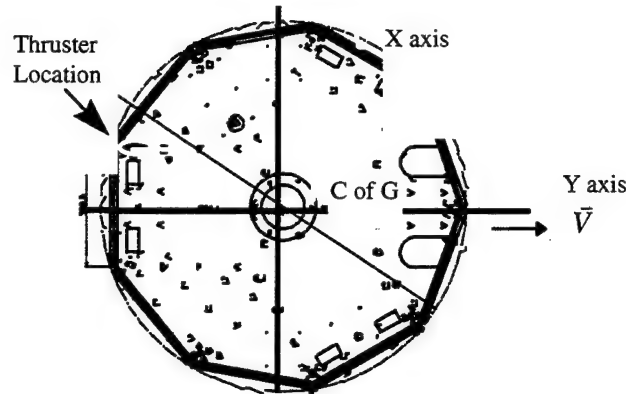


Figure 6-7: Top Down View of UoSAT-12 Showing the Resistojet Thruster Location

At this location, the 0.125 N resistojet can not be fired for any duration of any useful thrust time (at least 1 minute), without causing severe pitch and roll problems (>90 degrees) if the cold gas system is not fired to compensate. If the cold gas system is operated the satellite does not change attitude at all with respect to the three axes for the 0.125 N operation for the burn duration - 60 minutes. It is currently planned to fire for 60 minutes in 7 intervals for a total mission life of 7 hours. This lifetime is based upon a total propellant mass of 2.5 kg. Based upon this thrust level, and 2.5 kg of propellant (3.3 L of nitrous oxide, for the tanks to fit in the module box), the resistojet can change the semi-major axis of the spacecraft by 3 km with each firing for a total change of 21 km. This is enough distance to validate the performance of the system using GPS (resolution for semi-major axis changes >1 km) to determine the change in orbit. If the nozzle is canted through the centre of gravity, the cold gas firings can be significantly reduced to only take care of errors in the actual CG position from predicted and thrust misalignment from the resistojet [Williams, 98].

Since the system is designed for 100 W, 1 hour of continuous power is feasible during specific solar cycles of the orbit to directly run off of the solar arrays. If the self-sustained decomposition reaction can be demonstrated, then the power can be drastically reduced.

Figure 6-8 shows a picture of the flight and engineering model resistojet for UoSAT-12. Figure 6-9 presents the chamber and insulation subassemblies. The mass break down and system specifications for the thruster and components is shown in Table 6-5.

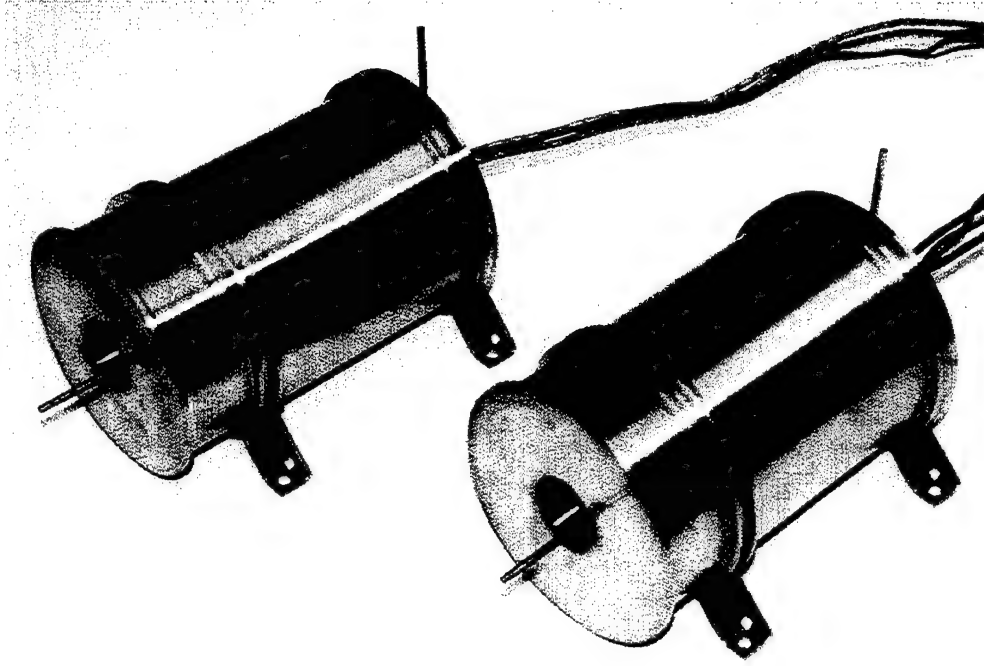


Figure 6-8: Picture of UoSAT-12 Engineering Model and Flight Resistojet

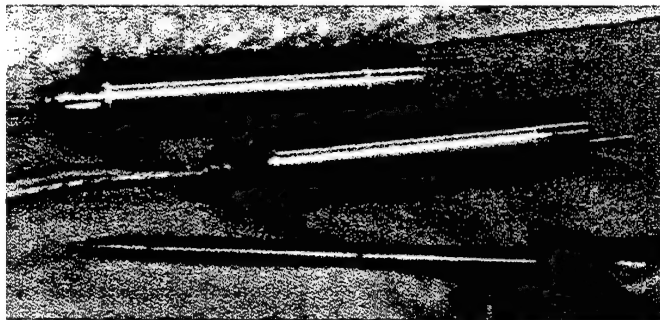


Figure 6-9: Flight Thruster Subassemblies

| Item | Mass |
|--|--|
| Outer shell (needed for Micropore Insulation - 0.06 W/mK in vacuum since it is very porous (90%) and chalky for integration) | s.s. - 337 g |
| Micropore Insulation | 212 g |
| Inner shell | s.s. 195 g |
| Silicon Carbide | 253 g (assumes 42 % porosity - measured) |
| Heater (no power conditioning needed runs right off of 28 V input) | 100 g |
| Injector | 75 g |
| Nozzle assembly | 80 g |
| Expulsion System (pressure switch, 3 tanks, 2 solenoids, pressure transducer) *Pressure tank not required | 9.5 kg |
| Thermocouple pipe | 20 g |
| Total thruster mass (Estimated) | 1.27 kg |
| Total Thruster Mass (Measured) | 1.24 kg |
| propellant | 2.5 kg |
| Total: | 13.2 kg |

| Item | Specification |
|--|---|
| Dry Mass | 10.75 kg |
| Isp (steady state) | 127 sec |
| Power | 100 W @ 28 V |
| Thrust | 125 mN |
| massflow rate: | 0.0001 kg/s |
| Chamber pressure | 4 bar |
| Nozzle | 0.4 mm throat spark eroded |
| Propellant mass | 2.5 kg @ 48 bar (710 kg / m ³) |
| ΔV (assuming steady state Isp) | 10.4 m/s |
| Burn Time: 1 hr (7 total firings) | Change in semi-major axis for 300 kg platform : 21 km |
| Assembly | electron beam welded |


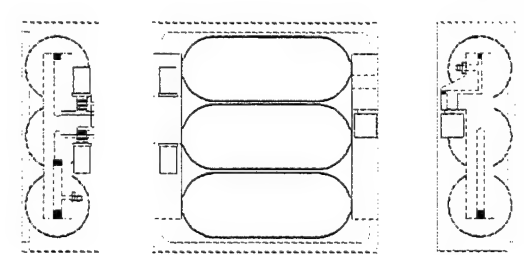
Table 6-5: System mass and specifications

Figure 6-10 shows the Polyflex (UK firm) expulsion system inside the module box. The three tanks will store 3.3 litres of propellant for a total propellant mass of 2.5 kg. A 4th tank will act as an accumulator or buffer volume. The expulsion system is planned to have a simple mode of operation. A pressure switch will open flow from the tanks to the accumulator by opening one of the solenoids

(have two solenoids in the system for redundancy) and fill the volume of the accumulator. The switch will then open/close the solenoid to an accuracy of 1 bar. As long as the accumulator fills to 10 bar from the 48 bar storage pressure, there will not be two phase flow coming into the chamber. If the pressure switch does not work within the pressure tolerance, then a transducer will be added with some control logic to run the system. There will be a slight mass flow decay as the pressure bleeds out of the accumulator, but since the burn times are on the order of 1 hour and this is a stationkeeping manoeuvre, this will not be a problem. Preliminary feed system tests have been conducted using a breadboard model provided by Polyflex. The pressure switch fires the solenoid every 2 seconds to maintain 10 bar at the 0.1 g/s flow rate. The pressure switch and solenoid consume 7 W of power each time. The mass flow rate is steady over the period. The time to reach zero flow from shutoff is 2 minutes - small delay since the total burn time is 60 minutes. The system has been able to support the 7 hour life time at the desired flow rate.

The expulsion tests have served as another means of checking the flowmeter calibration. The entire expulsion system was weighed to ensure proper filling of the nitrous tanks before thruster operation. The tanks are filled using nitrogen pressure gas above the vapour pressure of the nitrous oxide. Once the tanks are filled and checked with the scale, the scale is used to monitor flow rate over time. For a 4 hour and 48 minutes test, the flow meter and scale were within 99.25 % of each other.

Qualification tests will be conducted in the end of October of 1998 with integration beginning in November of 1998. UoSAT-12 is due to be launched on the Dnepr launch vehicle in Baikonour Russia in April 1999.

| | | | | | | | |
|---|--|-------------------------|--|----------------------|--|--|--|
| DRC No. | | THIRD ANGLE PROJECTION | | DO NOT SCALE DRAWING | |  Polyflex Air Tech | |
|  | | | | | | | |
| CAD GENERATED - NO MANUAL CHANGES PERMITTED - UNLESS OTHERWISE STATED, DIMENSIONS ARE IN mm - IF IN DOUBT ASK | | | | | | | |
| DES No. | | POLYFLEX | | MATERIAL | | TITLE | |
| DCN No. | | UNLESS OTHERWISE STATED | | SPEC. | | SSTL_NZO_2.dwg | |
| DESIGN | | 0.0000 | | FRESH | | | |
| CHECK'D | | 1.0000 | | HEAT | | | |
| APPROVED | | 2.0000 | | TREATMENT | | | |
| DATE | | 3.0000 | | BY 308 | | [1] DRC:ML | |

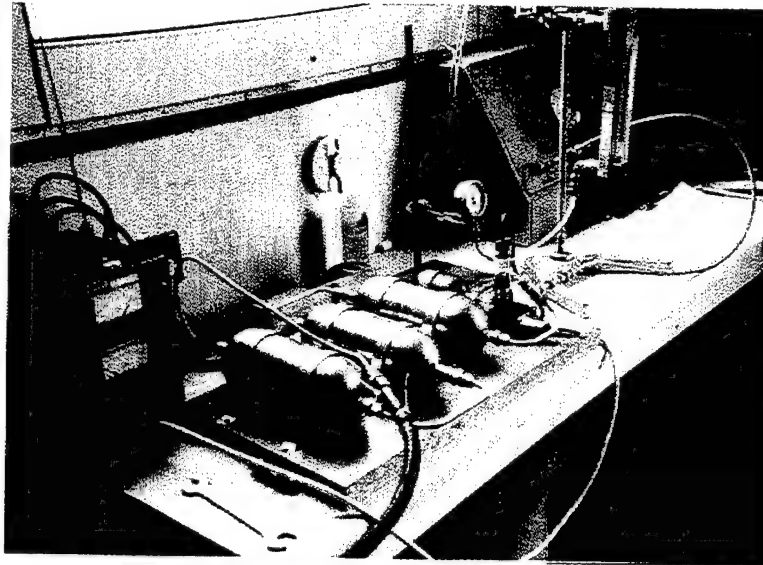


Figure 6-10 Polyflex Expulsion System. Picture shows breadboard system

6.3. MightySatII.1

6.3.1. Mission and Spacecraft

The MightySATII.1 is a flagship mission of the USAF AFRL for small satellite application. Using the theme, “faster, cheaper, better”, the USAF has decided that low cost small satellite platforms are useful for launching its own DOD payloads from the research laboratories in a quick and cheap manner. The MightySAT series is a test bed spacecraft to demonstrate this concept. It is developed with a target total cost budget of \$ 10 million. Spectrum Astro is the prime contractor. Figure 6-11 shows the spacecraft and the bus components. Figure 6-12 shows the various payloads.

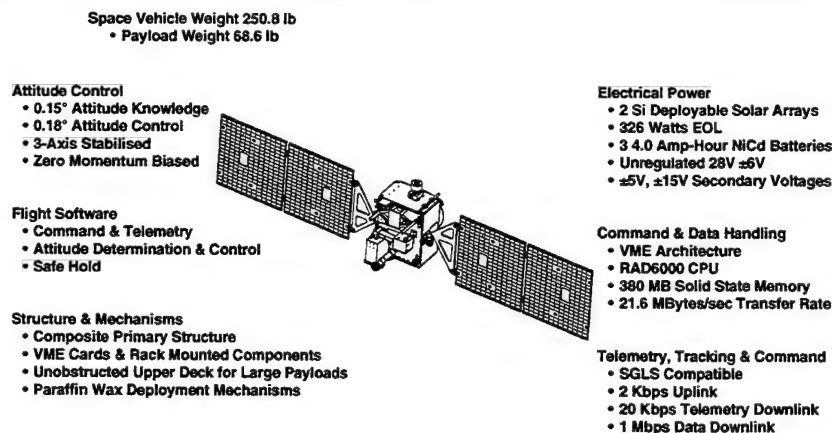


Figure 6-11: MightySATII.1 Spacecraft bus [Spectrum , 98]

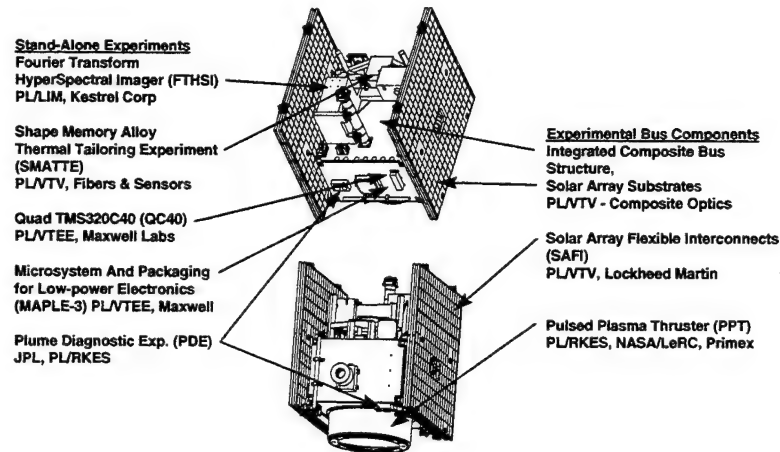


Figure 6-12: MightySAT II.1 Payloads [Spectrum, 98] The water resistojet replaces the PPT system.

The system was going to fly a 100 W Pulsed Plasma Thruster for orbit insertion. The primary vehicle was the space shuttle, and in order to increase mission life, propulsion was needed - see Figure 6.14.

PPT

Total Mission = 75 days
 - Trip time ~ 75 days
 = Available ~ 0 days
 Science days

Water Resistojet

Total Mission = 80 days
 - Trip time ~ 10 days
 = Available ~ 70 days
 Science days

No Propulsion

Total Mission = 40 days
 - Trip time ~ 0 days
 = Available ~ 40 days
 Science days

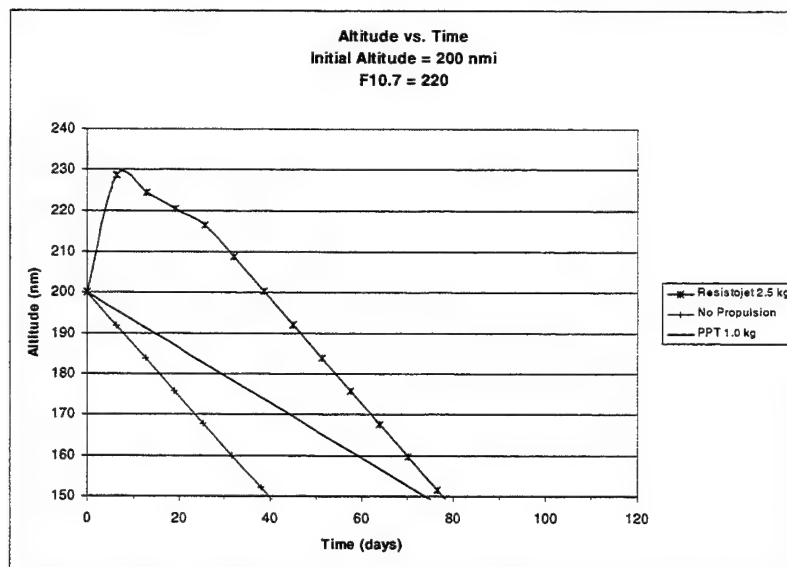


Figure 6-13: Mission Tradeoffs for high drag orbit [AFRL, 98]

This trade-off showed that the PPT could not provide any science days (all power goes to propulsion during maneuvers) assuming a 200 nm orbit under high drag conditions. In Dec 98, when the protoflight programme was underway for UoSAT-12, the results shown in Chapter 5 impressed the personnel at the USAF AFRL Electric Propulsion Laboratory. There was also a problem in that the PPT could not function at 100 W - burned out after minutes of operation. Thus, the USAF decided to pursue a 100 W water resistojet system.

Table 6-6 shows the system specifications. The configuration is very similar to UoSAT-12, except for the different nozzle size and no exit pipe attached to the nozzle for thermocouple measurements. All

of the engineering drawings for the thrusters are attached in Appendix B. Figure 6-15 shows the flight thruster integrated onto the expulsion system provided by Allied Signal, Tempe, Az.

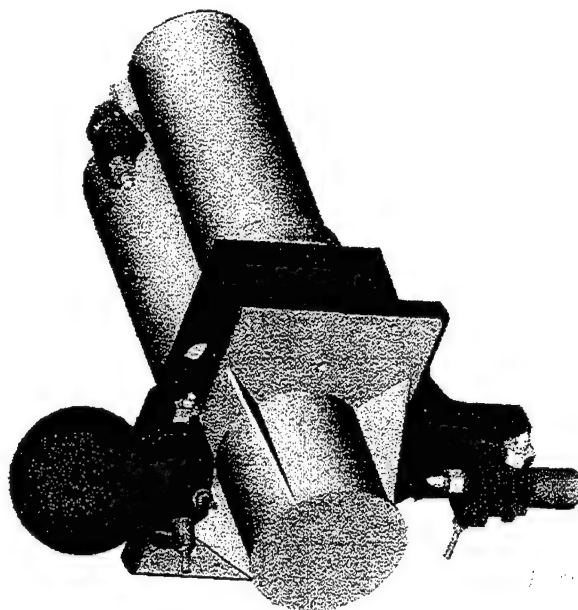


Figure 6-14: MightySAT11.1 Flight Design integrated to the expulsion system [Allied, 98]

| Item | Specification |
|--|---|
| Resistojet mass | 1.5 kg (same as UoSAT-12 plus attachment fins & viscojet) |
| Expulsion system mass | 6 kg |
| Water mass | 1.1 kg |
| Mass flow rate | 0.00003 kg/s |
| Pressure | 10 bar inlet, 5 bar chamber |
| Isp (steady state) | 152 sec |
| Thrust | 45 mN |
| ΔV (assuming steady state Isp) | 14 m/s |
| Nozzle | 0.3 mm throat - spark eroded |
| Burn Time | 10 hours continuous |
| Power | 100 W |
| Assembly | Electron Beam Welded |

Table 6-6: System Specifications

At the time at the start of the effort, the primary launch vehicle was the space shuttle. As of October 1998, the launch vehicle has been changed to the Minotaur. Since its initial orbit is ~ 660 km, mission lifetime can be guaranteed without propulsion. Thus, deorbit, circulization, or slight altitude changes for remote sensing and stationkeeping burns similar to UoSAT-12 are being considered.

The expulsion system is being designed by Allied Signal. Table 6-7 lists the system components. Figure's 6-15 and 6-16 show the flow system schematic with integration interfaces.

| COMPONENT | PEDIGREE | FEATURES |
|---------------------------------|------------|--|
| Pressure Vessel | Qualified | Existing unit needed to meet schedule due to length of certification process |
| Manifold | New | Design to meet package and component selection |
| Fill Port/ Test Port | Commercial | Check valve and cap |
| Initiator (Optional) | Qualified | Used for over 20 years on missile and space vehicle programs |
| Filter | Commercial | 3 micron (Abs) |
| Limit Orifice | Commercial | Lee Viscojet or Equivalent |
| Pressure Control Solenoid Valve | Qualified | Satellite usage proven component to be selected |
| Burst Disk | Commercial | Standard proven disk to be selected |
| Relief Valve | Commercial | Production part to be selected with acceptable usage history |
| Pressure Transducer | Commercial | Selection to be based on history |
| Water tank | New | New Piston accumulator design to meet package and schedule |
| Control Solenoid | Qualified | Satellite usage proven component to be selected |
| Tubing | New | Welded connection for gas side and standard fitting for water side. |

Table 6-7: Expulsion System Components [Allied, 98]

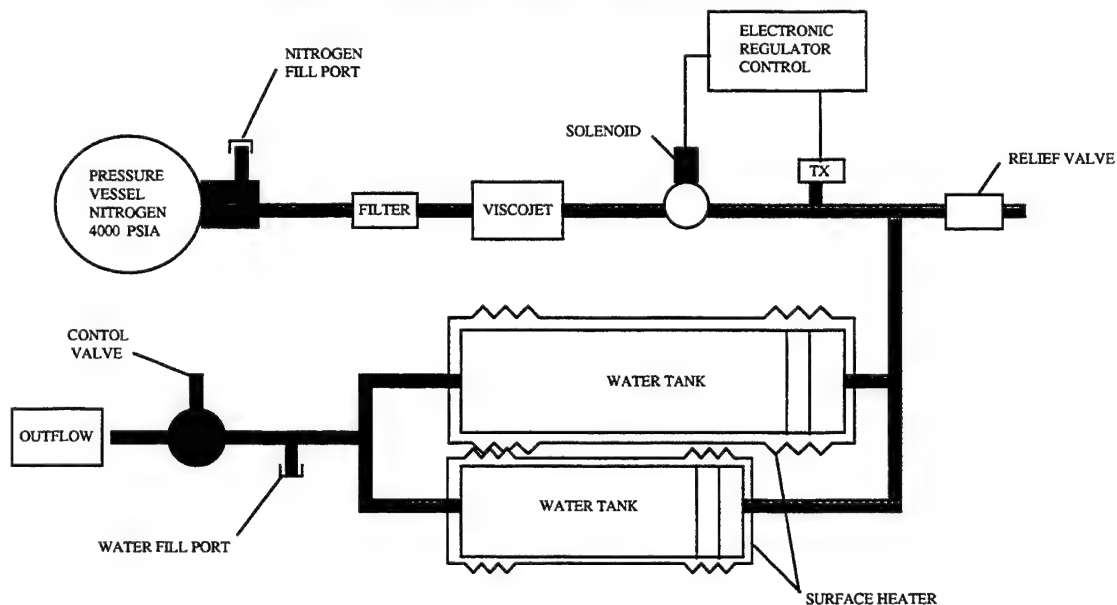
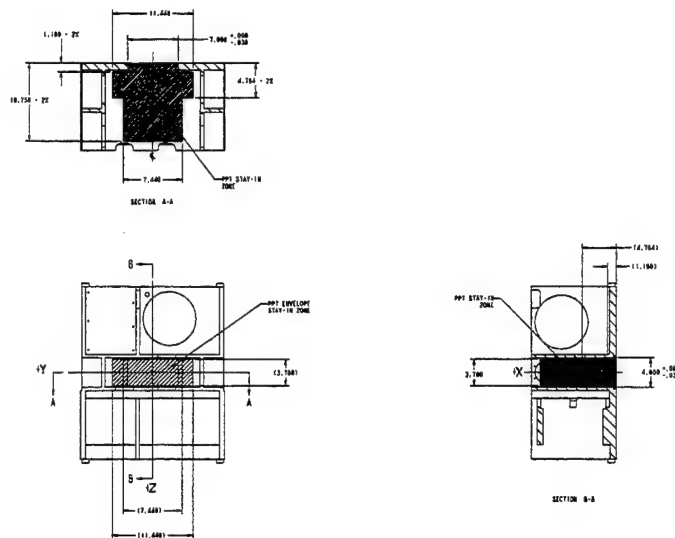


FIGURE 6-15: PRESSURIZED FEED SYSTEM SCHEMATIC [Allied, 98]**FIGURE 6-16: INSTALLATION ENVELOPE [Allied, 98]**

The available pressure vessel from the ARRIS program is a 3.46 dia sphere of 15.6 cu in capacity which was designed for 10,000 psia operating pressure with a burst factor of 2.25 (MIL- STD- 1522). Under STS rules this would allow a maximum fill pressure of 5625 psia to be used unless the vessel can be tested and certified to a higher value or a lower burst factor accepted. Packaging constraints using this vessel limit water capacity thereby reducing nitrogen gas required by 30%. This vessel can meet all the STS requirements. Should external water tanks be used to raise the water quantity to 4 liters (a requirement for an STS launch) then this pressure vessel charged to the 5625 psia will meet the expulsion requirements. However, at this time it appears that the maximum water capacity is 1.1 liters.

The manifold is a machined titanium block directly attached to the pressure vessel and is ported to receive all the pneumatic system components. The manifold assembly includes an electro-explosive device (EED) used to open the pressure vessel, a filter to protect critical downstream orifices from contamination, and a Viscojet orifice sized to control flow of the nitrogen gas into the water tanks.

The pressure vessel may be filled and factory sealed with a knockoff seal which is broken by initiating the EED. This design option enables the manifold to remain unpressurized throughout storage and launch and to be pressurized on orbit when propulsion is required.

An alternate approach to a factory filled and sealed pressure vessel is to design a manual fill port into the manifold in place of the EED. This approach leaves the pressure vessel unsealed at the time of

shipment and will require on-site capability to charge the pressure vessel to the required system operating pressure under controlled environmental conditions.

Pressed into the manifold and located downstream of the fill port or initiator is a sintered metal, 3 micron absolute, filter. This filter will protect all downstream orifices against contamination generated in pressurizing the system.

Immediately downstream of the filter is the Viscojet orifice. The Viscojet is currently sized with an effective diameter of .003 to .005 inches. The outlet of the manifold is sealed off by the pressure control solenoid valve.

The manifold is designed to the same pressure ratings as the pressure vessel.

This Pressure Control Solenoid valve is an ultra low leakage poppet valve with a soft sealing surface. Upstream pressure activates the seat and provides sealing force. The valve is partially pressure balanced with upstream pressure to minimize solenoid force requirements and therefore solenoid size. The closing force is overcome by the force generated in the solenoid when the coils are energized. (Redundant coils are optional).

This valve is a key item to successful system operation due to the requirement for extremely low leakage. Typical valves in this size range have leakage rates of 10% of that required to maintain the expected water flowrate. Therefore, this valve will have to be selected from a limited number of ultra low leakage repeatable seating valves. These valves have been developed for long term satellite use by several sources and typically have long lead procurement cycle times. Early evaluation and selection of this component is critical to the schedule.

There are no burst disks due to the pressure tolerance specified by the solenoid valve manufacturer.

The relief valve is designed to protect against rupture of the water tanks in the event of an over-pressure condition and will also prevent complete loss of pressurizing gas. This approach supports single point failure safety of the pneumatic system.

A 500 psi range variable reluctance type pressure transducer is recommended. This transducer design would provide good calibration stability and a resolution compatible with the regulation loop requirements. Alternates may be considered such as pressure actuated switches.

The electronics for signal conditioning of the pressure transducer, set point comparison and operation of a solenoid driver with current limiting represent a small standard circuit which can be incorporated into other circuit boards if space is available.

Should mechanical, reed or magnetic switches be used, then electronics may not be required as these can directly operate the solenoid valve through the direct closure of contacts on the power line to the solenoid.

The water tanks are positive expulsion piston interfaced tanks of cylindrical configuration with the outside diameter maximized to the available package. The tanks are designed with the same factors as those currently used for several launch vehicle hydraulic systems (Athena, Maxxus, Taurus, Vega, Hera, etc.).

The main tank body is anodized 6061-T6 aluminum with wall thickness of .060 inches. The gas end is integrally machined in the main body. The water end of the main body is threaded to mate with the titanium end cap. Titanium is utilized to minimize the overall outside tank diameter.

The piston will use a Teflon or equivalent 'T-seal and have an aspect ratio of .3 which will allow for approximately 3 cu.in. of ullage volume in each tank with over 98 % expulsion efficiency.

The initial evaluation gives the two tanks a water volume of 0.55 kg.

The tanks will be provided with a conformal self regulating surface heater to warm the tanks to 40° F prior to pressurization.

This solenoid valve is of the latching type to minimize electrical power usage (Single or dual coil is an option). This solenoid will require 20 volt at 1 amp minimum for 50 ms to actuate. Polarity reversal is required to de-activate. If bus power is lost, the valve will remain in the open position which could bring water into the thruster cavity with no power. This failure mode may require this valve be replaced with a non-latching solenoid [Allied, 98].

Integration tests began in October of 1998. Integration is expected in early Spring of 98 with the expulsion system CDR scheduled for end of November 1998. The MightySATII.1 is expected to be launched off of the Minotaur launch vehicle in January 2000. The statement of work for the effort is attached in Appendix D.

6.4. References

- [Allied Signal, 98] Allied Signal technical interchange meeting in support of the MightySATII.1 Programme, October 6, 1998, Tempe, Az.
- [AFRL, 98] Air Force Research Laboratory MightySATII.1 Mission Analysis Briefing, February, 1998.
- [Gomes, 98] Personal interview with Mr. Luis Gomes, SSTL thermal engineering, May, 1998.
- [Hashida, 96] Personal interview with Mr Yoshi Hashida and use of U12 attitude control software, 1996.
- [Morren, 87] Jones, R.E., Louviere A J and Sovey J.S., "Water Propellant Resistojets for Man-tended Platforms", 38th Astronautical Federation Congress, Brighton UK, October 10-17 1987.
- [Sellers, 96] Sellers, J.J. "Investigation into Low-Cost Propulsion Systems for Small Satellite Missions", Ph.D. Thesis, Department of Electrical Engineering, CSER, University of Surrey, Guildford, UK June, 1996.
- [Spectrum, 98] Spectrum Astro mission briefing slides for MightySATII.1, February, 1998.
- [Ward, 98] Ward, J.W. "UoSAT-12 System Description", SSTL Web Page, September, 1998.
- [Williams, 98] Williams, Trevor, Use of internal memorandum written on attitude control studies done in support of UoSAT-12, August, 1998.

Chapter 7

Conclusions

7. CONCLUSIONS

7.1. RESULTS

7.2. CONCLUSIONS

7.3. ACCOMPLISHMENTS

This final chapter summarises the key conclusions of this research effort. The significant results obtained through four research phases are as follows:

- At the start of this research effort, a water or nitrous oxide resistojets looked like the best option for the 6 tight mission constraints of small satellite stationkeeping. Based upon the test results and endurance tests, a low cost resistojets can be designed and qualified for small satellite missions.
- Characterisation of flow performance in a working water resistojets. Observation and characterisation of a controlled self-sustaining decomposition reaction of nitrous oxide in a working resistojets.
- Development of a thermal model to verify design performance and enable future design. Characterisation of heat transfer efficiency, nozzle friction losses, and rocket performance for various working fluids under different flow conditions.

Notable accomplishments and recommendations for future work are also included.

7. Conclusions

7.1. Results

The best way to present the results of this investigation is to return to the research plan and list the goals at the start of the research versus the specific results from each of these goals. Table 7-1 presents these results.

| Research Phase | Goals | Tasks | Result |
|-----------------------------|---|---|--|
| Proof of Concept | <ul style="list-style-type: none"> Design packed bed system @500 W using water as the working fluid - collect data to verify thermal analyses Collect data / observe fluid flow for thermal model | <ul style="list-style-type: none"> Built thruster that fired for 27 hours using 6 different bed materials. Identified engineering issues for next phase - efficiency, lifetime | System feasible for small satellite application, Constraints not satisfied - more efficient and longer life design needed in next phase - Move to Prototype phase |
| Prototype | <ul style="list-style-type: none"> Design 200 W thruster with new heater and SiC bed material for better efficiency Improve thermal model - use gases with easier properties for benchmark Calculate heat transfer efficiency, thrust, Isp | <ul style="list-style-type: none"> Two thrusters fired for 150 hours Friction losses in nozzle reduced performance up to 90 % Oxidation of bed material reduced lifetime - discovered by using Electron Microscope Issues for next phase : efficiency and lifetime | Chamber Temperatures of 900 K achieved at 100 W input power, friction and radiation losses produced unacceptably low Isp's . Nozzle clogged after 10's of hours of operation. Constraints not satisfied - Need longer life, more efficient system - Move to Protoflight phase |
| Protoflight | <ul style="list-style-type: none"> Improve Design Calculate heat transfer efficiency, thrust, Isp Improve thermal model Obtain endurance data obtainable for a flight system | <ul style="list-style-type: none"> Tested for a total of 450 hours in vacuum with He, N₂, H₂O, H₂O/Methanol, N₂O, and N₂O with MgO catalyst @powers from 0 - 600 W, pressures from 3 - 100 bar using a thrust stand Observed first self-sustaining N₂O reaction for resistojets . Density Isp of 182 sec for water and 105 sec for nitrous oxide with 0 power applications makes flight systems attractive modeling within 10 % of experimental results | Multiple working fluids helped improve thermal model Higher power, higher mass flow thruster achieved performance much closer to ideal (94- 100 %) Developed technique to determine when friction flow losses are occurring and ways of building a better performing system via the thermal model. Lifetime demonstrated and found ways to improve it further. |
| UoSAT-12 Flight System | <ul style="list-style-type: none"> Design flight system | <ul style="list-style-type: none"> Use ALL results to design 100 W N₂O system | 100 W Nitrous Oxide System: 125 mN, 127 sec, $\Delta V=10.4$ m/s Planned to fly ! |
| MightySATII.1 Flight System | <ul style="list-style-type: none"> Design flight system | <ul style="list-style-type: none"> Use ALL results to design 100 W H₂O system | 100 W Water System 45 mN, 152 sec, $\Delta V=14$ m/s Planned to fly ! |

Table 7-1: Summary of research goals, their specific corresponding tasks and the results obtained in the research programme.

7.2. Conclusions

This section first shows how the 6 small satellite stationkeeping constraints were solved through this research effort. It then summarizes the conclusions into three broad areas of research into resistojet rockets for small satellite applications:

- Engineering
- Scientific
- Performance

Recommendations for further research in each area will also be presented.

7.2.1. Small Satellite Constraints

Six constraints were identified as being key parameters for propulsion systems providing stationkeeping to small satellites. The constraint followed by the results presented in this research investigation are:

- Cost: £93,673 total programme cost (explained in section 7.3). Future thrusters will cost £5000.
- Mass: Water and Nitrous Oxide Isp's of 152 and 127 sec (better than cold gas and cost-effective compared to higher performing systems)
- Volume: water and nitrous oxide working fluids have a density Isp of 152 sec and 127 sec, but nitrous oxide does not require a pressurisation system
- Power: 45 mN and 125mN @ 100 W input power can overcome high drag orbits and also integrate into small satellite attitude control system with low disturbance torque
- Integration: non-toxic propellants, 354 demonstrated lifetime.
- Thrust: thrust/power allows flexible range to meet power budgets. Optimum firing is for 1 hour for stationkeeping manoeuvres.

The end result is a propulsion system fine-tuned to the small satellite user. It is low cost and designed with a thrust/power for low Earth orbiting small spacecraft. The outside funding and upcoming flights show the uniqueness of the effort.

7.2.2. Engineering Accomplishments

Approximately 700 hours of test data were collected on 7 different thrusters using 3 different designs. A 190 W water resistojet that fired for 354 hours was the most significant engineering accomplishment of the programme. The thrust did decay by 30 % over the length of this firing. Analysis and post-inspection of the chamber revealed that silicon oxide deposits had built up due to impurities in the silicon carbide bed material before firing. A "purer" bed material was discovered and a treatment method to remove the silicon oxide and prevent future problems in the flight design. Thus the key engineering discoveries were:

1. ISE Inc. heater - reliable at various power levels as long as inside temperature does not exceed 1000 C.
2. Micropore Insulation - 0.006 W/mK thermal conductivity properties inside vacuum. Used for reducing wall temperature to reduce radiation losses.
3. Viscojet - reduces thrust oscillations at start-up with water as the working fluid.
4. Silicon carbide bed material - 687 J/kg K heat capacity, 2970 kg/m³ density, and 1.046 W/mK thermal conductivity gives a good balance of heat transfer characteristics for good bed performance in a resistojet. Material issues discussed above show good compatibility for long duration burns.
5. Small nozzles - able to spark erode nozzles from 0.12 - 0.7 mm throat diameter - better than MEMS technology as of current literature survey.

6. Test approach - testing @ sea level and improving the design while not going to the thrust stand until close to flight qualification keeps the programme cost low.

The ultimate test of these conclusions will be when the resistojet presented in Chapter 6 flies in space for the UoSAT-12 and MightySATII.1 missions. However, there are some areas where the system could be researched further:

- higher temperature heater - since performance scales directly with Chamber Temperature - a higher performing heater @ 100 W (watt density, sheath temperature) would increase performance. Currently, one does not exist off the shelf.
- lower weight - since the chamber and insulation protection outer sleeve are made of stainless steel, the mass of the 100 W resistojet is just over 1 kg. If a low cost system can be built with lower weight materials, it would ease integration.
- better performing nozzle - the flight designs have as big as a throat to support the optimal chamber temperature and mass flow conditions. The contour has been rounded off of the throat and polished to reduce friction losses and prevent particulate (if any exists) from sticking to the surface. Other more complicated geometries may give better performance for the 100 W flow rates.

7.2.3. Scientific

With all of the test data collected with various working fluids under different flow conditions and powers for the three thrusters, it allowed characterization of the flow conditions use of the results to develop a scientific model for future design. This in turn allowed the design to improve from phase to phase. The culmination of the research will be obtained when the first water and nitrous oxide resistojets fly in space in the Spring of 1999 and Spring 2000. The specific results are:

- self-sustained nitrous oxide decomposition reaction for 18 hours with no power input for resistojet application. This is the first time ever this reaction has been recorded for resistojet application.
- 18 - 20 minutes to reach steady state (30 minutes typical in resistojet application) and proper start-up procedure for efficient operation - certain scenarios can produce problems
- Optimal conditions determined - scaling effects
- Thermal model for future design function of(input power, materials, thruster geometry (bed, straight tube, multi-pass, etc., inlet pressure, flowrate)

There are several scientific areas where further research is needed:

- Reduction of radiation losses to increase heat transfer efficiency
- Verification of thermal model in space - microgravity, changing temperature, tighter vacuum. Also validation of the model for future design applications.
- Better characterisation of nitrous oxide decomposition. Is heat transfer efficiency the driving factor in the self-sustaining decomposition? Bed temperature, mass flow, and pressure should be measured to see if they are contributing factors to the self-sustaining reaction. At what flow conditions does the reaction start / stop ? This type of chamber monitoring would drive the design back to something like the Proof of

Concept thruster, but with orbital welding, this would not lead to as many problems (leaks) associated with the screwed fittings in that programme. Catalysts could be investigated further. Hybrid options needed to be addressed. Use of the resistojet to start up a hybrid motor using nitrous oxide as the oxidiser for multi-restart missions is an interesting area. The resistojet time transient to reach steady state would need to be improved.

7.2.4. Performance

The vast test data is also very important in producing a good performance prediction for the thrusters. The use of the NASA JPL Inverted Pendulum Thrust Stand at the AFRL Edwards AFB Electric Propulsion Laboratory produced an error bar < 1% for the Prototype#4 tests, added to an error bar of < 3% in the flow meter, giving a highly accurate characterization of thrust and specific impulse which is used to compare with theoretical models and plan the future flight mission. The specific results achieved are as follows:

1. Characterization of friction losses - the thrust stand revealed that the nozzles in the Prototype and Protoflight- (0.12 - 0.194 mm throat diameters) experienced losses in specific impulse of 25 - 50 %. A Reynolds Number and Knudsen Number analysis showed that the geometry of the nozzle and viscosity of the working fluid allowed all of the thermal energy produced in the chamber to be lost due to friction in the nozzle (heat loss which is radiated to space) and subsequent reduction in kinetic energy in the nozzle (lower exit velocity - lower specific impulse).
2. Performance prediction method for current and future designs for various working fluids and flow conditions.
3. Optimal firing strategy (lower power, longer run time) developed looking at performance over time and spacecraft integration issues.
4. Comparison of various performance prediction methods - thermodynamic (some new to electric propulsion), and thrust stand..
5. Use of instruments in space for other methods of performance prediction.

There are also areas that performance prediction can be further researched:

- Validation of performance with qualification and flight data obtained for the two flight systems with two engineering model thrusters.
- In-house thrust stand vacuum facility needed
- Improved data acquisition (better flow meter for next phase < 1% error bar), automatic instead of recorded manually.

7.3. Accomplishments

This research has produced novel results that have made an impact to the small satellite and electric propulsion communities. Table 7-2 shows the complete cost break down (in £) for the research programme.

| Programme Phase | Hardware | Labour | Total |
|------------------------------------|----------|--------|--------|
| Proof of Concept | 2, 879 | 4,969 | 7,848 |
| Prototype | 7,640 | 3,765 | 11,405 |
| Protoflight | 11,071 | 14,537 | 25,608 |
| UoSAT-12 flight +expulsion | 35,000 | 13,812 | 48,812 |
| MightySATII.1 Water - expulsion | 15,000 | 21,250 | 36,250 |

Table 7-2: Resistojet Programme Cost Break Down

As stated in the introduction, there was a total of £40,000 of outside money put into this programme budget. Omitting the 40 K of outside money, the **TOTAL COST** for the University of Surrey to design, build, test, qualify, and fly the complete (+ expulsion system provided by Polyflex at £25,000, includes SSTL manpower man-hours) nitrous oxide resistojet on UoSAT-12 is £93,673. The current off-the-shelf price of a 300 W hydrazine system (quoted from Primex) is £93,750 for the thruster only. The selling price of a University of Surrey built thruster is £5,000 and its performance is applicable for the small satellite mission requirements. The cost constraint was the most important out of the six constraints. This is quite a remarkable accomplishment in just three years from programme start - hence the outside interest.

Besides cost, the following notable contributions have lead to the first ever:

- water resistojet for space application 100 W, 45 mN, 152 sec Isp (operation at higher powers also make it applicable to systems bigger than small satellites)
- nitrous oxide resistojet for space application 0 - 100 W, 125 mN, 127 sec Isp (self-sustained decomposition reaction observed in Protoflight#4)
- complete characterization of resistojet performance (heat transfer efficiency, nozzle friction losses) for small satellites
- new bed and thermal model for future resistojet design - documented system simulation for scaling / losses
- advanced the state of the art for low cost small satellite stationkeeping propulsion - hence 2 flight systems for Spring 1999 and 2000

This research has proved that affordable access to space for small satellite stationkeeping missions is achievable compared to current off the shelf systems. This work has made a significant contribution to the field of rocket propulsion, electric propulsion, and satellite engineering.

APPENDIX A

THERMAL MODEL

Figure A-1 shows the final thermal model flow chart developed in this research effort.

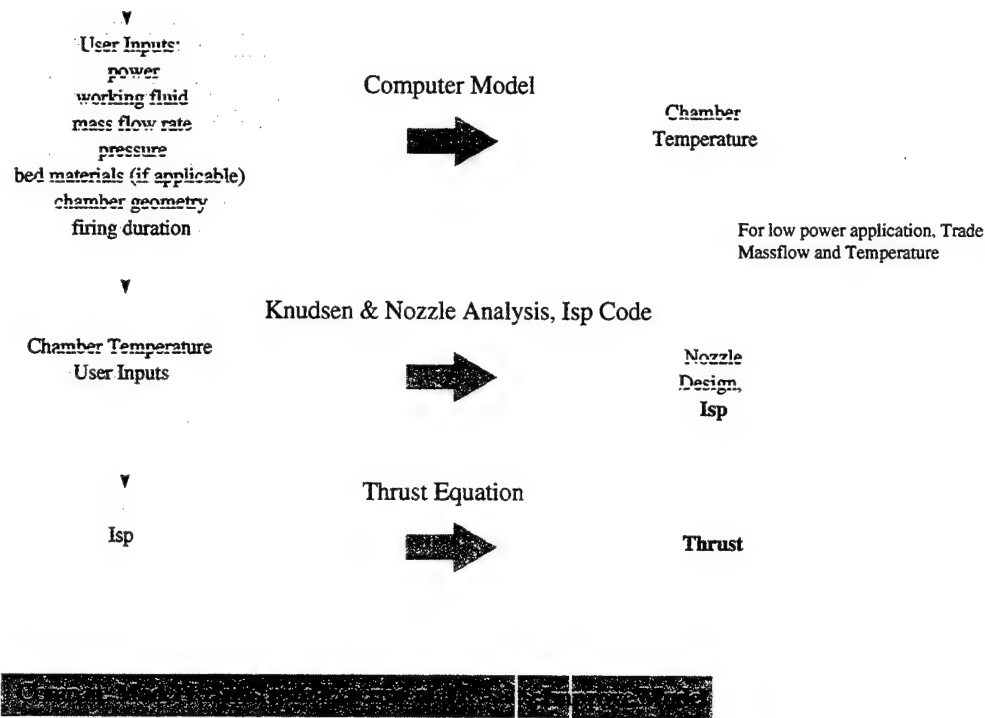


Figure A-1: Thermal Model

Figure A-2, shows the results of the model through the various research phases.

Proof of Concept
 Power: 560 W
 Thrust: 100 mN
 Isp: 78 sec
 Thermal Model Error: 15 %

Prototype
 Power: 100 - 250 W
 Thrust: 10 - 30 mN
 Isp: 82 - 101 sec
 Thermal Model Error: 50 %

Protoflight
 Power: 0 - 330 W
 Thrust: 500 mN
 Isp: 136 - 150 sec
 Thermal Model Error: 10%

Flight
 Power: 100 W
 Thrust: 125 mN
 Isp: 127
 Thermal Model Error: 3 % -- Measured
 Chamber temperature at steady state 809 K versus
 a predicted of 812 K.

Figure A-2: Thermal Model Results for Nitrous Oxide for the Various Research Phases

Figure A-2 shows the improvement in the model over time. The reasons for the error were:

- lumped thruster geometry (proof of concept)
- working fluid heat transfer properties (proof of concept)

- friction losses and flow losses in nozzle (prototype and protoflight)
- time to reach steady state based on continuum heat transfer between the bed particles (proof of concept, prototype)

Analysis of the empirical results over time led to the improved and final model. A “step by step” use of the model is shown below:

1. User inputs data into the thermal code. The inputs are (source code is attached after this description): chamber outer radius (not including Micropore insulation, code only studies particle to particle heat transfer to the fluid and is not used for radiation losses. Wall temperature measurements using the Stephan-Boltzmann Radiation equation were used for determining these losses. The sizing of the Micropore insulation was based upon these measurements and off the shelf options - 25 mm thickness.), bed outer radius, heater outer radius, heater centreline radius, bed porosity, bed particle diameter, particle dimensions, particle density, heat capacity, thermal conductivity, choice of working fluid from heph2.for (computer file), working fluid inlet temperature, pressure, and mass flow rate, power density (heater power divided by bed volume), and length of simulation. The heat transfer and pressure drop in the bed is based upon the Achenbach heat transfer and Ergun pressure drop correlation (Chapter 2).
2. The computer code outputs chamber temperature as a function of time. Each time data point should be multiplied by 4 due to the continuum time difference from the particle to particle heat transfer to the fluid (Chapter 4). This chamber temperature, along with the mass flow rate and pressure and other fluid properties are used to size the nozzle (Chapter 2). Once the nozzle is sized, an analysis of the Knudsen number and Reynolds number is needed to determine if flow separation and or boundary layers exist in the nozzle (Chapter 5). If this is the case, then the mass flow needs to be increased by growing the nozzle throat radius. With the new mass flow rate, step 1 is used again. This may require several iterations since as the mass flow rate increases, the chamber temperature in the bed decreases at a constant heater power input. The flight thruster represents this process. The chamber temperature was dropped from 1100 K to 800 K (0.13 mm throat diameter at a mass flow rate of 0.00005 kg/s to 0.4 mm throat diameter at a mass flow rate of 0.0001 kg/s).
3. Once the chamber temperature and nozzle size are determined, the Isp is determined by using the Isp code. The Isp code requires the working fluid pressure, expansion ratio, exit pressure, and temperature to calculate the Isp. If the Knudsen number is below 0.01, the ideal assumptions in the Isp code give a good approximation to the measured Isp. The thrust is determined from the mass flow rate and Isp (Chapter 2).

This method predicts that even though the chamber temperature drops by 300 K, the Isp increases due to a better performing nozzle for 100 W input power (measured result was 54

% of ideal due to nozzle losses @ 100 W in the prototype system). Thus the predicted Isp of 127 sec will give a better total impulse with the bigger nozzle. The model is a good use of scientific theory and empirical data and should be applied to other systems instead of the sole use of empirical data or just nozzle theory.

```

C *****
C TTTT RRRR IIII TTTT RRRR AAA N N 3333
C T R R I T R R A A NN N 3
C T RRRR I T RRRR AAAA N N N 333
C T R R I T R R A A N NN 3
C T R R IIII T R R A A N N 3333
C *****
C TRITRAN3 - THIS IS A PRELIMINARY CODE FOR PBR ANALYSIS
C THAT FIRST FINDS THE CONDITIONS
C FOR A FUEL ELEMENT, GIVEN THE BOUNDARY CONDITONS OF
C INLET PRESSURE, INLET TEMP, MASS FLOW RATE, AND
C POWER DENSITY. IT UTILIZES THE MIT-SNL CONTROL LAWS FOR THREE
C TRANSIENT RAMPS. THE FIRST TRANSIENT. THE MIT-SNL CONTROL LAWS
C ARE PATENTED UNDER NUMBERS 4,637,911; 4,710,341; 4,781,881.
C THE BASELINE ELEMENT IS 2 INLET CHANNELS, 6 SLOTS, 1 ELEMENT
C
C *** THIS CODE WAS MODIFIED FOR RESISTOJET SIMULATION BY TJL
C STARTING IN DEC 95. The first mod was
C to change the geometry from a particle bed reactor to
C a resistojet thruster. The new version
C predicts the heat transfer in a resistojet thrust
C chamber with a centrally mounted cartridge
C heater surrounded by a packed bed material. It
C studies the bed heat transfer for
C any bed material. The bed volume over heater input
C power should be used for the power
C density input. The programme uses the subroutine
C heph2.for for helium
C simulations and a modified heph2.for for water. The
C modified version use lumped
C values for the intial state properties (mixtures of
C steam/water- derived from experimental data).
C Other gases can use STP values for the initial
C conditions (nitrogen and nitrous oxide).
C The other modification was the time to reach
C steady state. According to Chapter 4, comparing the
C empricial continuum value to predicted for particle
C particle heat transfer can vary by a factor of 2- 4.
C The output time values are multiplied by 4 and reresent
C a good approximation to measured versus predicted
C steady state values. The output chamber temperature is then
C used in the flow chart shown in Appendix A.
C
C VERSION: 4 DATE:9/11/98
C NBSPH2 SUBROUTINE FOR HYDROGEN PROPERTIES BY JAMES WALTON, NASA LeRC
C Changed to H2O on 15/1/96 from Properties obtained in Todreas Book
C *****
C
C IMPLICIT REAL (A-H,O-Z)
C REAL MANIN,MANOUT,M1,M2,M3,NU,KCOND,MACH
C REAL LAMBDA(6),LAMBDAE,NLIFE,K1,K2,K3,KF
C DIMENSION AIN(9),AOUT(9),ABAR(9),FLEN(9)
C DIMENSION DH(9),VOL(9),RHOBAR(9),TYPMAN(9)
C DIMENSION C(6),C1(6),BETA(6),TEMP(60),DROP(9)
C DIMENSION REYN(9),RHOIN(10),VISC(9),RES(9)
C DIMENSION PIN(10),PIN1(10),PBAR(9),PBAR1(9)
C DIMENSION TIN(10),TBAR(9)
C
C COMMONS FOR THE INTERACT SUBROUTINE

```

```

C      COMMON /ELEMENT/ RORF,ORFLEN,RIC,WSL,TSL,RIP,PBRLN,RCF,RPB,RHF,
1      ROP,EXTLEN,ECF,EPB,EHF,DCF,DPB,DHF,MANIN,MANOUT
COMMON /PARTCLE/ RF,R1,R2,R3,RHOF,RHO1,RHO2,RHO3,
1      CPF,CP1,CP2,CP3,KF,K1,K2,K3
COMMON      /TRANS/ TINO,TINP1,TINP2,TINP3,PINO,PINP1,PINP2,PINP3,
1      FLOWO,FLOW1,FLOW2,FLOW3,PDENO,PDEN1,PDEN2,PDEN3,DURTRAN1,
1      DURTRAN2,DURTRAN3,DELAYT,AFTERT,DELTAT,ISAVE,WO
COMMON /RESTNC/ AIN,AOUT,ABAR,DH,TYPMAN,
1      REYN,RHOIN,RHOBAR

C
C DATA SETS FOR THE INLET CHANNEL, INLET SLOT DIMENSIONS
C AND THE REACTIVITY GROUP VALUES
C
DATA PI,NLIFE /3.14159265442,52.9E-6/
DATA BETA /.00028,.00159,.00141,.00305,.00096,.0002/
DATA LAMBDA /.01323,.039,.139,.359,1.41,4.03/
DATA ALPHAT,ALPHAP,ALPHAD,WORTH /-1.E-5,9.8E-10,-4.E-6,6.0/

C
C OPEN THE OUTPUT FILES
C
OPEN(UNIT=9, FILE= 'tritrans3.inp')
OPEN(UNIT=10, FILE= 'temps.csv')
OPEN(UNIT=11, FILE= 'wdot.csv')
OPEN(UNIT=12, FILE= 'react.csv')
OPEN(UNIT=13, FILE= 'mdot.csv')
OPEN(UNIT=14, FILE= 'pressure.csv')
WRITE(14,*) ' TIME,PORFIN,PICIN,PSLIN,PIPIN,PCFIN,
1      PPBIN,PHFIN,POPIN,PEXTIN,POUT'
OPEN(UNIT=15, FILE= 'RESIST.CSV')
WRITE(15,*) ' TIME,RESORF,RESIC,RESSL,RESIP,RESCF,
1      RESPB,RESHF,RESOP,RESEXT'
OPEN(16,FILE= 'press.csv')
OPEN(17,FILE= 'powers.csv')
OPEN(18,FILE= 'theta.csv')

C
C DETERMINE THE PROBLEM STATEMENT
C A. READ THE REFERENCE DATA FILE FOR BASELINE VALUES
C B. GET FUEL ELEMENT DIMENSIONS
C C. GET THE FUEL PARTICLE DIMENSIONS AND CHARACTERISTICS
C D. GET THE INITIAL AND TRANSIENT CONDITIONS
C
DO 10 I=1,60
    READ(9,*) TEMP(I)
10 CONTINUE
    READ(9,*) ORF
    CLOSE(9)
    CALL INTERACT(TEMP)

C
C SET UP THE FLOW AREAS AND VOLUMES FOR EACH CONTROL VOLUME
C
C INLET CHANNEL EXTENSION
    AIN(1)=PI*RORF**2*2*ORF
C      ! 2 CHANNELS PER ELEMENT
    AOUT(1)=AIN(1)
    VOL(1)=AIN(1)*ORFLEN
    FLEN(1)=ORFLEN
    DH(1)=2*RORF
C INLET CHANNEL
    AIN(2)=PI*RIC**2*2
C      ! 2 CHANNELS PER ELEMENT

```

```

      AOUT(2)=PBRLN*WSL*2*3
C      ! 2 CHANNELS,3 SLOTS PER ELEMENT
      VOL(2)=AIN(2)*PBRLN
      FLEN(2)=PBRLN/2.
C      ! 1/2 EFFECTIVE LENGTH
      DH(2)=2*RIC
C      INLET SLOT
      AIN(3)=AOUT(2)
      AOUT(3)=AIN(3)
      VOL(3)=AIN(3)*TSL
      FLEN(3)=TSL
      DH(3)=4*AIN(3)/(2*(WSL+PBRLN))/6.
C      ! TO GET TO 1 SLOT DH
C      INNER PLENUM REGION
      AIN(4)=PBRLN*2.*PI*RIP
      AOUT(4)=PBRLN*2.*PI*RCF
      VOL(4)=PBRLN*PI*(RIP**2-RCF**2)
      FLEN(4)=RIP-RCF
      DH(4)=2*PBRLN
C      AFLOWIP=PBRLN*(RIP-RCF)
C      DH(4)=4*AFLOWIP/(2*(PBRLN+RIP-RCF))
C      COLD FRIT
      AIN(5)=PBRLN*2.*PI*RCF*ECF
      AOUT(5)=PBRLN*2.*PI*RPB*ECF
      VOL(5)=PBRLN*PI*(RCF**2-RPB**2)*ECF
      FLEN(5)=RCF-RPB
C      DH(5)=DCF/(1-ECF)
      DH(5)=DCF*(1-ECF)/ECF*2./3.
C      FUEL PARTICLE BED
      AIN(6)=PBRLN*2.*PI*RPB*EPB
      AOUT(6)=PBRLN*2.*PI*RHF*EPB
      VOL(6)=PBRLN*PI*(RPB**2-RHF**2)*EPB
      FLEN(6)=RPB-RHF
C      DH(6)=DPB/(1-EPB)
C      DH(6)=DPB*(1-EPB)/EPB*2/3
      dh(6)=dph
C      HOT FRIT
      AIN(7)=PBRLN*2.*PI*RHF*EHF
      AOUT(7)=PBRLN*2.*PI*ROP*EHF
      VOL(7)=PBRLN*PI*(RHF**2-ROP**2)*EHF
      FLEN(7)=RHF-ROP
      DH(7)=DHF
C      OUTLET CHANNEL
      AIN(8)=PBRLN*2.*PI*ROP
      AOUT(8)=PI*ROP**2
      VOL(8)=PBRLN*AOUT(8)
      FLEN(8)=PBRLN/2.
C      ! 1/2 EFFECTIVE LENGTH
      DH(8)=2*ROP
C      OUTLET EXTENSION PIECE
      AIN(9)=AOUT(8)
      AOUT(9)=AIN(9)
      VOL(9)=EXTLEN*AOUT(9)
      FLEN(9)=EXTLEN
      DH(9)=DH(8)
C      LUMPED VOLUMES FOR HEAT BALANCE CALCULATIONS
      VOLI=VOL(1)+VOL(2)+VOL(3)+VOL(4)+VOL(5)
      VOLIII=VOL(7)+VOL(8)+VOL(9)
C      INITIALIZE VOLUME PRESSURES AND TEMPERATURES
      DO 20 J=1,9
        PIN(J)=PINO

```

```

        PIN1(J)=PINO
        PBAR(J)=PINO
        TIN(J)=TINO
        TBAR(J)=TINO
        TYPMAN(J)=0.0
        ABAR(J)=0.5*(AIN(J)+AOUT(J))
20    CONTINUE
        PIN(10)=PINO
        POUT=PIN(10)
        TIN(10)=TINO
        TYPMAN(2)=MANIN
        TYPMAN(8)=MANOUT
C
C    CALCULATE THE INITIAL AND STEADY STATE CONDITIONS
C
        PBARI=.5*(PIN(1)+PIN(6))
        PBARIII=.5*(PIN(7)+PIN(10))
        P=PIN(1)
        TT=TIN(1)
        CALL NBSPH2(HIN,P,TT,RHO,VIS,CP,PR,S,CND,SS,G,X,0)
        PDEN=PDENO
        QBED=PDEN*1.0E9*VOL(6)/EPB
        CLOSE(8)
        W=FLOWO
        ICNT2=0
        HOUT=QBED/W+HIN
        HO=HOUT
201    PO=PIN(10)
        CALL NBSPH2(HO,PO,TIN(10),RHOIN(10),VIS,CP,PR,SND,CND,SS,G,X,1)
        TIN(7)=TIN(10)
        TIN(8)=TIN(7)
        TIN(9)=TIN(8)
        DO 45 J=1,9
            PII=PIN(J)
            TI=TIN(J)
            PB=PBAR(J)
            TB=TBAR(J)
            CALL NBSPH2(HI,PII,TI,RHOIN(J),VIS,CP,PR,S,CND,SS,G,X,0)
            CALL NBSPH2(HI,PB,TB,RHOBAR(J),VISC(J),CP,PR,S,CND,SS,G,X,0)
            REYN(J)=W*DH(J)/(VISC(J)*ABAR(J))
45    CONTINUE
C
C    FLOW RESISTANCES FOR EACH CONTROL VOLUME
C
        RESTOT=0.0
        DO 50 J=1,9
            CALL RESIST(J,FLEN(J),VISC(J),W,RES(J))
            RESTOT=RESTOT+RES(J)
50    CONTINUE
C
C    CONVERGE ONTO EXIT PRESSURE & FIND PRESSURES
C
        DO 60 J=1,9
            DROP(J)=RES(J)*(W**2)
            PIN(J+1)=PIN(J)-DROP(J)
            PBAR(J)=0.5*(PIN(J)+PIN(J+1))
            TBAR(J)=0.5*(TIN(J)+TIN(J+1))
60    CONTINUE
        TF1=TBAR(6)
        PBARI=.5*(PIN(1)+PIN(6))
        PBARIII=.5*(PIN(7)+PIN(10))

```

```

      POWOUT=W*(HOUT-HIN)/1.0E9
      VOUT=W/(RHOIN(10)*AOUT(9))
      SOUND=SND
      MACH=VOUT/SOUND
      IF(MACH.GT.1.0) GOTO 946
      ICNT2=ICNT2+1
      IF(ICNT2.GT.100) GOTO 941
      PERROR=1-PIN(10)/POUT
      POUT=PIN(10)
      IF(ABS(PERROR).GT.1.0E-5) GOTO 201
C
C  CALCULATE THE FUEL CHARACTERISTICS
C
      OUTERA=3*R3**2
      FMA=RHO1/OUTERA*RF**3
      R1MA=RHO1/OUTERA*(R1**3-RF**3)
      R2MA=RHO2/OUTERA*(R2**3-R1**3)
      R3MA=RHO3/OUTERA*(R3**3-R2**3)
      TOTMA=FMA+R1MA+R2MA+R3MA
      RHOBARF=RHO1*(RF**3)+RHO1*(R1**3-RF**3)+RHO2*
1      (R2**3-R1**3)+RHO3*(R3**3-R2**3)
      RHOBARF=RHOBARF/R3**3
      BB=FMA*CPF+R1MA*CP1+R2MA*CP2+R3MA*CP3
      CPBAR=BB/TOTMA
      UF=2*KF/(3*R3)
      UR1=RF*R1*K1/(R3*R3*(R1-RF))
      UR2=R1*R2*K2/(R3*R3*(R2-R1))
      UR3=R2*R3*K3/(R3*(R3-R2))
      TOTU=1/(1/UF+1/UR1+1/UR2+1/UR3)
      FR3=TOTU/UR3
      FR2=TOTU/UR2+FR3
      FR1=TOTU/UR1+FR2
      FBAR=(FMA*CPF*(FR1+1)+R1MA*CP1*(FR1+FR2)+R2MA*CP2*
1      (FR2+FR3)+R3MA*CP3*FR3)/(2*TOTMA*CPBAR)
      AV=6*(1-EPB)/DPB
      VCV=VOL(6)/EPB
C      CALL GETTIM(IHR,IMIN,ISEC,IHUN)
C
C  SET UP THE ENTHALPIES AND PRESSURES
C
      HIN1=HIN
      HINPB=HIN
      HINPB1=HIN
      HINIII=HOUT
      HINIIII=HINIII
      HOUT1=HOUT
      DO 75 J=1,9
        PIN1(J)=PIN(J)
        PBAR1(J)=PBAR(J)
75    CONTINUE
      PIN1(10)=PIN(10)
      PBAR11=PBARI
      PBARIIII=PBARIII
      RESTOT1=RESTOT
C
C  INITIALIZE THE HEAT TRANSFER INFORMATION
C
      PB=PBAR(6)
      TB=TBAR(6)
      CALL NBSPH2(HH,PB,TB,RHO,VISC(6),CPM,PRAND,S,KCOND,SS,G,X,0)
      RN=W*DPB/ABAR(6)*EPB/VISC(6)

```

```

EPFS=1-EPB
NU=.70767*EPFS/EPB*(PRAND**.333)*(0.622926*(RN/EPFS)**2.32
1      +6.44603E-4*(RN/EPFS)**3)**0.25
HTTRANS=NU*KCOND/DPB
UBAR=TOTU*HTTRANS/(FBAR*HTTRANS+TOTU)
QS=PDEN*1.0E9/AV
TF1=QS/UBAR+TBAR(6)
QINT=QS*AV*VCV
PHI=(TIN(7)-TIN(6))/TIN(6)
RNIN=W*DPB/AIN(6)*EPB/VISC(5)

C
C INITIALIZE THE REACTIVITY INFORMATION
C
      CTOT=0.0
      CTOTL=0.0
      CTOTLL=0.0
      BETAE=0.0
      IF(PDEN.EQ.0.0) PDEN=PDEN+1E-16
      POW1=PDEN
      POW2=PDEN
      DO 80 KK=1,6
        C(KK)=BETA(KK)/NLIFE/LAMBDA(KK)*QS*AV/1.0E9
        C1(KK)=C(KK)
        CTOT=CTOT+C(KK)
        CTOTL=CTOTL+LAMBDA(KK)*C(KK)
        CTOTLL=CTOTLL+C(KK)*LAMBDA(KK)**2
        BETAE=BETAE+BETA(KK)
80    CONTINUE
      REACT=0.0
      REACTT=ALPHAT*(TBAR(6))
      REACTD=ALPHAD*(TF1)
      REACTP=ALPHAP*(PBAR1(6))
      REACF=REACTT+REACTD+REACTP
      REACF1=REACF
      REACC=-1*REACF
      REACC1=REACC
C      !CNTRL DRUM WORTH $ FOR 90 DEGREES
      SPAN=-1.*WORTH*BETAE
C      IF(ABS(REACC1).GT.ABS(SPAN)) GOTO 949
      THETA=ACOS(REACC/SPAN)
      CONV=180./PI
      RDOTMX=.8
      TAUINV=0.0
      TIME=0.0

C
C WRITE OUT THE INITIAL STARTING POINT DATA
C
      WRITE(10,*) 'TIME,TIN(1),TIN(10),TBAR(6),TF1'
      WRITE(11,*) 'TIME,WDOT,TAUINV,RNIN,PHI'
      WRITE(12,*) 'TIME,REACT1,REACF1,REACC1,BETAE'
      WRITE(13,*) 'TIME,W,VOUT,SOUND,MACH'
      WRITE(16,*) 'TIME,PIN(1),PIN(10),PIN(6),PBAR(6),'
      WRITE(17,*) 'TIME,PDEN,QINTW,PDENO,CTOT'
      WRITE(18,*) 'TIME,REACC1,RCDOT,THETA*CONV,THETADOT'
      WRITE(10,780) TIME,TIN(1),TIN(10),TBAR(6),TF1
      WRITE(11,780) TIME,WDOT,TAUINV,RNIN,PHI
      WRITE(12,780) TIME,REACT1,REACF1,REACC1,BETAE
      WRITE(13,780) TIME,W,VOUT,SOUND,MACH
      WRITE(14,778) TIME,(PIN(J)/1000., J=1,10)
      WRITE(15,779) TIME,(RES(J), J=1,9)
      WRITE(16,780) TIME,PIN(1),PIN(10),PIN(6),PBAR(6)

```



```

        WRITE(17,780) TIME,PDEN,PDENO,PDENO,CTOT
        WRITE(18,780) TIME,REACC1,RCDOT,THETA*CONV,THETADOT
778    FORMAT(1X,F6.3,2X,5(F7.2,2X),/,9X,5(F7.2,2X))
779    FORMAT(1X,F6.3,1X,5(E12.6,1X),/,8X,4(E12.6,1X))
780    FORMAT(1X,F8.4,4(' ',E12.6))
C
C    NOW SET UP THE TRANSIENT TIME CONSTANTS AND DURATIONS
C
        TIMEMAX=DELAYT+DURTRAN1+DURTRAN2+DURTRAN3+AFTERT
        TIMEPT1=DELAYT+DURTRAN1
        TIMEPT2=TIMEPT1+DURTRAN2
        TIMEPT3=TIMEPT2+DURTRAN3
        TIME=DELTAT
        PRNCNT=1
        OMEGA1=LOG(PDEN1/PDENO)/DURTRAN1
        OMEGA2=LOG(PDEN2/PDEN1)/DURTRAN2
        OMEGA3=LOG(PDEN3/PDEN2)/DURTRAN3
C
C    BEGIN TRANSIENT CALCULATIONS
C
C    PERFORM POINT KINETICS MIT-SNL APPROACH FOR POWER RAMP
C
100    IF (TIME.GT.TIMEMAX) GOTO 948
        IF ((TIME.GT.DELAYT).AND.(TIME.LE.TIMEPT1)) THEN
            OMEGA=OMEGA1
            TDT=(TIME-DELAYT)/DURTRAN1
            PIN1(1)=PINO+(PINP1-PINO)*TDT
            W=FLOWO+(FLOW1-FLOWO)*TDT
            TIN(1)=TINO+(TINP1-TINO)*TDT
        ELSEIF ((TIME.GT.TIMEPT1).AND.(TIME.LE.TIMEPT2)) THEN
            OMEGA=OMEGA2
            TDT=(TIME-TIMEPT1)/DURTRAN2
            PIN1(1)=PINP1+(PINP2-PINP1)*TDT
            W=FLOW1+(FLOW2-FLOW1)*TDT
            TIN(1)=TINP1+(TINP2-TINP1)*TDT
        ELSEIF ((TIME.GT.TIMEPT2).AND.(TIME.LE.TIMEPT3)) THEN
            OMEGA=OMEGA3
            TDT=(TIME-TIMEPT2)/DURTRAN3
            PIN1(1)=PINP2+(PINP3-PINP2)*TDT
            W=FLOW2+(FLOW3-FLOW2)*TDT
            TIN(1)=TINP2+(TINP3-TINP2)*TDT
        ELSEIF (TIME.GT.TIMEPT3) THEN
            OMEGA=LOG(PDEN3/POW1)/(50.*DELTAT)
            PIN1(1)=PINP3
            W=FLOW3
            TIN(1)=TINP3
        ENDIF
C
C    FIND THE NEW INLET ENTHALPY
C
        P=PIN(1)
        TT=TIN(1)
        CALL NBSPH2(HIN1,P,TT,RHO,VIS,CP,PR,S,CND,SS,G,X,0)
C
C    NOW DO THE POINT KINETICS
C
        LAMBDAB=CTOTLL/CTOTL
        SUMBL=0.0
        DO 105 KK=1,6
            SUMBL=SUMBL+BETA(KK)*(LAMBDA(KK)-LAMBDAB)
105    CONTINUE

```

```

WDOT=(OMEGA-TAUINV)/(5.0*DELTAT)
RFDOT=(REACF1-REACF)/DELTAT
RCDOT=(BETAE-REACT)*OMEGA-LAMBDABE*REACT-SUMBL-RFDOT+
1 NLIFE*WDOT+OMEGA*NLIFE*(OMEGA+LAMBDABE)
REACC1=REACC+RCDOT*DELTAT
REACC=AMIN1(-.999*SPAN,REACC1)
REACC1=AMAX1(.999*SPAN,REACC)
THETAD=ACOS(REACC1/SPAN)
THETADOT=(THETAD-THETA+0.000001)/DELTAT
TSIGN=THETADOT/ABS(THETADOT)
IF(ABS(THETADOT*CONV).GT.180.) THETADOT=180./CONV*TSIGN
THETA1=THETA+THETADOT*DELTAT
THETA=THETA1
REACC1=SPAN*COS(THETA)
RCDOT=-1*SPAN*SIN(THETA)*THETADOT
RDOT=RCDOT+RFDOT
REACT1=REACT+RDOT*DELTAT
C FOLLOWING WAS AN ATTEMPT AT REACTIVITY CONTRAINT, BUT NOT COMPLETED
C RTEMP=RDOTMX/LAMBDABE
C REACT1=REACT+DELTAT*(OMEGA*(BETAE+NLIFE*(OMEGA+LAMBDABE))-SUMBL)-
C 1 (REACFEED1-REACFEED)+NLIFE*WDOT*DELTAT
C REACT1=REACT1/(1+DELTAT*(OMEGA+LAMBDABE))
C IF(REACT1.LE.1.0E-4) REACT1=0.0
C RCNST1=RDOTMX/LAMBDABE
C RCNST2=RDOTMX*(1/LAMBDABE+1/TAUINV*LOG(PDEN3/PDEN))
C IF(REACT1.GT.RCNST1) REACT1=RCNST1
C IF(REACT1.GT.RCNST2) REACT1=RCNST2
C POW1=(PDEN+DELTAT*CTOTL)/(1+DELTAT*(BETAE-REACT1)/NLIFE)
C CTOT=0.0
C CTOTL=0.0
C CTOTLL=0.0
C DO 110 JJ=1,6
C LINEAR POWER EXTRAPOLATION
C VAR1=EXP(-1*LAMBDA(JJ)*DELTAT)
C VAR2=(1-VAR1)/(DELTAT*LAMBDA(JJ)**2)
C VAR3=BETA(JJ)*(1/LAMBDA(JJ)-VAR2)/NLIFE
C VAR4=BETA(JJ)*(VAR2-VAR1/LAMBDA(JJ))/NLIFE
C C1(JJ)=VAR1*C(JJ)+VAR3*POW1+VAR4*PDEN
C SIMPLE IMPLICIT TIME DIFFERENCE SCHEME
C C1(JJ)=(C(JJ)+DELTAT*BETA(JJ)*PDEN/NLIFE)/(1+LAMBDA(JJ)*DELTAT)
C CTOT=CTOT+C1(JJ)
C CTOTL=CTOTL+LAMBDA(JJ)*C1(JJ)
C CTOTLL=CTOTLL+C1(JJ)*LAMBDA(JJ)**2
110 CONTINUE
TB=TBAR(6)
PB=PBAR(6)
CALL NBSPH2(HH,PB,TB,RHO,VISC(6),CPM,PRAND,S,KCOND,SS,G,X,0)
RN=W*DPB/ABAR(6)*EPB/VISC(6)
NU=.70767*EPFS/EPB*(PRAND**.333)*(0.622926*(RN/EPFS)**2.32
1 +6.44603E-4*(RN/EPFS)**3)**0.25
HTTRANS=NU*KCOND/DPB
UBAR=TOTU*HTTRANS/(FBAR*HTTRANS+TOTU)
QS=POW1*1.0E9/AV
C
C CONTROL VOLUME CALCULATIONS
C
C INLET PLENUM AND COLD FRIT CONTROL VOLUME
C
M1=0.0
DO 135 II=1,5
M1=M1+RHOBAR(II)*VOL(II)

```

```

135  CONTINUE
      HINPB1=(HINPB+(DELTAT/M1)*((VOLI*(PBARI1-PBARI)/DELTAT)
1      +W*HIN1+0.0*QINT))/(1+DELTAT*W/M1)
C
C  PARTICLE FUEL BED CONTROL VOLUME
C
      TF2=(TF1+DELTAT*(QS+UBAR*TBAR(6))/BB)
      TF2=TF2/(1+DELTAT*UBAR/BB)
      QINT=UBAR*VCV*AV*(TF2-TBAR(6))
      TF1=TF2
      M2=(RHOBAR(6)*VOL(6))
      HINIIII1=(HINIIII+(DELTAT/M2)*((VCV*(PBAR1(6)-PBAR(6))/DELTAT)
1      +W*HINPB1+1.0*QINT))/(1+DELTAT*W/M2)
C
C  HOT FRIT AND OUTLET CHANNEL CONTROL VOLUME
C
      M3=RHOBAR(7)*VOL(7)+RHOBAR(8)*VOL(8)+RHOBAR(9)*VOL(9)
      HOUT1=(HOUT+(DELTAT/M3)*((VOLIII*(PBARIIII1-PBARIII)/DELTAT)
1      +W*HINIIII1+0.0*QINT))/(1+DELTAT*W/M3)
C
C  UPDATE THERMODYNAMIC PROPERTIES
C
      PBARI=PBARI1
      PBARIIII=PBARIIII1
      DO 140 JJ=1,9
          PIN(JJ)=PIN1(JJ)
          PBAR(JJ)=PBAR1(JJ)
140  CONTINUE
C
C  FIND THE TEMPS AND PROPERTIES FROM THE PRESSURES AND ENTHALPIES
C
      PIN(10)=PIN1(10)
      HO=HINPB1
      PP=PIN(6)
c  write(*,*) 'ho,pp,tin(6)',ho,pp,tin(6)
      CALL NBSPH2(HO,PP,TIN(6),RHO,VIS,CP,PR,S,CND,SS,G,X,1)
      RNIN=W*DPB/AIN(6)*EPB/VIS
      HO=HINIIII1
      PP=PIN(7)
c  write(*,*) 'ho,pp,tin(7)',ho,pp,tin(7)
      CALL NBSPH2(HO,PP,TIN(7),RHO,VIS,CP,PR,S,CND,SS,G,X,1)
      PHI=(TIN(7)-TIN(6))/TIN(6)
      HO=HOUT1
      PP=PIN(10)
c  write(*,*) 'ho,pp,tin(10)',ho,pp,tin(10)
      CALL NBSPH2(HO,PP,TIN(10),RHOIN(10),VIS,CP,PR,SND,CND,SS,G,X,1)
      TIN(9)=TIN(10)
      TIN(8)=TIN(9)
      DO 145 J=1,9
          PII=PIN(J)
          TI=TIN(J)
          PB=PBAR(J)
          TBAR(J)=0.5*(TIN(J)+TIN(J+1))
          TB=TBAR(J)
          CALL NBSPH2(HI,PII,TI,RHOIN(J),VIS,CP,PR,S,CND,SS,G,X,0)
          CALL NBSPH2(HI,PB,TB,RHOBAR(J),VISC(6),CP,PR,S,CND,SS,G,X,0)
          REYN(J)=W*DH(J)/(VISC(J)*ABAR(J))
145  CONTINUE
      HIN=HIN1
      HINPB=HINPB1
      HINIIII=HINIIII1

```

```

      HOUT=HOUT1
C
C   FLOW RESISTANCES FOR EACH CONTROL VOLUME
C
      RESTOT1=0.0
      DO 150 J=1,9
        CALL RESIST(J,FLEN(J),VISC(J),W,RES(J))
        RESTOT1=RESTOT1+RES(J)
150    CONTINUE
C
C   FIND THE PRESSURE DROPS AND OUTLET PRESSURE
C
      RESTOT=RESTOT1
      DO 155 J=1,9
        DROP(J)=RES(J)*(W**2)
        PIN1(J+1)=PIN1(J)-DROP(J)
        PBAR1(J)=0.5*(PIN1(J)+PIN1(J+1))
155    CONTINUE
      PBARI1=.5*(PIN1(1)+PIN1(6))
      PBARIII1=.5*(PIN1(7)+PIN1(10))
      POWOUT=W*(HOUT1-HIN1)/1.0E9
      VOUT=W/(RHOIN(10)*AOUT(9))
      SOUND=SND
      MACH=VOUT/SOUND
      IF(MACH.GT.1.0) GOTO 946
C
C   UPDATE THE REACTIVITY INFORMATION
C
      REACF=REACF1
      REACT=REACT1
      REACC=REACC1
      REACTT=ALPHAT*(TBAR(6))
      REACTD=ALPHAD*(TF1)
      REACTP=ALPHA*(PBAR1(6))
      REACF1=REACTT+REACTD+REACTP
      DO 160 KK=1,6
        C(KK)=C1(KK)
160    CONTINUE
      TAUINV=LOG(POW1/POW2)/(2.0*DELTAT)
      POW2=PDEN
      PDEN=POW1
C
C   DETERMINE IF NEED TO PRINT OUT RESULTS
C
      IF(PRNCNT.NE.ISAVE) GOTO 301
      QINTW=QINT/1.0E9/VOL(6)*EPB
      WRITE(10,780) TIME,TIN(1),TIN(10),TBAR(6),TF1
      WRITE(11,780) TIME,WDOT,TAUINV,RNIN,PHI
      WRITE(12,780) TIME,REACT1,REACF1,REACC1,BETA
      WRITE(13,780) TIME,W,VOUT,SOUND,MACH
      WRITE(14,778) TIME,(PIN(J)/1000., J=1,10)
      WRITE(15,779) TIME,(RES(J), J=1,9)
      WRITE(16,780) TIME,PIN(1),PIN(10),PIN(6),PBAR(6)
      WRITE(17,780) TIME,PDEN,QINTW,PDENO,CTOT
      WRITE(18,780) TIME,REACC1,RCDOT,THETA*CONV,THETADOT*CONV
      PRNCNT=0
      WRITE(*,*) 'TIME IS NOW AT ',TIME,' sec.  END TIME= ',TIMEMAX
301    TIME=TIME+DELTAT
      IF(TIME.GT.DELAYT) TRANSTIME=TRANSTIME+DELTAT
      PRNCNT=PRNCNT+1
      GOTO 100

```

```

C
C   ABORT AND FINISH STATEMENTS
C
941  WRITE(*,*) ' FAIL TO CONVERGE ON PIN; ICNT2=100'
      GOTO 948
942  WRITE(*,*) ' FAIL TO CONVERGE ON COMMON DP; ICNT1=100'
      GOTO 948
944  WRITE(*,*) ' FAIL TO CONVERGE ON TINPB; ICNT4=600'
      GOTO 948
945  WRITE(*,*) ' FAIL TO CONVERGE ON TINIII; ICNT5=800'
      GOTO 948
946  WRITE(*,*) ' ERR - MACH NUMBER AT OUTLET IS GREATER THAN 1.0'
      GOTO 948
949  WRITE(*,*) ' ERR - CONTROL REACTIVITY REQUIRED IS > DRUM WORTH'
      WRITE(*,*) ' REACC = $',REACC1/BETAE
948  CONTINUE
C    CALL GETTIM(JHR,JMIN,JSEC,JHUN)
C    WRITE(*,777) IHR,IMIN,ISEC,IHUN
C    WRITE(*,777) JHR,JMIN,JSEC,JHUN
C777  FORMAT(1X,I2,':',I2,':',I2,':',I2,':',I2)
      DO 999 K=10,18
      CLOSE(K)
999  CONTINUE
      STOP
      END

C
C *****
C
C    RESISTANCE SUBROUTINE
C
C *****
C
      SUBROUTINE RESIST(J,FL,VIS,WW,REST)
      IMPLICIT REAL (A-H,O-Z)
      REAL MANIN,MANOUT
      DIMENSION AIN(9),AOUT(9),ABAR(9),DH(9)
      DIMENSION REYN(9),RHOIN(10),RHOBAR(9),TYPMAN(9)
      COMMON /ELEMENT/ RORF,ORFLEN,RIC,WSL,TSL,RIP,PBRLN,RCF,RPB,RHF,
1      ROP,EXTLEN,ECF,EPB,EHF,DCF,DPB,DHF,MANIN,MANOUT
      COMMON /RESTNC/ AIN,AOUT,ABAR,DH,TYPMAN,
1      REYN,RHOIN,RHOBAR

C
C    RESISTANCE DUE TO FRICTION
C
      IF((J.LT.5).OR.(J.GT.6)) THEN
C
C    MODIFIED TURBULENT FRICTION FACTOR FROM CASEY & TUDDENHAM THESES
C
      RESF=.138*(REYN(J)**(-.151))*(FL/DH(J))
      RESF=RESF/(2*RHOBAR(J)*ABAR(J)**2)
      ELSE
C
C    ERGUN RELATION FOR PARTICLE BEDS
C
      ETA=EPB
      DPART=DPB
      IF(J.EQ.5) THEN
        ETA=ECF
        DPART=DCF
      ENDIF
      RESIST1=(150.*VIS*(1-ETA)**2)

```

```

RESIST1=RESIST1/(RHOBAR(J)*ABAR(J)*WW*(DPART*ETA)**2)
RESIST2=(1.75*(1-ETA))/(RHOBAR(J)*ETA*DPART*ABAR(J)**2)
RESF=FL*(RESIST1+RESIST2)
ENDIF

C
C RESISTANCE DUE TO AREA ACCELERATION
C
RESA=(AIN(J)+AOUT(J))/(2*AIN(J)*AOUT(J))
RESA=RESA*(1/(RHOIN(J+1)*AOUT(J))-1/(RHOIN(J)*AIN(J)))

C
C RESISTANCE DUE TO FORM
C
ASMALL=AMIN1(AIN(J),AOUT(J))
ALARGE=AMAX1(AIN(J),AOUT(J))
BETA=ASMALL/ALARGE
IF(AIN(J).EQ.ASMALL) THEN
    COEF=1.0
ELSE
    COEF=0.5
ENDIF
RESK=COEF*((1-BETA)**2)/(2*RHOBAR(J)*ASMALL**2)

C
C RESISTANCE DUE TO MANIFOLD EFFECTS
C
IF(TYPMAN(J).EQ.0.0) THEN
    RESM=0.0
ELSE
    RESM=TYPMAN(J)/RHOBAR(J)
    RESM=RESM*(1/(AIN(J)**2)+1/(AOUT(J)**2))
ENDIF

C
C NOW TOTAL RESISTANCES FOR THE ZONE
C
REST=RESF+RESA+RESK+RESM
RETURN
END

C
C *****
C
C SUBROUTINE INTERACT - USED TO GET THE BASELINE DATA AND VERIFY
C DATA FOR DIMENSIONS, CHARACTERISTICS, AND INITIAL CONDITIONS
C *****
C
SUBROUTINE INTERACT(T)
IMPLICIT REAL (A-H,O-Z)
REAL KF,K1,K2,K3
REAL MANIN,MANOUT
DIMENSION T(60)
COMMON /ELEMENT/ RORF,ORFLEN,RIC,WSL,TSL,RIP,PBRLN,RCF,RPB,RHF,
1 ROP,EXTLEN,ECF,EPB,EHF,DCF,DPB,DHF,MANIN,MANOUT
COMMON /PARTICLE/ RF,R1,R2,R3,RHOF,RHO1,RHO2,RHO3,
1 CPF,CP1,CP2,CP3,KF,K1,K2,K3
COMMON /TRANS/ TINO,TINP1,TINP2,TINP3,PINO,PINP1,PINP2,PINP3,
1 FLOW,FLOW1,FLOW2,FLOW3,PDENO,PDEN1,PDEN2,PDEN3,DURTRAN1,
1 DURTRAN2,DURTRAN3,DELAYT,AFTERT,DELTAT,ISAVE,WO

C
C WRITE FUEL ELEMENT DATA TO SCREEN AND ASK FOR UPDATE
C

```

```

RORF=T(1)
ORFLEN=T(2)
RIC=T(3)
WSL=T(4)
TSL=T(5)
RIP=T(6)
RCF=T(7)
RPB=T(8)
RHF=T(9)
ROP=T(10)
PBRLEN=T(11)
EXTLEN=T(12)
ECF=T(13)
EPB=T(14)
EHF=T(15)
DCF=T(16)
DPB=T(17)
DHF=T(18)
MANIN=T(19)
MANOUT=T(20)
100 WRITE(*,600) RORF,ORFLEN,RIC,WSL,TSL,RIP,RCF,RPB,RHF,ROP
WRITE(*,660) PBRLEN,EXTLEN,ECF,EPB,EHF,DCF,DPB,DHF,MANIN,MANOUT
600 FORMAT(/,/ ,
1      ' STANDARD FLOW DIMENSION DATA' ,/ ,
1      ' 1. ORIFICE RADIUS (m) ',F8.5,/ ,
1      ' 2. ORIFICE LENGTH (m) ',F8.5,/ ,
1      ' 3. INLET CHANNEL RADIUS (m) ',F8.5,/ ,
1      ' 4. INLET SLOT WIDTH (m) ',F8.5,/ ,
1      ' 5. INLET SLOT LENGTH (m) ',F8.5,/ ,
1      ' 6. INLET REGION RADIUS (m) ',F8.5,/ ,
1      ' 7. RESISTOJET CHAMBER RADIUS (m) ',F8.5,/ ,
1      ' 8. FUEL BED OUTER RADIUS (m) ',F8.5,/ ,
1      ' 9. HEATER OUTER RADIUS (m) ',F8.5,/ ,
1      ' 10. HEATER CENTERLINE (m) ',F8.5)
660 FORMAT(' 11. CHAMBER LENGTH (m) ',F8.5,/ ,
1      ' 12. OUTLET EXTENSION LENGTH (m) ',F8.5,/ ,
1      ' 13. COLD FRIT POROSITY ',F8.5,/ ,
1      ' 14. FUEL BED POROSITY ',F8.5,/ ,
1      ' 15. HOT FRIT POROSITY ',F8.5,/ ,
1      ' 16. COLD FRIT PARTICLE DIAM. (m) ',F9.7,/ ,
1      ' 17. FUEL PARTICLE DIAM (m) ',F8.5,/ ,
1      ' 18. HOT FRIT FLOW DIAM. (m) ',F8.5,/ ,
1      ' 19. INLET MANIFOLD FACTOR ',F8.5,/ ,
1      ' 20. OUTLET MANIFOLD FACTOR ',F8.5,/ ,
1      ' ENTER [NUMBER] [VALUE] TO CHANGE (eg 2 .002)' ,/ ,
1      ' ENTER 0 0. TO MOVE ON' ,/)
101 READ (*,*) NUM,VALUE
IF(NUM.EQ.0) GO TO 199
IF(NUM.EQ.1) RORF=VALUE
IF(NUM.EQ.2) ORFLEN=VALUE
IF(NUM.EQ.3) RIC=VALUE
IF(NUM.EQ.4) WSL=VALUE
IF(NUM.EQ.5) TSL=VALUE
IF(NUM.EQ.6) RIP=VALUE
IF(NUM.EQ.7) RCF=VALUE
IF(NUM.EQ.8) RPB=VALUE
IF(NUM.EQ.9) RHF=VALUE
IF(NUM.EQ.10) ROP=VALUE
IF(NUM.EQ.11) PBRLEN=VALUE
IF(NUM.EQ.12) EXTLEN=VALUE
IF(NUM.EQ.13) ECF=VALUE

```

```

IF(NUM.EQ.14) EPB=VALUE
IF(NUM.EQ.15) EHF=VALUE
IF(NUM.EQ.16) DCF=VALUE
IF(NUM.EQ.17) DPB=VALUE
IF(NUM.EQ.18) DHF=VALUE
IF(NUM.EQ.19) MANIN=VALUE
IF(NUM.EQ.20) MANOUT=VALUE
IF((NUM.GE.1).AND.(NUM.LE.20)) GO TO 100
WRITE(*,*) 'TRY AGAIN WITH A VALID SELECTION'
GOTO 101
199 CONTINUE
C
C NOW DO THE SAME FOR THE FUEL PARTICLE CHARACTERISTICS
C
RF=T(21)
R1=T(22)
R2=T(23)
R3=T(24)
RHOF=T(25)
RHO1=T(26)
RHO2=T(27)
RHO3=T(28)
CPF=T(29)
CP1=T(30)
CP2=T(31)
CP3=T(32)
KF=T(33)
K1=T(34)
K2=T(35)
K3=T(36)
200 WRITE(*,601) RF,R1,R2,R3,RHOF,RHO1,RHO2,RHO3,
1 CPF,CP1
WRITE(*,661) CP2,CP3,KF,K1,K2,K3
601 FORMAT(/,/ /,/ /,/ /,/ /,/ /,/ /,
1 ' FUEL PARTICLE BASELINE DATA',/ ,
1 ' 1. FUEL KERNEL RADIUS (m) ',F8.5,/ ,
1 ' 2. LAYER 1 RADIUS (m) ',F8.5,/ ,
1 ' 3. LAYER 2 RADIUS (m) ',F8.5,/ ,
1 ' 4. LAYER 3 RADIUS (m) ',F8.5,/ ,
1 ' 5. FUEL DENSITY (Kg/m3) ',F8.2,/ ,
1 ' 6. LAYER 1 DENSITY (Kg/m3) ',F8.2,/ ,
1 ' 7. LAYER 2 DENSITY (Kg/m3) ',F8.2,/ ,
1 ' 8. LAYER 3 DENSITY (Kg/m3) ',F8.2,/ ,
1 ' 9. FUEL Cp (J/Kg) ',F8.3,/ ,
1 ' 10. LAYER 1 Cp (J/Kg) ',F8.3)
661 FORMAT(' 11. LAYER 2 Cp (J/Kg) ',F8.3,/ ,
1 ' 12. LAYER 3 Cp (J/Kg) ',F8.3,/ ,
1 ' 13. FUEL k (W/m2/K) ',F8.3,/ ,
1 ' 14. LAYER 1 k (W/m2/K) ',F8.3,/ ,
1 ' 15. LAYER 2 k (W/m2/K) ',F8.3,/ ,
1 ' 16. LAYER 3 k (W/m2/K) ',F8.3,/ / / ,
1 ' ENTER [NUMBER] [VALUE] TO CHANGE (eg 2 .002)',/ ,
1 ' ENTER 0 0. TO MOVE ON',/ )
201 READ(*,*) NUM,VALUE
IF(NUM.EQ.0) GO TO 299
IF(NUM.EQ.1) RF=VALUE
IF(NUM.EQ.2) R1=VALUE
IF(NUM.EQ.3) R2=VALUE
IF(NUM.EQ.4) R3=VALUE
IF(NUM.EQ.5) RHOF=VALUE
IF(NUM.EQ.6) RHO1=VALUE

```


[illegible]

```

IF (NUM.EQ.3) TINP2=VALUE
IF (NUM.EQ.4) TINP3=VALUE
IF (NUM.EQ.5) PINO=VALUE
IF (NUM.EQ.6) PINP1=VALUE
IF (NUM.EQ.7) PINP2=VALUE
IF (NUM.EQ.8) PINP3=VALUE
IF (NUM.EQ.9) FLOWO=VALUE
IF (NUM.EQ.10) FLOW1=VALUE
IF (NUM.EQ.11) FLOW2=VALUE
IF (NUM.EQ.12) FLOW3=VALUE
IF (NUM.EQ.13) PDENO=VALUE
IF (NUM.EQ.14) PDEN1=VALUE
IF (NUM.EQ.15) PDEN2=VALUE
IF (NUM.EQ.16) PDEN3=VALUE
IF ((NUM.GE.1).AND.(NUM.LE.16)) GO TO 300
WRITE(*,*) 'TRY AGAIN WITH A VALID SELECTION'
GOTO 301
399 CONTINUE
WO=FLOWO

C
C CONVERT kPa TO Pa
PINO=PINO*1000.
PINP1=PINP1*1000.
PINP2=PINP2*1000.
PINP3=PINP3*1000.

C
C NOW DO FOR THE TRANSIENT DATA
C
DELAYT=T(53)
DURTRAN1=T(54)
DURTRAN2=T(55)
DURTRAN3=T(56)
AFTERT=T(57)
DELTAT=T(58)
ISAVE=T(59)
400 WRITE(*,603) DELAYT,DURTRAN1,DURTRAN2,DURTRAN3,AFTERT,
1 DELTAT,ISAVE
603 FORMAT(/,/ /,/ /,/ /,/ /,/ /,/ /,
1 ' TRANSIENT DURATION TIMING DATA',/,
1 ' 1. TIME DELAY BEFORE TRANSIENT (sec) ',F8.4,/,
1 ' 2. DURATION OF RAMP 1 (sec) ',F8.4,/,
1 ' 3. DURATION OF RAMP 2 (sec) ',F8.4,/,
1 ' 4. DURATION OF RAMP 3 (sec) ',F8.4,/,
1 ' 5. RUN TIME AFTER TRANSIENT OVER (sec) ',F8.4,/,
1 ' 6. TIME STEP (sec) ',F8.4,/,
1 ' 7. INFO SAVED EVERY X TIME STEPS (#)
',I5,/ /,/ /,/ /,/ /,
1 ' ENTER [NUMBER] [VALUE] TO CHANGE (eg 2 .5)',/,/,
1 ' ENTER 0 0. TO MOVE ON',/,)
401 READ(*,*) NUM,VALUE
IF (NUM.EQ.0) GO TO 499
IF (NUM.EQ.1) DELAYT=VALUE
IF (NUM.EQ.2) DURTRAN1=VALUE
IF (NUM.EQ.3) DURTRAN2=VALUE
IF (NUM.EQ.4) DURTRAN3=VALUE
IF (NUM.EQ.5) AFTERT=VALUE
IF (NUM.EQ.6) DELTAT=VALUE
IF (NUM.EQ.7) ISAVE=VALUE
IF ((NUM.GE.1).AND.(NUM.LE.7)) GO TO 400
WRITE(*,*) 'TRY AGAIN WITH A VALID SELECTION'
GOTO 401

```

499 RETURN
END

```

C  SUBROUTINE FOR HELIUM PROPERTIES USING THE NBSPH2 SUBROUTINE CALLS
C
      SUBROUTINE NBSPH2 (H,P,T,RHO,VIS,CP,PR,SND,CND,SS,GAM,X,ISS)
      IMPLICIT REAL (A-H,O-Z)
C
C  USE IDEAL GAS RELATIONS FROM 101000Pa, 310K
C
      RGAS=8314.34
      HEMW=44.02
      CP=1000.0
      CV=CP-RGAS/HEMW
      GAM=CP/CV
C
C  DUMMY VARIABLES AND REFERENCE STATE POINTS
C
      X=1.0
      SS=1.0
      HREF=20279.18
      PREF=101000.0
      TREF=310.0
      RREF=1.997
      VREF=1.54E-5
C
C  NOW FOR THE CALCULATIONS ISS=1, INPUT H,P
C
      IF (ISS.EQ.1) T=(H-HREF)/CP+TREF
      IF (ISS.EQ.0) H=CP*(T-TREF)+HREF
      VIS=VREF*(T/TREF)**0.7
      CND=(CP+5.*RGAS/4./HEMW)*VIS
      PR=VIS*CP/CND
      SND=SQRT(GAM*RGAS/HEMW*T)
      RHO=RREF*P/PREF*TREF/T
      RETURN
      END

```

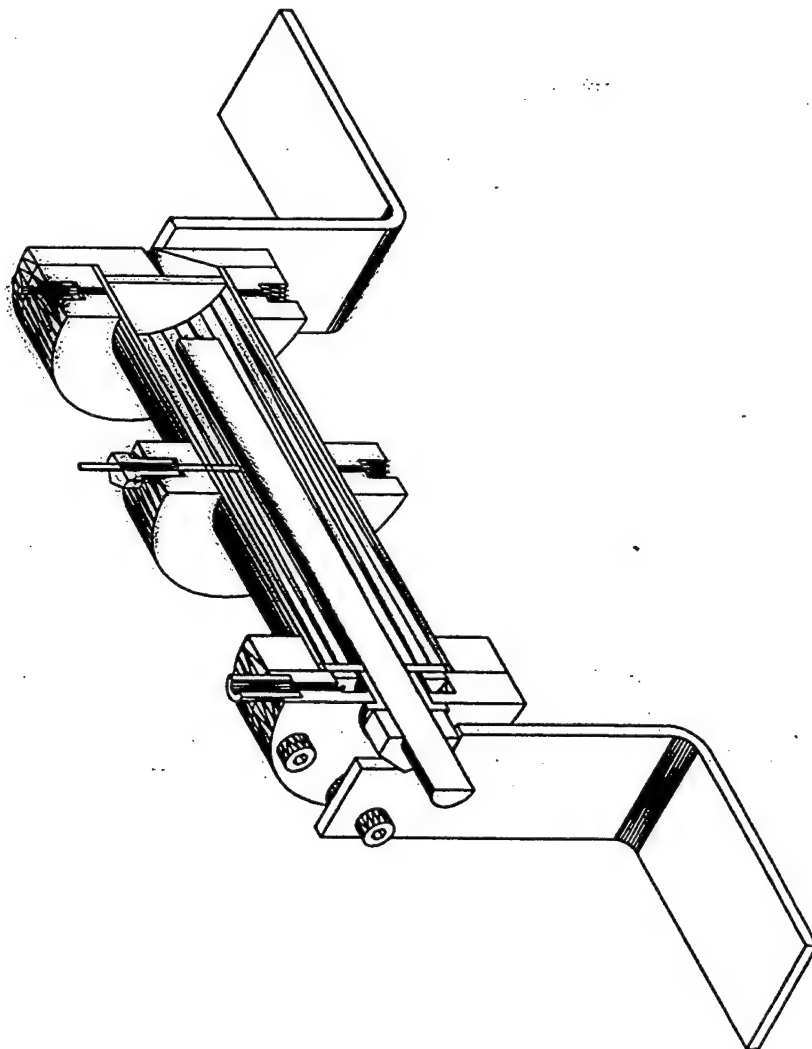
```

C SUBROUTINE FOR HELIUM PROPERTIES USING THE NBSPH2 SUBROUTINE CALLS
C Modified by tjl for water
  SUBROUTINE NBSPH2(H,P,T,RHO,VIS,CP,PR,SND,CND,SS,GAM,X,ISS)
    IMPLICIT REAL (A-H,O-Z)
C
C USE IDEAL GAS RELATIONS FROM 101000Pa, 310K
C
  RGAS=8314.34
  HEMW=4.0026
  CP=5193.
  CV=CP-RGAS/HEMW
  GAM=CP/CV
C
C DUMMY VARIABLES AND REFERENCE STATE POINTS
C
  X=1.0
  SS=1.0
  HREF=164241.33
  PREF=101000.0
  TREF=310.
  RREF=.157021849
  VREF=2.11E-5
C
C NOW FOR THE CALCULATIONS ISS=1, INPUT H,P
C
  IF(ISS.EQ.1) T=(H-HREF)/CP+TREF
  IF(ISS.EQ.0) H=CP*(T-TREF)+HREF
  VIS=VREF*(T/TREF)**0.7
  CND=(CP+5.*RGAS/4./HEMW)*VIS
  PR=VIS*CP/CND
  SND=SQRT(GAM*RGAS/HEMW*T)
  RHO=RREF*P/PREF*TREF/T
  RETURN
  END

```

APPENDIX B

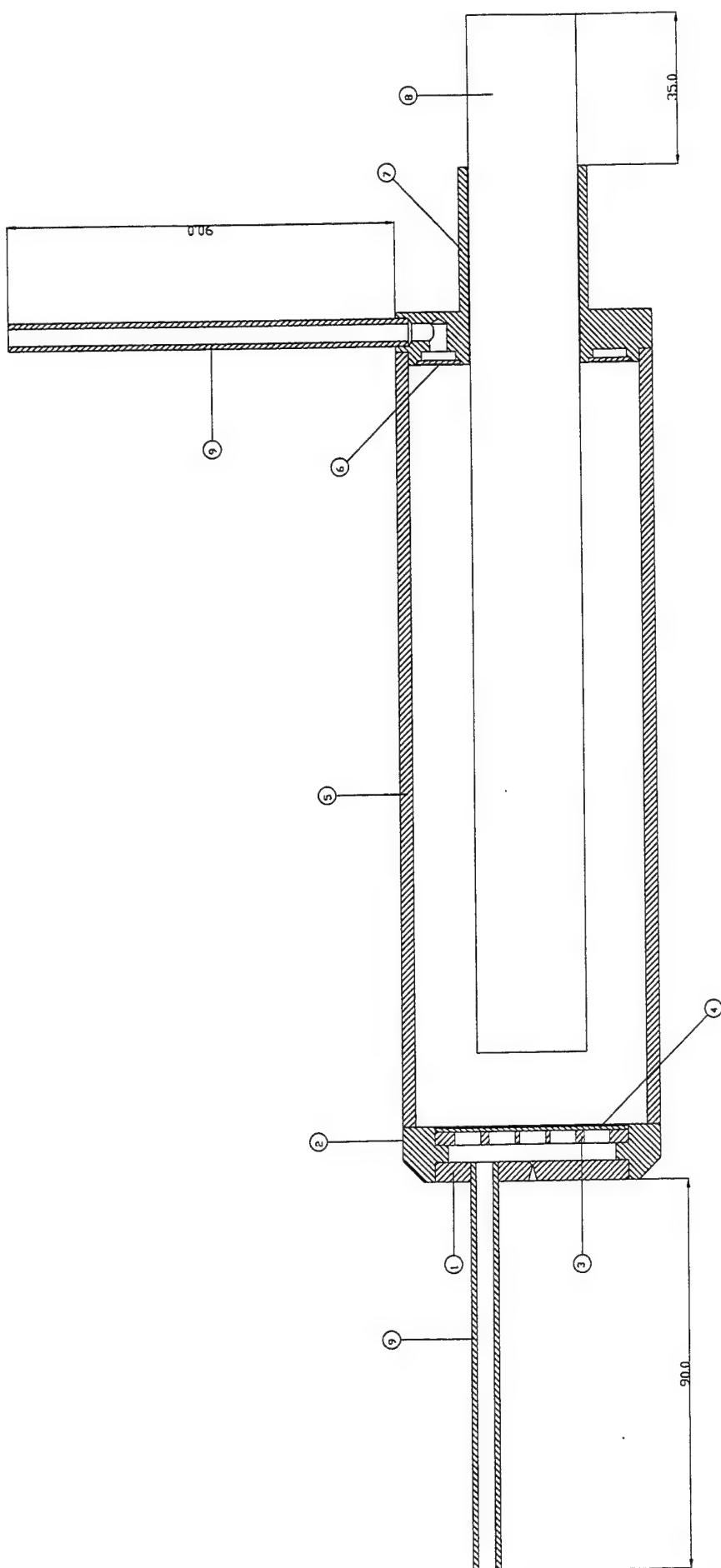
ENGINEERING DRAWINGS



All Dimensions in Millimeters
General Tolerance -- 0.2 UDS
All Radii R2 UDS
Surface Texture R7

| | | | | |
|---------------------|--|---|----------|---------|
| TITLE | |  | FILENAME | not set |
| not set | | | DRAWN BY | not set |
| Copyright SS&L 1995 | | | PROJECT | not set |
| | | | ISSUE | not set |
| | | | DATE | not set |
| | | | APPROVED | not set |

| REVISIONS | | | |
|-----------|---|-----------|----------|
| REV | DESCRIPTION | DATE | APPROVED |
| B | Heater position added | 3/Nov/97 | |
| C | Transducer pipes lengthened and dimensioned | 11/Nov/97 | |
| D | Parts 1 and 2 uplissed | 17/Nov/97 | |
| E | Part 2 uplissed to enable C.B. welding | 18/Nov/97 | |



Notes:
 1. Prior to welding thoroughly clean items 1, 2, 3 and 4 to ensure that no loose particulate can block the nozzle orifice

| Item No. | Qty. | Part or Identifying No. | Description |
|----------|------|-------------------------|-----------------------|
| 1 | 1 | RDDM008 | 02mm Nozzle Plate |
| 2 | 1 | RDDM002 | Front End Cap |
| 3 | 1 | RDDM003 | Support Plate |
| 4 | 1 | RDDM004 | Sintered Mesh Disk |
| 5 | 1 | RDDM005 | Heater Housing |
| 6 | 1 | RDDM006 | Sintered Mesh Annulus |
| 7 | 1 | RDDM007 | Cold End Cap |
| 8 | 1 | | Heater |
| 9 | 2 | | 1/4" Pipe |

UNLESS OTHERWISE SPECIFIED
 DIMENSIONS IN MILLIMETERS
 TOLERANCES ARE
 DECIMAL X +/- .02
 ANGULAR +/- .05
 .XX +/- .01

SURREY SATELLITE TECHNOLOGY LIMITED

PROJECT Rocket Development

DATE 18/Nov/97

DRAWN BY M.Tucknott

APPROVED

TITLE ResistoJet Assembly

Copyright © SSTL 1997

FILENAME RDDM800

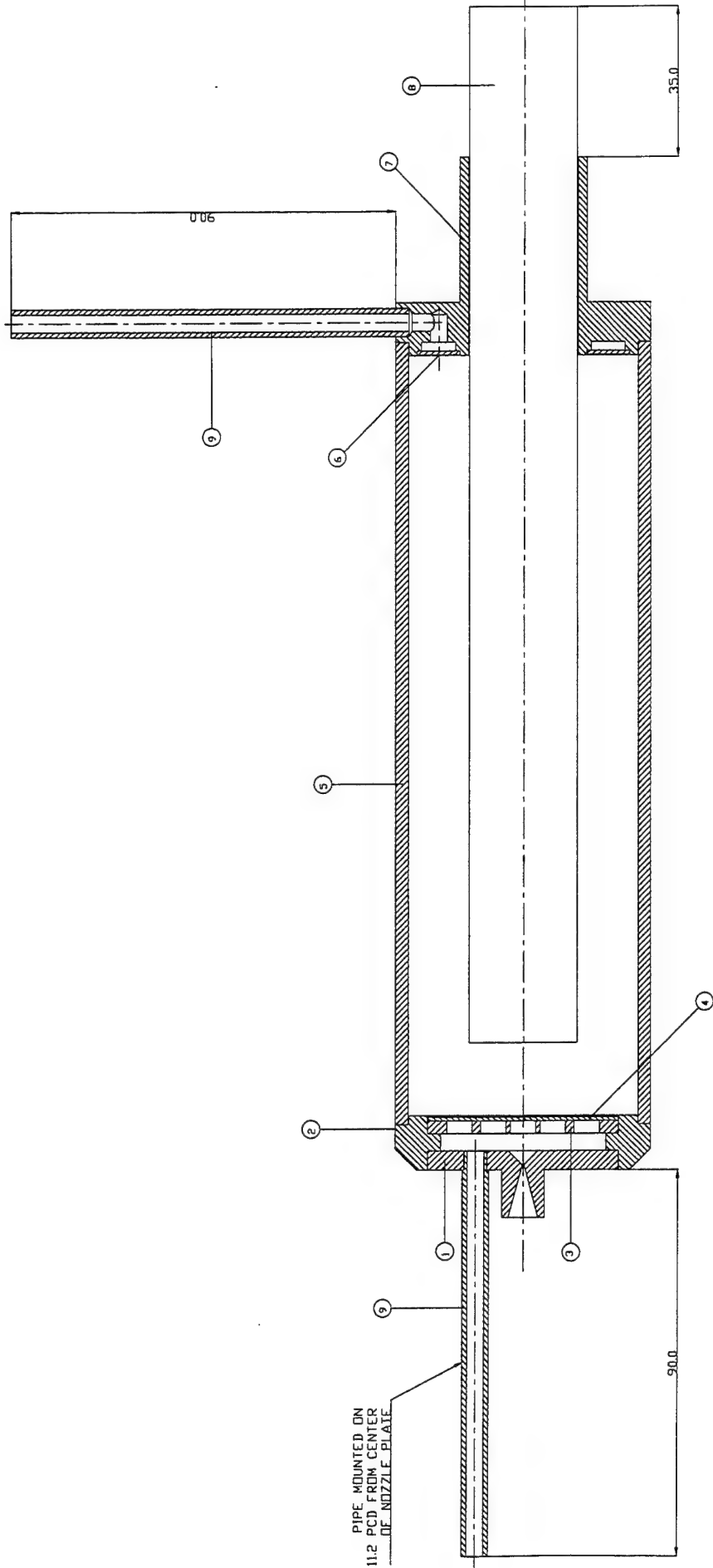
REV E

SHEET 1 OF 1

SIZE A3

SCALE 1:1

| REVISIONS | | | |
|-----------|---|----------|----------|
| REV | DESCRIPTION | DATE | APPROVED |
| B | Revised End Cap and Heater Housing Included | 1/Dec/97 | |



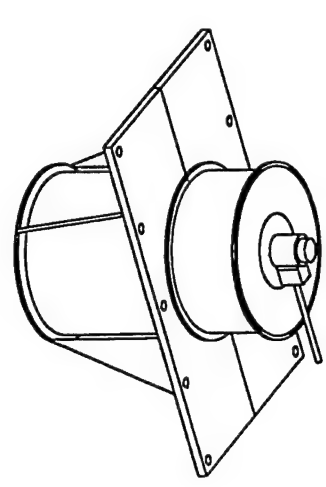
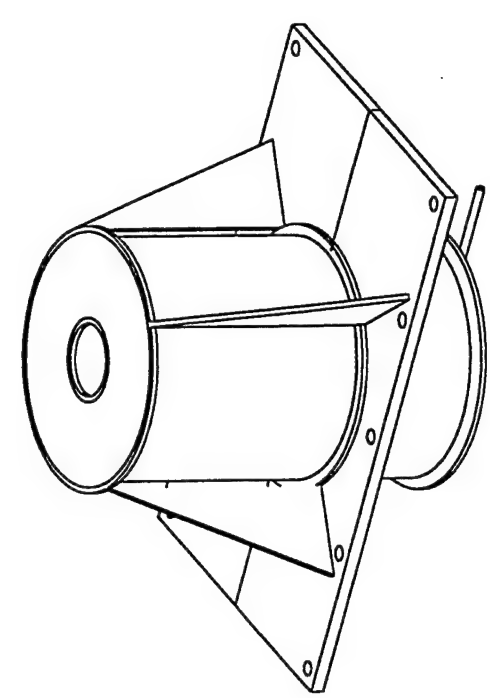
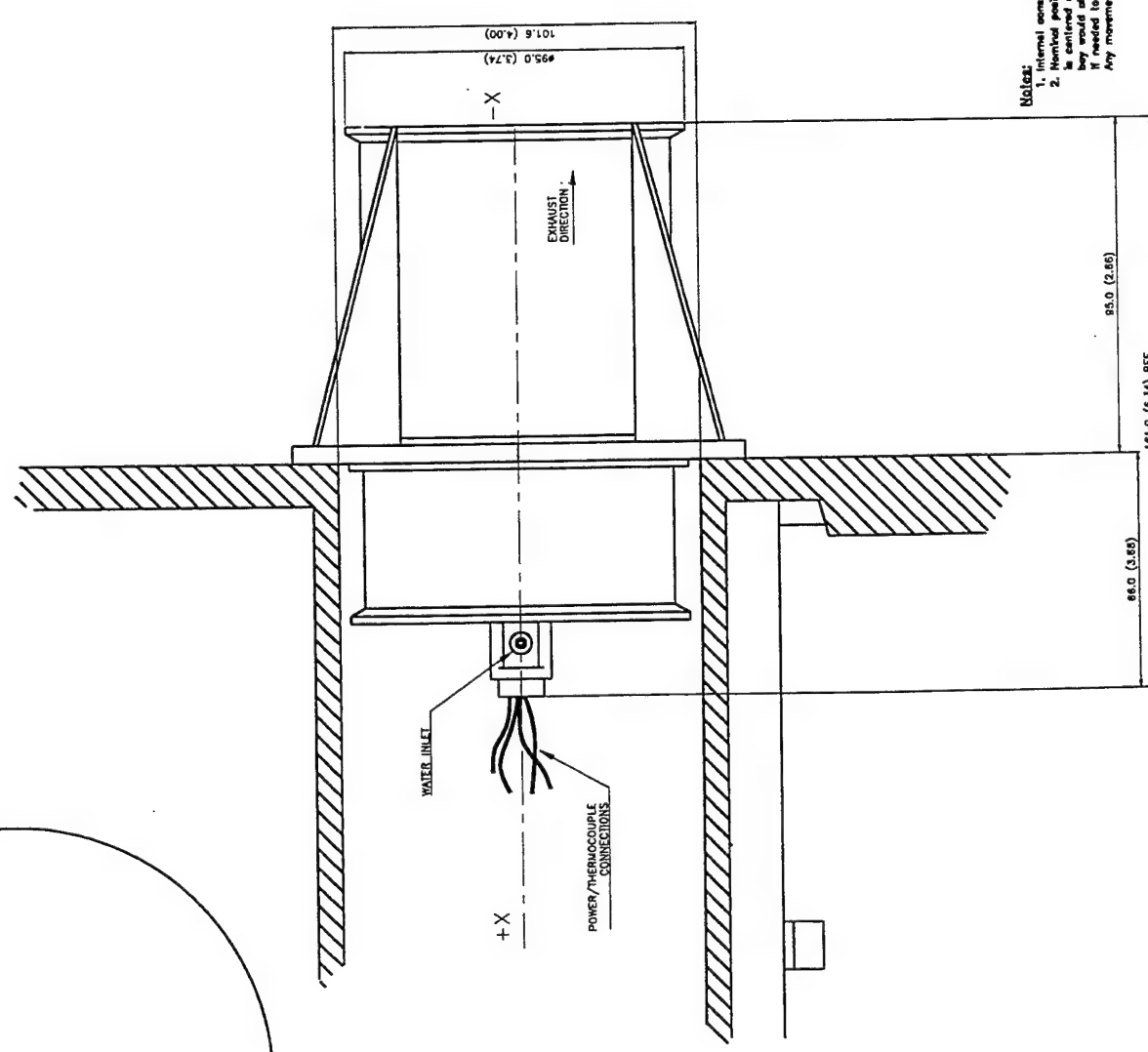
Notes:
 1. Prior to welding thoroughly clean items 1, 2, 3 and 4 to ensure that no loose particulate can block the nozzle orifice

| Item No. | Qty | Part or Identifying No. | Description |
|----------|-----|-------------------------|----------------------|
| 1 | 1 | RDDM001 | 0.7mm Nozzle Plate |
| 2 | 1 | RDDM002 | Front End Cap |
| 3 | 1 | RDDM003 | Support Plate |
| 4 | 1 | RDDM004 | Sintered Mesh Disk |
| 5 | 1 | RDDM005 | Heater Housing |
| 6 | 1 | RDDM006 | Sintered Mesh Anulus |
| 7 | 1 | RDDM007 | Cold End Cap |
| 8 | 1 | | Heater |
| 9 | 2 | | 1/4" Pipe |

| | | | | | | | | | | | | |
|---------|--------------------|-------|----------|----------|-------------|----------|-------|-------|----------------------------------|-----------------------|----------|---------|
| PROJECT | Rocket Development | DATE | 1/Dec/97 | DRAWN BY | M. Tucknott | APPROVED | | TITLE | Large Nozzle ResistoJet Assembly | Copyright © SSTL 1997 | FILENAME | RDDM802 |
| REV | B | SHEET | 1 | DF | 1 | SCALE | 1 : 1 | SIZE | A3 | | | |

UNLESS OTHERWISE SPECIFIED DIMENSIONS IN MILLIMETERS ARE
 DECIMAL X +/- 0.2 ANGULAR XX +/- 0.1
 DO NOT SCALE

| REVISIONS | | |
|-----------|--|---------|
| REV | DESCRIPTION | DATE |
| B | Minor revised drawings to meet in order of quality and to increase possible storage volume | 6/10/98 |
| C | Changed to 180mm height clear wall | 6/10/98 |



Notes:
 1. Internal construction as per RDDM804
 2. Nominal position of the thrust in the Y plane is centered on the Z axis. The width of the thrust bay would allow up to +/- 30mm (1.2in) of lateral movement. If needed to ease packaging of the test system. Any movement in the plane would result in an air venting thrust vector.

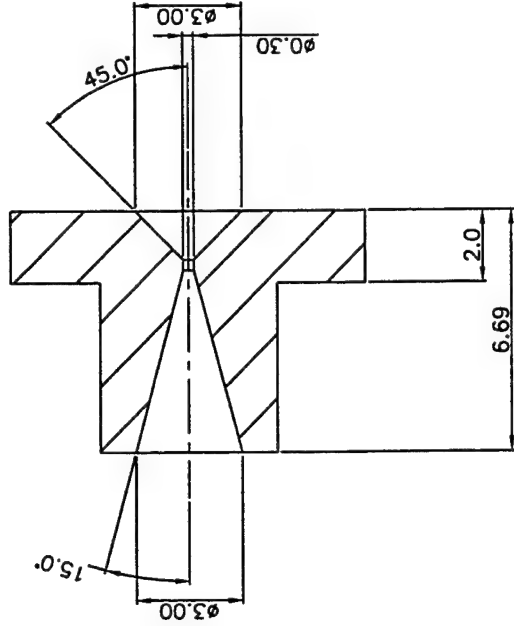
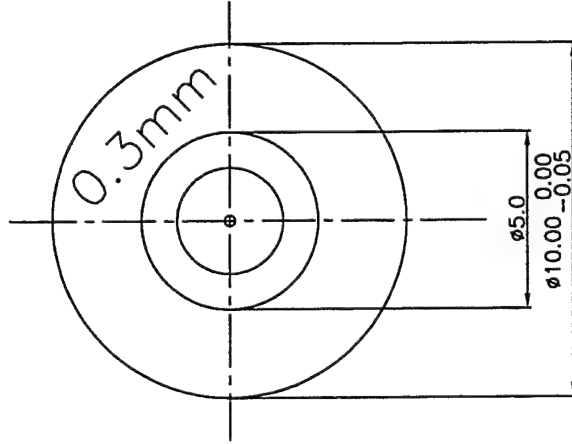
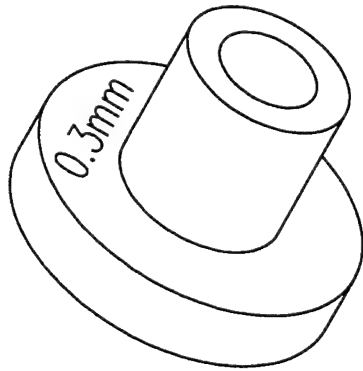
| | | | |
|-----------|--------------------|------------------------------------|----------|
| PROJECT | Rocket Development | DATE | 1/Jan/98 |
| DESIGN BY | M. Tucknott | APPROVED BY | ASK |
| MILE | | MightySat Resistor Mounting Scheme | |
| SHEET | | OF 1 | |
| TARE A7 | | SIZE 1:1 UOS | |

| | |
|-----------------------------|---------|
| MAXIMUM DIMENSION SPECIFIED | 181.0 |
| MINIMUM DIMENSION SPECIFIED | 66.0 |
| TOLERANCES ARE | ±0.5 |
| UNLESS OTHERWISE SPECIFIED | ±0.5 |
| NO HOLE | NO HOLE |

SECTION THROUGH Z PLANE OF MOUNTING STRUCTURE
 EXCEPT FOR THRUSTER AND SATELLITE STRUCTURE IS NOT TO SCALE

| | |
|------------------------------------|--------------------|
| PROJECT | Rocket Development |
| DATE | 1/Jan/98 |
| DESIGN BY | M. Tucknott |
| APPROVED BY | ASK |
| MILE | |
| MightySat Resistor Mounting Scheme | |
| SHEET | |
| OF 1 | |
| TARE A7 | |
| SIZE 1:1 UOS | |

| REVISIONS | | | | 4 | 5 | 6 |
|-----------|-------------|------|----------|---|---|---|
| REV | DESCRIPTION | DATE | APPROVED | | | |
| | | | | | | |



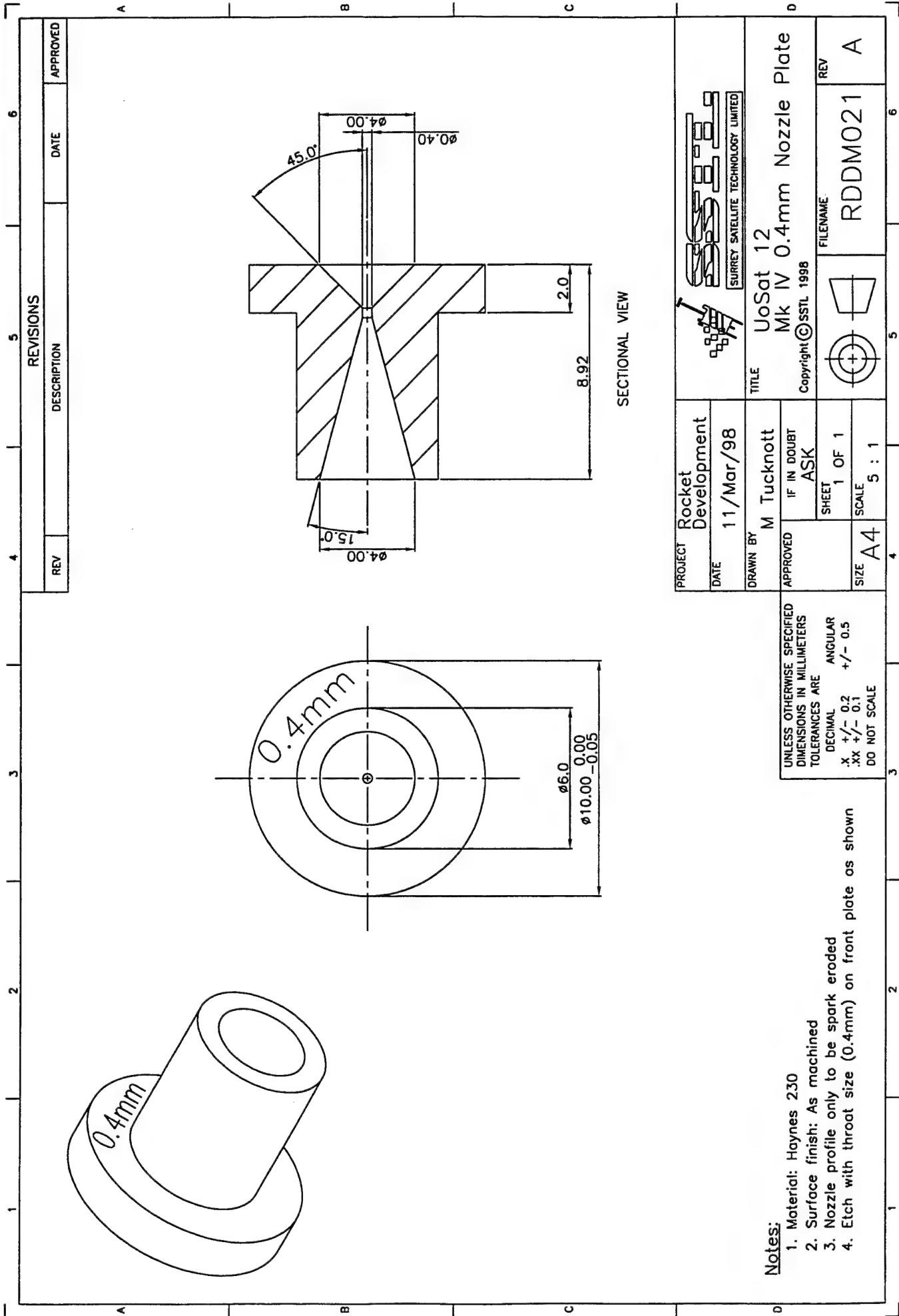
SECTIONAL VIEW

Notes:

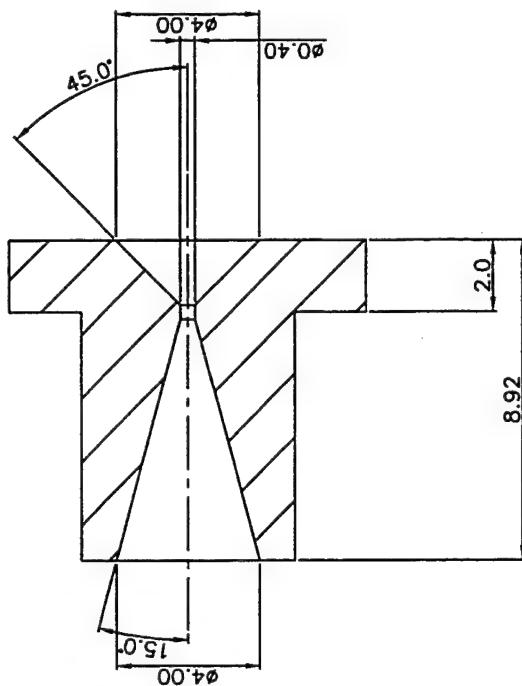
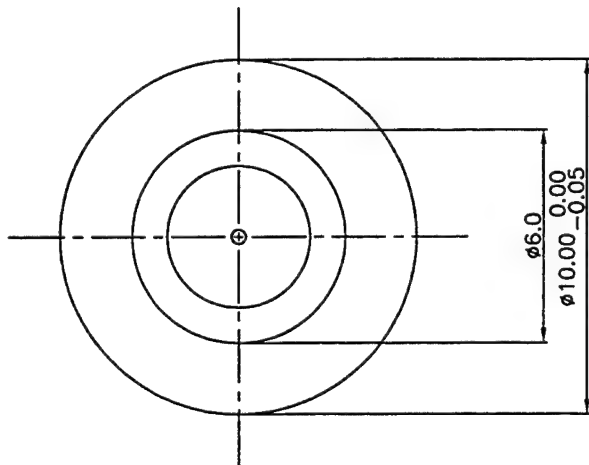
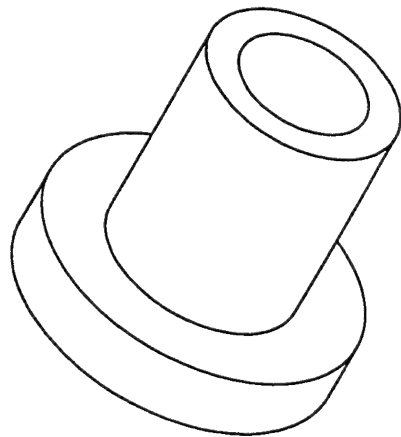
1. Material: Haynes 230
2. Surface finish: As machined
3. Nozzle profile only to be spark eroded
4. Etch throat size (0.3mm) in front plate as shown

| | | | |
|----------------------------|--------------------------|-------------------------------------|-------|
| PROJECT Rocket Development | | Surrey Satellite Technology Limited | |
| DATE 11/Mar/98 | TITLE MightySat 2.1 | | |
| DRAWN BY M Tucknott | Mk IV 0.3mm Nozzle Plate | | |
| APPROVED IF IN DOUBT ASK | Copyright © SSTL 1998 | | |
| SHEET 1 OF 1 | FILENAME RDDM020 | | REV A |
| SCALE 5 : 1 | SIZE A4 | | |




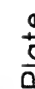

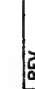










UNLESS OTHERWISE SPECIFIED
DIMENSIONS IN MILLIMETERS
TOLERANCES ARE
DECIMAL ANGULAR
.X +/- 0.2 +/- 0.5
.XX +/- 0.1
DO NOT SCALE



| REVISIONS | | | |
|-----------|-------------|------|----------|
| REV | DESCRIPTION | DATE | APPROVED |
| 4 | | | |
| 5 | | | |
| 6 | | | |

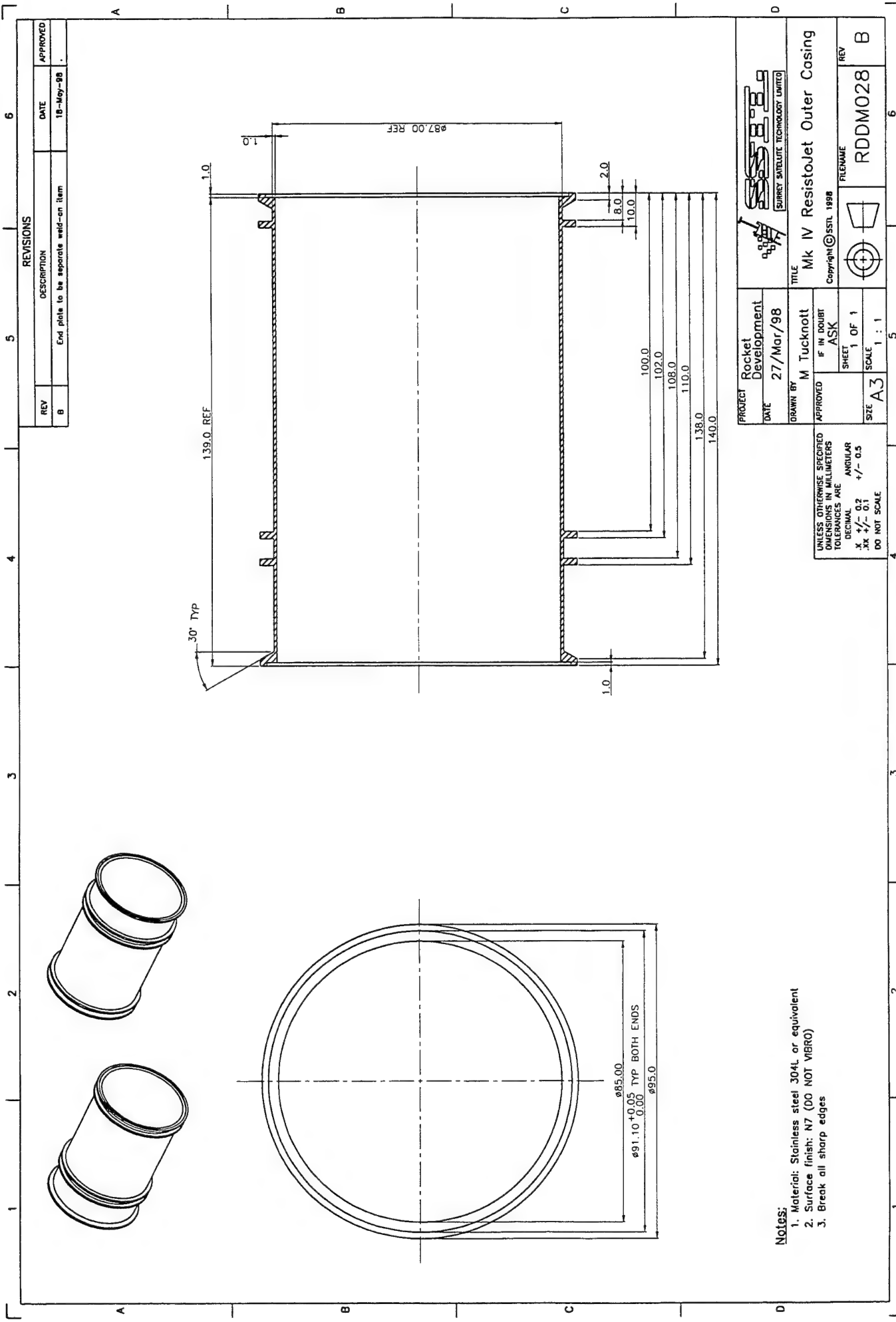


SECTIONAL VIEW



| | | | | | | | | | | | | | | | | | | | | | | | | | | | | | | | | | | | | | | | | | | | | | | | | | | | | | | | | | | | | | | | | | | | | | | | | | | | | | |
|---------|--------------------|--|--|--|--|--|--|--|--|--|--|--|--|--|--|--|--|--|--|--|--|--|--|--|--|--|--|--|--|--|--|--|--|--|--|--|--|--|--|--|--|--|--|--|--|--|--|--|--|--|--|--|--|--|--|--|--|--|--|--|--|--|--|--|--|--|--|--|--|--|--|--|--|--|--|--|--|
| PROJECT | Rocket Development | |  |  |  |  |  |  |  |  |  |  |  |  |  |  |  |  | | | | | | | | | | | | | | | | | | | | | | | | | | | | | | | | | | | | | | | | | | | | | | | | | | | | | | | | | | | |
|---------|--------------------|--|--|--|--|--|--|--|--|--|--|--|--|--|--|--|--|--|--|--|--|--|--|--|--|--|--|--|--|--|--|--|--|--|--|--|--|--|--|--|--|--|--|--|--|--|--|--|--|--|--|--|--|--|--|--|--|--|--|--|--|--|--|--|--|--|--|--|--|--|--|--|--|--|--|--|--|

Notes:

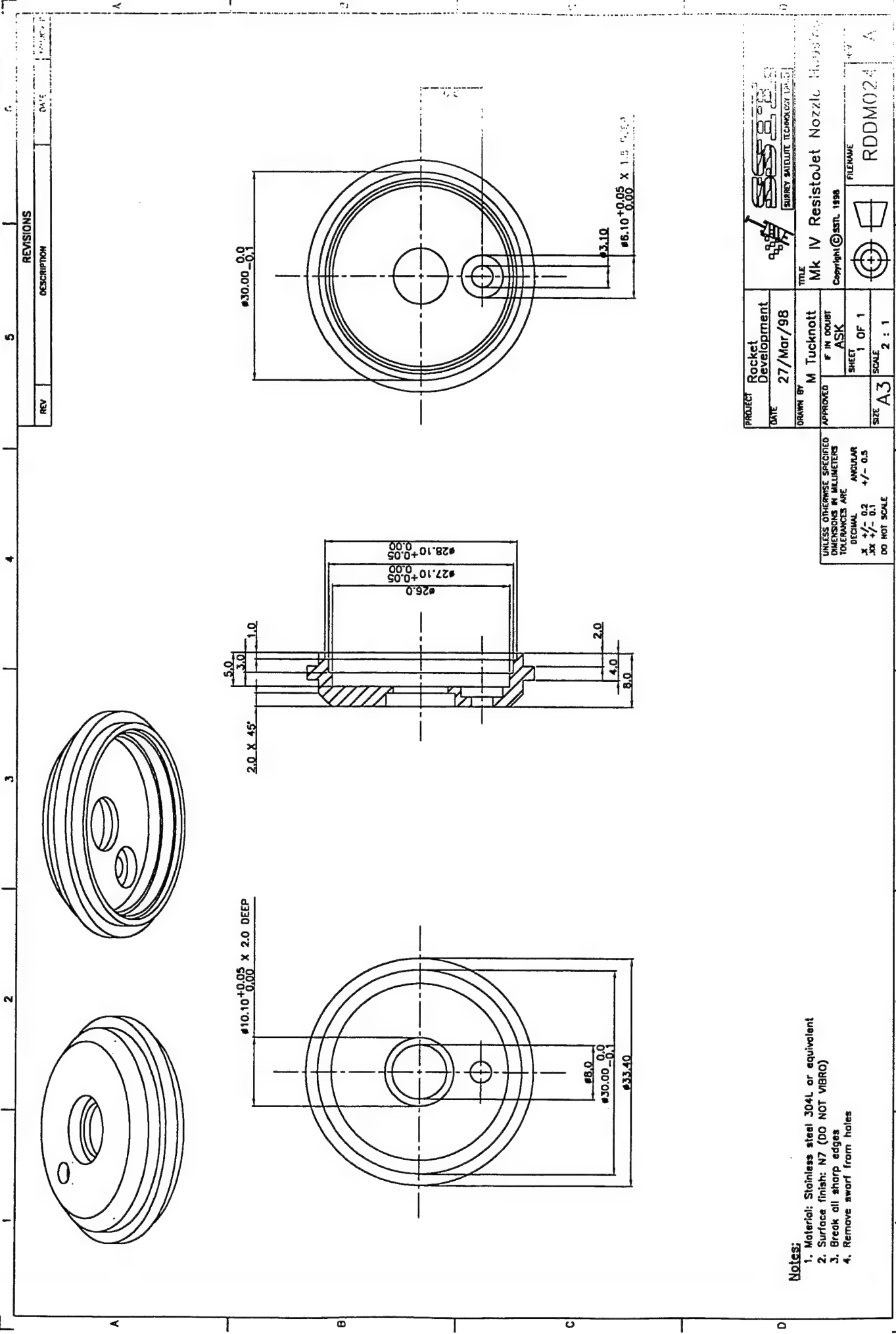
1. Material: Haynes 230
2. Surface finish: As machined
3. Nozzle profile only to be spark eroded








| | | | | | |
|-------------------------------|-----------|------------------------|--|---|----------|
| PROJECT Rocket Development | 27/Mar/98 | DRAWN BY M Tucknott | TITLE Mk IV ResisitoJet Front Plate | | REV A |
| | | | Copyright © SSTL 1998 | | |
| DATE | | | IF IN DOUBT ASK | FILENAME | |
| | | | SHEET 1 OF 1 |   | |
| SIZE A4 | | | SCALE 1 : 1 | RDDM022 | |

1. Material: Stainless steel 304L or equivalent
2. Surface finish N7 (DO NOT VIBRO)
3. Break all sharp edges

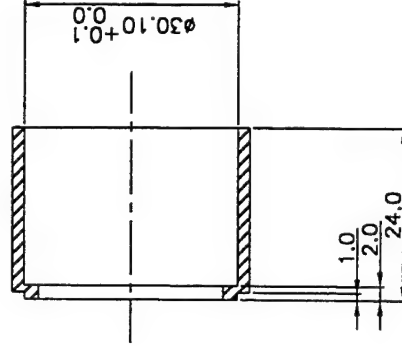
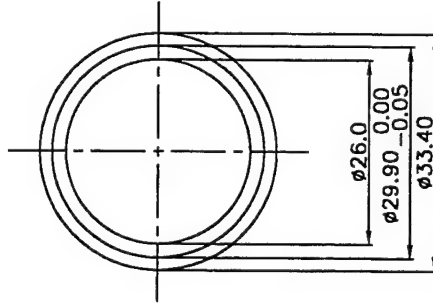
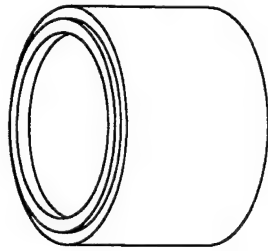


| REV | DESCRIPTION | DATE |
|-----|-------------|------|
| | | |

| | | | | | | | | | | | | | | | | | |
|---|--------------------|--|--|------|-----------|----------|------------|----------|--------------------|--|-------|--------|-------|-------|------|----|--|
| PROJECT | Rocket Development | | | DATE | 27/Mar/98 | DRAWN BY | M Tucknott | APPROVED | IF IN DOUBT ASK | | SHEET | 1 OF 1 | SCALE | 2 : 1 | SIZE | A3 | |
| <div><div></div><div><div>Mk IV Resistojet Nozzle</div><div>Copyright © SSTL 1998</div></div></div> | | | | | | | | | | | | | | | | | |
| <div><div></div><div>FILENAME</div><div>RDDM024</div></div> | | | | | | | | | | | | | | | | | |

UNLESS OTHERWISE SPECIFIED
DIMENSIONS IN MILLIMETERS
TOLERANCES ARE
DECIMAL
X +/- 0.2
XX +/- 0.1
ANGULAR
+/- 0.5
DO NOT SCALE

Notes:
1. Material: Stainless steel 304L or equivalent
2. Surface finish: N7 (DO NOT VIBRO)
3. Break all sharp edges
4. Remove swarf from holes



Notes:

1. Material: Stainless steel 304L or equivalent
2. Surface finish: N7 (DO NOT VIBRO)
3. Break all sharp edges

REVISIONS

| REV | DESCRIPTION | DATE | APPROVED |
|-----|-------------|------|----------|
|-----|-------------|------|----------|

PROJECT Rocket Development

DATE 27/Mar/98

DRAWN BY

M Tucknott

APPROVED

IF IN DOUBT ASK

SHEET 1 OF 1

SCALE 1 : 1

SIZE A4

UNLESS OTHERWISE SPECIFIED
DIMENSIONS IN MILLIMETERS
TOLERANCES ARE

DECIMAL ANGULAR

.X +/- 0.2 +/- 0.5

.XX +/- 0.1
DO NOT SCALE



TITLE

Mk IV ResistJet Front Sleeve

Copyright © SSTL 1998

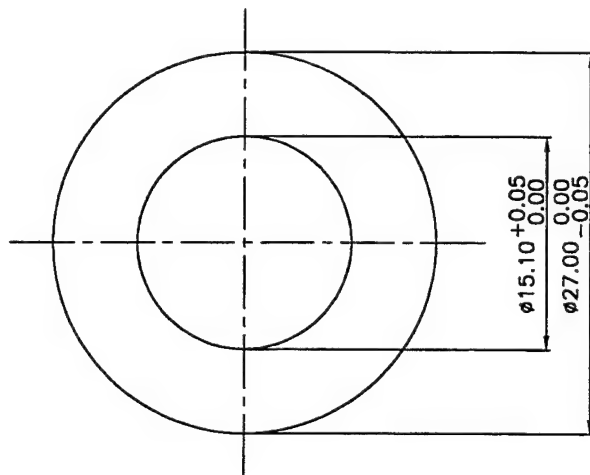


FILENAME

RDDM023

REV

A



Notes:

1. Material: 50B stainless steel mesh
Porosity 50 microns
(Sheet thickness 1mm)

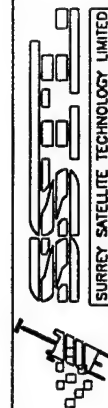
REVISIONS

| REV | DESCRIPTION | DATE | APPROVED |
|-----|-------------|------|----------|
|-----|-------------|------|----------|

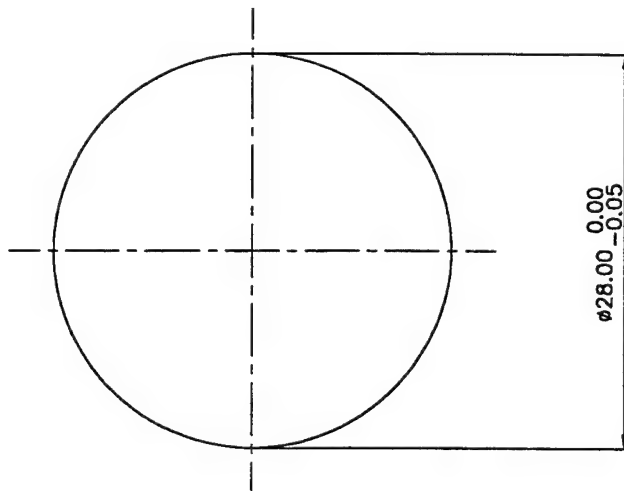
| | |
|----------|--------------------|
| PROJECT | Rocket Development |
| DATE | 31/Mar/98 |
| DRAWN BY | M Tucknott |
| APPROVED | IF IN DOUBT ASK |
| SHEET | 1 OF 1 |
| SCALE | 2 : 1 |
| SIZE | A4 |

| | |
|-----------|----------------------------------|
| TITLE | Mk IV ResisitJet Sintered Anulus |
| Copyright | ©SSTL 1998 |
| FILENAME | RDDM029 |
| REV | A |

UNLESS OTHERWISE SPECIFIED
DIMENSIONS IN MILLIMETERS
TOLERANCES ARE
DECIMAL ANGULAR
.X +/- 0.2 +/- 0.5
.XX +/- 0.1
DO NOT SCALE



| REVISIONS | | | |
|-----------|-------------|------|----------|
| REV | DESCRIPTION | DATE | APPROVED |
| 1 | 1 | 2 | 3 |




Notes:

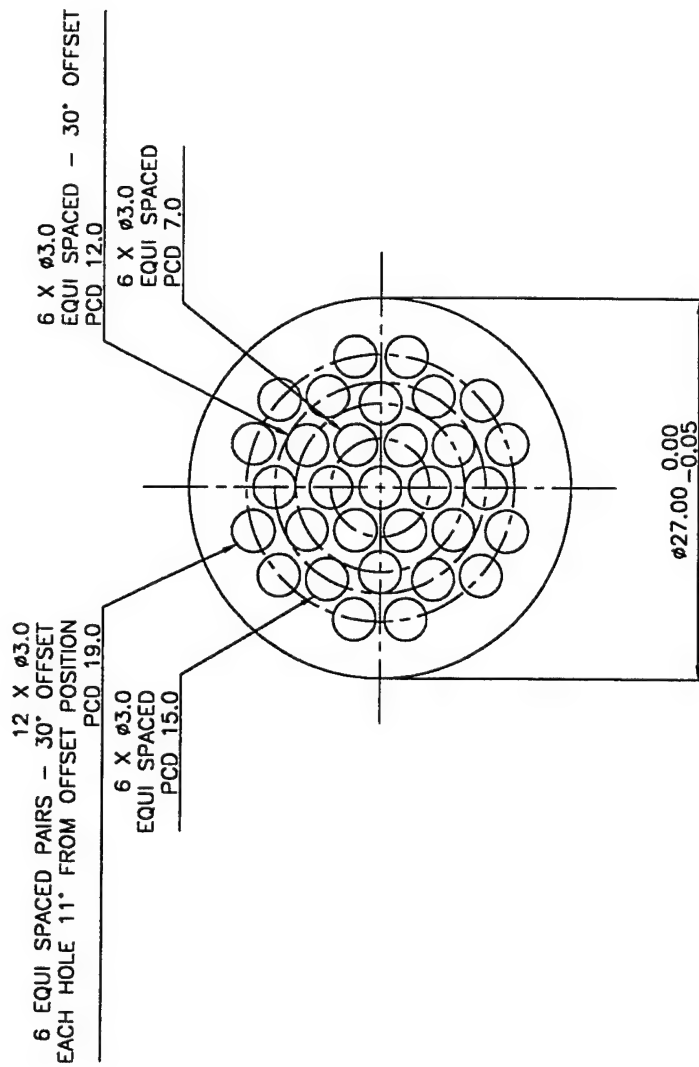
1. Material: 50B sintered stainless steel mesh
Porosity 50 microns
(Sheet thickness 1mm)

UNLESS OTHERWISE SPECIFIED
DIMENSIONS IN MILLIMETERS
TOLERANCES ARE






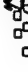






















| | DECIMAL | ANGULAR |
|----|---------|---------|
| X | +/- 0.2 | +/- 0.5 |
| XX | +/- 0.1 | |

DO NOT SCALE

| | | | | | | |
|---------|--------------------|----------|-----------------------|---|---------|----------|
| PROJECT | Rocket Development | DRAWN BY | M Tucknott | TITLE | REV | |
| | DATE | | 27/Mar/98 | IF IN DOUBT ASK | | FILENAME |
| SIZE | A4 | SHEET | 1 OF 1 |  | RDDM026 | 6 |
| | SCALE | 2 : 1 | Copyright © SSTL 1998 | | | |
| | | | | SURREY SATELLITE TECHNOLOGY LIMITED | | 4 |



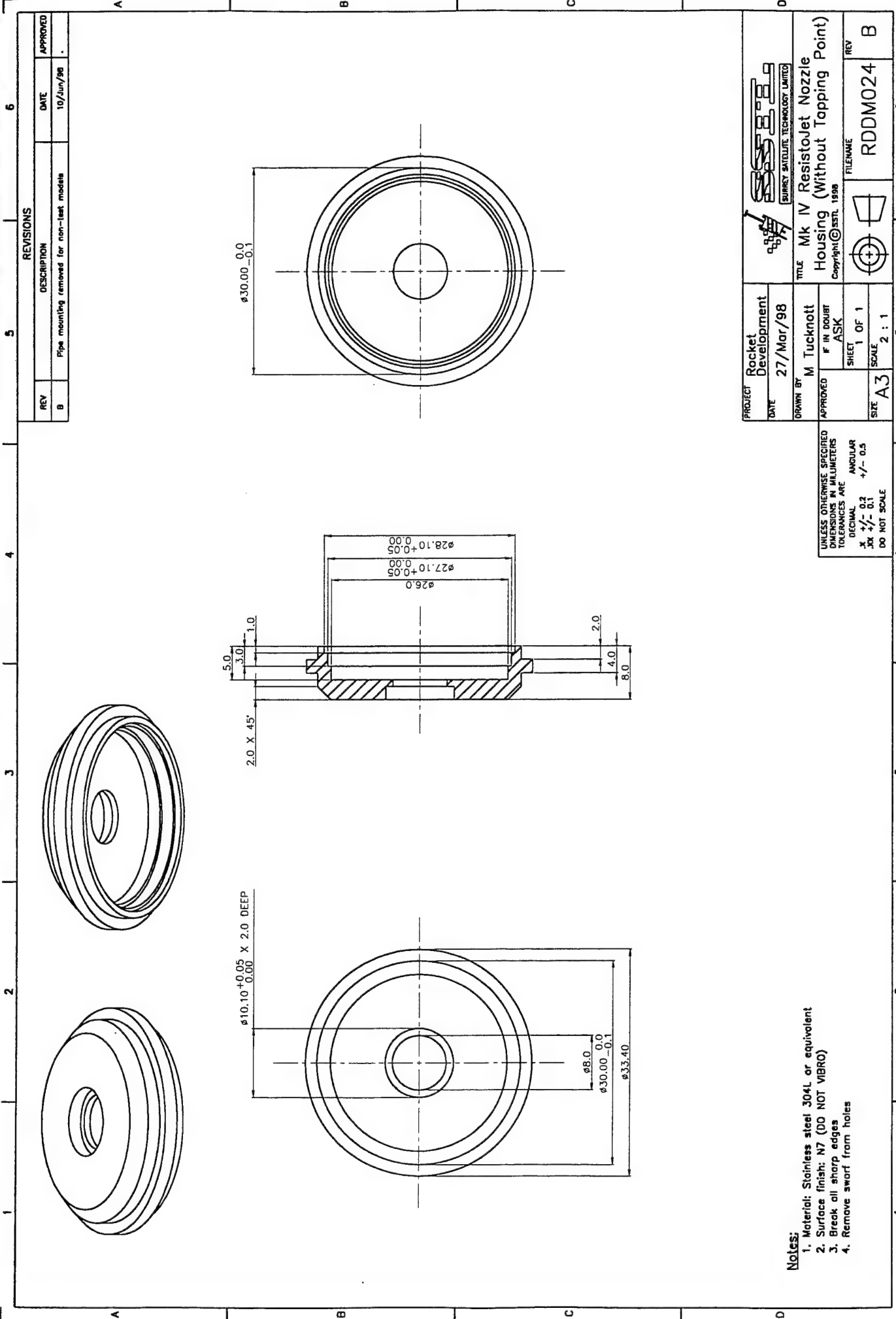
1. Material: Stainless steel 304L or equivalent
2. All holes $\phi 3.0$
3. Surface finish N7 (DO NOT VIBRO)
4. Break all sharp edges
5. Remove swarf from holes

| | | | | | | | | | | | | | | | | | | | | | | | | | | | | | | | | | | | | | | | | | | | | | | | | | | | | | | | | | | | | | | | | | | | | | | | | | | | | | | | | | | | | | | | | | | | | | | | |
|---------|--------------------|--|---|---|---|---|---|---|---|---|---|---|---|--|---|---|---|---|---|---|---|---|---|---|---|---|---|---|---|---|---|---|---|---|---|---|---|---|---|---|---|---|---|---|---|---|---|---|---|---|---|---|---|---|---|---|---|---|---|---|---|---|---|---|---|---|---|---|---|---|---|---|---|---|---|---|---|---|---|---|---|---|---|---|---|---|---|---|---|---|---|---|---|---|---|
| PROJECT | Rocket Development | |  |  |  |  |  |  |  |  |  |  |  |  |  |  |  |  |  |  |  |  |  |  |  |  |  |  |  |  | | | | | | | | | | | | | | | | | | | | | | | | | | | | | | | | | | | | | | | | | | | | | | | | | | | | | | | | | | | | | | | | | |
|---------|--------------------|--|---|---|---|---|---|---|---|---|---|---|---|--|---|---|---|---|---|---|---|---|---|---|---|---|---|---|---|---|---|---|---|---|---|---|---|---|---|---|---|---|---|---|---|---|---|---|---|---|---|---|---|---|---|---|---|---|---|---|---|---|---|---|---|---|---|---|---|---|---|---|---|---|---|---|---|---|---|---|---|---|---|---|---|---|---|---|---|---|---|---|---|---|---|

UNLESS OTHERWISE SPECIFIED
DIMENSIONS IN MILLIMETERS
TOLERANCES ARE




| | DECIMAL | ANGULAR |
|-----|---------|---------|
| X | +/- 0.2 | +/- 0.5 |
| .XX | +/- 0.1 | |

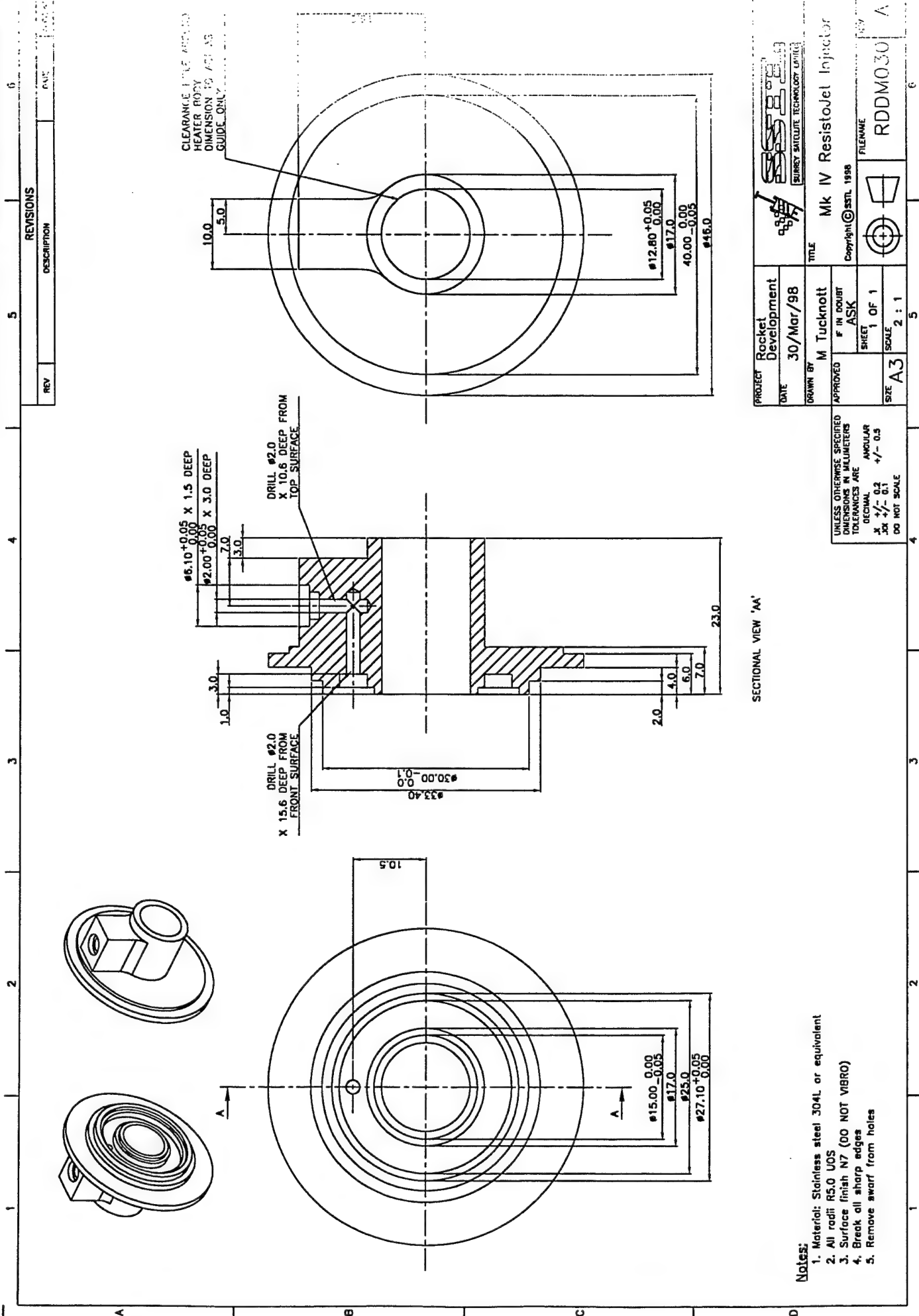
DO NOT SCALE



Notes:

1. Material: Stainless steel 304L or equivalent
2. Surface finish: N7 (DO NOT VIBRO)
3. Break all sharp edges
4. Remove swarf from holes

| | | | | | | | | | |
|----------|--|--------------------|--|---|--|---|--|-------------------------------------|--|
| PROJECT | | Rocket Development | |  | |  | | SURREY SATellite TECHNOLOGY LIMITED | |
| DATE | | 27/Mar/98 | | | | | | | |
| DRAWN BY | | M Tucknott | | TITLE Mk IV Resistotet Nozzle Housing (Without Tapping Point) | | | | | |
| APPROVED | | F IN DOUBT ASK | | Copyright © SSTL 1998 | | | | | |
| SIZE A3 | | SHEET 1 OF 1 | |  | | FILENAME RDDM024 | | REV B | |
| | | SCALE 2 : 1 | | | | | | | |

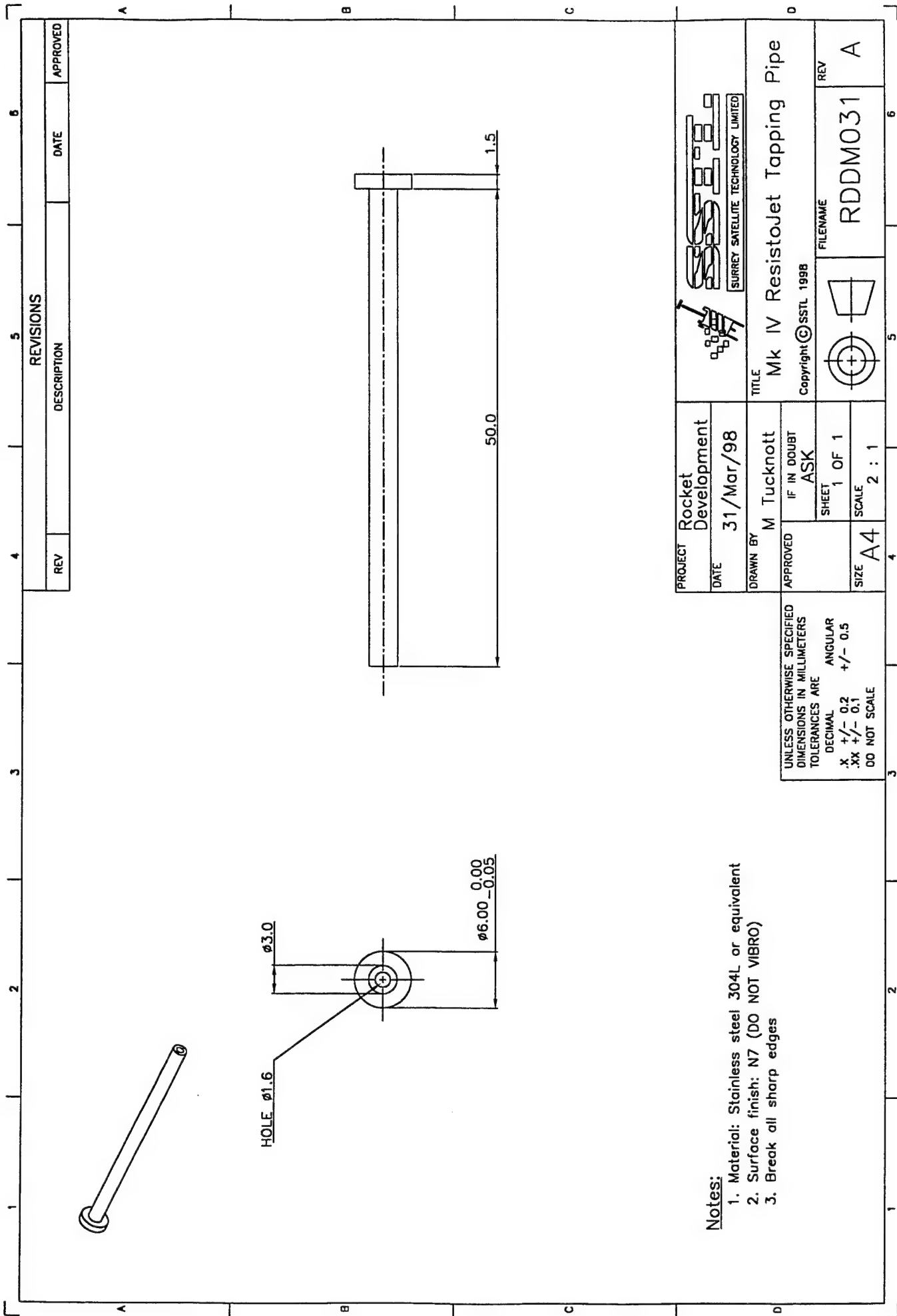


- Notes:**
1. Material: Stainless steel 304L or equivalent
 2. All radii R5.0 UOS
 3. Surface finish N7 (DO NOT VIBRO)
 4. Break all sharp edges
 5. Remove swarf from holes

SECTIONAL VIEW 'AA'


| | | | |
|----------|--------------------|-----------|---------------------------|
| PROJECT | Rocket Development | TITLE | Mk IV Resistojet Injector |
| DATE | 30/Mar/98 | DRAWN BY | M Tucknott |
| APPROVED | "I" IN DOUBT ASK | COPYRIGHT | © STL 1998 |
| SHEET | 1 OF 1 | FILENAME | RDDM030 |
| SCALE | 2 : 1 | SIZE | A3 |

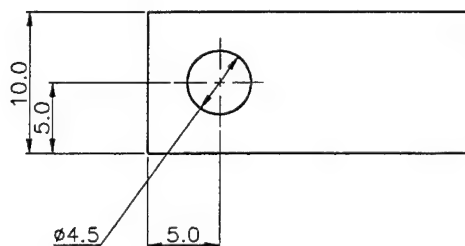
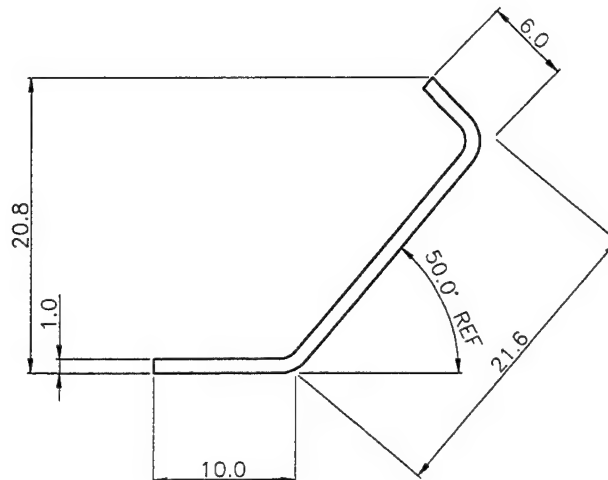
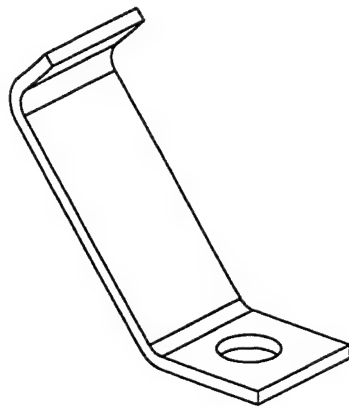
UNLESS OTHERWISE SPECIFIED
DIMENSIONS IN MILLIMETERS
TOLERANCES ARE
DECIMAL ANGULAR
X +/- 0.2 +/- 0.5
XX +/- 0.1
DO NOT SCALE



Notes:

1. Material: Stainless steel 304L or equivalent
2. Surface finish: N7 (DO NOT VIBRO)
3. Break all sharp edges


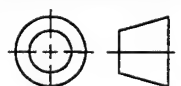
| | | |
|----------|--------------------|--|
| PROJECT | Rocket Development |  SURREY SATELLITE TECHNOLOGY LIMITED |
| DATE | 31/Mar/98 | |
| DRAWN BY | M Tucknott | TITLE |
| APPROVED | IF IN DOUBT ASK | Mk IV ResistoJet Tapping Pipe |
| SHEET | 1 OF 1 | Copyright © SSTL 1998 |
| SCALE | 2 : 1 | FILENAME |
| SIZE | A4 | RDDM031 |
| | | REV |
| | | A |



Notes:

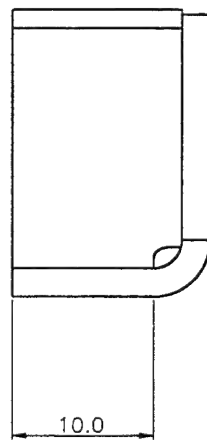
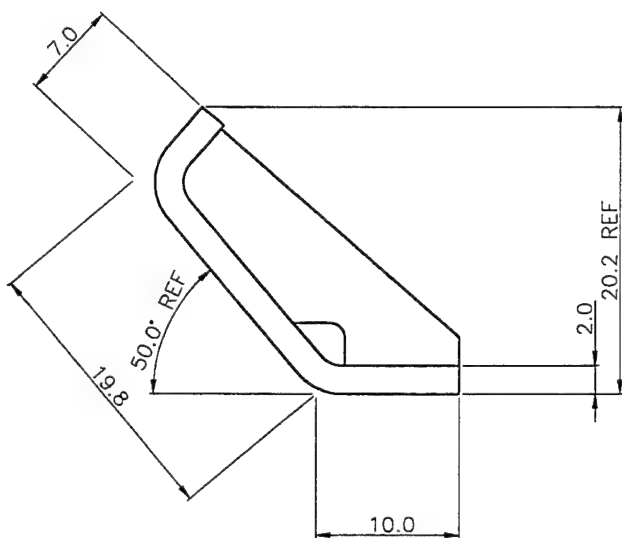
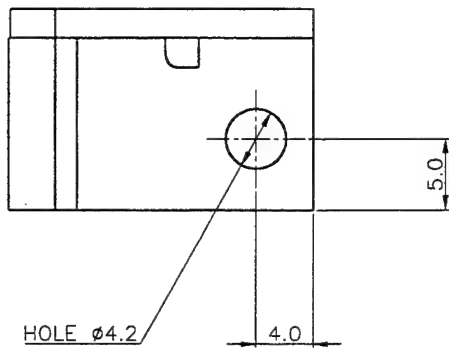
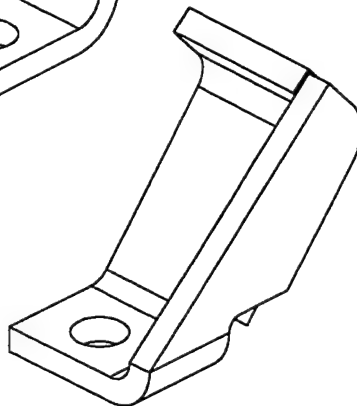
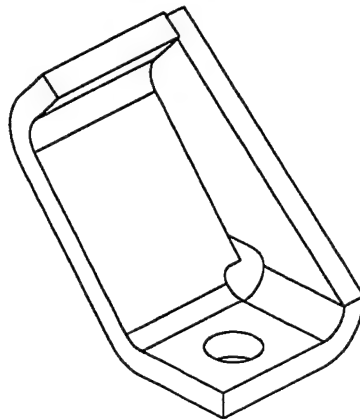
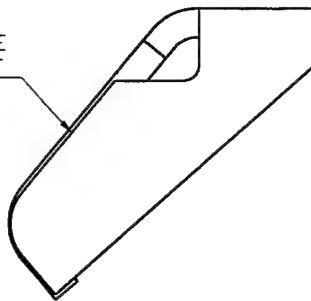
1. Material: Stainless steel 304L
2. All internal bend radii R2.0 max
3. Surface finish N7 (DO NOT VIBRO)

UNLESS OTHERWISE SPECIFIED
DIMENSIONS IN MILLIMETERS
TOLERANCES ARE
DECIMAL ANGULAR
.X +/- 0.2 +/- 0.5
.XX +/- 0.1
DO NOT SCALE

| | | | |
|----------------------------|-----------------|---|------------------|
| PROJECT Rocket Development | |  SURREY SATELLITE TECHNOLOGY LIMITED | |
| DATE 6/Apr/98 | | | |
| DRAWN BY M Tucknott | | TITLE Mk IV Resistojet Leg | |
| APPROVED | IF IN DOUBT ASK | Copyright © SSTL 1998 | |
| | SHEET 1 OF 1 |  | FILENAME RDDM032 |
| | SIZE A4 | | SCALE 2 : 1 |

| REVISIONS | | | |
|-----------|--------------------------------------|-----------|----------|
| REV | DESCRIPTION | DATE | APPROVED |
| B | Stiffening following stress analysis | 11/Jun/98 | . |

WELD EDGE
SHUT



Notes:

1. Material: Stainless Steel 304L
2. All internal bend radii R2.0 max
3. Surface finish N7 (DO NOT VIBRO)

UNLESS OTHERWISE SPECIFIED
DIMENSIONS IN MILLIMETERS
TOLERANCES ARE
DECIMAL ANGULAR
X ± 0.2 ± 0.5
XX ± 0.1
DO NOT SCALE

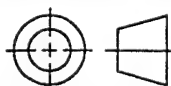
| | |
|------------------------|--------------------|
| PROJECT Rocket | |
| DATE 6/Apr/98 | |
| DRAWN BY M Tucknott | |
| APPROVED | IF IN DOUBT ASK |
| SHEET 1 OF 1 | SIZE A4 |
| SCALE 2 : 1 | |



SURREY SATELLITE TECHNOLOGY LIMITED

TITLE
Mk IV ResistoJet Leg

Copyright © SSTL 1998

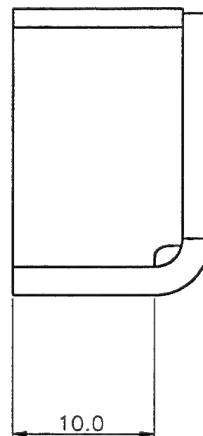
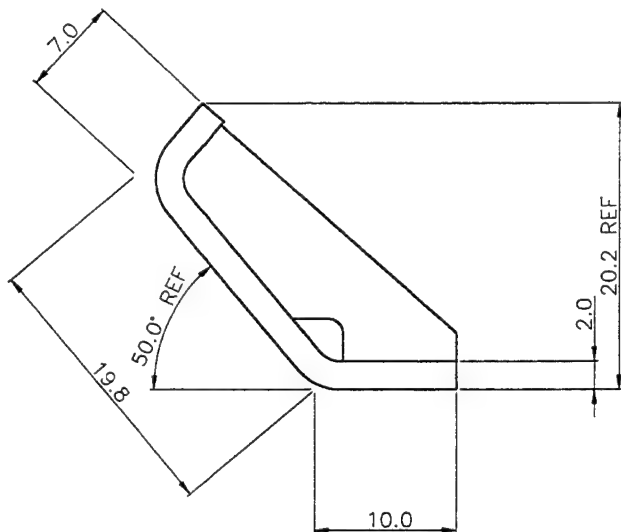
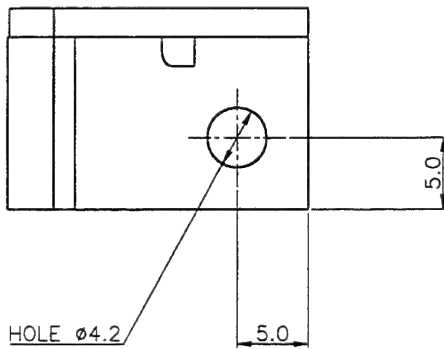
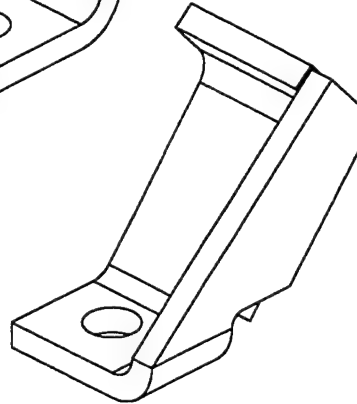
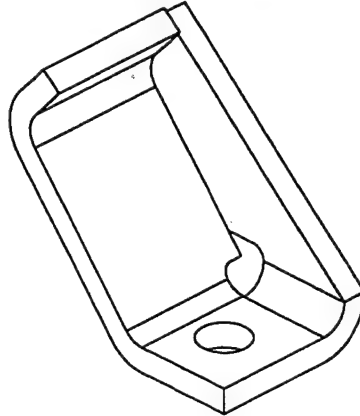
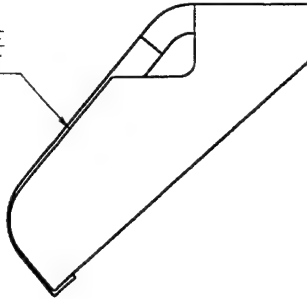


FILENAME
RDDM032

REV
B

| REVISIONS | | | |
|-----------|--------------------------------------|-----------|----------|
| REV | DESCRIPTION | DATE | APPROVED |
| B | Stiffening following stress analysis | 11/Jun/98 | . |
| C | Mounting hole repositioned | 23/Jun/98 | . |

WELD EDGE
SHUT


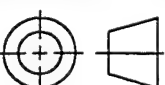
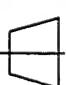
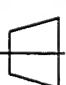
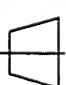


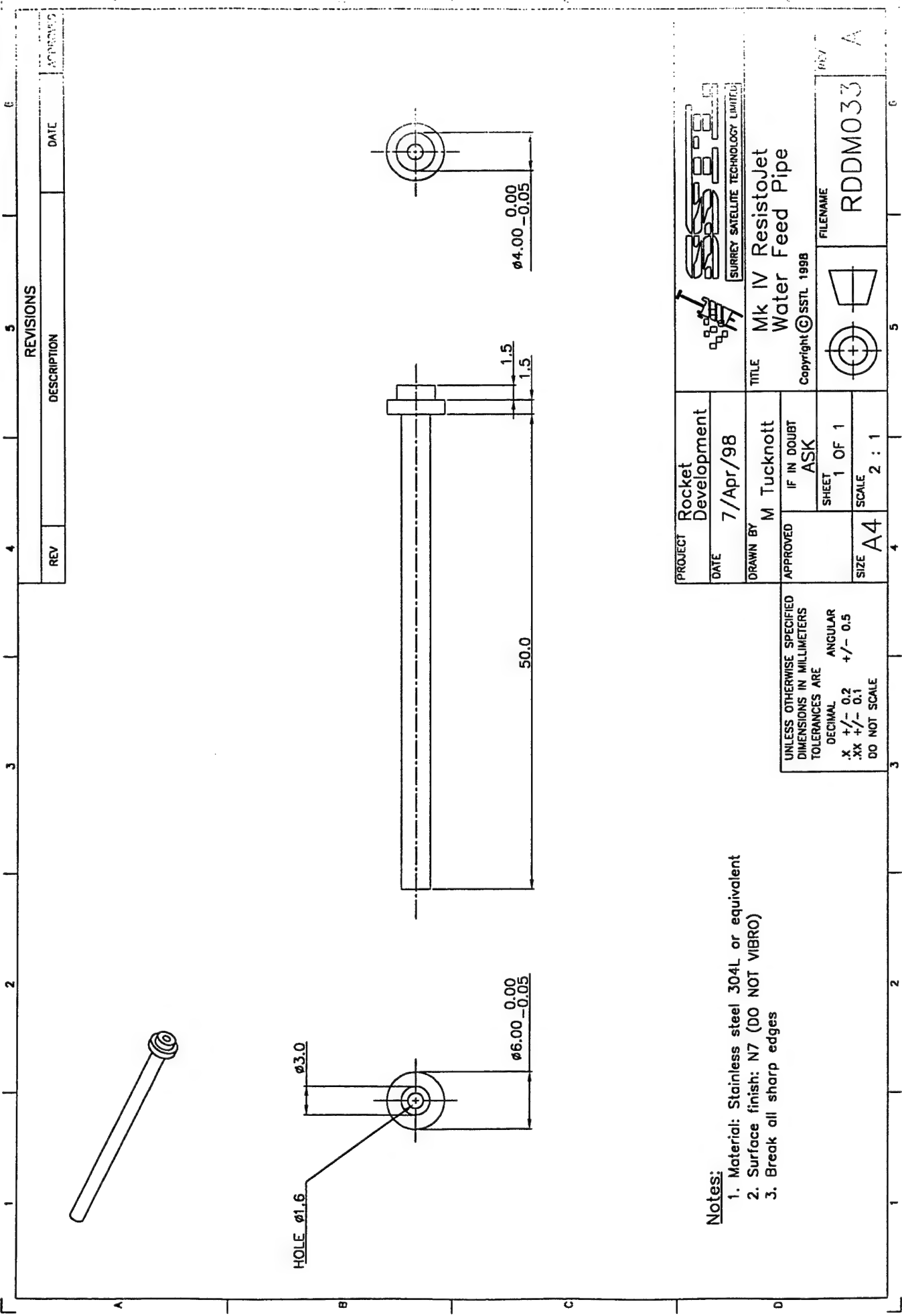
Notes:

1. Material: Stainless Steel 304L
2. All internal bend radii R2.0 max
3. Surface finish N7 (DO NOT VIBRO)

UNLESS OTHERWISE SPECIFIED
DIMENSIONS IN MILLIMETERS
TOLERANCES ARE



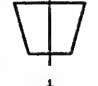
| DECIMAL | ANGULAR |
|--------------|-----------|
| X ± 0.2 | ± 0.5 |
| XX ± 0.1 | |
| DO NOT SCALE | |

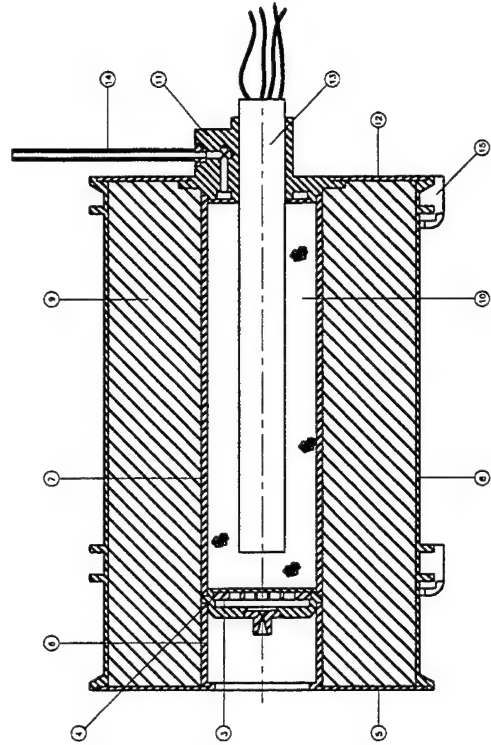
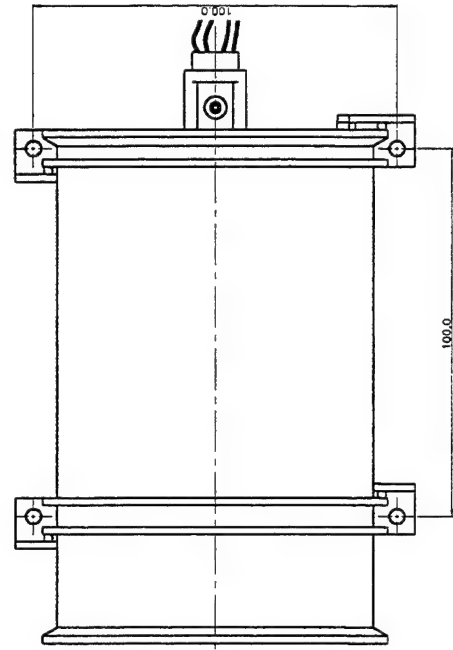
| | | | |
|----------|--------------------|--|----------|
| PROJECT | Rocket |  SSTL SURREY SATELLITE TECHNOLOGY LIMITED | |
| DATE | 6/Apr/98 | | |
| DRAWN BY | M Tucknott | TITLE | |
| APPROVED | IF IN DOUBT ASK | Mk IV ResistoJet Leg | |
| SIZE | A4 | Copyright © SSTL 1998 | REV |
| | |  | FILENAME |
| | |  | RDDM032 |
| | |  | C |
| | |  | |























































































Notes:

1. Material: Stainless steel 304L or equivalent
2. Surface finish: N7 (DO NOT VIBRO)
3. Break all sharp edges

| | | | |
|---|--------------|--|--|
| PROJECT Rocket Development | |  SURREY SATELLITE TECHNOLOGY LIMITED | |
| DATE | 7 / Apr / 98 | TITLE | |
| DRAWN BY | | M Tucknott | |
| APPROVED | | IF IN DOUBT | |
| | | ASK | |
| SHEET | | 1 OF 1 | |
| SCALE | | 2 : 1 | |
| SIZE | | A4 | |
| UNLESS OTHERWISE SPECIFIED DIMENSIONS IN MILLIMETERS TOLERANCES ARE DECIMAL ANGULAR .X +/- 0.2 +/- 0.5 .XX +/- 0.1 DO NOT SCALE | | | |
|  | |  | |
| FILENAME | | RDDM033 | |
| REV | | A | |



| 18 | 4 | ROMA02C | Leg |
|-----|---|---------|-----------------|
| 14 | 1 | ROMA02A | Water Fuel Pipe |
| 15 | 1 | ROMA02A | Header |
| 16 | 1 | ROMA02A | Back Pipe |
| 17 | 1 | ROMA02A | Flange |
| 18 | 1 | ROMA02A | Flange |
| 19 | 1 | ROMA02A | Flange |
| 20 | 1 | ROMA02A | Flange |
| 21 | 1 | ROMA02A | Flange |
| 22 | 1 | ROMA02A | Flange |
| 23 | 1 | ROMA02A | Flange |
| 24 | 1 | ROMA02A | Flange |
| 25 | 1 | ROMA02A | Flange |
| 26 | 1 | ROMA02A | Flange |
| 27 | 1 | ROMA02A | Flange |
| 28 | 1 | ROMA02A | Flange |
| 29 | 1 | ROMA02A | Flange |
| 30 | 1 | ROMA02A | Flange |
| 31 | 1 | ROMA02A | Flange |
| 32 | 1 | ROMA02A | Flange |
| 33 | 1 | ROMA02A | Flange |
| 34 | 1 | ROMA02A | Flange |
| 35 | 1 | ROMA02A | Flange |
| 36 | 1 | ROMA02A | Flange |
| 37 | 1 | ROMA02A | Flange |
| 38 | 1 | ROMA02A | Flange |
| 39 | 1 | ROMA02A | Flange |
| 40 | 1 | ROMA02A | Flange |
| 41 | 1 | ROMA02A | Flange |
| 42 | 1 | ROMA02A | Flange |
| 43 | 1 | ROMA02A | Flange |
| 44 | 1 | ROMA02A | Flange |
| 45 | 1 | ROMA02A | Flange |
| 46 | 1 | ROMA02A | Flange |
| 47 | 1 | ROMA02A | Flange |
| 48 | 1 | ROMA02A | Flange |
| 49 | 1 | ROMA02A | Flange |
| 50 | 1 | ROMA02A | Flange |
| 51 | 1 | ROMA02A | Flange |
| 52 | 1 | ROMA02A | Flange |
| 53 | 1 | ROMA02A | Flange |
| 54 | 1 | ROMA02A | Flange |
| 55 | 1 | ROMA02A | Flange |
| 56 | 1 | ROMA02A | Flange |
| 57 | 1 | ROMA02A | Flange |
| 58 | 1 | ROMA02A | Flange |
| 59 | 1 | ROMA02A | Flange |
| 60 | 1 | ROMA02A | Flange |
| 61 | 1 | ROMA02A | Flange |
| 62 | 1 | ROMA02A | Flange |
| 63 | 1 | ROMA02A | Flange |
| 64 | 1 | ROMA02A | Flange |
| 65 | 1 | ROMA02A | Flange |
| 66 | 1 | ROMA02A | Flange |
| 67 | 1 | ROMA02A | Flange |
| 68 | 1 | ROMA02A | Flange |
| 69 | 1 | ROMA02A | Flange |
| 70 | 1 | ROMA02A | Flange |
| 71 | 1 | ROMA02A | Flange |
| 72 | 1 | ROMA02A | Flange |
| 73 | 1 | ROMA02A | Flange |
| 74 | 1 | ROMA02A | Flange |
| 75 | 1 | ROMA02A | Flange |
| 76 | 1 | ROMA02A | Flange |
| 77 | 1 | ROMA02A | Flange |
| 78 | 1 | ROMA02A | Flange |
| 79 | 1 | ROMA02A | Flange |
| 80 | 1 | ROMA02A | Flange |
| 81 | 1 | ROMA02A | Flange |
| 82 | 1 | ROMA02A | Flange |
| 83 | 1 | ROMA02A | Flange |
| 84 | 1 | ROMA02A | Flange |
| 85 | 1 | ROMA02A | Flange |
| 86 | 1 | ROMA02A | Flange |
| 87 | 1 | ROMA02A | Flange |
| 88 | 1 | ROMA02A | Flange |
| 89 | 1 | ROMA02A | Flange |
| 90 | 1 | ROMA02A | Flange |
| 91 | 1 | ROMA02A | Flange |
| 92 | 1 | ROMA02A | Flange |
| 93 | 1 | ROMA02A | Flange |
| 94 | 1 | ROMA02A | Flange |
| 95 | 1 | ROMA02A | Flange |
| 96 | 1 | ROMA02A | Flange |
| 97 | 1 | ROMA02A | Flange |
| 98 | 1 | ROMA02A | Flange |
| 99 | 1 | ROMA02A | Flange |
| 100 | 1 | ROMA02A | Flange |

| | | | | | | | | | |
|---------|--------------------|------|-----------|---|-------------|-------------|-----|-----|---|
| PROJECT | Social Development | DATE | 24/Jun/98 | DESIGNED BY | M. Tucknoll | APPROVED BY | ASK | REV | A |
| | | | |                   | | | | | |
| | | | |                   | | | | | |
| | | | |                   | | | | | |
| | | | |                   | | | | | |
| | | | |             | | | | | |

APPENDIX C

UoSAT-12 ATTITUDE CONTROL SIMULATIONS

U12.txt
oms simulator sysin data file ver 1.0

D000_simulation_epoch_in_calender = 951230000000.0

if 21st century follow this example "010225123530.0"
this corresponds 12:35:30 utc 25/02/2001

D001_epoch_semi_major_axis_in_kilometre = 7200.0
D002_epoch_eccentricity = 0.0001
D003_epoch_inclination_in_degrees = 63.7
D004_epoch_ascending_node_in_degrees = 335.0
D005_epoch_argument_perigee_in_degrees = 120.0
D006_epoch_mean_anomaly_in_degrees = 210.0

initial keplerian

D007_epoch_roll_in_degrees = 0.0
D008_epoch_pitch_in_degrees = 0.0
D009_epoch_yaw_in_degrees = 0.0

initial attitude euler 2-1-3 system w.r.t. local orbit

D010_epoch_x_angular_vel_in_deg_sec = 0.0
D011_epoch_y_angular_vel_in_deg_sec = -0.0
D012_epoch_z_angular_vel_in_deg_sec = 0.0

initial inertial angular velocity w.r.t. body

D013_moment_of_inertia_ix_in_kgm2 = 5.34
D014_moment_of_inertia_iy_in_kgm2 = 5.34
D015_moment_of_inertia_iz_in_kgm2 = 0.237

momentum of inertia

D016_product_of_inertia_iyz_in_kgm2 = -0.0
D017_product_of_inertia_izx_in_kgm2 = -0.0
D018_product_of_inertia_ixy_in_kgm2 = 0.0

product of inertia (cross term)

D019_simulation_duration_in_hours = 1.0

desired simulation duration in hours

D020_integration_step_in_seconds = 1.0

integration step size (fixed)

D021_inertia_momentum_of_wheel = 0.000

inertia momentum of pitch momentum wheel

```

                                U12.txt
D022_tai_utc_offset_in_seconds      =      30.0
D023_utc_utl_offset_in_seconds      =      0.0

    time offset

D024_max_allowable_igrf_err_in_nT    =      5000.0

    igrf mask (for kalman filtering)

D025_epoch_roll_err_in_degrees      =      -2.0
D026_epoch_pitch_err_in_degrees     =      1.0
D027_epoch_yaw_err_in_degrees       =      5.0

    initial attitude estimation error (for kalman)

D028_epoch_x_angular_vel_err_in_deg_sec =      0.001
D029_epoch_y_angular_vel_err_in_deg_sec =     -0.005
D030_epoch_z_angular_vel_err_in_deg_sec =     -0.001

    initial angular velocity estimation error (for kalman)

D031_epoch_rol_covariance_in_deg2    =      100.0
D032_epoch_pch_covariance_in_deg2    =      100.0
D033_epoch_yaw_covariance_in_deg2    =      100.0
D034_epoch_rol_rate_cov_in_deg_sec2  =      4.e-4
D035_epoch_pch_rate_cov_in_deg_sec2  =      4.e-4
D036_epoch_yaw_rate_cov_in_deg_sec2  =      4.e-4

    initial covariance matrix diagonals (for kalman)

D037_kalman_process_noise_x_in_nm    =      1.e-7
D038_kalman_process_noise_y_in_nm    =      1.e-7
D039_kalman_process_noise_z_in_nm    =      1.e-7

    process noise variances (for kalman)

D040_kalman_magnav_x_noise_var_in_nT2 =      9.e5
D041_kalman_magnav_y_noise_var_in_nT2 =      9.e5
D042_kalman_magnav_z_noise_var_in_nT2 =      9.e5

    observation noise variances (for kalman)

D043_emulated_magnav_noise_in_nT     =      300.0

    emulated magnetometer observation noise 1-sigma

D044_emulated_x_disturb_torque_in_nm =      1.e-8
D045_emulated_y_disturb_torque_in_nm =      1.e-8
D046_emulated_z_disturb_torque_in_nm =      1.e-8

    emulated unmodelled disturbance torque 1-sigma

```

U12.txt

| | | |
|--------------------------------------|---|-------|
| D047_emulated_x_disturb_force_in_ms2 | = | 1.e-8 |
| D048_emulated_y_disturb_force_in_ms2 | = | 1.e-8 |
| D049_emulated_z_disturb_force_in_ms2 | = | 1.e-8 |

emulated unmodelled disturbance force 1-sigma

| | | |
|---------------------------------------|---|------|
| D050_pitch_m_wheel_spin_in_rpm | = | -0.0 |
| D051_pitch_m_wheel_spin_rate_in_degs2 | = | 0.0 |

pitch momentum wheel status

| | | |
|-------------------------------------|---|--------|
| D052_cg_pos_x_wrt_strbody_in_metres | = | -0.089 |
| D053_cg_pos_y_wrt_strbody_in_metres | = | -0.089 |
| D054_cg_pos_z_wrt_strbody_in_metres | = | -0.295 |

cg position vector

strbody : structural body coordinate [max defined]

| | | |
|--------------------------------------|---|--------|
| D055_oms_pos_x_wrt_strbody_in_metres | = | -0.089 |
| D056_oms_pos_y_wrt_strbody_in_metres | = | -0.089 |
| D057_oms_pos_z_wrt_strbody_in_metres | = | -0.0 |

oms position vector

| | | |
|--|---|-------------|
| _D058_thruster_force_unit_vct_x_wrt_body | = | 0.958665525 |
| _D059_thruster_force_unit_vct_y_wrt_body | = | 0.28453543 |
| _D060_thruster_force_unit_vct_z_wrt_body | = | 0.0 |

these parameters (above) are only valid for
d055 = -0.438 and d056 = -0.130

| | | |
|---|---|-----|
| D058_thruster_force_unit_vct_x_wrt_body | = | 0.1 |
| D059_thruster_force_unit_vct_y_wrt_body | = | 0.1 |
| D060_thruster_force_unit_vct_z_wrt_body | = | 0.8 |

thruster force direction unit vector
must be with respect to body not strbody:

D061_thruster_force_in_newton = 8000.0

thruster force

D062_rcs_x_torque_in_nm = 0.05

D063_rcs_y_torque_in_nm = 0.05

D064_rcs_z_torque_in_nm = 0.05

rcs torque

D065_oms_burn_time_per_orbit_in_second = 2.5

oms firing time per orbit

D066_spacecraft_mass_in_kg = 15.0

mass

D067_lqr_p_weight_matrix_p00 = 1.0

D068_lqr_p_weight_matrix_p11 = 1.0

D069_lqr_p_weight_matrix_p22 = 1.0

D070_lqr_p_weight_matrix_p33 = 1.0

D071_lqr_p_weight_matrix_p44 = 1.0

D072_lqr_p_weight_matrix_p55 = 1.0

lqr controller system parameter weight diagonals
recommend not to change

D073_lqr_q_weight_matrix_q00 = 1.0

D074_lqr_q_weight_matrix_q11 = 1.0

D075_lqr_q_weight_matrix_q22 = 1.0

lqr controller control parameter weight diagonals
if stronger pulse is required, try to make these
weights smaller

stronger ---> smaller

weaker ---> bigger

D076_3d_graphic_view_point_az_in_deg = 0.0

D077_3d_graphic_view_point_el_in_deg = 0.0

U12.txt

3d graphic your view points

| | | |
|------------------------------|---|-------|
| D078_mxy_0_strength_in_am2 | = | 40.0 |
| D079_mxy_1_strength_in_am2 | = | 40.0 |
| D080_mxy_2_strength_in_am2 | = | 40.0 |
| D081_mz_strength_in_am2 | = | 40.0 |
| | | |
| D082_mxy_0_azimuth_in_degree | = | 60.0 |
| D083_mxy_1_azimuth_in_degree | = | 180.0 |
| D084_mxy_2_azimuth_in_degree | = | 300.0 |

uosat-12 magnetorquer specification

| | | |
|--------------------------|---|---------|
| D085_cpl_roll_rate_gain | = | 10000.0 |
| D086_cpl_pitch_rate_gain | = | 10000.0 |
| D087_cpl_yaw_rate_gain | = | 10000.0 |
| | | |
| D088_cpl_roll_gain | = | 100.0 |
| D089_cpl_pitch_gain | = | 100.0 |
| D090_cpl_yaw_gain | = | 100.0 |

magnetorquer control [cross product law] gain

| | | |
|--------------------------------|---|-----|
| I000_data_save_span_in_intstep | = | 120 |
|--------------------------------|---|-----|

history data save span

| | | |
|-------------------------------|---|----|
| I001_kalman_update_in_intstep | = | 10 |
|-------------------------------|---|----|

kalman update timing

| | | |
|-------------------------------------|---|----|
| I002_igrf_harmonic_order_for_ref | = | 10 |
| I003_igrf_harmonic_order_for_filter | = | 10 |

igrf95 model: harmonic order must be <= 10

| | | |
|----------------------------------|---|---|
| I004_geopotential_harmonic_order | = | 0 |
|----------------------------------|---|---|

wgs84 defined model: harmonic order must be <= 8
set 0 (zero) if simple two body is preferable

| | | |
|----------------------------|---|----|
| I005_lqr_update_in_intstep | = | 20 |
|----------------------------|---|----|

lqr update timing

| | | |
|------------------------------|---|----|
| I006_xfer_loop_number_in_lqr | = | 10 |
|------------------------------|---|----|

recommend not to change

| | | |
|---------------------------------|---|---|
| I007_how_many_oms_mnvr_in_total | = | 1 |
|---------------------------------|---|---|

U12.txt

total manoeuvre time is therefore $d065 \cdot i007$ seconds

I008_kalman_determination_system_switch = 0

= 0 : off -> controller can know true attitude state
(assume perfect attitude determination)

= 1 : on -> controller can only know determined attitude
state which may not be true
(assume realistic kalman determination)

I009_rcs_mnvr_limit_per_cntl_in_intstep = 10

if control loop is 20 seconds then obviously this parameter
must be smaller than 20

I010_cpl_update_in_intstep = 20

cpl controller update timing

I011_cpl_mtq_firing_time_in_intstep = 10

magnetorquer firing time : must be < i010

I012_apply_deadbeat_manoeuvre_or_not = 0

0: no / 1: yes

APPENDIX D

MIGHTYSATIL.1 STATEMENT OF WORK

Surrey Satellite Technology, Ltd.

F61775-98-WE099

Page 004

NON PERSONAL CONSULTING SERVICES AS FOLLOWS:

ANY CHANGE IN THE ITINERARY OR ADDITIONAL TIME ON SITE AND/OR PERFORMANCE WHICH WOULD REQUIRE FUNDS EXCEEDING THE AMOUNT SET FORTH ON THE SF 1449 MUST BE AUTHORIZED BY AN ORDER MODIFICATION APPROVED BY A US GOVERNMENT CONTRACTING OFFICER

F7LEOB81310100

Schedule of Supplies/ServicesAmount: \$57,322.00Item 0001

\$40,000.00

The contractor will investigate the application of H2O resistojet propulsion technology for the AFRL Mightysat II satellite program. Three proto-flight models will be built and tested. Two models will be delivered to AFRL/PRR (Edwards, AFB, CA). Following testing, the third model will be sectioned and examined to prepare the final report. First payment will be made upon receipt and acceptance of two proto-flight models of a resistojet to AFRL/PRR (Edwards AFB, CA). Delivery is due no later than 2 months after contract award.

Report Due: 16 Aug 98Item 0002

\$17,322.00

Second payment will be made upon receipt and acceptance of a complete test report. This test report is due no later than 4 months after contract award.

Report Due: 16 Oct 98

SPECIAL PROJECT SPC-98-4064

THE CONTRACTOR IS RESPONSIBLE FOR ANY TAX PAYMENTS AND COMPLIANCE WITH ALL APPLICABLE STATE, LOCAL, FOREIGN TAX AND/OR SOCIAL SECURITY LEGISLATION.

5783600 298 47C3 636340 E22300 586 63302F 672300 F72300 43730002
H98G740134

\$57,322.00